

**THE DESIGN, SYNTHESIS, AND  
APPLICATION OF RUTHENIUM  
METATHESIS CATALYSTS FOR THE  
PREPARATION OF SMALL  
MOLECULES AND POLYMERS**

Thesis by

Renee M. Thomas

In Partial Fulfillment of the Requirements for the Degree of  
Doctor of Philosophy

CALIFORNIA INSTITUTE OF TECHNOLOGY

Pasadena, California

2012

(Defended May 7, 2012)

© 2012

Renee Thomas

All Rights Reserved

## ***ACKNOWLEDGEMENTS***

I want to begin by thanking my advisor, Professor Robert Grubbs. I really value his guidance and support, and the independence that he gives us in lab to explore our research interests. My time in his lab has been very educational and enjoyable. I also deeply appreciate that he has been very supportive of my career goals and choices, and has really done a lot to help me reach them. Additionally, I want to acknowledge my committee members: Professors Brian Stoltz, Harry Gray, and Dennis Dougherty. I am very thankful for all of their support over the years.

The Grubbs group has been a great group to work with, and I especially want to thank Jean Li, Rosemary Conrad, and Pinky Patel for being good friends. I have enjoyed our many activities together, both in and outside of the lab. Postdoctoral fellows AJ Boydston, Rosemary Conrad, Pinky Patel, Alexey Federov, and Jeremiah Johnson have been wonderful scientific resources. I have enjoyed learning alongside the graduate students in the Grubbs group that I have overlapped with: John Matson, Matt Whited, Kevin Kuhn, Paul Clark, Yan Xia, Jean Li, Chris Daffler, Matthew Van Wingerden, Keith Keitz, Myles Herbert, Ben Sveinbjornsson, Zach Wickens, Brendan Quigley, and Raymond Weitekamp. Caltech has been a wonderful school to study at and has a very collaborative environment. I value the many friendships that I have made here with my fellow graduate students in other groups: Madalyn Radlauer, Kaycie Deyle, Lindsay Repka, Kristina McCleary, and Catrina Pheeny.

Dr. Scott Virgil has been very willing and available for helpful scientific discussions as well as assistance with many instruments for analyzing data. Dr. David VanderVelde has

been a great resource for questions involving NMR spectroscopy. Dr. Lawrence Henling and Dr. Michael Day obtained the crystal structures of my catalysts.

Finally I would like to thank my family for being so supportive of me over the years. My mom, dad, Kristen, Tricia, and my dear friend Annie have always been there for me and believed in me, and I would not be where I am now without them.

## ***ABSTRACT***

Olefin metathesis is a widely used method for constructing carbon–carbon double bonds. This methodology has broad applications in organic and polymer chemistry, and the continued design of highly efficient catalysts has been critical to the success of this reaction. The main goal of this thesis was to design and synthesize new catalysts for better selectivity and for improved properties for targeted applications, as well as to explore different ligand structures for optimal catalyst performance in olefin metathesis.

The application of ruthenium catalysts for the ring-opening metathesis polymerization of challenging monomer 1,5-dimethyl-1,5-cyclooctadiene in the presence of a chain transfer agent is discussed in chapter 2. A variety of complexes were explored to find the ideal catalyst for this transformation, enabling the synthesis of telechelic polyisoprene, which has extensive applications in block copolymerization.

Chiral *N*-alkyl, *N*-aryl NHC ruthenium catalysts were designed and synthesized to improve the enantioselectivity during asymmetric ring-opening cross-metathesis. Mechanistic studies of these catalysts revealed a preference for methylenide propagation compared to previous NHC catalysts. Chapter 3 describes these studies, in addition to the screening of a variety of chiral ligands for optimal enantioselectivity. Some of these catalysts gave very high enantioselectivity, comparable to the best reported ruthenium catalysts. Insights into the stability of these complexes as a propagating methylenide led to investigating them in applications where propagation as a methylenide is desirable.

*N*-aryl, *N*-alkyl NHC ruthenium catalysts were designed and synthesized for improved selectivity during ethenolysis reactions, which require a ruthenium methylenide species

to react with an internal olefin to yield a terminal olefin and a ruthenium alkylidene species. Subsequent reaction of this ruthenium alkylidene species with ethylene gives the other terminal olefin. This reaction can be applied to the internal olefin of seed oils to generate valuable products that are typically derived from petroleum sources, thus providing an environmentally friendly route to the same products. An important component of ethenolysis catalysts is stability to existing as a methyldiene, a property of the *N*-aryl, *N*-alkyl NHC ruthenium catalysts described in chapter 4.

Chapter 5 describes the design and synthesis of sterically hindered *N*-aryl, *N*-alkyl NHC ruthenium catalysts for application in latent metathesis. These complexes also show excellent stability at elevated temperatures for extended periods of time.

Appendix A contains NMR spectra for catalysts described in chapter 4, as well as X-ray crystal structures for two of the catalysts.

Appendix B contains NMR spectra for catalysts described in chapter 5, as well as X-ray crystal structures for two of those catalysts.

***TABLE OF CONTENTS***

<b>Chapter 1</b>	<b>1</b>
<b>Chapter 2</b>	<b>9</b>
<b>Chapter 3</b>	<b>26</b>
<b>Chapter 4</b>	<b>52</b>
<b>Chapter 5</b>	<b>95</b>
<b>Appendix A</b>	<b>122</b>
<b>Appendix B</b>	<b>140</b>

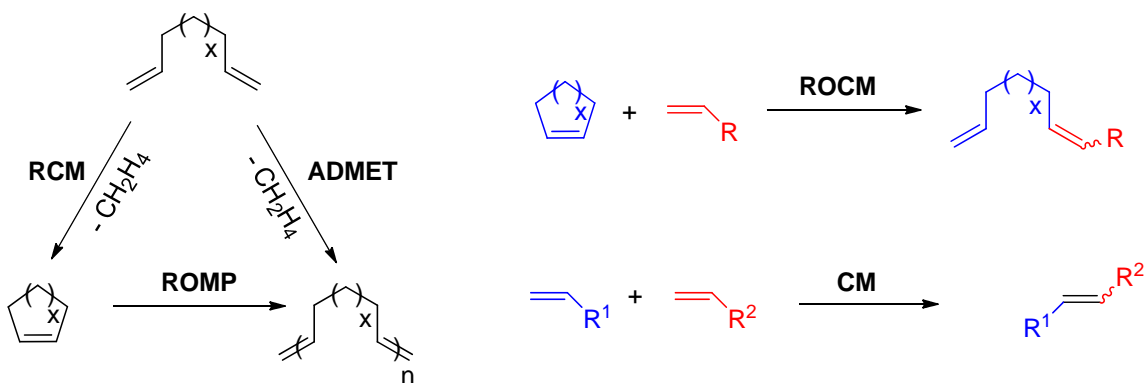
## *Chapter 1*

### INTRODUCTION TO OLEFIN METATHESIS: RUTHENIUM CATALYST DEVELOPMENT

#### **Abstract**

Olefin metathesis is one of the most versatile methods for forming carbon–carbon bonds. Metathesis reactions have extensive applications, ranging from natural product and pharmaceutical synthesis, to polymers and materials. Research efforts have been directed toward developing efficient catalysts tailored to specific applications. In particular, ruthenium catalysts have been especially attractive due to their stability, enabling them to be easily handled, and their functional group tolerance, making them useful for a broad substrate scope.

#### *Metathesis Reactions*



Metathesis reactions are used for a variety of synthetic purposes, including ring-opening metathesis polymerization (ROMP), ring-closing metathesis (RCM), cross-metathesis (CM), ring-opening cross-metathesis (ROCM), and acyclic diene metathesis polymerization (ADMET), as shown above. This methodology allows access to small

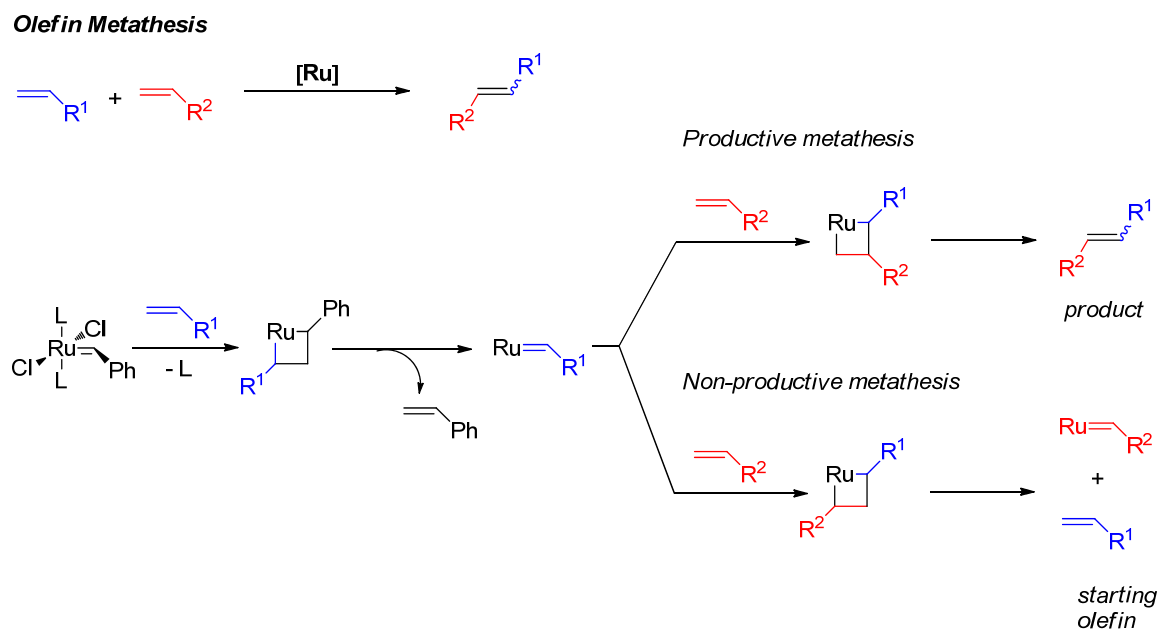


molecules and polymers that often would be very challenging or impossible to synthesize otherwise. Due to the wide applicability of metathesis reactions, improvement and modification of catalysts are an ongoing endeavor to provide more efficient, stable, and selective complexes.

## Introduction

In olefin metathesis, the formation of new carbon–carbon double bonds occurs through the metal mediated reaction of two olefins via an intermediate metallacyclobutane, which can break down to give a new olefin (productive metathesis) or the original olefin (non-productive metathesis) (Scheme 1.1).

**Scheme 1.1.** Olefin metathesis mechanism.



As one of the best methods for making carbon-carbon bonds, this methodology has broad use in organic and polymer chemistry and can be utilized through a variety of reactions,

including CM, RCM, ROCM, and ROMP. Important to the success of this reaction has been the continued design and development of highly efficient catalysts. The design and synthesis of new metathesis catalysts has been ongoing since the initial discovery of olefin metathesis in the 1960s.<sup>1-4</sup> However, the first catalysts were not well-defined and commonly consisted of metal salts, where the metal was typically titanium,<sup>1</sup> molybdenum,<sup>2</sup> tungsten,<sup>5</sup> or rhenium.<sup>6</sup> The active species of these mixtures were not characterized, making the process of developing better catalysts challenging as there was no known catalyst structure/activity relationship from which to derive new models.

The first well-defined metathesis catalysts were reported in the early 1980s by Schrock.<sup>7</sup> Niobium, tantalum, and tungsten complexes were synthesized, characterized, and shown to be active for metathesis turnovers. Further catalyst development by Schrock focused on molybdenum systems, which proved to have superior activity and selectivity during metathesis reactions.<sup>8,9</sup> Recently, highly selective molybdenum catalysts have been reported for enantioselective metathesis,<sup>10</sup> as well as *Z*-selective metathesis.<sup>11</sup> However, molybdenum catalysts are air and moisture sensitive, and their functional group tolerance is limited. Accordingly, more stable and robust metathesis catalysts are needed for many applications and for easy handling and manipulation.

In order to prepare a catalyst system with improved stability and functional group tolerance, Grubbs and co-workers observed that ruthenium trichloride hydrate salts were capable of carrying out the ROMP of 7-oxanorbornene derivatives in water.<sup>12</sup> This system, although not well-defined, gave significant improvement over other metal systems in functional group tolerance, and could be used in water and protonated solvents. Subsequently, Grubbs reported the first well-defined ruthenium metathesis

catalysts in the early 1990s (Figure 1.1), which exhibited the same functional group tolerance and stability as the undefined system, although suffered from low initiation rates.<sup>13,14</sup> As a result, a broad polydispersity index (PDI) was observed during ROMP, and RCM required long reaction times. Therefore, efforts were focused on improving these well-defined catalysts by ligand modification to produce a catalyst with better initiation rates and yields.

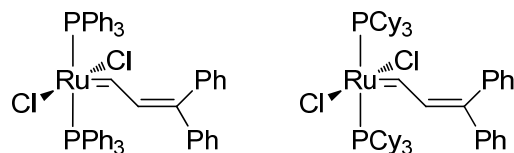


**Figure 1.1.** Early well-defined ruthenium metathesis catalysts.

Grubbs and co-workers reported the first generation ruthenium metathesis catalyst in 1995 (**1.1**, Figure 1.2).<sup>14</sup> This catalyst gave improved initiation rates and yields, and showed good stability, making it attractive for synthetic purposes. Complex **1.1** is stable in air, whereas the earlier complexes were not stable in air, and **1.1** initiates ROMP over 1000 times faster than the earlier catalysts. Complex **1.1** also catalyzed the living ROMP of norbornene and substituted cyclobutenes, and afforded polymers with very low PDIs, indicative of excellent initiation. However, molybdenum-based catalysts, although air and moisture sensitive, generally still had a broader substrate scope and were more efficient at RCM. Additionally, catalyst **1.1** underwent appreciable decomposition at elevated temperatures, a feature limiting its utility in some applications.

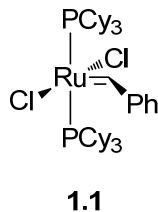


**Figure 1.2.** First generation ruthenium metathesis catalyst.

Toward improving ruthenium metathesis catalysts' thermal stability and functional group tolerance, Grubbs and co-workers developed unsaturated *N*-heterocyclic carbene (NHC) ligands in place of one of the phosphine ligands (**1.2**, Figure 1.3).<sup>15</sup> While complex **1.2** showed low reactivity at ambient temperature for RCM, the reactivity was substantially superior to **1.1** at 40 °C. Additionally, **1.2** catalyzed the RCM of more sterically demanding olefins that **1.1** did not, including tetra-substituted olefins. Variations of the unsaturated NHC were explored and found to give similar results to **1.2**.<sup>16,17</sup>

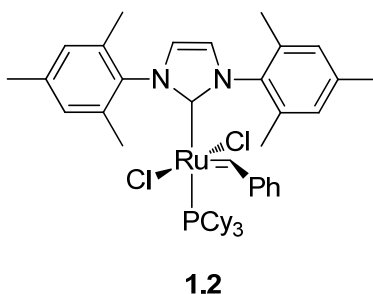


**Figure 1.3.** Unsaturated NHC ruthenium metathesis catalyst.

In order to improve catalyst efficiency, a second generation, saturated NHC ruthenium metathesis catalyst (**1.3**) was prepared by Grubbs and co-workers in 1999 (Figure 1.4).<sup>18</sup> This catalyst showed excellent activity, stability, and functional group tolerance compared to **1.2**,<sup>19</sup> and as a result, its applications in synthetic, polymer, and materials chemistry has been extensive. Indeed, due to its easy manipulation, catalyst **1.3** is one of

the most widely used metathesis catalysts in organic laboratories. Subsequent catalyst improvements have largely been focused on modifying this very successful motif for specific applications requiring particular catalyst properties. Hoveyda and co-workers designed a variation of catalyst **1.3** with a chelating ether benzylidene initiator instead of a phosphine initiator (**1.4**, Figure 1.4).<sup>20</sup>

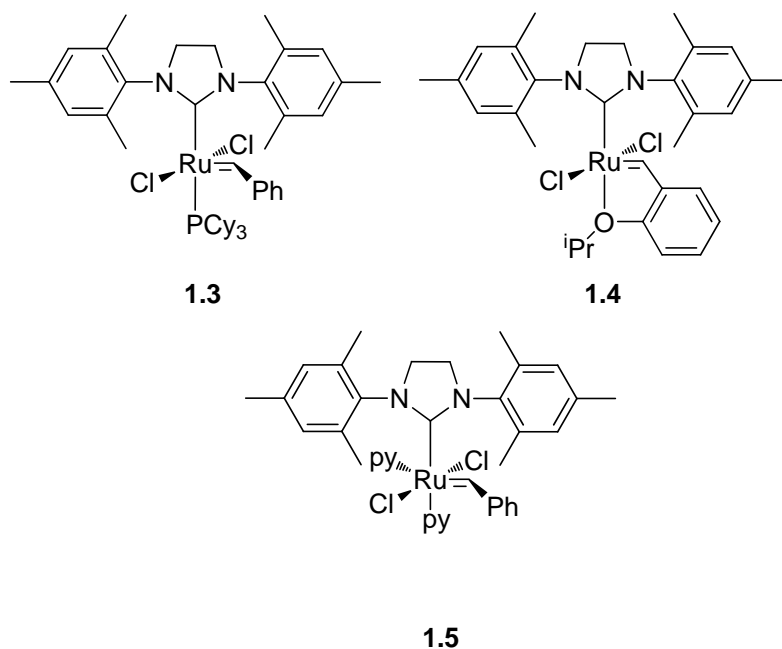


**Figure 1.4.** Second generation ruthenium metathesis catalysts.

Complex **1.4**, while generally a slower initiator than complex **1.3**, has remarkable stability, making it an ideal catalyst for applications where the reaction conditions are harsh or where the substrates or products contain highly reactive functionalities. Additionally, its stability renders it an attractive choice for the metathesis of substrates that are slow to react, since it will remain active for a long period of time before it begins to decompose. Another advancement in catalyst development came with the synthesis of complex **1.5**, with two readily displaceable pyridine ligands (Figure 1.4).<sup>21</sup> Catalyst **1.5** is

highly efficient and a very fast initiator, and while not as long-lived as catalysts **1.3** and **1.4**, its high activity and efficiency enable it to complete metathesis reactions in a much shorter amount of time.<sup>22</sup> Since polymerization reactions require good catalyst initiation for controlled molecular weight and narrow PDIs, catalyst **1.5** is excellent for use in ROMP of norbornenes and strained cyclic olefins.

Further catalyst development has been primarily focused on varying the NHC ligand backbone and *N*-substituents to improve selectivity, stability, and efficiency.<sup>23</sup> Designing selective catalysts is particularly important as this increases the utility of metathesis reactions in synthesis.<sup>24</sup> Specifically, changing the steric and electronic properties of the NHC has been employed to access complexes that, for example, are selective for the cross-metathesis of two different olefins over homodimerization,<sup>25</sup> selectivity for the formation of *Z* over *E* olefins during cross-metathesis,<sup>26</sup> and enantioselective olefin metathesis.<sup>27</sup> Enantioselectivity is significant as this enables stereochemical control during synthesis, an important component in natural product and pharmaceutical drug synthesis.<sup>28</sup> There is continued need for catalyst improvement, and ongoing research in ligand modification is directed toward producing better catalysts for broader applications.

## REFERENCES

1. Truett, W. L.; Johnson, D. R.; Robinson, I. M.; Montague, B. A. *J. Am. Chem. Soc.* **1960**, *82*, 2337–2340.
2. Banks, R. L.; Bailey, G. C. *Ind. Eng. Chem. Prod. R.D.* **1964**, *3*, 170–173.
3. Hérissou, J.-L.; Chauvin, Y. *Makromol. Chem.* **1971**, *141*, 161–176.
4. Schrock, R. R. *J. Am. Chem. Soc.* **1974**, *96*, 6796–6797.
5. (a) Calderon, N.; Chen, H. Y.; Scott, K. W. *Tet. Lett.* **1967**, *34*, 3327–3329. (b) Calderon, N.; Ofstead, E. A.; Ward, J. P.; Judy, W. A.; Scott, K. W. *J. Am. Chem. Soc.* **1968**, *90*, 4133–4140. (c) Lewandos, G. S.; Pettit, R. *J. Am. Chem. Soc.* **1971**, *93*, 7087–7088. (d) Grubbs, R. H.; Brunck, T. K. *J. Am. Chem. Soc.* **1972**, *94*, 2538–2540. (e) Casey, C. P.; Burkhardt, T. J. *J. Am. Chem. Soc.* **1974**, *96*, 7808–7809. (f) Grubbs, R. H.; Burk, P. L.; Carr, D. D. *J. Am. Chem. Soc.* **1975**, *97*, 3265–3267. (g) McGinnis, J.; Katz, T. J.; Hurwitz, S. *J. Am. Chem. Soc.* **1976**, *98*, 605–606.
6. Katz, T. J.; McGinnis, J. *J. Am. Chem. Soc.* **1975**, *97*, 1592–1594.
7. Schrock, R. R.; Rocklage, S.; Wengrovius, J.; Rupprecht, G.; Fellmann, J. *J. Mol. Cat.* **1980**, *8*, 73–83.
8. Schrock, R. R.; Murdzek, J. S.; Bazan, G. C.; Robbins, J.; DiMare, M.; O'Regan, M. *J. Am. Chem. Soc.* **1990**, *112*, 3875–3886.
9. Bazan, G. C.; Oskam, J. H.; Cho, H.-N.; Park, L. Y.; Schrock, R. R. *J. Am. Chem. Soc.* **1991**, *113*, 6899–6907.
10. Hoveyda, Amir H.; Schrock, Richard R. *Organic Synthesis Highlights V* **2003**, 210–229.
11. Flook, M. M.; Jiang, A. J.; Schrock, R. R.; Muller, P.; Hoveyda, A. H. *J. Am. Chem. Soc.* **2009**, *131*, 7962–7963.
12. Novak, B. M.; Grubbs, R. H. *J. Am. Chem. Soc.* **1988**, *110*, 7542–7543.
13. Nguyen, S. T.; Johnson, L. K.; Grubbs, R. H. *J. Am. Chem. Soc.* **1992**, *114*, 3974–3975.
14. Schwab, P.; France, M. B.; Ziller, J. W. Grubbs, R. H. *Angew. Chem. Int. Ed.* **1995**, *34*, 2039–2041.
15. Scholl, M.; Trnka, T. M.; Morgan, J. P.; Grubbs, R. H. *Tet. Lett.* **1999**, *40*, 2247–2250.
16. Huang, J.; Stevens, E. D.; Nolan, S. P.; Petersen, J. L. *J. Am. Chem. Soc.* **1999**, *121*, 2674–2678.
17. Ackermann, L.; Fürstner, A.; Weskamp, T.; Kohl, F. J.; Herrmann, W. A. *Tet. Lett.* **1999**, *40*, 4787–4790.
18. Scholl, M.; Ding, S.; Lee, C. W.; Grubbs, R. H. *Org. Lett.* **1999**, *1*, 953–956.
19. (a) Sanford, M. S.; Ulman, M.; Grubbs, R. H. *J. Am. Chem. Soc.* **2001**, *123*, 749–750. (b) Sanford, M. S.; Love, J. A.; Grubbs, R. H. *J. Am. Chem. Soc.* **2001**, *123*, 6543–6554.
20. Garber, S. B.; Kingsbury, J. S.; Gray, B. L.; Hoveyda, A. H. *J. Am. Chem. Soc.* **2000**, *122*, 8168–8179.
21. Sanford, M. S.; Love, J. A.; Grubbs, R. H. *Organometallics* **2001**, *20*, 5314–5318.
22. Ritter, T.; Hejl, A.; Wenzel, A. G.; Funk, T. W.; Grubbs, R. H. *Organometallics* **2006**, *25*, 5740–5745.

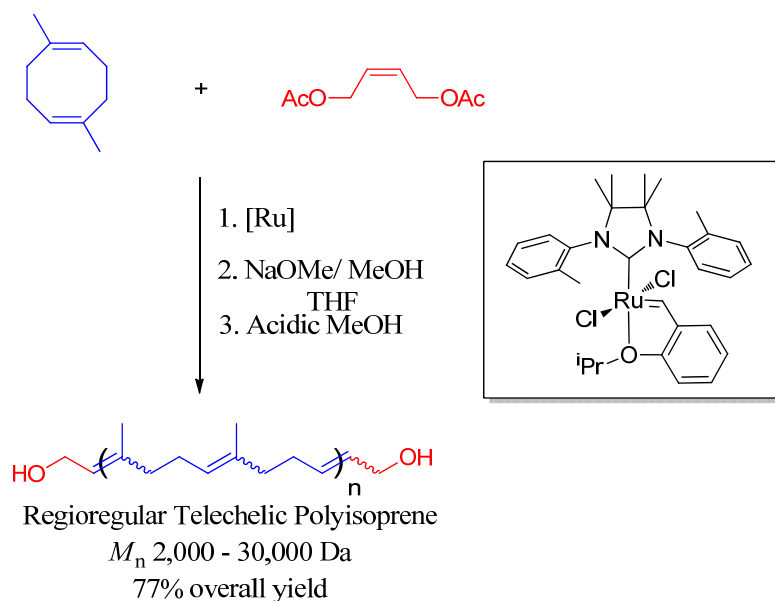
23. (a) Trnka, T. M.; Grubbs, R. H. *Acc. Chem. Res.* **2001**, *34*, 18–29. (b) Kuhn, K. M.; Bourg, J.-B.; Chung, C. K.; Virgil, S. C.; Grubbs, R. H. *J. Am. Chem. Soc.* **2009**, *131*, 5313–5320. (c) Love, J. A.; Morgan, J. P.; Trnka, T. M.; Grubbs, R. H. *Angew. Chem. Int. Ed.* **2002**, *41*, 4035–4037.
24. Hoveyda, A. H.; Zhurgralin, A. R. *Nature* **2007**, *450*, 243–251.
25. (a) Chatterjee, A. K.; Choi, T.-L.; Sanders, D. P.; Grubbs, R. H. *J. Am. Chem. Soc.* **2003**, *125*, 11360–11370. (b) Chatterjee, A. K.; Morgan, J. P.; Scholl, M.; Grubbs, R. H. *J. Am. Chem. Soc.* **2000**, *122*, 3783–3784.
26. Endo, K.; Grubbs, R. H. *J. Am. Chem. Soc.* **2011**, *133*, 8525–8527.
27. (a) Hoveyda, A. H.; Schrock, R. R. *Comprehensive Asymmetric Catalysis*, Supplement **2004**, *1*, 207–233. (b) Connon, S. J.; Blechert, S. *Topics in Organometallic Chemistry* **2004**, *11*, 93–124. (c) Hoveyda, A. H.; Schrock, R. R. *Organic Synthesis Highlights V* **2003**, 210–229.
28. (a) Gillingham, D. G.; Hoveyda, A. H. *Angew. Chem. Int. Ed.* **2007**, *46*, 3860–3864. (b) Takao, K.; Yasui, H.; Yamamoto, S.; Sasaki, D.; Kawasaki, S.; Watanabe, G.; Tadano, K. *J. Org. Chem.* **2004**, *69*, 8789–8795. (c) Cortez, G. A.; Schrock, R. R.; Hoveyda, A. H. *Angew. Chem. Int. Ed.* **2007**, *46*, 4534–4538. (d) Savoie, J.; Stenne, B.; Collins, S. K. *Advanced Synthesis & Catalysis* **2009**, *351*, 1826–1832. (e) Fournier, P. A.; Savoie, J.; Stenne, B.; Bedard, M.; Grandbois, A.; Collins, S. K. *Chemistry—A European Journal* **2008**, *14*, 8690–8695. (f) Funk, T. W.; Berlin, J. M.; Grubbs, R. H. *J. Am. Chem. Soc.* **2006**, *128*, 1840–1846.



## Chapter 2

### SYNTHESIS OF TELECHELIC POLYISOPRENE VIA RING-OPENING METATHESIS POLYMERIZATION IN THE PRESENCE OF CHAIN TRANSFER AGENT

#### Abstract



Telechelic polyisoprene was synthesized via the ring-opening metathesis polymerization (ROMP) of 1,5-dimethyl-1,5-cyclooctadiene (DMCOD) in the presence of *cis*-1,4-diacetoxy-2-butene as a chain transfer agent (CTA). This method afforded telechelic polymer in excellent yield, and the acetoxy groups were successfully removed to yield  $\alpha,\omega$ -hydroxy end-functionalized polyisoprene with potential for subsequent reactions. Efficient, quantitative incorporation of the CTA was achieved, and NMR spectroscopy was utilized to confirm the chemical identity of the polymer end groups. Polymerization of discrete DMCOD monomer generated polyisoprene with excellent regioregularity in the polymer backbone. Successful ROMP of sterically challenging DMCOD in the presence of a CTA

for chain end-functionalization was discovered through screening of a variety of Ru-based olefin metathesis catalysts.

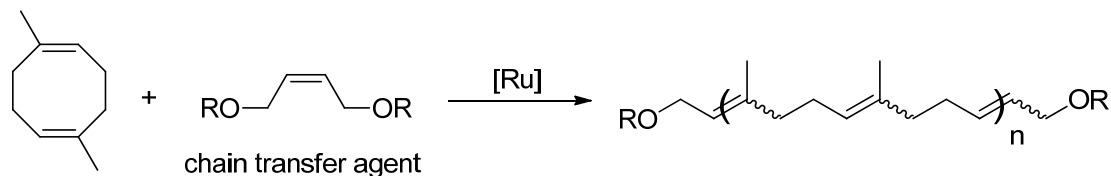
## **Introduction**

Ring-opening metathesis polymerization (ROMP) in the presence of a functionalized allylic olefin as a chain transfer agent has been successfully employed to synthesize telechelic polymers,<sup>1</sup> which are valuable commodities due to their versatility toward subsequent polymerization initiated from the chain ends to afford ABA triblock copolymers. ABA triblock copolymers have extensive utility for materials applications, including use in thermoplastic elastomeric films,<sup>2</sup> adhesives,<sup>3</sup> and biocompatible materials.<sup>4</sup> The center B-block of the ABA copolymer is commonly used to generate a material with desirable physical properties,<sup>5</sup> while A-blocks are often incorporated to render the material biocompatible or biodegradable.<sup>6</sup> In other cases, the A-blocks have been used to control the surface properties of the resulting macromolecules.<sup>7</sup>

An advantage of using ROMP to construct a telechelic center B-block is that this methodology allows access to a wide range of polymer compositions and tolerates a broad scope of functionality. One class of monomers that has been underutilized in the synthesis of telechelic ROMP polymers are sterically encumbered, strained cyclic olefins, despite the fact that substituted cyclic olefins can give rise to a broad range of functional polymers. Specifically, ROMP of DMCOD would give rise, nominally, to polyisoprene, a polymer of industrial importance (Scheme 2.1).

**Scheme 2.1.** Synthesis of telechelic polyisoprene via ROMP of DMCOD with a generic CTA.

1,5-dimethyl-1,5-cyclooctadiene



The potential of telechelic polyisoprene has attracted considerable attention due to the wide variety of commercial applications of this material. To date, the synthesis of telechelic polyisoprene has been primarily realized by reversible addition-fragmentation chain-transfer polymerization<sup>8</sup> or modification of natural rubber to functionalize the chain ends.<sup>9</sup> However, this method often requires harsh reaction conditions for functionalization.<sup>10</sup> Pilard and coworkers reported the synthesis of telechelic polyisoprene via degradation of natural rubber through Ru-mediated olefin metathesis in the presence of a functionalized allylic chain transfer agent.<sup>11</sup> The reported polydispersity indexes (PDI) of the obtained polymers were broad, indicating poor molecular weight control. This example highlights one of the most prominent inherent barriers for the synthesis of telechelic polyisoprene using ROMP—steric hindrance of the methyl substituted double bond significantly retards olefin metathesis during both polymerization and chain transfer events. ROMP of DMCOD in the presence of a CTA would provide a one-pot synthesis of telechelic polyisoprene with good molecular weight control, regioregularity in the polymer backbone, and a broad range of end-group functionalities. Recent advancements in Ru-based olefin metathesis catalysts was expected to provide new opportunities for the synthesis of telechelic polyisoprene by overcoming previous insufficiencies in catalyst activity.

Ruthenium metathesis catalysts have proven to be efficient initiators for ROMP of norbornenes and cyclooctadiene (COD) with a variety of chain transfer agents.<sup>12</sup> The ring-strain energy of metathesis substrates has been shown to significantly affect the monomer reactivity toward ring-opening metathesis, with strained substrates such as norbornenes exhibiting significantly enhanced reactivity over less-strained COD. Trisubstituted olefins are traditionally challenging substrates for metathesis catalysts, with noticeably decreased reactivity compared to disubstituted olefins.<sup>13</sup>

Collectively, DMCOD is a challenging ROMP substrate due to both the lower reactivity of the trisubstituted olefins and low ring-strain energy, rendering it significantly less reactive than previously reported monomers. Accordingly, a range of metathesis catalysts were explored to identify an effective system for the quantitative incorporation of CTA during polymerization of this challenging monomer. The one-pot synthesis of telechelic polyisoprene from DMCOD monomer, with control over the final polymer molecular weight and well-defined microstructure is reported herein.

## Results and Discussion

The activity of a series of known ruthenium metathesis catalysts (**1a-g**, Figure 2.1) was compared for the ROMP of trisubstituted 1,5-dimethyl-1,5-cyclooctadiene (DMCOD) in the presence of *cis*-1,4-diacetoxy-2-butene (**2**) as the chain transfer agent (Scheme 2.2). The ligand structure of ruthenium metathesis catalysts has been reported to significantly affect both activity and catalyst stability, and labile ligands have been shown to improve initiation, although often such complexes exhibit reduced catalyst lifetime.<sup>14</sup> A catalyst screen was therefore conducted to identify an efficient catalyst for rapid monomer

polymerization and quantitative incorporation of chain transfer agent with this less-reactive monomer. These attributes of the polymerization are essential for incorporating chain transfer agents on both ends of the polymer and for achieving molecular weight control.

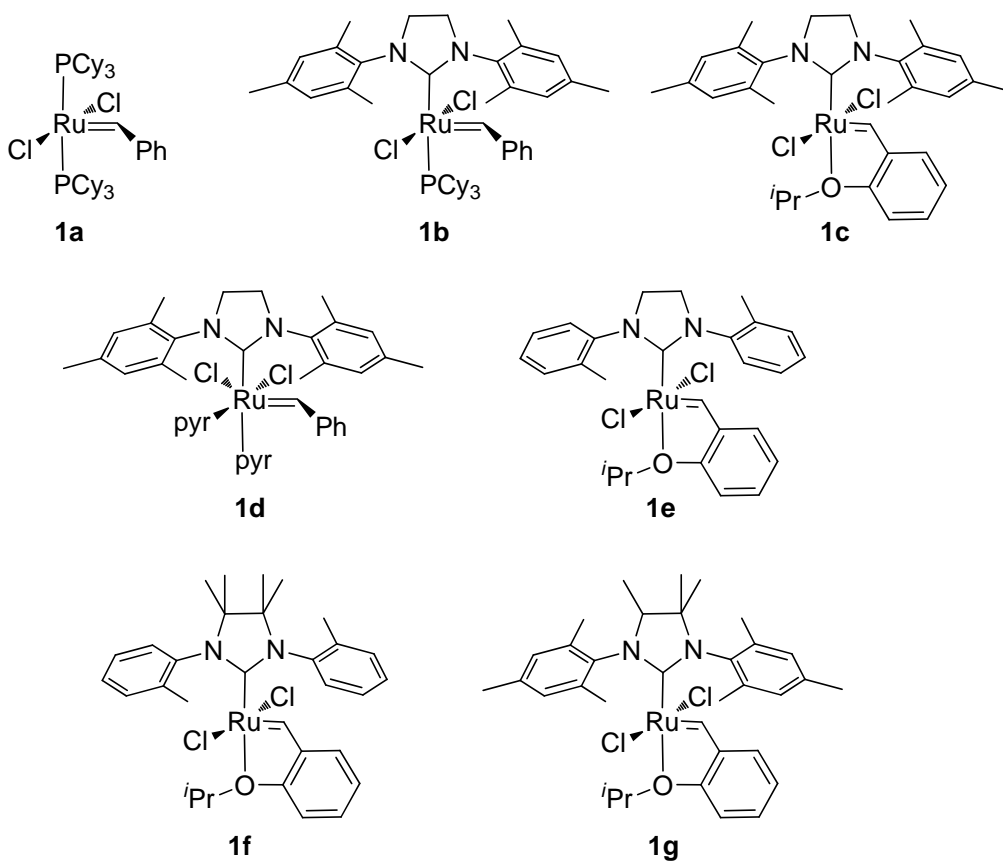
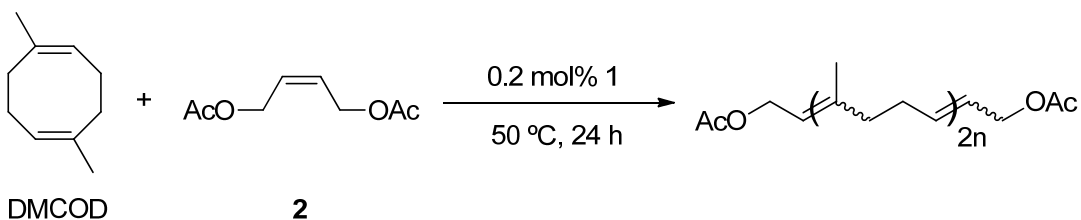


**Figure 2.1.** Ruthenium catalysts screened for ROMP of DMCOD with CTA.

**Scheme 2.2.** Synthesis of  $\alpha,\omega$ -end-functionalized polyisoprene via ROMP.



Accordingly, ruthenium catalysts representing a range of ligand substituents were chosen for polymerization screening to identify the ideal catalyst for optimal activity and stability (Figure 2.1). Catalyst stability and activity during the course of the polymerization is critical to producing difunctionalized polymer in high yield without monofunctionalized polymer impurity. Since DMCOD is a challenging ROMP substrate due to steric encumbrance of the trisubstituted olefins and has relatively low ring-strain energy compared to traditional ROMP monomers such as norbornenes, the identification of an active catalyst for the polymerization with equilibration of molecular weights with CTA presented a significant challenge.

**Table 2.1.** Catalyst activity screening for the ROMP of DMCOD in the presence of CTA **2**.

Entry <sup>a</sup>	Catalyst <sup>b</sup>	% Conv. <sup>c</sup>	% Yield	$M_n$ (NMR) <sup>d</sup>	$M_n$ (GPC)	$M_w$	PDI
<b>1</b>	<b>1a</b>	0	NA	NA	NA	NA	NA
<b>2</b>	<b>1b</b>	99	86	6,620	9,990	14,400	1.44
<b>3</b>	<b>1c</b>	85	74	6,550	9,650	13,100	1.39
<b>4</b>	<b>1d</b>	93	84	7,680	10,700	15,100	1.40
<b>5</b>	<b>1e</b>	0	NA	NA	NA	NA	NA
<b>6</b>	<b>1f</b>	>99	85	7,170	10,300	15,300	1.49
<b>7</b>	<b>1g</b>	73	64	6,240	8,330	11,600	1.40

<sup>a</sup>Polymerizations were conducted at 50 °C for 24 h. [DMCOD]<sub>0</sub> was 2 M in toluene. The molar ratio of DMCOD/**2** was 110/1. <sup>b</sup>Catalyst loading was 0.2 mol%. <sup>c</sup>Conversions were determined by <sup>1</sup>H NMR spectroscopy. <sup>d</sup> $M_n$  was determined by <sup>1</sup>H NMR spectroscopy by relative integration of polymer chain-end olefin protons to internal olefin protons, assuming complete incorporation of **2**.

First generation ruthenium metathesis catalyst **1a**, as well as those comprising *N*-heterocyclic carbene (NHC) ligands (**1b-1g**), were screened. Rigorously air-free conditions were required for high monomer conversion. Catalysts **1b**, **1c**, and **1d** were compared for initial rates as well as stability throughout the course of the polymerization. Sterics in the

NHC backbone as well as substituents on the *N*-arene were evaluated for their impact on activity and stability.

Complex **1a** did not polymerize DMCOD, despite being a successful initiator for the ROMP of COD (Table 2.1, entry 1). Catalyst **1b** exhibited good activity for the polymerization, reaching 99% conversion in 24 h (Table 2.1, entry 2). While catalysts **1c** and **1d** were also active, complete consumption of monomer was not observed after 24 h (Table 2.1, entries 2 and 4, respectively). Interestingly, the less sterically hindered *N*-tolyl complex **1e** was found to be completely inactive for the polymerization of DMCOD (Table 2.1, entry 5). In contrast, backbone substitution on *N*-tolyl complex **1f** resulted in excellent activity for the polymerization, giving greater than 99% conversion of monomer to polymer (Table 2.1, entry 6). Maintaining NHC backbone substitution while increasing the size of the *N*-aryl groups (**1g**) resulted in lower activity in comparison with the other active complexes (Table 2.1, entry 7). Collectively, the data suggests that smaller *N*-aryl groups are advantageous for activity, but that concurrent substitution on the NHC backbone is necessary for stability.<sup>15</sup>

Following these results, catalyst rates were compared by following conversion of DMCOD to polymer over time. The kinetics of the reactions were monitored by NMR spectroscopy. Catalyst **1g** was not evaluated as it was less active than the other complexes, reaching only 73% conversion in 24 h. Interestingly, while complex **1b** displayed the fastest initial rate, catalyst **1f** reached 99% conversion in the shortest reaction time (12 h). Although complex **1d** is often reported to initiate faster than **1b** or **1c**, complex **1d** was found to be comparable to **1c** and surprisingly slower than both **1b** and **1f** (Figure 2.2).<sup>16</sup> Considering the data from

each of the catalysts, we focused our attention on complexes **1b** and **1f** as the most viable systems for accomplishing controlled synthesis of telechelic polyisoprene via ROMP.

The CTA was chosen as *cis*-1,4-diacetoxy-2-butene (**2**) since it can be easily deprotected to give hydroxyl groups, which could then be further reacted to make ABA block polymers. Allylic alcohols were not used directly as the chain transfer agent due to possible interference of the hydroxyl groups with the metathesis reaction. Hydroxyl groups are ideal end groups due to their flexibility for further functional group transformations, and their potential to be used directly as initiators in subsequent polymerizations.

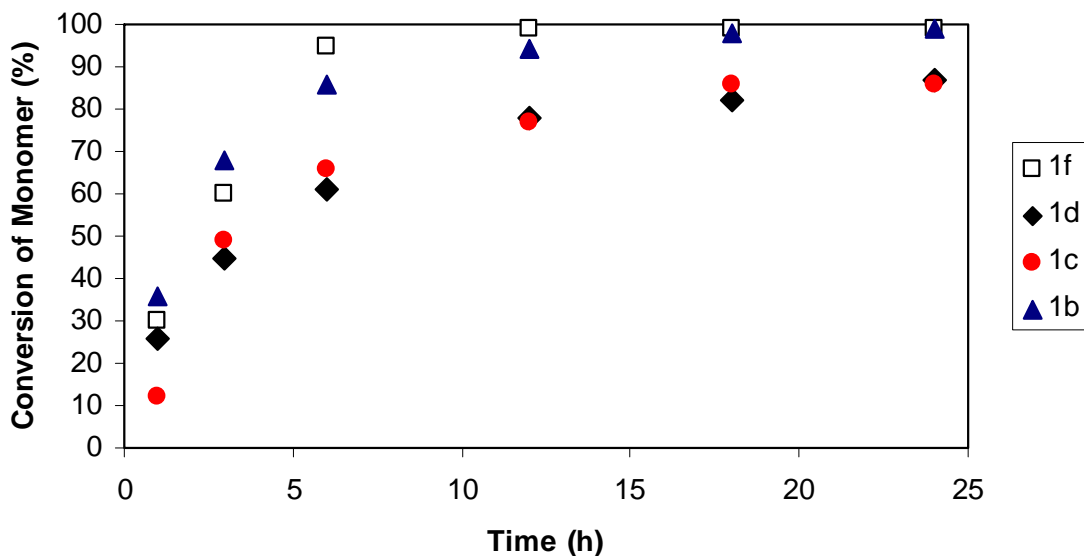


**Figure 2.2.** Conversion of DMCOD to polyisoprene versus time for complexes **1b-1d**, **1f**. Polymerization conditions: 0.2 % **1**, 0.009 equivalents of **2**, [DMCOD] = 2 M in toluene, 50 °C.

The ratio of the initial concentration of CTA **2** to DMCOD was varied to yield telechelic polymer with a range of target molecular weights. The ability to control molecular weight by means of the ratio of  $[\text{DMCOD}]_0/[\mathbf{2}]_0$  is an essential component of the method, allowing



access to various polymer chain lengths for a number of applications. A study of molecular weight control was first carried out using catalyst **1b** since it is commercially available and relatively inexpensive (Table 2.2).

By varying  $[\text{DMCOD}]_0/[\mathbf{2}]_0$ , polymers with molecular weights ranging from 2,000 g/mol to 25,000 g/mol were successfully synthesized. At high CTA loading, the conversion of DMCOD to polymer was lower (Table 2.2, entries 1 and 2), possibly due to greater catalyst decomposition. Control of polymer molecular weight with precise ratios of DMCOD to **2** was achieved (Table 2.2, entries 1-7). For high ratios of DMCOD to **2**, targeting polymers of molecular weights greater than about 35,000 g/mol, the discrepancy between observed and theoretical molecular weight increased (example, Table 2.2, entry 8).

**Table 2.2.** Varying the ratio of DMCOD to **2** with complex **1b**.

Entry <sup>a</sup>	$[\text{DMCOD}]_0/[\mathbf{2}]_0$	% Conv. <sup>b</sup>	% Yield	Theoretical $M_n$ (g/mol) <sup>c</sup>	$M_n$ (NMR) <sup>d</sup>	$M_n$ (GPC)	PDI
<b>1</b>	28	55	28	3,800	1,670	2,440	1.22
<b>2</b>	56	77	51	7,600	4,220	6,740	1.27
<b>3</b>	84	83	58	11,400	7,120	10,700	1.28
<b>4</b>	110	86	56	15,000	8,030	12,800	1.27
<b>5</b>	184	89	68	25,000	11,700	17,000	1.26
<b>6</b>	220	87	79	30,000	20,400	21,300	1.35
<b>7</b>	257	85	63	35,000	28,200	25,100	1.26
<b>8</b>	294	85	55	40,000	25,400	25,400	1.29

<sup>a</sup>Polymerizations were conducted at 50 °C for 20 h.  $[\text{DMCOD}]_0$  was 2 M in toluene. The catalyst loading was 0.1 mol%. <sup>b</sup>Conversion was determined by <sup>1</sup>H NMR spectroscopy. <sup>c</sup>Assumes 100% conversion. <sup>d</sup>Determined by <sup>1</sup>H NMR spectroscopy by relative integration of the polymer chain-end olefin protons to the internal olefin protons, assuming complete incorporation of **2**.

Polymers exhibiting a range of target molecular weights were then synthesized with catalyst **1f** with the goal of increasing monomer conversion (Table 2.3). The conversion of

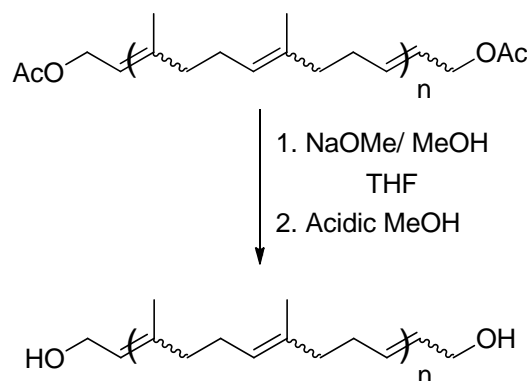
DMCOD to polymer was complete for all reactions and the yields were significantly improved from complex **1b**.

**Table 2.3.** Varying the ratio of DMCOD to **2** using complex **1f**.

Entry <sup>a</sup>	[DMCOD] <sub>0</sub> /[ <b>2</b> ] <sub>0</sub>	% Conv. <sup>b</sup>	% Yield	Theoretical M <sub>n</sub> (g/mol) <sup>c</sup>	M <sub>n</sub> (NMR) <sup>d</sup>	M <sub>n</sub> (GPC)	PDI
<b>1</b>	50	98	80	6,800	4,130	6,320	1.52
<b>2</b>	100	99	75	13,600	7,550	10,600	1.63
<b>3</b>	150	99	76	20,400	11,200	18,100	1.43
<b>4</b>	200	>99	82	27,300	14,300	21,500	1.39
<b>5</b>	250	>99	80	34,100	15,300	24,200	1.39
<b>6</b>	500	>99	80	68,100	25,100	30,300	1.35

<sup>a</sup>Polymerizations were run at 50 °C for 15 h. [DMCOD]<sub>0</sub> was 2 M in toluene. The catalyst loading was 0.2 mol%. <sup>b</sup>Conversion was determined by <sup>1</sup>H NMR spectroscopy. <sup>c</sup>Assumes 100% conversion. <sup>d</sup>Determined by relative integration of the end group olefin protons compared to the internal polymer olefin protons, assuming complete incorporation of **2**.

**Scheme 2.3.** Hydroxy telechelic polyisoprene via deprotection of acetoxy end groups.



The polymerization was successfully conducted on a larger scale to ensure practical synthesis. To this end, DMCOD (13 g) was polymerized in the presence of CTA **2** to afford acetoxy end-functionalized polyisoprene in 87% isolated yield. The polymer was subsequently deprotected to give hydroxy end-functionalized polymer in high yield

(Scheme 2.3). The experimental molecular weight of  $\alpha,\omega$ -hydroxy functionalized polyisoprene (20,190 g/mol) closely matched the theoretical molecular weight of 20,050 g/mol.

The polyisoprene functionality ( $F_n$ ) was determined to be two based on NMR spectroscopy (see experimental section). Two dimensional HSQC, HMBC, and DOSY were utilized to identify the presence of polymer acetate end groups, as well as demonstrate the absence of any terminal olefin groups or end groups corresponding to the catalyst alkylidene initiator within the detection limits of the NMR spectrometer. The DOSY spectrum verified that all the signals except for  $\text{CDCl}_3$  came from polymer. The presence of a methyl signal in the edited HMBC at 2.0/21.0 ppm was demonstrated to be the acetate methyl group by its correlation to the carbonyl carbon at 171 ppm; the methylene signal at 4.6 ppm correlates to the same carbonyl carbon. No terminal  $=\text{CH}_2$  groups were observed in the HSQC. The absence of aryl signals in the  $^1\text{H}$  NMR excluded any alkylidene initiator. Upon deprotection to afford hydroxy end groups, an upfield shift in the NMR signal was observed from 4.6 to 4.1 ppm for the terminal hydroxy  $\text{CH}_2$ . HMBC showed the disappearance of the acetate group.

## Conclusion

Ring-opening metathesis polymerization of DMCOD in the presence of chain transfer agent was successfully employed for efficient one pot synthesis of telechelic  $\alpha,\omega$ -end functionalized polyisoprene. A series of ruthenium metathesis catalysts were screened, and viable complexes were identified that give good control of target molecular weights and afford polymer in excellent yields. This route is particularly attractive and advantageous in

that the polymerization of a well-defined monomer (DMCOD) affords polyisoprene with controlled, defined polymer microstructure. The acetoxy groups were deprotected to give hydroxy end groups that can subsequently undergo a variety of reactions, rendering these telechelic polymers valuable precursors for the synthesis of triblock copolymers.

## Experimental

### General Considerations

All polymerizations were conducted under a nitrogen atmosphere using a drybox.  $^1\text{H}$  and  $^{13}\text{C}$  NMR spectra were recorded on a Varian Mercury ( $^1\text{H}$ , 300 MHz) or an automated Varian Inova 500 ( $^1\text{H}$ , 500 MHz;  $^{13}\text{C}$  125 MHz) spectrometer and referenced to residual protio solvent. HSQC, HMBC, and DOSY were carried out using a Varian Inova 600. Gel permeation chromatography (GPC) analyses were carried out in HPLC grade tetrahydrofuran on two PLgel 10  $\mu\text{m}$  mixed-B LS columns connected in series with a DAWN EOS multiangle laser light scattering (MALLS) detector and an Optilab DSP differential refractometer. No calibration standards were used, and  $dn/dc$  values were obtained for each injection by assuming 100% mass elution from the columns.

### Materials

Toluene was purified by passage through solvent purification systems. *cis*-1,2-Diacetoxy-2-butene was purchased from Aldrich and distilled over  $\text{CaH}_2$  under argon prior to use. 1,5-Dimethyl-1,5-cyclooctadiene was degassed by three freeze-pump-thaw cycles prior to use. Ruthenium complexes were received from Materia or synthesized according to published

procedures.<sup>17</sup> All other reagents and solvents were used as purchased without further purification.

**Representative Ring-Opening Metathesis Polymerization of 1,5-dimethyl-1,5-cyclooctadiene with *cis*-1,4-diacetoxy-2-butene as Chain Transfer Agent**

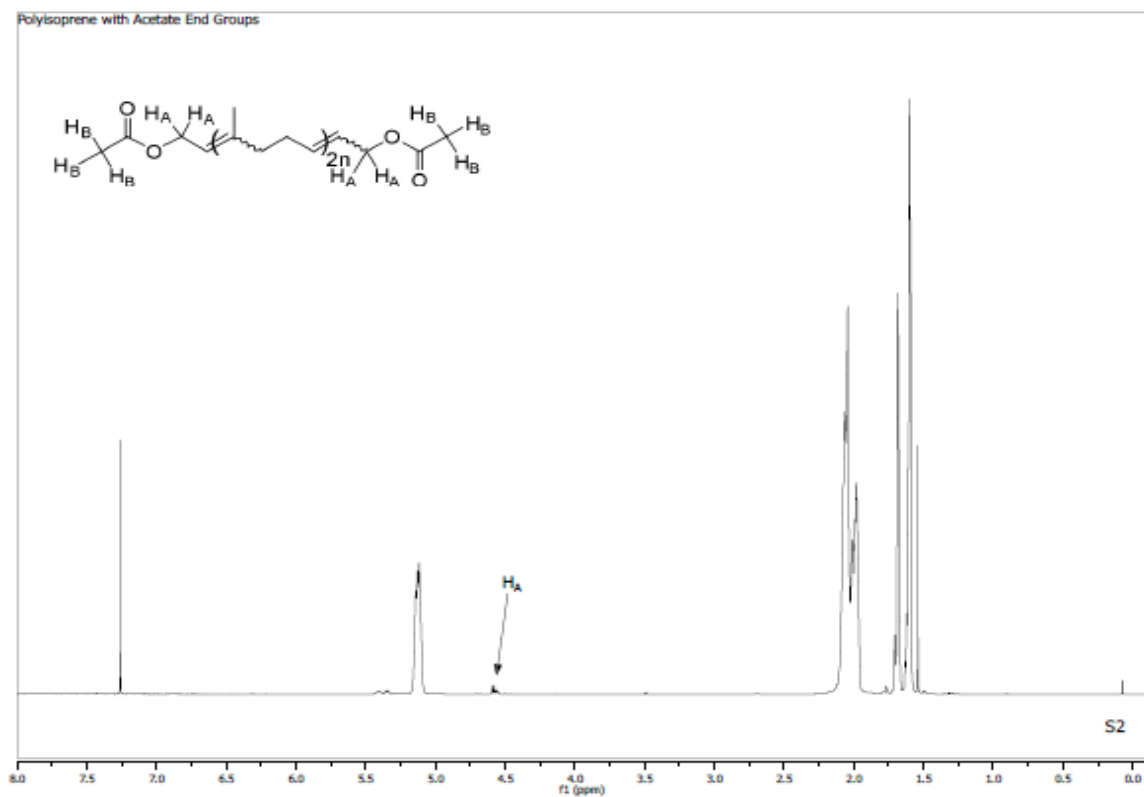
In a nitrogen atmosphere glovebox, a 100 mL round bottom flask containing a magnetic stir bar was charged with 1,5-dimethyl-1,5-cyclooctadiene (13.19 g, 96.8 mmol). Subsequently, toluene (16 mL) was added and the solution was stirred at 22 °C. Catalyst **1b** (0.082 grams, 0.1 mol%) was added to the flask with stirring, after which chain transfer agent *cis*-1,4-diacetoxy-2-butene (105  $\mu$ L, 0.0068 equivalents relative to DMCOD) was added via syringe. The round bottom flask was sealed with a glass stopper in the glovebox and then brought out and heated to 50 °C in an oil bath for 24 h. An aliquot was taken out by syringe for <sup>1</sup>H NMR spectroscopy, and the conversion to polymer was determined to be 92% by relative integration of the olefin peaks. The polymerization was terminated by the addition of ethyl vinyl ether (2 mL), and the polymer was precipitated by dropwise addition into a flask containing 175 mL of anhydrous methanol. The supernatant was decanted, and the polymer residue was washed twice more with methanol. The polymer was then redissolved in 50 mL of toluene and slowly added via an addition funnel to 400 mL of methanol with stirring. The methanol solution was again decanted off, and the resulting polymer was dried under vacuum on a Schlenk manifold for 48 h. The polymer was isolated in 87% yield (11.44 g). <sup>1</sup>H NMR (CDCl<sub>3</sub>, 500 MHz):  $\delta$  5.10-5.13 (m, 2H), 2.00-2.06 (br, m, 8H), 1.68 (br, s, 3H), 1.59-1.60 (br, m, 3H) ppm. Acetate end groups: CH<sub>2</sub> 4.55-4.60 ppm, CH<sub>3</sub> 2.0

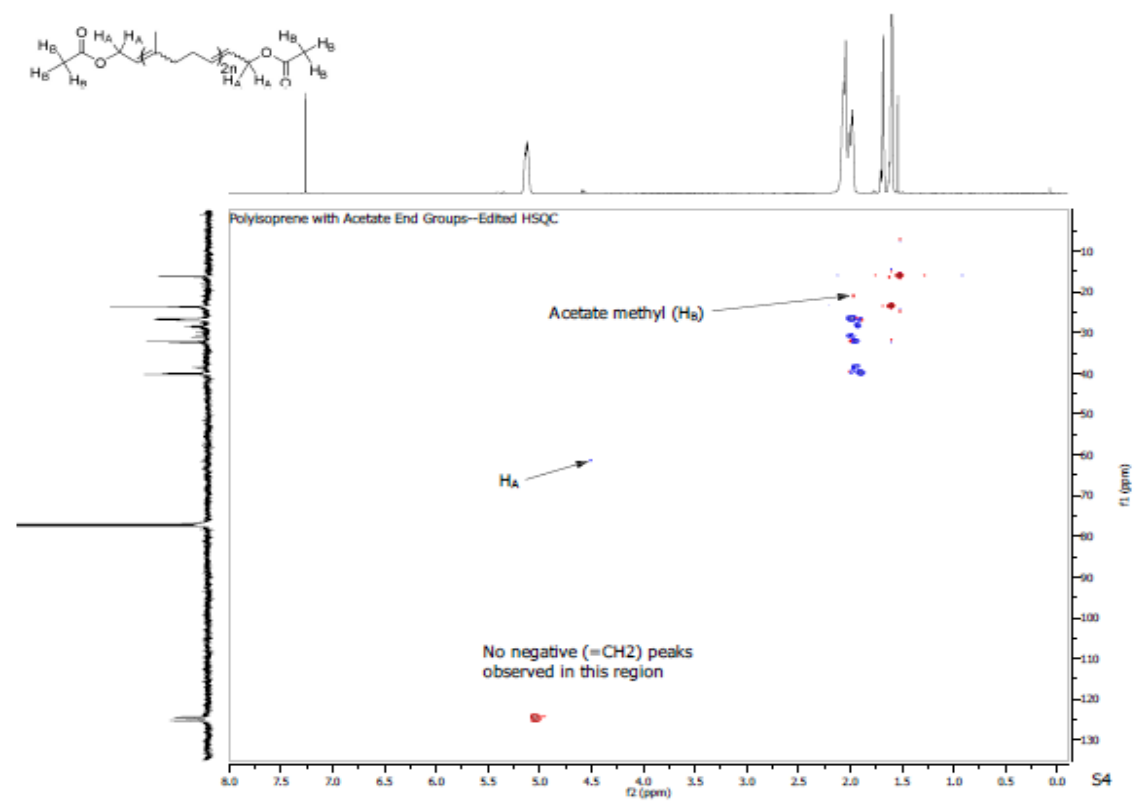
ppm. The polymer end groups contained both *cis* and *trans* isomers.  $^{13}\text{C}$  NMR ( $\text{CDCl}_3$ , 125 MHz):  $\delta$  135.1, 125.1, 124.2, 40.1, 39.8, 32.2, 32.0, 26.5, 23.5, 16.0 ppm.

### **Representative Deprotection of Polymer Acetate End Groups**

Functionalized  $\alpha,\omega$ -diacetoxypolyisoprene (10.28 g) was dissolved in 100 mL of THF and cooled to 0 °C in an ice bath. A 25 wt% solution of NaOMe in methanol (15 mL) was added slowly and the mixture was stirred for 72 h at 22 °C. The reaction mixture was then added dropwise via an addition funnel into 600 mL of acidic methanol (0.5 mL of concentrated HCl in 600 mL of anhydrous methanol). The acidic methanol solution was decanted off, and the precipitate was washed three more times with acidic methanol, followed by washing three times with a 1:1 methanol/water solution. The polymer was subsequently washed three times with anhydrous methanol, then dried under vacuum using a Schlenk manifold for 48 h. The polymer (9.10 g) was isolated in 89% yield.  $^1\text{H}$  NMR ( $\text{CDCl}_3$ , 500 MHz):  $\delta$  5.12-5.13 (m, 2H), 4.08-4.17 (m, 2H), 1.98-2.05 (br, m, 8H), 1.69 (br, s, 3H), 1.60-1.61 (br, m, 3H) ppm. Hydroxy end groups:  $\text{CH}_2$  4.05-4.15 ppm. The polymer end groups contained both *cis* and *trans* isomers.  $^{13}\text{C}$  NMR ( $\text{CDCl}_3$ , 125 MHz):  $\delta$  135.1, 125.1, 124.3, 40.1, 39.8, 32.2, 32.0, 26.6, 26.5, 26.4, 23.5, 16.0 ppm.

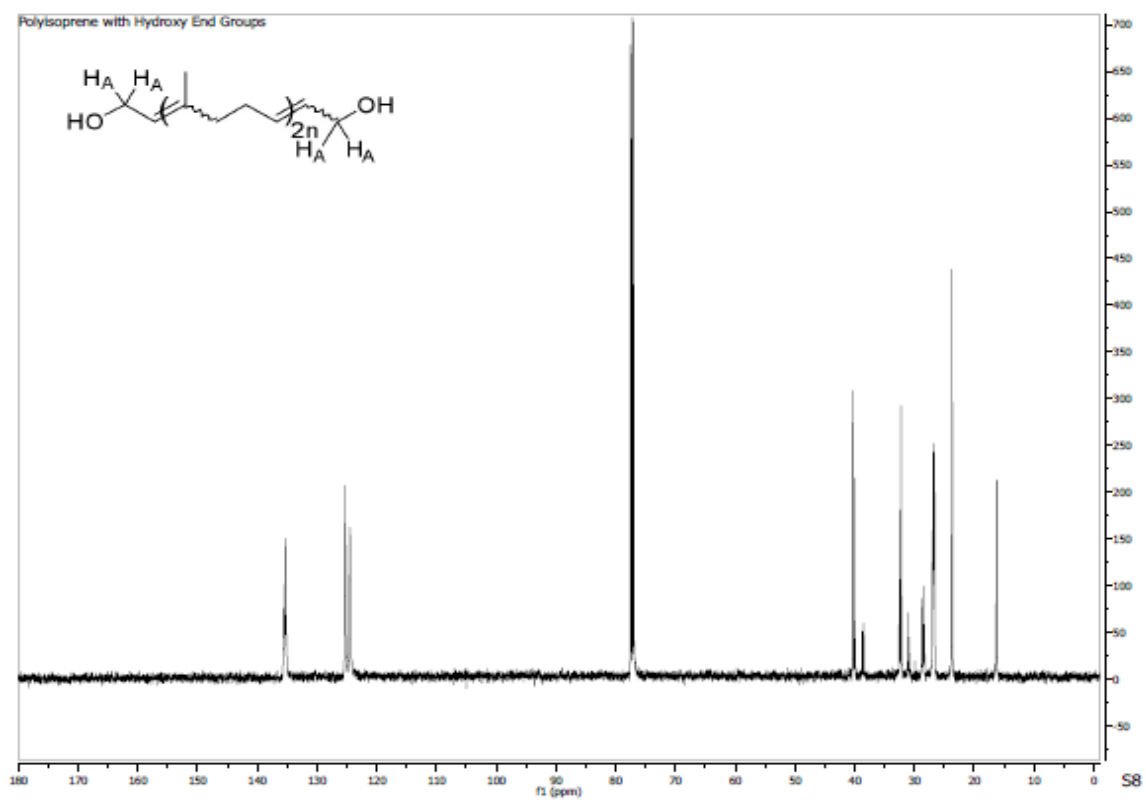
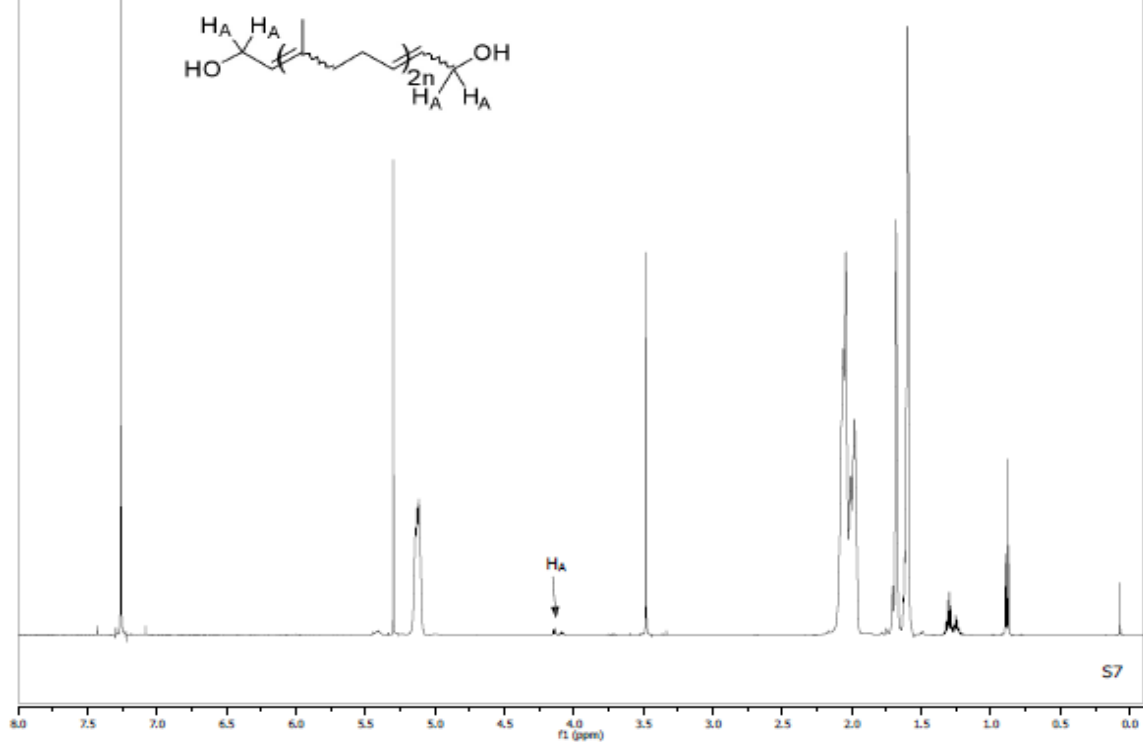
## Polymer NMR Spectra

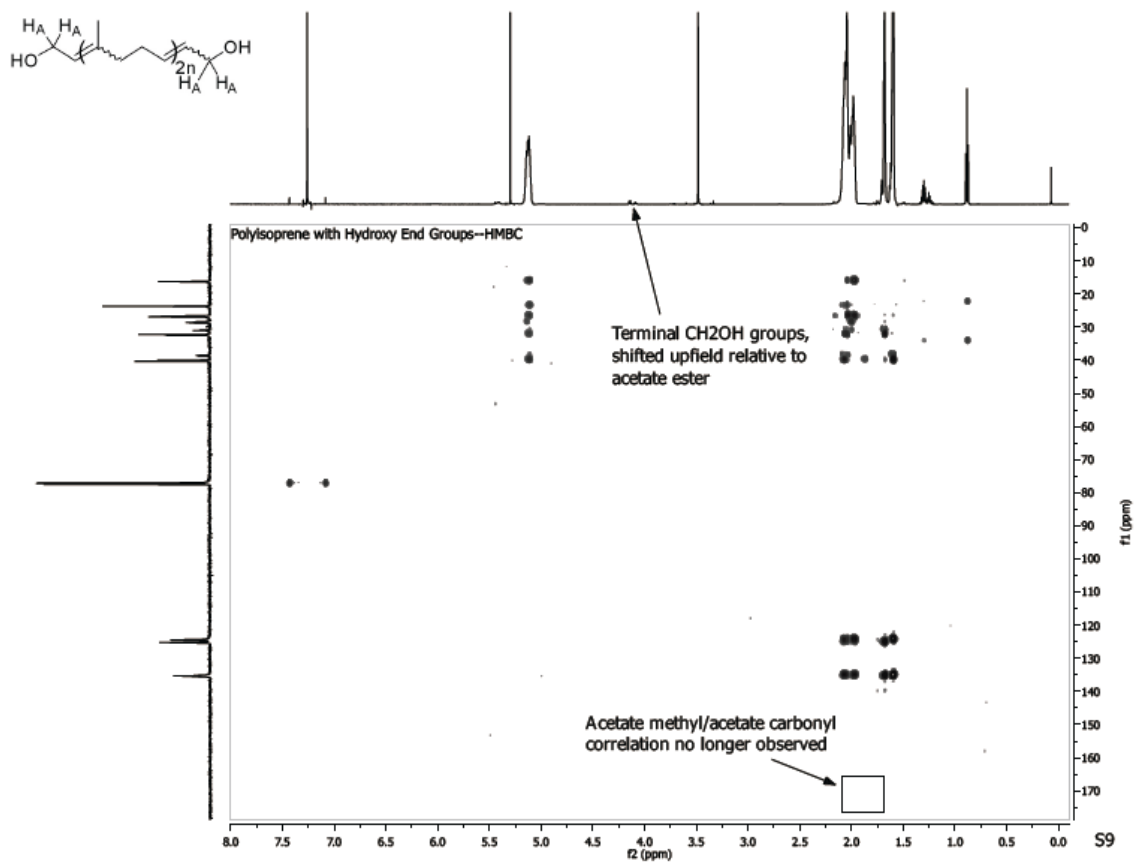












**Acknowledgment.** The author thanks *American Chemical Society* for permission for the contents of this chapter. This research has been published in *Macromolecules*. Article reference: Thomas, R. M.; Grubbs, R. H. *Macromolecules* **2010**, *43*, 3705–3709.

## REFERENCES

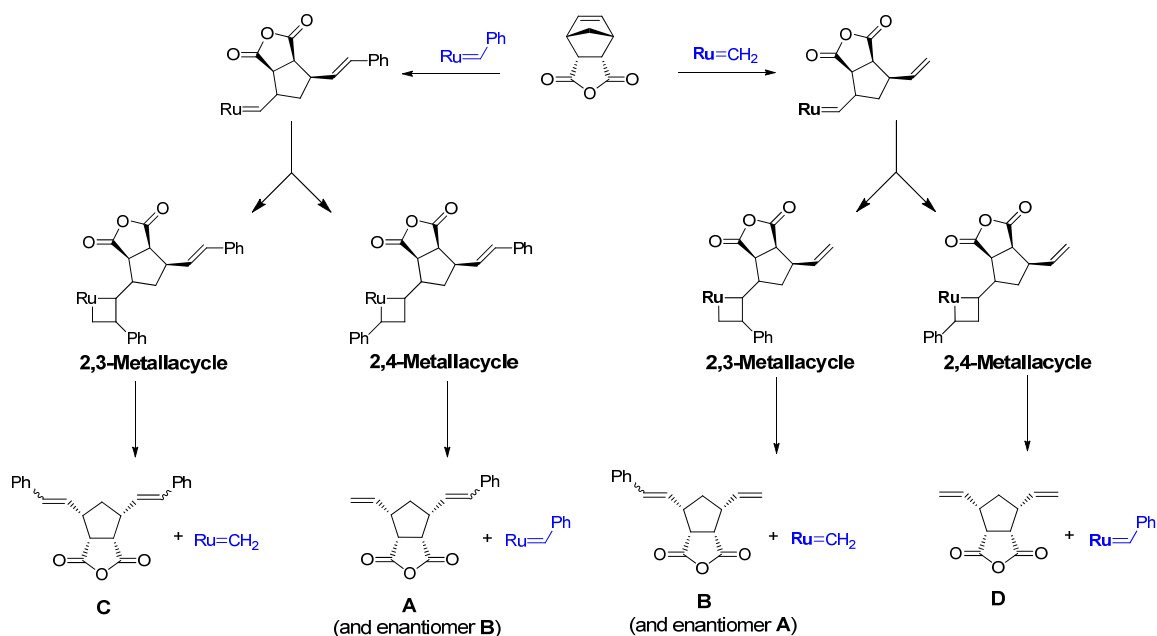
1. (a) Hillmyer, M. A.; Grubbs, R. H. *Macromolecules* **1993**, *26*, 872. (b) Hillmyer, M. A.; Nguyen, S. T.; Grubbs, R. H. *Macromolecules* **1997**, *30*, 718. (c) Mahanthappa, M. K.; Bates, F. S.; Hillmyer, M. A. *Macromolecules* **2005**, *38*, 7890.
2. Yonghua, Z.; Faust, R.; Richard, R.; Schwarz, M. *Macromolecules* **2005**, *38*, 8183.
3. Phillips, J. P.; Deng, X.; Stephen, R. R.; Fortenberry, E. L.; Todd, M. L.; McClusky, D. M.; Stevenson, S.; Misra, R.; Morgan, S.; Long, T. E. *Polymer* **2007**, *48*, 6773.
4. K  bir, N.; Campistron, I.; Laguerre, A.; Pilard, J. F.; Bunel, C.; Jouenne, T. *Biomaterials* **2007**, *28*, 4200.
5. Pitet, L. M.; Hillmyer, M. A. *Macromolecules* **2009**, *42*, 3674.
6. Young, A. M.; Ho, S. M. *Journal of Controlled Release* **2008**, *127*, 162.
7. O'Reilly, R. K.; Hawker, C. J.; Wooley, K. L. *Chem. Soc. Rev.* **2006**, *35*, 1068.
8. Germack, D.; Wooley, K. L. *J. Polym. Sci., Part A: Polym. Chem.* **2007**, *45*, 4100.
9. Gillier-Ritoit, S.; Reyx, D.; Campistron, I.; Laguerre, A.; Singh, R. P. *J. Appl. Polym. Sci.* **2003**, *87*, 42.
10. Morandi, G.; Kebir, N.; Campistron, I.; Gohier, F.; Laguerre, A.; Pilard, J. F. *Tet. Lett.* **2007**, *48*, 7726.
11. Solanky, S. S.; Campistron, I.; Laguerre, A.; Pilard, J. F. *Macromol. Chem. Phys.* **2005**, *206*, 1057.
12. (a) Morita, T.; Maughon, B. R.; Bielawski, C. W.; Grubbs, R. H. *Macromolecules* **2000**, *33*, 6621. (b) Lexer, C.; Saf, R.; Slugovc, C. *J. Polym. Sci., Part A: Polym. Chem.* **2009**, *47*, 299.
13. Ritter, T.; Hejl, A.; Wenzel, A. G.; Funk, T. W.; Grubbs, R. H. *Organometallics* **2006**, *25*, 5740.
14. Love, J. A.; Sanford, M. S.; Day, M. W.; Grubbs, R. H. *J. Am. Chem. Soc.* **2003**, *125*, 10103.
15. (a) Kuhn, K. M.; Bourg, J. B.; Chung, C. K.; Virgil, S. C.; Grubbs, R. H. *J. Am. Chem. Soc.* **2009**, *131*, 5313. (b) Chung, C. K.; Grubbs, R. H. *Org. Lett.* **2008**, *10*, 2693.

16. Stewart, I. C.; Ung, T.; Pletnev, A. A.; Berlin, J. M.; Grubbs, R. H.; Schrodi, Yann. *Org. Lett.* **2007**, 9, 1589.
17. For the synthesis of complex **1d**, see reference 14. For the synthesis of complexes **1e**, **1f**, and **1g**, see reference 15.

### Chapter 3

## MECHANISTIC STUDIES OF ENANTIOSELECTIVE *N*-ARYL, *N*-ALKYL *N*-HETEROCYCLIC CARBENE RUTHENIUM METATHESIS CATALYSTS IN ASYMMETRIC RING-OPENING CROSS-METATHESIS

### Abstract



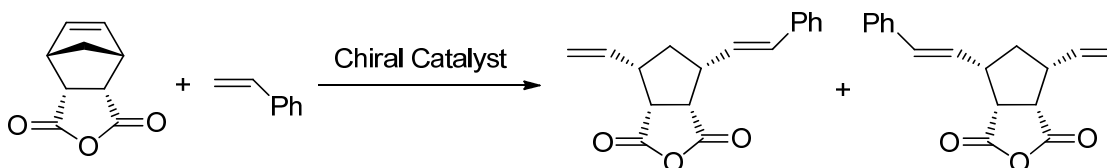
Chiral *N*-aryl, *N*-alkyl NHC ruthenium metathesis catalysts were designed and synthesized for asymmetric ring-opening cross-metathesis (AROCM). The *N*-alkyl ligands were designed to bring the chiral center on the ligand in closer proximity to the metal to enhance its influence on the product enantioselectivity. Several complexes gave very high enantiomeric excess (ee) for the AROCM of *cis*-5-norbornene-*endo*-2,3-dicarboxylic anhydride with styrene, comparable to the best ruthenium catalysts reported in the literature for this reaction. All of the *N*-aryl, *N*-alkyl NHC catalysts were observed to generate two additional products, and mechanistic studies revealed that these side products are formed

by the propagation of a ruthenium methyldene species. The formation of the expected product versus the side products was found to depend on whether the catalyst proceeds through a 2,3-metallacycle or a 2,4-metallacycle, with the preference of the catalyst for one metallacycle versus the other determining the ratio of the products.

## Introduction

Olefin metathesis is widely used for the construction of carbon-carbon double bonds and has extensive applications in organic and polymer synthesis,<sup>1</sup> as well as materials chemistry.<sup>2</sup> Asymmetric metathesis provides an attractive methodology for synthesizing enantiopure molecules, and significant efforts have been directed toward the development of enantioselective catalysts.<sup>3</sup> Since the chirality of pharmaceutical drugs and natural products often significantly affects their biological activity, efficient and controlled means for constructing a particular stereocenter are highly desirable. Asymmetric ring-opening cross-metathesis (AROCM) (Scheme 3.1) has been employed as the key step in several total syntheses, affording the desired product in excellent enantiomeric excess (ee).<sup>4,5</sup> Applications of AROCM have also been pursued in the synthesis of biologically relevant molecules.<sup>6</sup> Imparting chirality from the catalyst to the substrate is challenging, and has been the focus of catalyst design.<sup>7</sup>

**Scheme 3.1.** Asymmetric ring-opening cross-metathesis.



Early studies in AROCM focused on molybdenum-based metathesis catalysts, which displayed good selectivity for the reaction of substituted norbornenes with styrene.<sup>8</sup> The enantioselectivities of the molybdenum complexes were substrate dependent, but generally high (>80% ee).<sup>9,10</sup> While AROCM usually yields *E*-olefin products, sterically hindered stereogenic-at-molybdenum catalysts were demonstrated to give excellent *Z*-selectivity in AROCM, currently unique selectivity to molybdenum catalysts, although ruthenium catalysts can give *Z*-selectivity in cross-metathesis.<sup>11</sup> Ruthenium catalysts were explored due to their stability to air and moisture, a feature that enables them to be easily handled.<sup>12</sup> Comparison studies showed chiral ruthenium complexes to be comparable, and sometimes superior, to chiral molybdenum complexes in their enantioselectivity, and the preferred catalyst was found to be dependent on the particular reaction and substrate.<sup>13</sup>

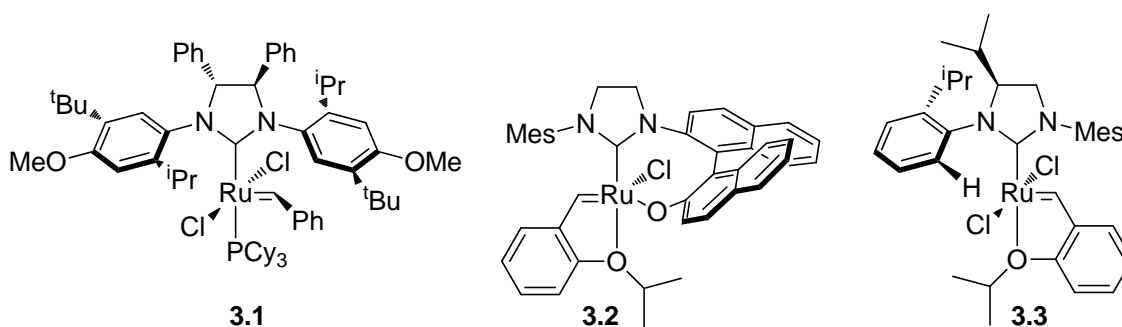


**Figure 3.1.** Ruthenium catalysts reported in AROCM.

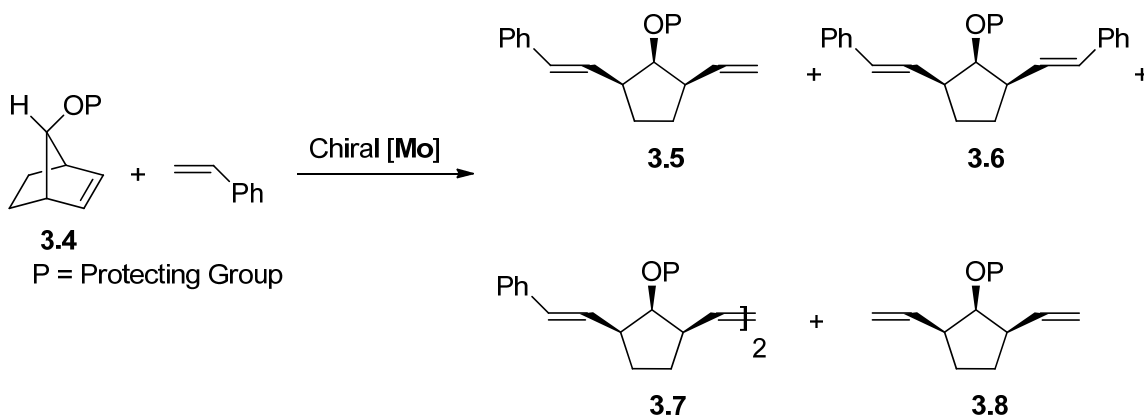
Chirality has been built into ruthenium complexes primarily in the *N*-heterocyclic carbene (NHC) backbone (Figure 3.1, **3.1**).<sup>14</sup> Hoveyda and coworkers improved the enantioselectivity of ruthenium catalysts through the synthesis of a *N*-binaphthol NHC with the hydroxyl group chelating to the ruthenium metal (Figure 3.1, **3.2**); however, the catalytic activity was decreased.<sup>15,16</sup> The enhanced selectivity of this complex is likely due



to the closer proximity of the chiral ligand to the reaction center, where it can impart a stronger influence on the stereochemistry of the transition state. Recently, Blechert and coworkers reported the synthesis of a chiral mono-substituted NHC backbone that achieved high enantioselectivity while maintaining activity during AROCM of various functionalized norbornenes (Figure 3.1, **3.3**).<sup>17</sup> The NHC backbone substituent, an isopropyl group, was proposed to induce the *N*-aryl ring to twist, creating the desired chiral environment. This is analogous to the mechanism by which the chiral diphenyl NHC backbone catalysts, such as **3.1**, are believed to impart chirality.<sup>14</sup>

At this time, there have been no detailed investigations into the other products produced during AROCM catalyzed by ruthenium complexes, and these products could reveal important mechanistic information. Schrock and coworkers have reported a discussion of possible side products, including the observation of such products, albeit in low yield, for molybdenum catalysts (Scheme 3.2).<sup>8,9</sup> In addition to product **3.5**, molybdenum catalysts were noted to give ring-opened products **3.6** and **3.8**, as well as in some cases homometathesis product **3.7**.

**Scheme 3.2.** Products of AROCM catalyzed by molybdenum complexes.



The authors detailed the mechanism leading to the desired (**3.5**) and undesired products (**3.6** and **3.8**), which has significance for ultimate enantioselectivity, as well as providing information regarding the propagating metal species (alkylidene versus methylidene).<sup>9</sup> Product **3.8** requires ring-opening by a methylidene species. After ring-opening of **3.4** by a molybdenum methylidene moiety, the styrene cross-partner can react to form either a 2,3- or 2,4-metallacycle to give the major product **3.5** or product **3.8**, respectively. The enantiomer of **3.5** could also be produced depending on the propagating Ru species. Presuming the catalyst methylidene species has the same facial selectivity as the catalyst alkylidene species, the cross-metathesis reaction with styrene and the methylidene-opened substrate will lead to the opposite enantiomer as that provided by ring-opening with the alkylidene species.<sup>9</sup> This information is valuable for gaining insight into catalyst behavior, including preference for alkylidene versus methylidene propagation and formation of a 2,4- versus 2,3-metallacycle. These catalyst attributes are essential to its application in metathesis reactions.

Mechanistic studies of chiral *N*-aryl, *N*-alkyl NHC ruthenium catalysts in AROCM will be described herein. The reaction pathways are discussed, as well as the enantioselectivity of the chiral *N*-aryl, *N*-alkyl NHC complexes studied. Some of the complexes investigated appeared to exhibit unusual preference for methylidene propagation compared to standard second generation ruthenium catalysts. Evidence suggests that these *N*-aryl, *N*-alkyl NHC ruthenium catalysts proceed through both a 2,4-metallacycle and a 2,3-metallacycle during AROCM, accounting for the observed product ratios and distribution. This catalyst behavior has significant implications for catalyst design and targeted application, as

methyldiene propagation and metallacycle orientation directly determine product outcome, and can be utilized accordingly.

## Results and Discussion

We designed ruthenium catalysts bearing an *N*-aryl, chiral *N*-alkyl NHC, with the goal of bringing ligand chirality in close proximity to the metal center for increased enantioselectivity during asymmetric metathesis reactions. Since *N*-alkyl, *N*-alkyl NHC ruthenium catalysts are reported to be less active than *N*-aryl, *N*-aryl NHC catalysts,<sup>18</sup> we chose to synthesize *N*-aryl, *N*-alkyl catalysts to ideally maintain a balance of good activity while achieving better selectivity.<sup>19</sup> NHC precursor salts **3.9-3.14** (Figure 3.2) were synthesized in an analogous procedure to that outlined by Kotschy and coworkers and purified by silica gel chromatography.<sup>20</sup>

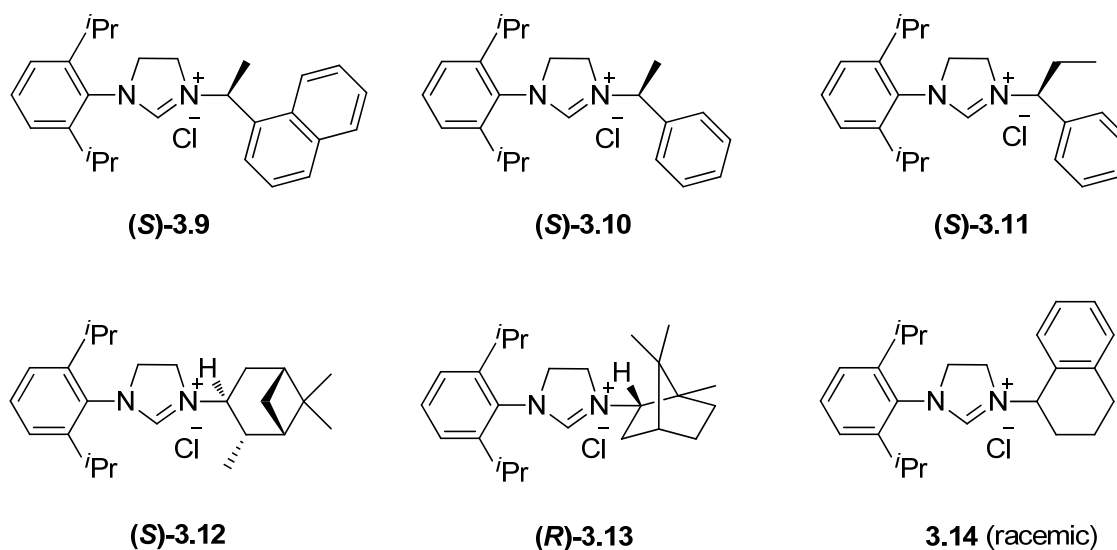


**Figure 3.2.** NHC precursor salts prepared.

The NHC salts were subsequently metallated as previously reported in the literature to give complexes **3.15-3.20**, which were also readily purified by silica gel chromatography (Figure 3.3).<sup>21</sup> The *N*-alkyl ligands were chosen to represent varying degrees of steric hindrance as well as different substituents for maximizing enantioselectivity, stability, and activity. Due to better catalyst stability, complexes with bulkier *N*-aryl groups (2,6-diisopropyl versus mesityl) were screened.

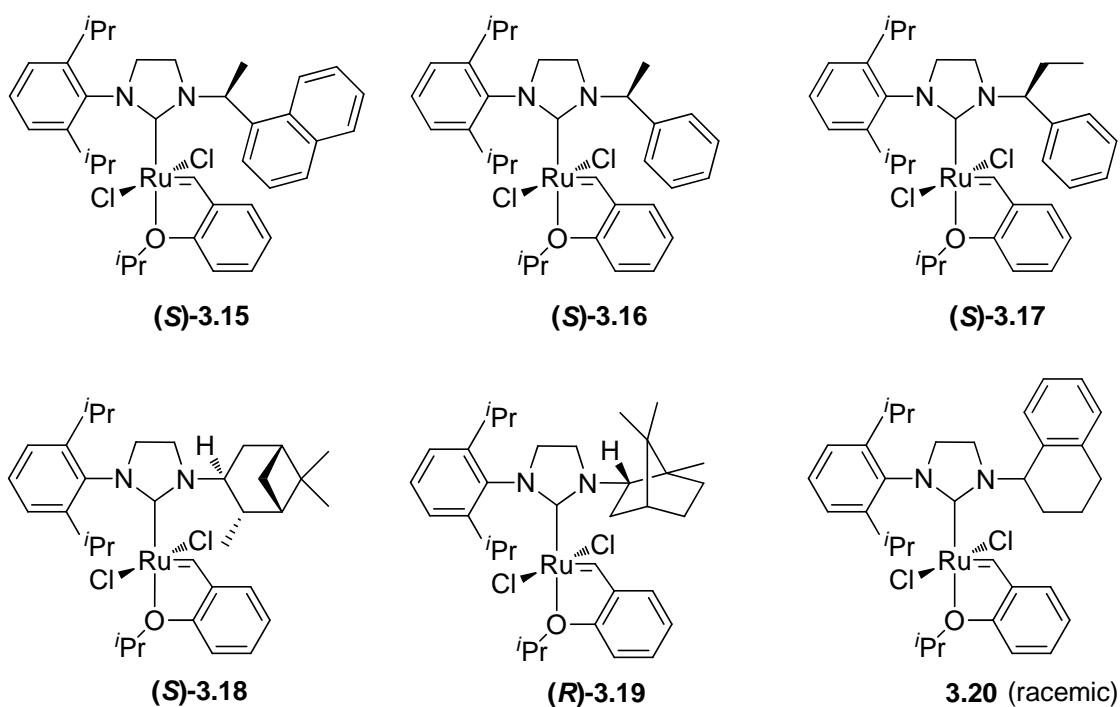
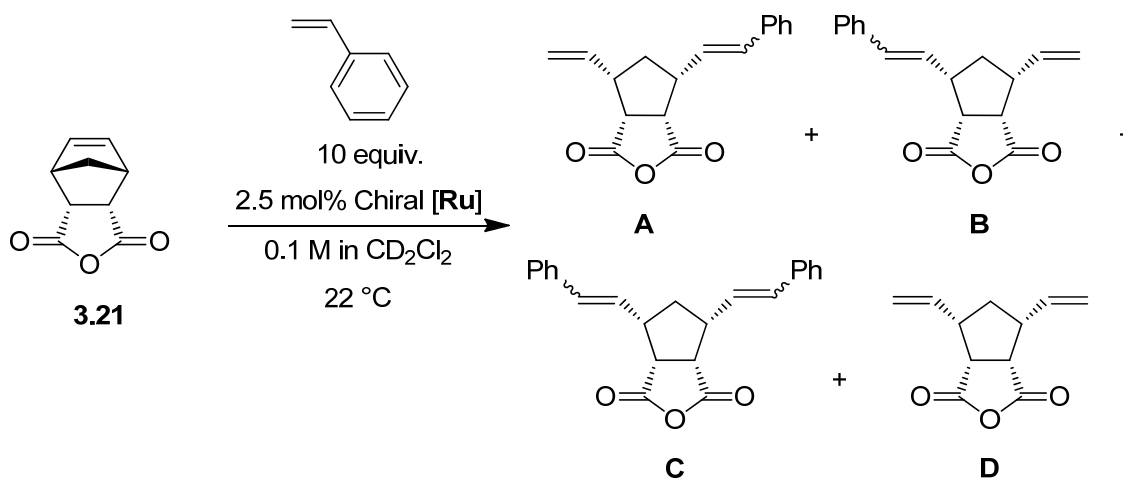


**Figure 3.3.** Catalysts synthesized.

Complex **3.15** was initially screened for AROCM, since it was anticipated that the large difference in the sterics of the substituents at the chiral carbon (naphthyl versus methyl versus H) would provide for a highly enantioselective reaction. Substrate *cis*-5-norbornene-*endo*-2,3-dicarboxylic anhydride (**3.21**) was reacted with 10 equivalents of styrene to yield product **A** in 69% ee over its enantiomer **B** (Scheme 3.3) after 2 hours at room temperature

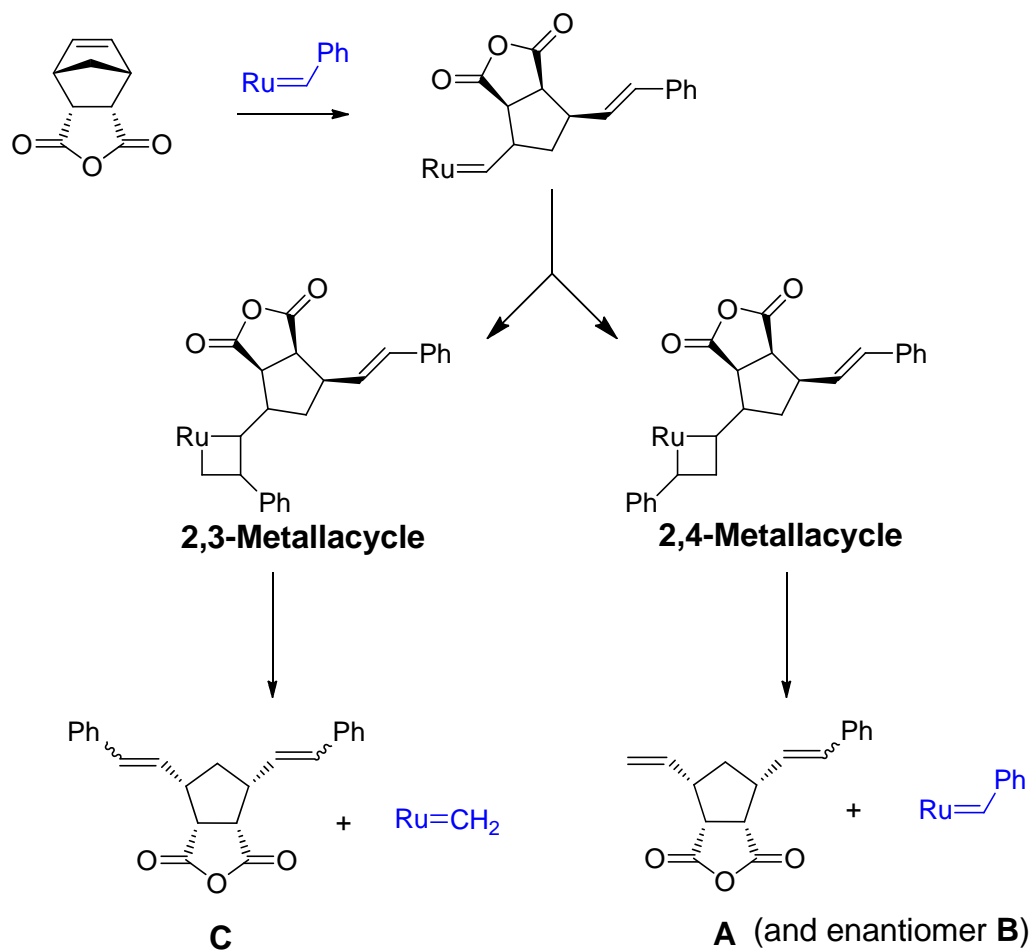
(99% conversion). Interestingly, side products **C** and **D** were also observed, in 17% and 10% of the product mixture, respectively. Subsequent experiments were therefore directed toward elucidating the pathway to the formation of these two side products. No polymer or homometathesis product was observed in the reaction mixture, although stilbene was formed from the cross-metathesis of styrene. The products all had *trans* stereochemistry, with no detectable *cis* isomers.

**Scheme 3.3.** AROCM catalyzed by ruthenium complexes: observation of side products.

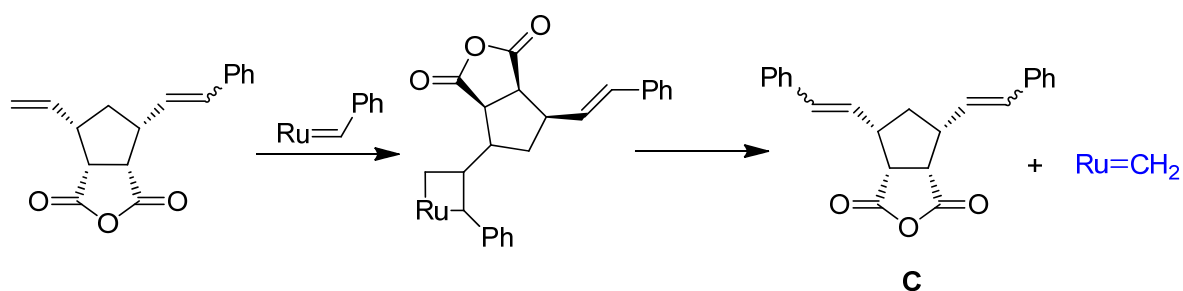


Formation of product **C** could result from the cross-metathesis reaction proceeding via a 2,3-metallacycle, and/or by secondary metathesis of products **A** and **B** with styrene. Breakdown of the 2,3-metallacycle to yield product **C** generates a ruthenium methylidene species, whereas reaction via a 2,4-metallacycle to afford the major products **A** and **B** gives a ruthenium alkylidene species (Scheme 3.4). Secondary metathesis of products **A** and **B** with styrene, reacting via a 2,3-metallacycle, also generates a ruthenium methylidene species (Scheme 3.5). Accordingly, formation of product **C** results in production of a ruthenium methylidene species, regardless of which pathway is taken.

**Scheme 3.4.** Mechanism for the formation of product **C** via a 2,3-metallacycle.



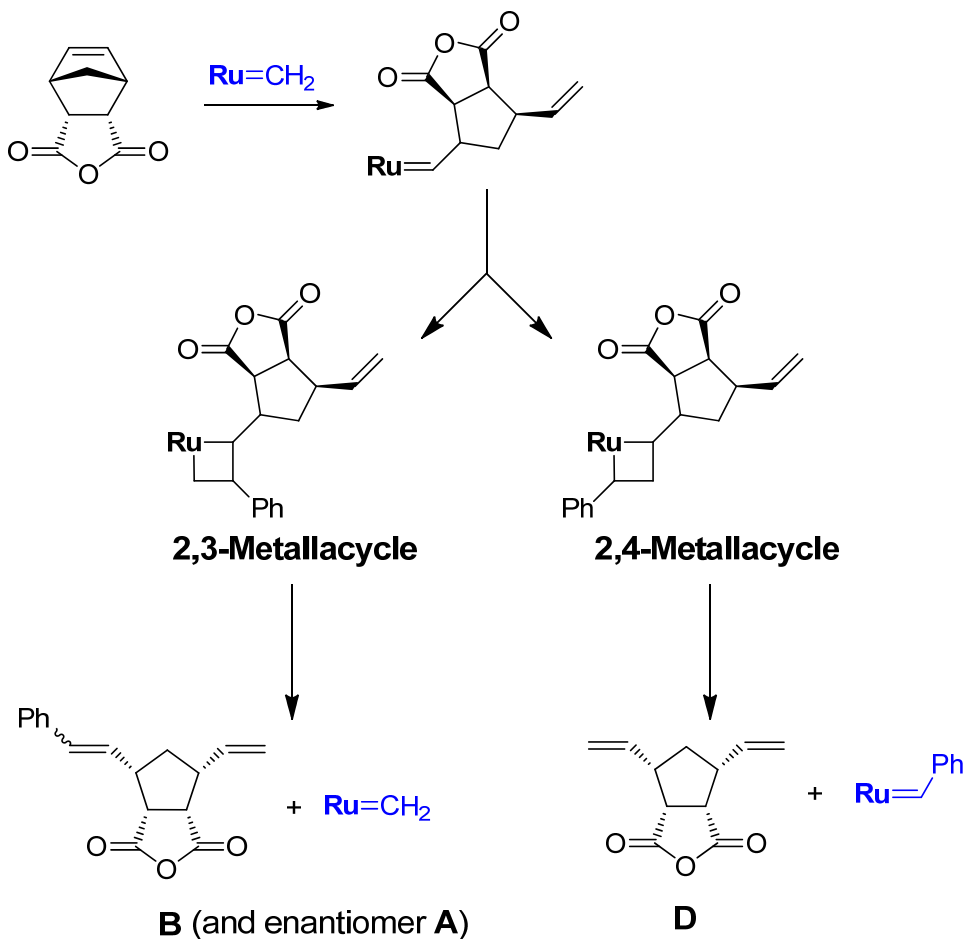
**Scheme 3.5.** Mechanism for the formation of product **C** via secondary metathesis.



Reaction kinetics can be used to determine the likely pathway through which the catalyst proceeds to generate product **C**. If formation of product **C** is solely the result of secondary metathesis, then the ratio of product **C** relative to products **A** and **B** would be expected to be dependent on conversion. This would be an indication of the production of **C** being dependent on the concentration of **A** and **B** in the reaction. With increasing concentration of **A** and **B** (through conversion of substrate), the relative amount of **C** would be expected to increase. Thus a graph of the ratio of **C** relative to **A** and **B** as a function of conversion would be expected to have an upward slope if secondary metathesis were the primary mechanism. However, if formation of **C** were the result of the catalyst proceeding through a 2,3-metallacycle, then the ratio of **C** relative to **A** and **B** would be anticipated to be constant, reflecting the inherent preference of the catalyst for a 2,4-metallacycle versus a 2,3-metallacycle. If that is the case, plotted as a function of conversion, the ratio of product **C** relative to products **A** and **B** should be a horizontal line.

Accessing product **D** requires ring-opening of **3.21** by a ruthenium methyldiene species to generate the first terminal olefin, followed by reaction with styrene through a 2,4-metallacycle to give the second terminal olefin (Scheme 3.6). Product **D** could also be formed by the ethenolysis of products **A** and **B**, although this mechanism of formation is highly unlikely considering the low concentration of ethylene in solution. If product **D** were made by the ethenolysis of **A** and **B**, then the ratio of **D** relative to products **A** and **B** would be expected to be dependent on the concentration of ethylene in solution. If the ratio of **D** relative to **A** and **B** is independent of ethylene concentration, then presumably **D** is formed by ring-opening of **3.21** with a ruthenium methyldiene species.

**Scheme 3.6.** Formation of product **D**: ring-opening of **3.21** via a ruthenium methyldene species.



Kinetic studies were carried out with catalyst **3.15** to elucidate the pathways to products **C** and **D**. The ratio of product **C** relative to products **A** and **B** was followed with conversion by proton NMR and plotted (Figure 3.4). This ratio is constant (0.16:1.0) up to complete consumption of substrate **3.21**, indicating product **C** is formed as a result of formation and breakdown of the 2,3-metallacycle. After complete conversion of substrate **3.21**, the ratio of product **C** relative to products **A** and **B** increases, indicating that secondary metathesis is occurring, but primarily only after **3.21** has completely reacted. Hence during the reaction product **C** is formed as a result of the catalyst proceeding via a 2,3-metallacycle, and after



the reaction is complete, secondary metathesis of products **A** and **B** generate more product **C** (Figure 3.4).

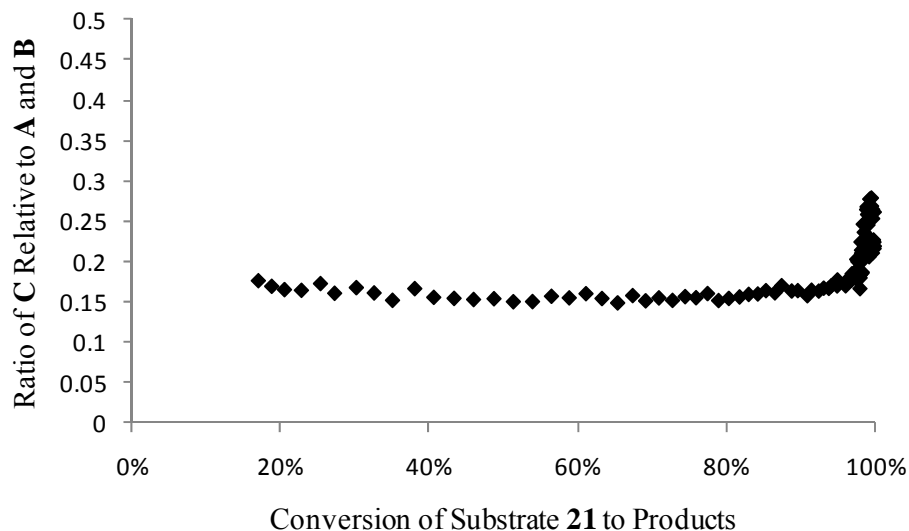


**Figure 3.4.** Ratio of product **C** relative to products **A** and **B** as a function of conversion catalyzed by **3.15**.

The ratio of product **D** relative to products **A** and **B** was constant as a function of conversion (Figure 3.5), suggesting ring-opening of **3.21** by a methyldiene species, followed by reaction of styrene through a 2,4-metallacycle. No dependence was observed on the concentration of ethylene in solution, indicating that ethenolysis of products **A** and **B** is not a major contributing pathway to the formation of compound **D**. Therefore, the production of **D** indicates propagation of ruthenium methyldiene species. This ruthenium methyldiene species can be generated by several reactions, including self-metathesis of styrene and formation of product **C**.

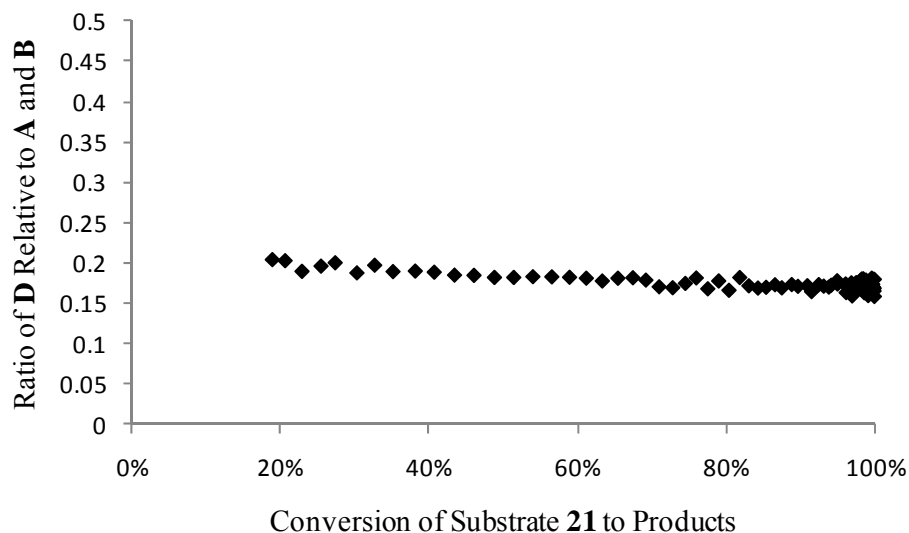
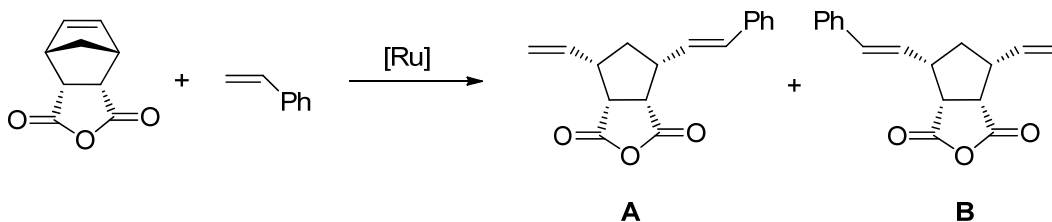


**Figure 3.5.** Ratio of product **D** relative to products **A** and **B** as a function of conversion catalyzed by **3.15**.

Complexes **3.16-3.20** were also screened to determine both their enantioselectivity and if they afforded products **C** and **D** in addition to products **A** and **B**. The reactions were monitored by NMR to determine when they were complete. The mixtures were worked up immediately to prevent any secondary metathesis from potentially eroding or enhancing the ee of the products. As discussed, complex **3.15** gave good enantioselectivity at 69% ee of **A** (Table 3.1, entry 1). Interestingly, **3.16** gave 14% ee of the opposite enantiomer **B**, despite having the same stereochemistry as **3.15** (both *S* configuration). The most plausible explanation is that **3.16** is less enantioselective than **3.15**; additionally, the ring-opening of **3.21** by the methyldiene species of **3.16**, followed by formation of the 2,3-metallacycle, occurs at a high enough frequency to ultimately favor enantiomer **B**. Since the methyldiene species presumably has the same facial selectivity as the alkylidene species (leading to the formation of the opposite enantiomer of product), (*S*)-**3.16** could afford **B** as the major

enantiomer (Table 3.1, entry 2), compared to enantiomer **A** yielded by (*S*)-**3.15**. Complex **3.17** also gave **B** in 9% ee, likely for the aforementioned reasons (Table 3.1, entry 3). While the different structural features of the chiral *N*-alkyl groups of the same stereochemical configuration could spatially alter which enantiomer they select for, complexes **3.15-3.17** seem similar enough to render this unlikely to be the cause of the difference in the preferred enantiomer.

**Table 3.1.** Enantioselectivity of catalysts **3.15-3.19** in AROCM of substrate **3.21**.



Entry <sup>a</sup>	Catalyst	Time (h)	% Conv. <sup>b</sup>	% Yield <sup>c</sup>	% ee <sup>d</sup>
1	<b>3.15</b>	5.5	60	60	69 ( <b>A</b> )
2	<b>3.16</b>	0.5	99	69	14 ( <b>B</b> )
3	<b>3.17</b>	0.5	99	73	9 ( <b>B</b> )
4	<b>3.18</b>	5.5	98	65	33 ( <b>A</b> )
5	<b>3.19</b>	10.5	98	54	82 ( <b>A</b> )

<sup>a</sup>Catalyst loading was 2 mol%. Concentration of **3.21** was 0.2 M in CH<sub>2</sub>Cl<sub>2</sub>. The reaction temperature was 22 °C. <sup>b</sup>Conversion was determined by <sup>1</sup>H NMR spectroscopy using disappearance of **3.21**. <sup>c</sup>Isolated yield of **A** + **B** + **C** + **D**. <sup>d</sup>Enantiomeric excess was determined by chiral HPLC. <sup>e</sup>Catalyst loading was 3 mol%.

By comparison to **3.15**, catalyst **3.18** showed only moderate enantioselectivity, affording product **A** in 33% ee (Table 3.1, entry 4). Complex **3.19** showed the highest selectivity at 82% ee of **A**, comparable to the best ruthenium catalysts reported to date for this particular substrate (Table 3.1, entry 5). Although complex **3.19** (*R* configuration) yields the same enantiomer as complex **3.15** (*S* configuration), we believe the *N*-alkyl structures are unique enough that a direct comparison between these catalysts cannot be made. Complex **3.19**

was significantly slower than the other catalysts screened, but showed no signs of decomposition throughout the reaction. Only the *trans* products were observed in all cases.

The effect of temperature on enantiomeric excess for AROCM catalyzed by **3.15** was studied, and as expected, the ee increased with decreasing temperature, and decreased with increasing temperature (Table 3.2). Complex **3.15** gave up to 72% ee of **A** at 0 °C, and afforded only 42% ee of **A** at 60 °C. The reaction was also noticeably slower at lower temperatures, reaching only 50% conversion after 4 hours at 0 °C, compared to 99% conversion at 50 °C in 3.5 hours.

**Table 3.2.** Effect of temperature on the enantioselectivity of **3.15**.

Entry <sup>a</sup>	Time (h)	Temp. (°C)	% Conv. <sup>b</sup>	% ee <sup>c</sup>
<b>1</b>	4	0	50	72
<b>2</b>	7	22	99	69
<b>3</b>	3.5	40	99	51
<b>4</b>	3.5	50	99	50
<b>5</b>	3.5	60	99	42

<sup>a</sup>Catalyst loading was 2.5 mol%. Temperature was 22 °C. Concentration of **3.21** was 0.1 M in methylene chloride. <sup>b</sup>Conversion was determined by <sup>1</sup>H NMR spectroscopy. <sup>c</sup>Enantiomeric excess was determined by chiral HPLC.

Complexes **3.16-3.20** also gave side products **C** and **D** during the AROCM of **3.21** (Table 3.3). Since complex **3.20** is racemic, its product distribution should not be effected by any potential enantiospecificity of a reaction step. With the exception of complex **3.19**, the catalysts generated approximately the same amount of product **C** relative to major products **A** and **B**, indicating that the inherent preference for a 2,4-metallacycle versus a 2,3-metallacycle is similar for these *N*-aryl, *N*-alkyl NHC catalysts. Complex **3.19** proceeds almost exclusively by a 2,4-metallacycle however, as shown by its low ratio of **C** to **A** and **B**

(0.08:1). The ratio of product **D** relative to products **A** and **B** varied significantly for the different catalysts. Complex **3.19** gave an unusually high ratio of product **D** relative to **A** and **B** (0.43:1), suggesting that this complex has a high propensity to propagate via a methyldiene species (Table 3.3, entry 5).

**Table 3.3.** The amount of side products **C** and **D** formed by different catalysts.

Entry <sup>a</sup>	Catalyst	Time (h)	% Conv. <sup>b</sup>	% C <sup>c</sup>	% D <sup>d</sup>
1	3.15	1	99	16	12
2	3.16	0.5	99	15	19
3	3.17	0.25	99	14	23
4	3.18	1	99	12	18
5	3.19	6	82	8	43
6	3.20	0.5	99	17	18

<sup>a</sup>Catalyst loading was 2.5 mol%. Concentration of **3.21** was 0.2 M in methylene chloride. <sup>b</sup>Conversion was determined by <sup>1</sup>H NMR spectroscopy. <sup>c</sup>Percent of product **C** relative to products **A** and **B**. <sup>d</sup>Percent of product **D** relative to products **A** and **B**.

The ratios of **C** to **A** and **B** and **D** to **A** and **B** were calculated as a function of temperature in order to determine the effect of temperature on alkylidene versus methyldiene propagation and the formation and breakdown of the 2,4-metallacycle versus 2,3-metallacycle. Complex **3.15** was used as the catalyst at a loading of 2.5 mol%, and the respective ratios were determined upon completion of the AROCM of **3.21** (0.1 M in methylene chloride) by <sup>1</sup>H NMR spectroscopy. With higher temperature, the amount of both products **C** and **D** yielded in the reaction increased (Figure 3.6). This is possibly a result of the higher temperature providing the necessary energy for the reaction to proceed down the less favorable pathways, thereby giving more of the end products of those pathways, **C** and **D**.

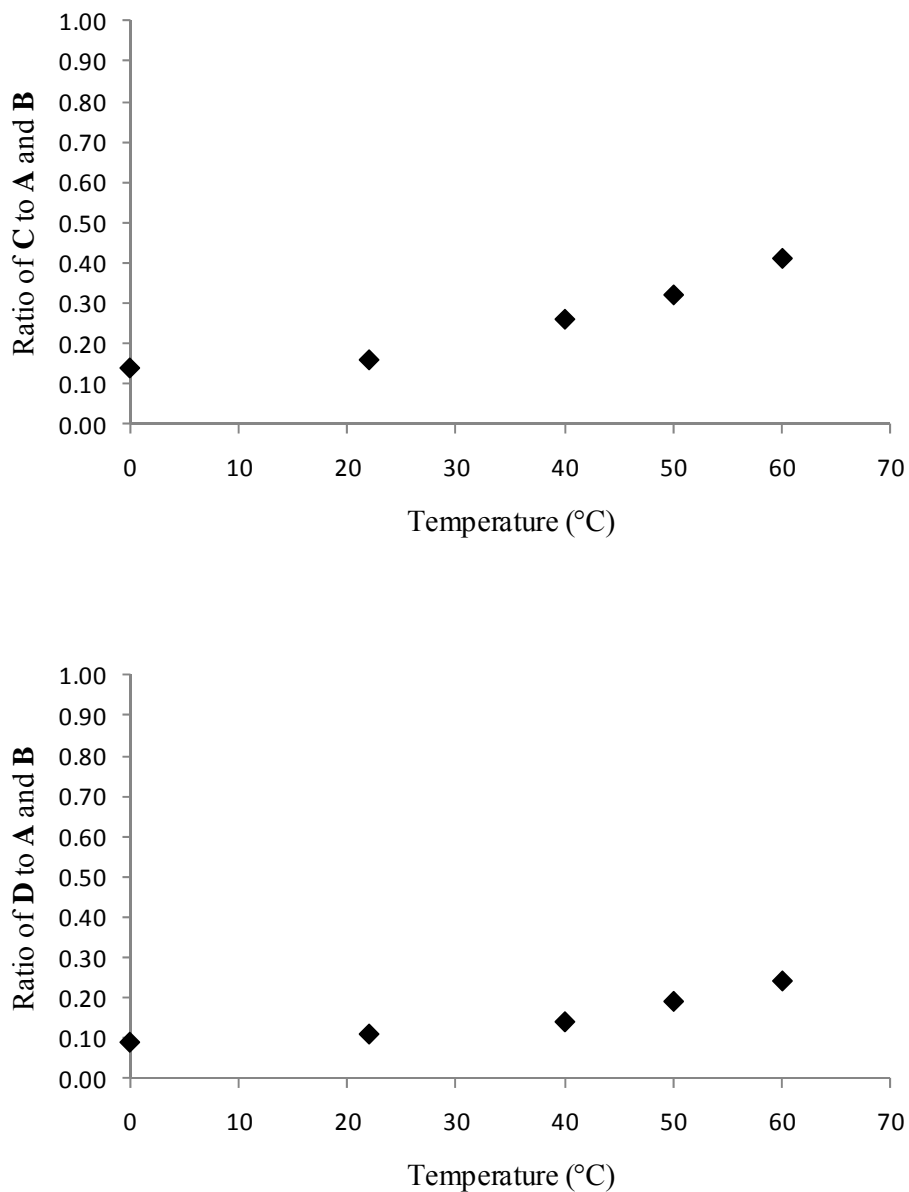


**Figure 3.6.** Effect of temperature on the yields of products **C** and **D**.

In order to confirm that product **C** was being formed as a result of the catalysts proceeding via a 2,3-metallacycle as a general principle, and not unique to complex **3.15**, the ratio of **C** relative to **A** and **B** was plotted as a function of conversion for catalysts **3.17**, **3.18**, and **3.20** as well. In all cases, the ratio of **C** to **A** and **B** was constant up to complete

consumption of substrate **3.21**, after which secondary metathesis occurred to increase the amount of **C** in the reaction mixture. Similarly, the ratio of product **D** to products **A** and **B** was shown to be constant throughout the reaction, confirming that these pathways are general to the complexes investigated in this study.

## Conclusion

Complexes **3.15-3.20** yield side products during AROCM reactions resulting from the catalysts proceeding through a 2,3-metallacycle in addition to a 2,4-metallacycle, as well as propagating by a methylidene species, and these pathways were found to be general to this class of ruthenium catalysts investigated. The inherent preference of a given catalyst for the formation and breakdown of a 2,4-metallacycle versus a 2,3-metallacycle affects its product distribution, and this catalyst behavior can be utilized to target products and particular applications. It also can be considered in new catalyst design, as the ligand structure was shown to have an effect on the propensity of the catalyst to undergo a 2,3- versus 2,4-metallacycle. Similarly, high preference for methylidene propagation alters product ratios and can be used for applications where this is a desirable pathway. Additionally, methylidene propagation generally shortens catalyst lifespan, a necessary consideration in choice of catalyst for a given reaction. Catalysts **3.15** and **3.19** gave high enantioselectivities, with catalyst **3.19** showing comparable enantioselectivity to the best ruthenium catalysts reported to date. The steric bulk of catalyst **3.19** could contribute to it being more stable as a methylidene species compared to the other catalysts, as well as making it slower. The propensity of catalyst **3.19** to propagate as a methylidene renders it

attractive for applications requiring complex stability as a methyldiene species. Future directions are focused toward exploited these catalyst properties for targeted reactions.

## Experimental Section

**General considerations.** All manipulations of air- or water-sensitive compounds were carried out under dry nitrogen using a glovebox or under dry argon utilizing standard Schlenk line techniques. NMR spectra were recorded on a Varian Mercury ( $^1\text{H}$ , 300 MHz), Varian Inova 400 ( $^1\text{H}$ , 400 MHz), or a Varian Inova 500 ( $^1\text{H}$ , 500 MHz;  $^{13}\text{C}$ , 125 MHz) spectrometer and referenced to residual protio solvent. Enantiomeric excesses were determined by chiral HPLC. Column: chiralcel AD; Solvent system: 8% isopropanol in hexanes. Flow rate: 0.75 mL per min.

**Materials.** Deuterated methylene chloride was dried over calcium hydride and vacuum distilled, followed by three cycles of freeze-pump-thawing. *cis*-5-Norbornene-*endo*-2,3-dicarboxylic anhydride (**3.21**) was obtained from Aldrich and used without further purification. Styrene was purchased from Aldrich and filtered through a silica gel plug prior to use.

**Representative AROCM reaction of *cis*-5-norbornene-*endo*-2,3-dicarboxylic anhydride with styrene.** Substrate *cis*-5-norbornene-*endo*-2,3-dicarboxylic anhydride (60 mg, 0.36 mmol) was added to a 100 mL round bottom flask containing a vacuum adaptor, and the flask was placed under an argon atmosphere. Dry methylene chloride (6 mL) was added via syringe, followed by styrene (0.42 mL, 3.6 mmol). Catalyst **3.15** (6.5 mg, 2.5 mol%) was then added, and the reaction was stirred for 4 hours. The mixture was



concentrated, and a crude proton NMR was taken to calculate the relative ratios of products **A/B**, **C**, and **D**. The products were purified by column chromatography (silica gel, 50% ether in pentane). Stilbene came off with an  $R_f$  of 0.91. Product **D** came off with an  $R_f$  of 0.43 and was recovered in trace amounts; product **A/ B** had an  $R_f$  of 0.33 (49 mg, 47% yield); and product **C** had an  $R_f$  of 0.27 (12 mg, 10% yield). Enantiomeric excess was determined by chiral HPLC, with enantiomer **A** showing a retention time of 28.95 min, and enantiomer **B** showing a retention time of 32.98 min. Product **A** was obtained in 69% ee over product **B**. The enantiomers were identified by comparison to the retention times under the same chiral HPLC conditions outlined in reference 14.  $^1\text{H}$  NMR of product **A/B** ( $\text{CDCl}_3$ , 500 MHz):  $\delta$  7.42 – 7.35 (m, 2H), 7.35 – 7.29 (m, 2H), 7.25 – 7.21 (m, 1H), 6.52 (d,  $J$  = 15.8 Hz, 1H), 6.30 (dd,  $J$  = 15.8, 8.0 Hz, 1H), 6.03 – 5.90 (m, 1H), 5.23 (d,  $J$  = 1.1 Hz, 1H), 5.20 (dt,  $J$  = 7.5, 1.3 Hz, 1H), 3.61 – 3.47 (m, 2H), 3.22 – 3.11 (m, 1H), 3.10 – 2.99 (m, 1H), 2.14 (dt,  $J$  = 12.8, 5.5 Hz, 1H), 1.57 (q,  $J$  = 12.9 Hz, 1H) ppm.  $^{13}\text{C}$  NMR of product **A/B** ( $\text{CDCl}_3$ , 125 MHz):  $\delta$  170.79, 136.84, 134.99, 132.48, 128.81, 127.96, 126.68, 126.57, 117.62, 50.06, 49.62, 47.00, 46.43, 36.78 ppm.  $^1\text{H}$  NMR of product **C** ( $\text{CDCl}_3$ , 500 MHz):  $\delta$  7.39 (m, 4H), 7.35 – 7.29 (m, 4H), 7.24 (m, 2H), 6.55 (d,  $J$  = 15.8 Hz, 2H), 6.31 (dd,  $J$  = 15.7, 8.0 Hz, 2H), 3.63 – 3.56 (m, 2H), 3.22 (m, 2H), 2.22 (dt,  $J$  = 12.7, 5.4 Hz, 1H), 1.66 (q,  $J$  = 12.9 Hz, 1H) ppm.  $^{13}\text{C}$  NMR of product **C** ( $\text{CDCl}_3$ , 125 MHz):  $\delta$  170.77, 134.98, 132.55, 128.82, 127.98, 126.70, 126.54, 50.00, 46.57, 37.55 ppm.  $^1\text{H}$  NMR of product **D** ( $\text{CDCl}_3$ , 500 MHz):  $\delta$  6.01 – 5.91 (m, 2H), 5.23 – 5.20 (m, 2H), 5.19 (dt,  $J$  = 10.0, 1.2 Hz, 2H), 3.54 – 3.44 (m, 2H), 3.06 – 2.94 (m, 2H), 2.07 (dt,  $J$  = 12.9, 5.5 Hz, 1H), 1.49 (q,  $J$  = 13.0 Hz, 1H) ppm.  $^{13}\text{C}$  NMR of product **D** ( $\text{CDCl}_3$ , 125 MHz):  $\delta$  170.74, 135.00, 117.59, 49.68, 46.90, 36.04 ppm.

**Representative kinetic experiment for the pathway to the formation of products C and D.** In a nitrogen atmosphere glovebox, an NMR tube was charged with *cis*-5-norbornene-*endo*-2,3-dicarboxylic anhydride (20 mg, 0.12 mmol) and 0.5 mL of deuterated methylene chloride. The NMR tube was sealed with a septum cap and brought out of the glovebox. Styrene was added via syringe through the septum cap, and a proton NMR spectrum ( $\text{CD}_2\text{Cl}_2$ , 500 MHz) was taken for time = 0. An NMR array was set up with pad increments of 10 sec, 16 scans per spectrum, 200 spectra. Catalyst solution (**3.15** in 0.25 mL dry  $\text{CD}_2\text{Cl}_2$ ; 1.7 mg, 2 mol%) was injected by syringe into the NMR tube, and the sample was inserted into the spectrometer. The data was collected and analyzed using MestReNova software. This same procedure was used for catalysts **3.17**, **3.18**, and **3.20**. The data is shown below. The kinetics experiments were not conducted for complex **3.19** since this catalyst is very slow and would take a long time to reach complete conversion. From the data collected for this catalyst in other experiments, catalyst **3.19** gives only trace conversion to product **C** during AROCM. The NMR array was also not run for catalyst **3.16**, as this complex was expected to be very similar to **3.17**.

The substrate conversion (**21**) to products (**A** and **B**, **C**, **D**) and the relative ratios of products **A** and **B**, **C**, and **D** were determined by integrating the respective proton NMR peaks (Figure 3.7). The  $^1\text{H}$  NMR array spectra were overlaid and worked up as a unit during data analysis. The ratio of **C** relative to **A** and **B** (and analogously the ratio of **D** relative to **A** and **B**) was plotted versus conversion for all of these spectra to generate the graphs.

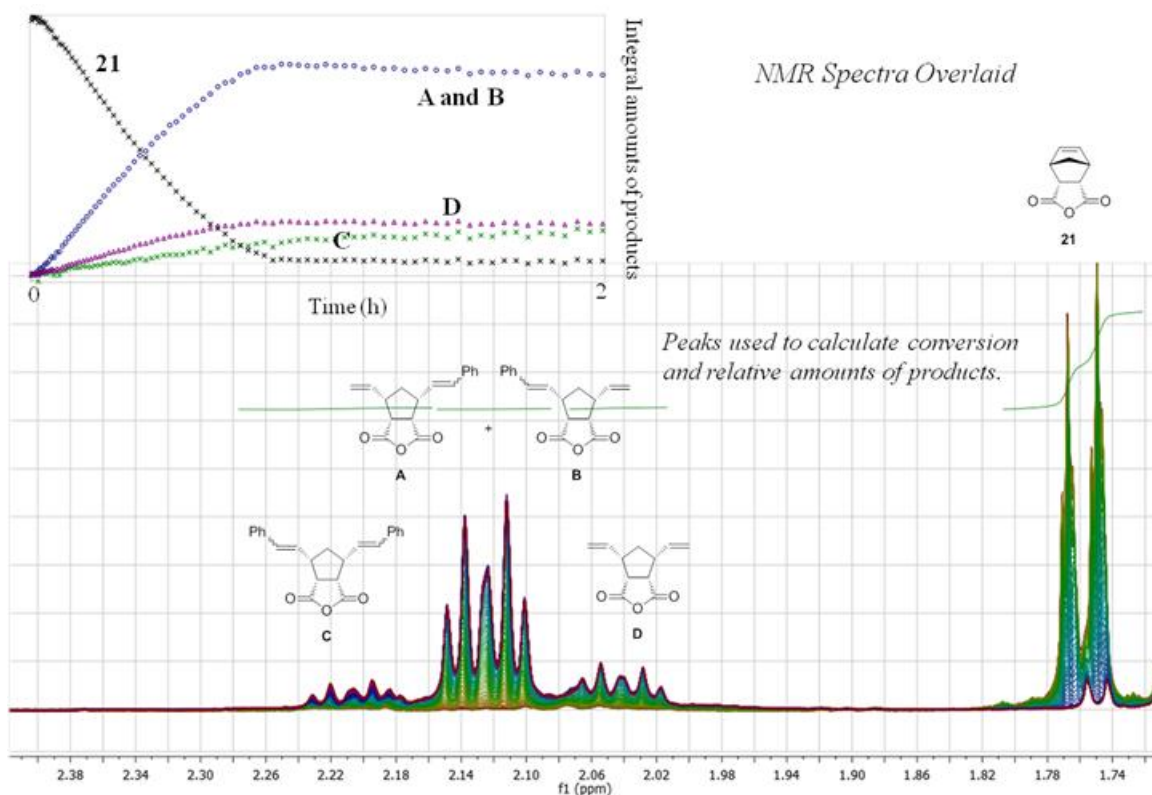


**Figure 3.7.**  $^1\text{H}$  NMR peaks used to calculate product ratios and conversion of **21**. The representative NMR overlay shown here is from a kinetic study with catalyst **3.20**.

The distribution of products as a function of time is shown in Figure 3.8. Substrate **21** disappears linearly over time, as expected. Products **A** and **B**, **C**, and **D** grow in linearly until **21** is consumed, at which point the amount of **D** remains constant. Product **C** continues to increase slowly due to secondary metathesis of products **A** and **B**. There does not appear to be detectable secondary metathesis of product **D**, possibly due to **D** undergoing more non-productive metathesis than productive metathesis. This could result from different sterics about product **D** affecting the preference and stability of the resulting metallacycles leading to productive and non-productive metathesis.

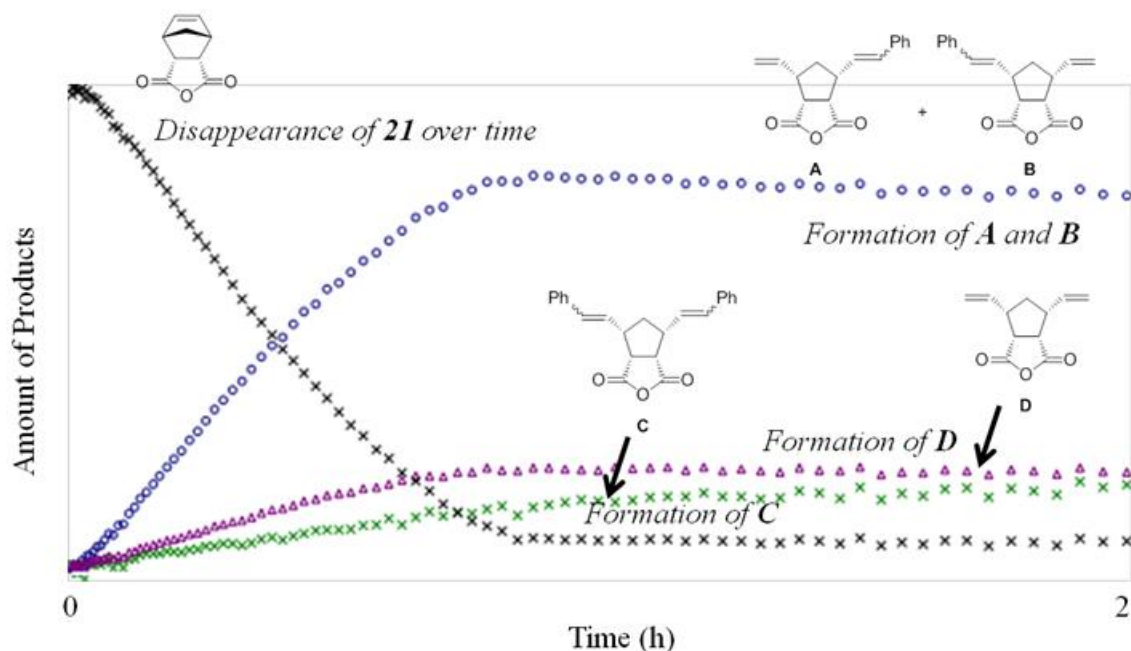
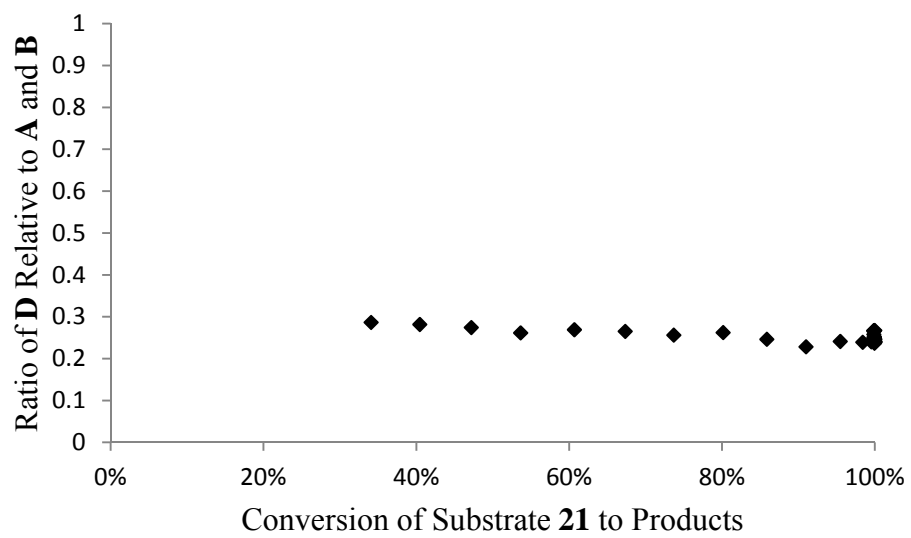
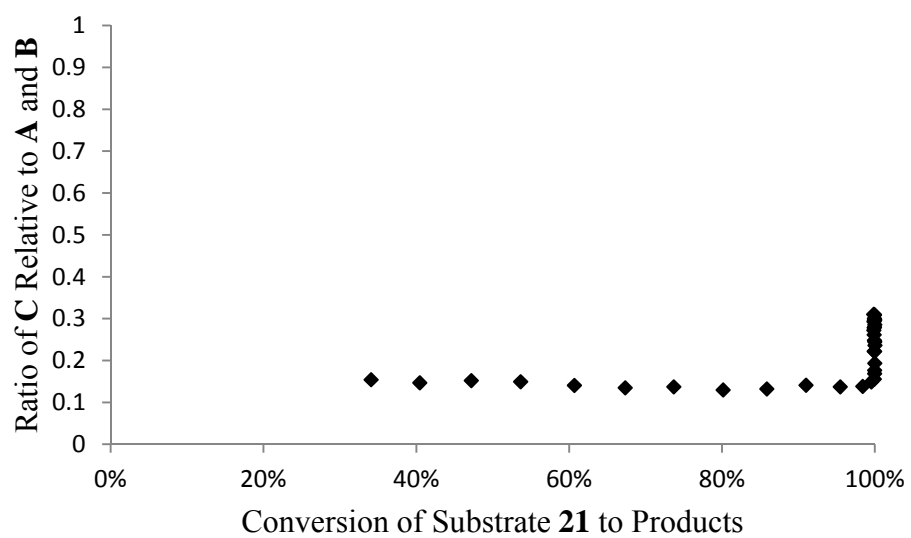


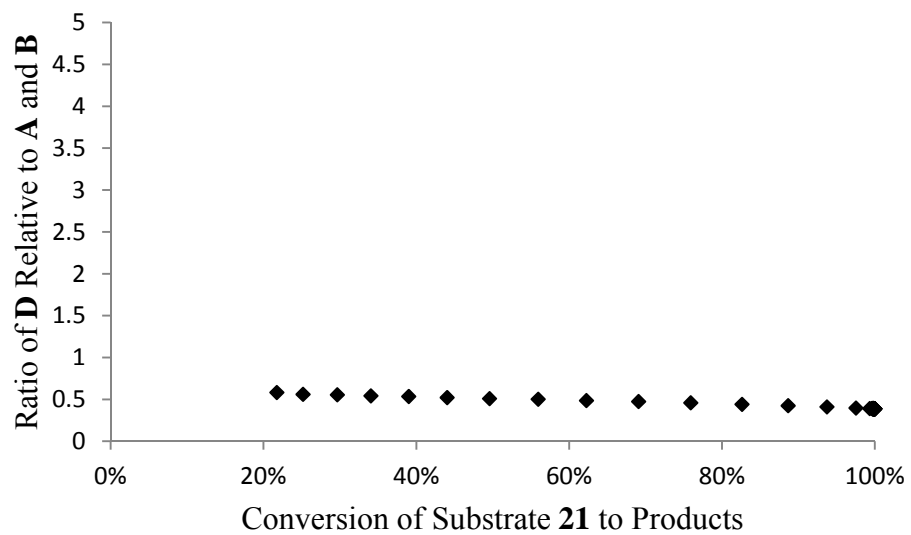
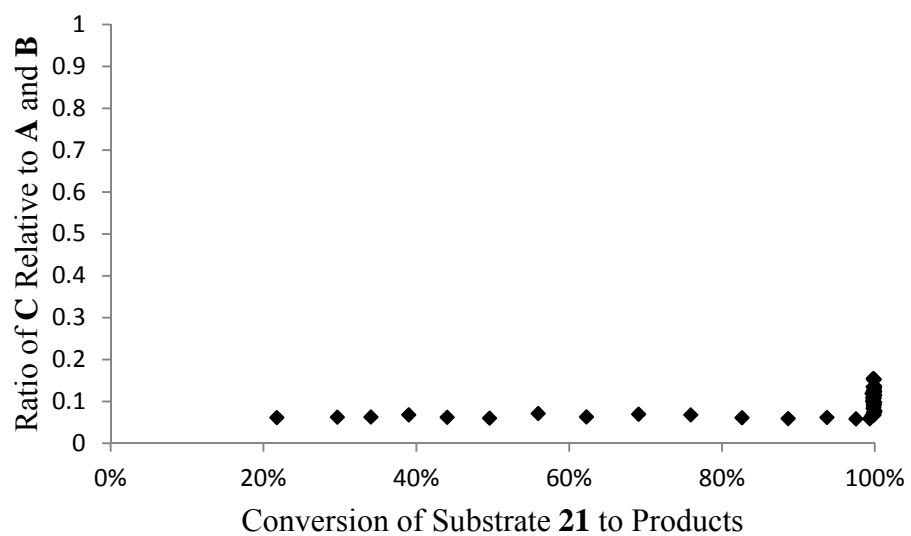
**Figure 3.8.** A graph showing the amounts of products, abstract units reflecting integral values, as a function of time during a kinetic experiment with catalyst **3.20**.

In the graphs of product ratios as a function of conversion, data points for low conversion are not shown due to greater error in product peak integrations when product is present in trace quantities. The ratio of product **C** relative to **A** and **B** is constant for the different catalysts during consumption of **21**, after which secondary metathesis results in an increase in product **C**, shown in the graphs as the ratio of **C** to **A** and **B** increases after complete conversion of **21**. The ratio of **D** remains constant throughout the reaction as well. These plots support the proposed metallacycle explanation for the formation of products **C** and **D**. The formation of product **D**, which requires methyldene propagation, indicates that these complexes are moderately stable to existing as a methyldene species.

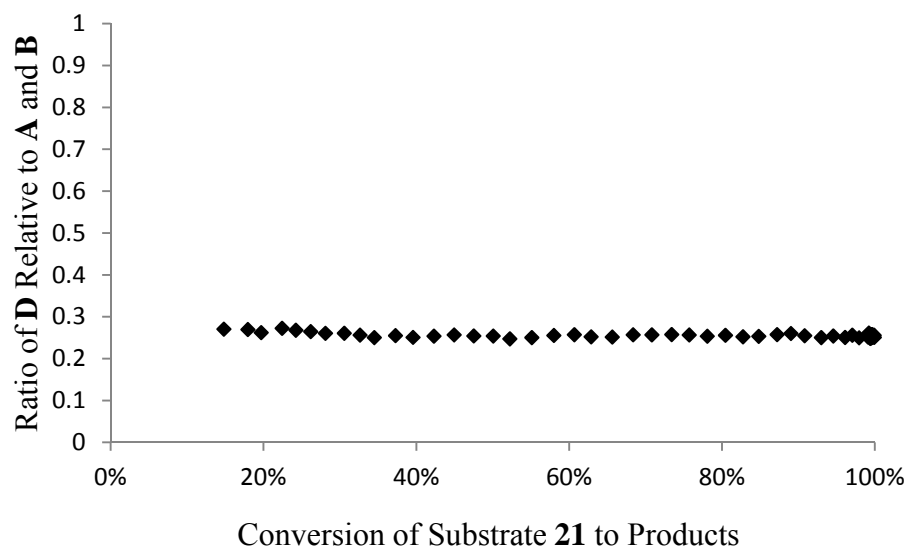
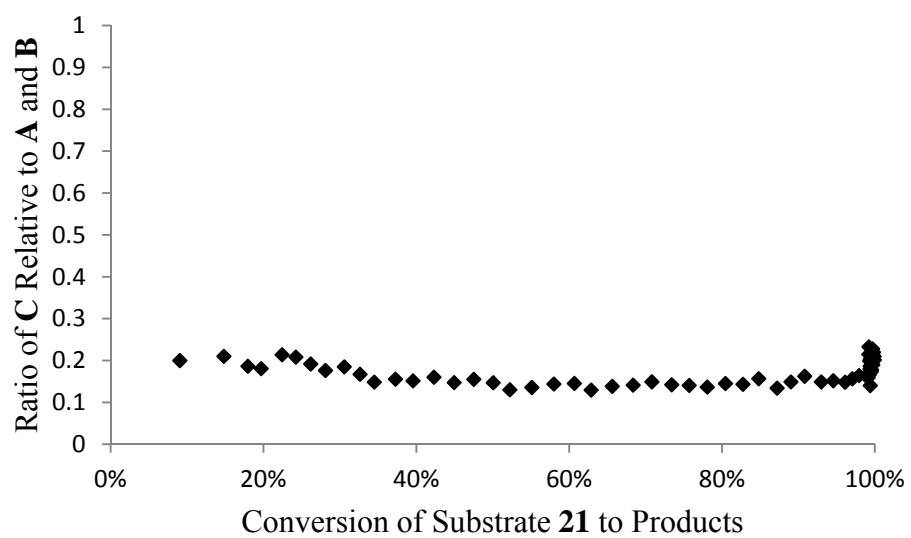
**Scheme 3.7.** Product ratios for AROCM of **21** with styrene catalyzed by complex **3.17**.



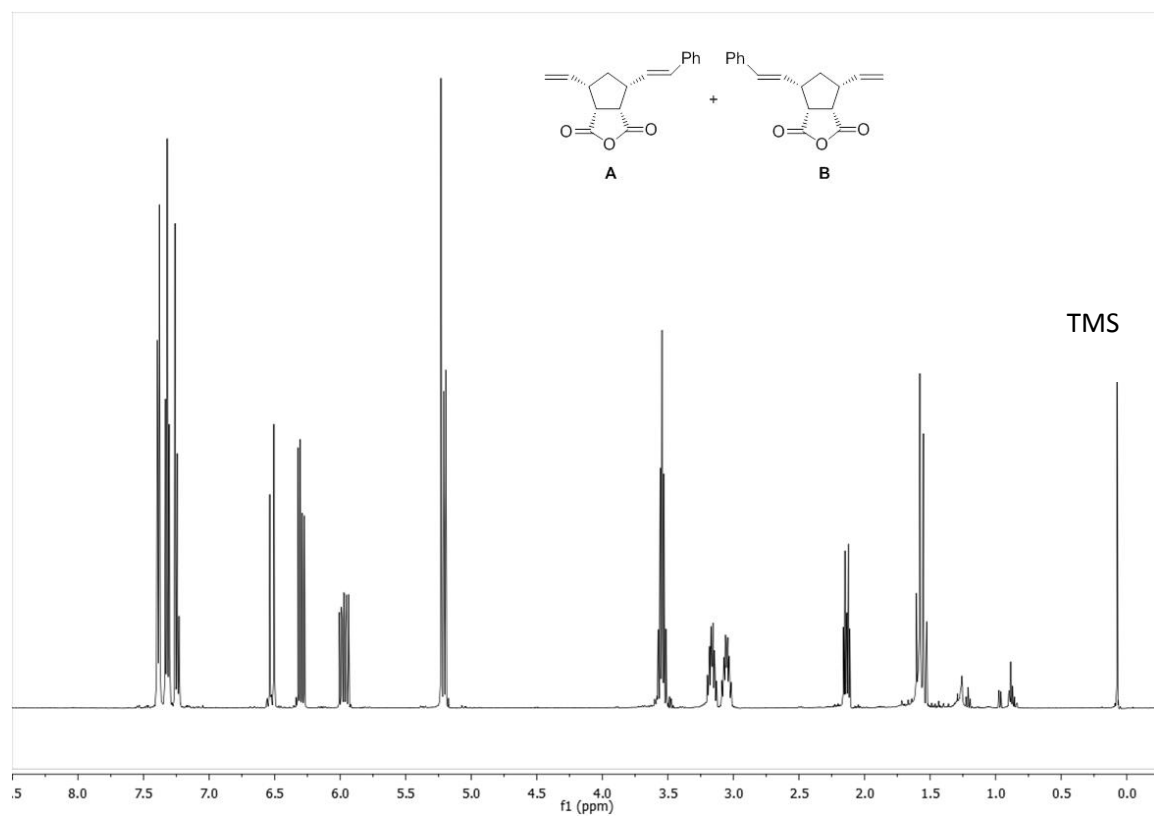
**Scheme 3.8.** Product ratios for AROCM of **21** with styrene catalyzed by complex **3.18**.



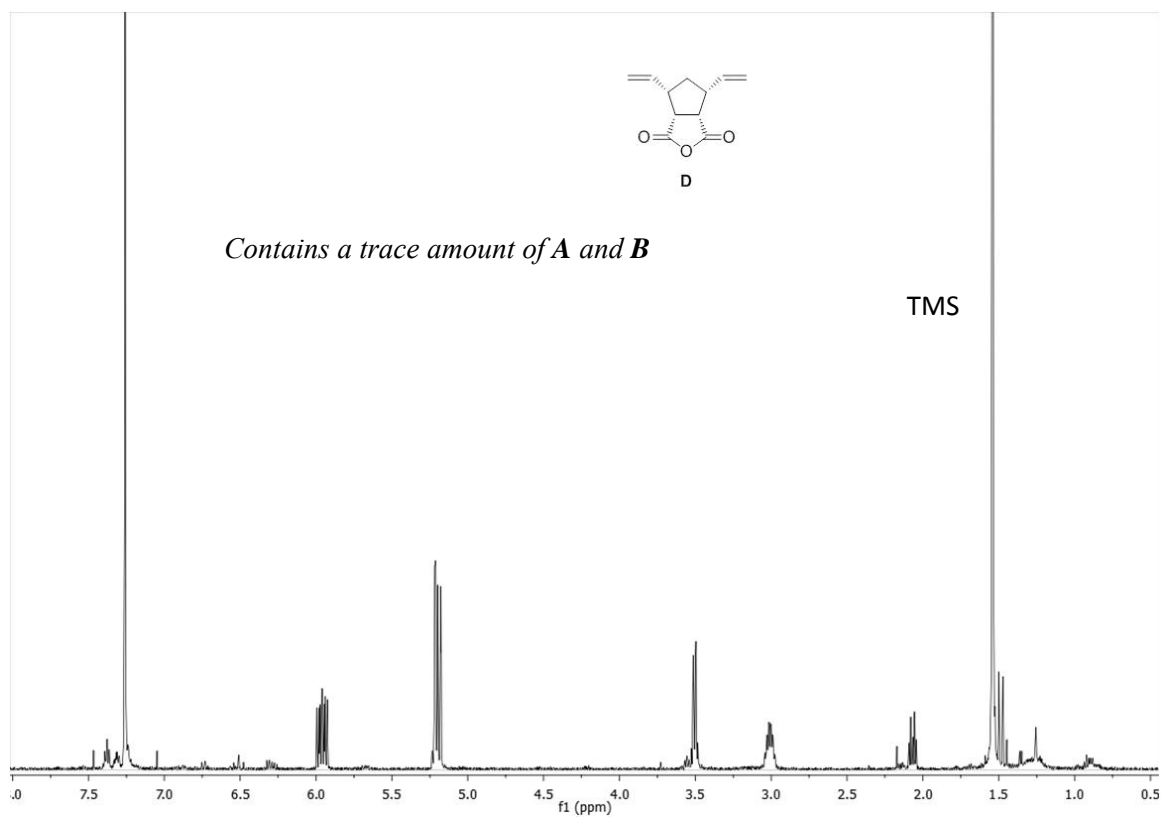
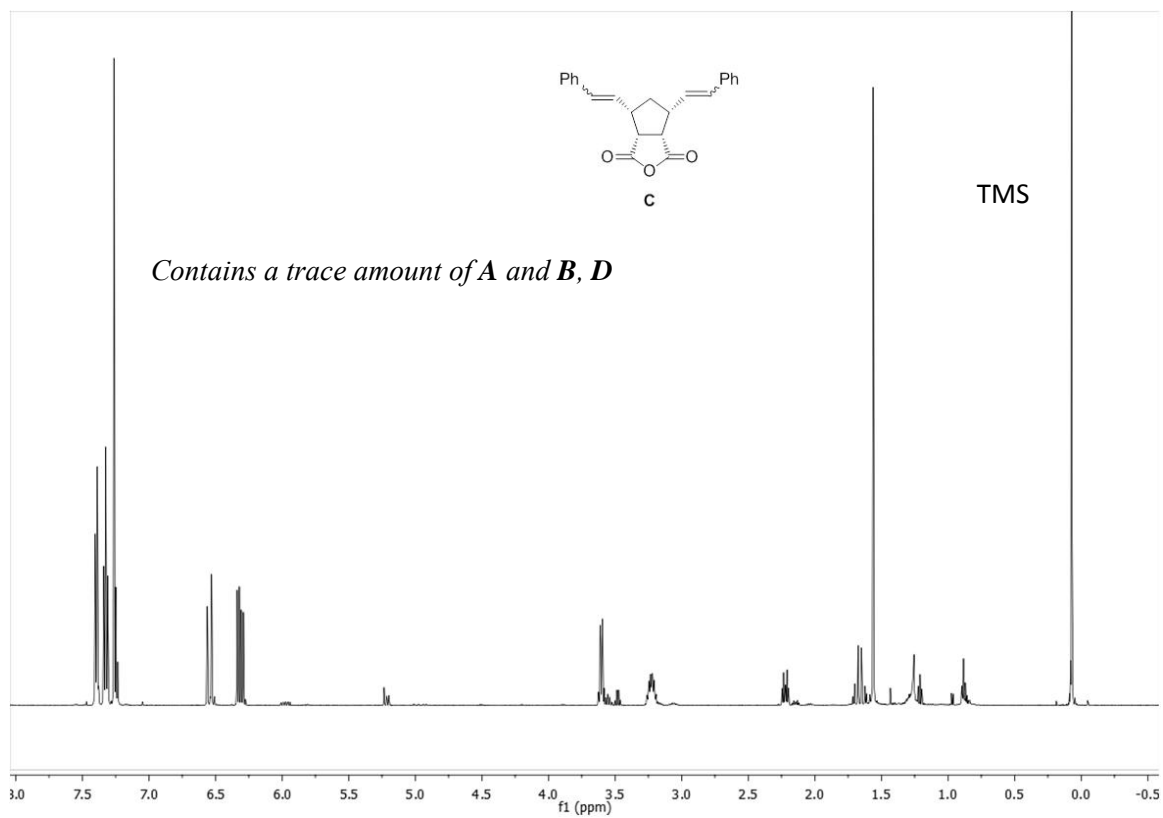
**Scheme 3.9.** Product ratios for AROCM of **21** with styrene catalyzed by complex **3.20**.



$^1\text{H}$  NMR spectra of products **A–D** in  $\text{CDCl}_3$  + TMS.







**Acknowledgment.** The author thanks *Chemistry in New Zealand* for permission for the contents of this chapter. This research has been published in *Chemistry in New Zealand*. Article reference: Thomas, R. M.; Grubbs, R. H. *Chemistry in New Zealand* **2011**, 75, 65–71.

## REFERENCES

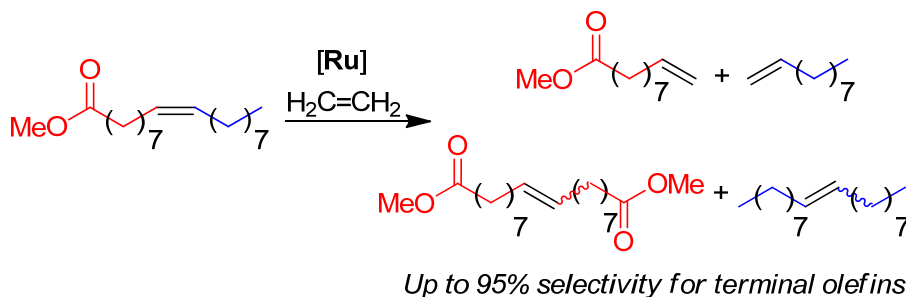
1. (a) Grubbs, R. H. *Handbook of Metathesis*; Wiley-VCH: Weinheim, Germany, 2003. And references cited therein. (b) Cossy, J.; Arseniyadis, S.; Meyer, C. *Metathesis in Natural Product Synthesis*; Wiley-VCH: Weinheim, Germany, 2010.
2. (a) Mutlu, H.; de Espinosa, L. M.; Meier, M. A. R. *Chem. Soc. Rev.* **2011**, *40*, 1404–1445. (b) Buchmeiser, M. R. *Macromolecular Symposia* **2010**, *298*, 17–24. (c) Khaja, S. D.; Lee, S.; Murthy, N. *Biomacromolecules* **2007**, *8*, 1391–1395. (d) Grubbs, R. H.; Trnka, T. M. *Ruthenium in Organic Synthesis* **2004**, 153–177.
3. (a) Hoveyda, A. H.; Schrock, R. R. *Comprehensive Asymmetric Catalysis*, Supplement **2004**, *1*, 207–233. (b) Connon, S. J.; Blechert, S. *Topics in Organometallic Chemistry* **2004**, *11*, 93–124. (c) Hoveyda, A. H.; Schrock, R. R. *Organic Synthesis Highlights V* **2003**, 210–229.
4. Gillingham, D. G.; Hoveyda, A. H. *Angew. Chem. Int. Ed.* **2007**, *46*, 3860–3864.
5. Takao, K.; Yasui, H.; Yamamoto, S.; Sasaki, D.; Kawasaki, S.; Watanabe, G.; Tadano, K. *J. Org. Chem.* **2004**, *69*, 8789–8795.
6. Cortez, G. A.; Schrock, R. R.; Hoveyda, A. H. *Angew. Chem. Int. Ed.* **2007**, *46*, 4534–4538.
7. (a) Savoie, J.; Stenne, B.; Collins, S. K. *Advanced Synthesis & Catalysis* **2009**, *351*, 1826–1832. (b) Fournier, P. A.; Savoie, J.; Stenne, B.; Bedard, M.; Grandbois, A.; Collins, S. K. *Chemistry- A European Journal* **2008**, *14*, 8690–8695. (c) Funk, T. W.; Berlin, J. M.; Grubbs, R. H. *J. Am. Chem. Soc.* **2006**, *128*, 1840–1846.
8. La, D. S.; Ford, J. G.; Sattely, E. S.; Bonitatebus, P. J.; Schrock, R. R.; Hoveyda, A. H. *J. Am. Chem. Soc.* **1999**, *121*, 11603–11604.
9. La, D. S.; Sattely, E. S.; Ford, J. G.; Schrock, R. R.; Hoveyda, A. H. *J. Am. Chem. Soc.* **2001**, *123*, 7767–7778.
10. Pilyugina, T. S.; Schrock, R. R.; Müller, P.; Hoveyda, A. H. *Organometallics* **2007**, *26*, 831–837.
11. (a) Ibrahim, I.; Yu, M.; Schrock, R. R.; Hoveyda, A. H. *J. Am. Chem. Soc.* **2009**, *131*, 3844–3845. (b) Endo, K.; Grubbs, R. H. *J. Am. Chem. Soc.* **2011**, *133*, 8525–8527.
12. (a) Mol, J. C. *J. Mol. Cat. A: Chem.* **2004**, *213*, 39–45. (b) Kuhn, K. M.; Bourg, J. –B.; Chung, C. K.; Virgil, S. C.; Grubbs, R. H. *J. Am. Chem. Soc.* **2009**, *131*, 5313–5320.
13. Cortez, G. A.; Baxter, C. A.; Schrock, R. R.; Hoveyda, A. H. *Org. Lett.* **2007**, *9*, 2871–2874.
14. Berlin, J. M.; Goldberg, S. D.; Grubbs, R. H. *Angew. Chem. Int. Ed.* **2006**, *45*, 7591–7595.
15. Van Veldhuizen, J. J.; Garber, S. B.; Kingsbury, J. S.; Hoveyda, A. H. *J. Am. Chem. Soc.* **2002**, *124*, 4954–4955.
16. Gillingham, D. G.; Kataoka, O.; Garber, S. B.; Hoveyda, A. H. *J. Am. Chem. Soc.* **2004**, *126*, 12288–12290.

17. Tiede, S.; Berger, A.; Schlesiger, D.; Rost, D.; Lühl, A.; Blechert, S. *Angew. Chem. Int. Ed.* **2010**, *49*, 3972–3975.
18. Grisi, F.; Costabile, C.; Gallo, E.; Mariconda, A.; Tedesco, C.; Longo, P. *Organometallics* **2008**, *27*, 4649–4656.
19. Vehlow, K.; Maechling, S.; Blechert, S. *Organometallics* **2006**, *25*, 25–28.
20. Paczal, A.; Bényei, A. C.; Kotschy, A. *J. Org. Chem.* **2006**, *71*, 5969–5979.
21. (a) Kuhn, K. M.; Bourg, J. B.; Chung, C. K.; Virgil, S. C.; Grubbs, R. H. *J. Am. Chem. Soc.* **2009**, *131*, 5313–5320. (b) Thomas, R. M.; Keitz, B. K.; Champagne, T. M.; Grubbs, R. H. *J. Am. Chem. Soc.* **2011**, *133*, 7490–7496.

## Chapter 4

### HIGHLY SELECTIVE RUTHENIUM METATHESIS CATALYSTS FOR ETHENOLYSIS

#### Abstract



*N*-aryl, *N*-alkyl *N*-heterocyclic carbene (NHC) ruthenium metathesis catalysts are highly selective toward the ethenolysis of methyl oleate, giving selectivity as high as 95% for the kinetic, ethenolysis products over the thermodynamic, self-metathesis products. The examples described herein represent some of the most selective NHC-based ruthenium catalysts for ethenolysis reactions to date. Furthermore, many of these catalysts show unusual preference and stability toward propagating as a methyldiene species, and provide good yields and turnover numbers (TONs) at relatively low catalyst loading (<500 ppm). A catalyst comparison shows that ruthenium complexes bearing sterically hindered NHC substituents afford greater selectivity and stability, and exhibit longer catalyst lifetimes. Comparative analysis of the catalyst preference for kinetic versus thermodynamic product formation was achieved via evaluation of their steady-state conversion in the cross-metathesis reaction of terminal olefins. These results coincided with the observed

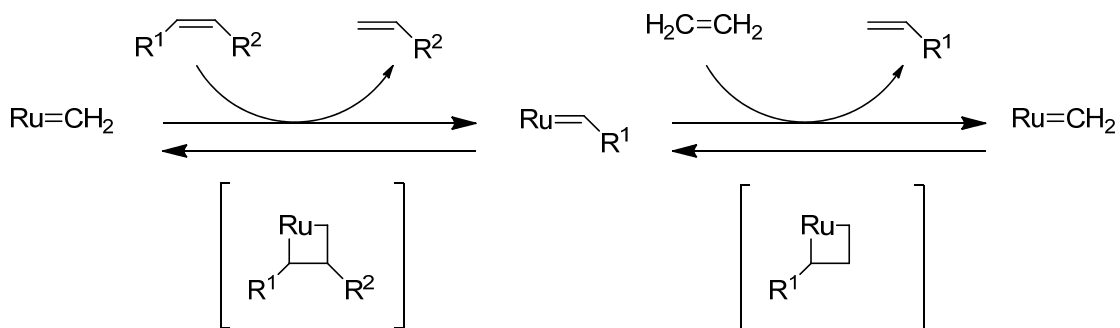
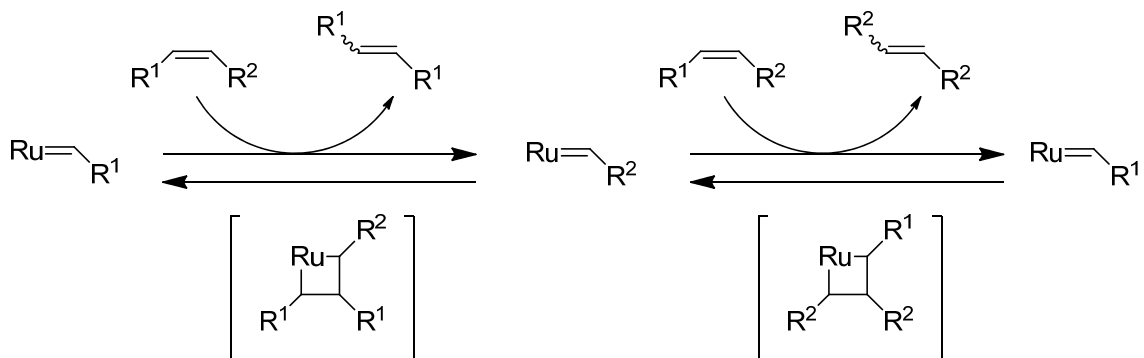
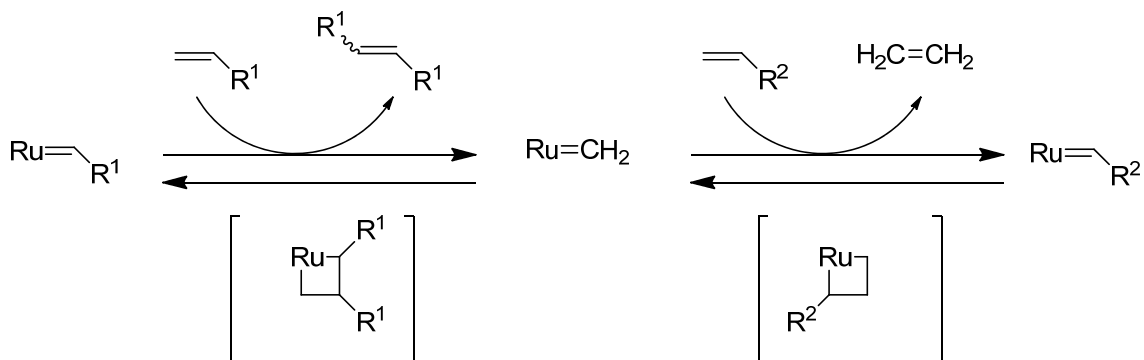
ethenolysis selectivities, in which the more selective catalysts reach a steady-state characterized by lower conversion to cross-metathesis products compared to less selective catalysts, which show higher conversion to cross-metathesis products.

## **Introduction**

Olefin metathesis is widely used in both organic and polymer synthesis and has become a standard methodology for constructing carbon-carbon double bonds.<sup>1</sup> Metathesis catalysts have been successfully designed for stability,<sup>2</sup> functional group tolerance,<sup>3</sup> activity,<sup>4</sup> and selectivity,<sup>5</sup> enabling metathesis to be broadly applied. The development of catalysts exhibiting preference for kinetically versus thermodynamically controlled product ratios continues to be a challenging area in olefin metathesis.<sup>6</sup> An example of a metathesis reaction which requires kinetic selectivity is ethenolysis, the reaction of an internal olefin with ethylene to generate thermodynamically disfavored terminal olefin products. There is significant interest for selective formation of terminal olefins due to the potential conversion of fatty acids derived from renewable biomass to valuable commercial products.<sup>7</sup> Such a process would enable the green synthesis of commercial commodities from renewable sources such as natural seed oils and their derivatives instead of petroleum feedstocks.<sup>8</sup> Natural seed oils are particularly attractive due to their built-in functionality, widespread availability, and relatively low cost. Specifically, ethenolysis of methyl oleate (MO) affords chemically desirable products with extensive applications including use in cosmetics, detergents, soaps,<sup>7</sup> and polymer additives,<sup>9</sup> as well as potential applications as a renewable biofuel source.<sup>10</sup>

Most reported studies have focused on ruthenium complexes in the development of an efficient ethenolysis catalyst due to their functional group tolerance and stability to air and water, which renders them easy to handle and does not require extensive purification of starting material.<sup>11</sup> High selectivities and yields for the ethenolysis of methyl oleate and cyclooctene have been disclosed by Schrock and coworkers using molybdenum systems.<sup>12</sup> Molybdenum metathesis catalysts give up to 99% selectivity for the ethenolysis of methyl oleate in up to 95% yield, with TONs as high as 4,750. Ideally, selective ethenolysis would be carried out by robust catalysts exhibiting high turnover numbers (TONs) for an efficient process. Since ruthenium catalysts are very stable and readily handled, research efforts were directed toward the development of ruthenium-based metathesis catalysts designed to exhibit these attributes for selective ethenolysis.

Ethenolysis reactions require catalyst stability as a propagating methyldiene species for high product selectivity and TON.<sup>6,13</sup> The desirable ethenolysis catalytic cycle involves crossing an internal olefin onto the active metal complex to generate an alkylidene species, followed by reaction with ethylene to form a 1,2-disubstituted metallacycle (Scheme 4.1). Breakdown of this metallacycle then yields the desired terminal olefin and a ruthenium methyldiene species. This methyldiene complex can then react with the substrate to release a terminal olefin and afford a ruthenium alkylidene species, which can subsequently react with ethylene and repeat the cycle. Most olefin metathesis catalysts are unstable as methyldiene complexes and possibly as the corresponding unsubstituted metallacycle, and undergo rapid decomposition.<sup>13</sup> This catalyst degradation significantly limits TON during ethenolysis reactions.

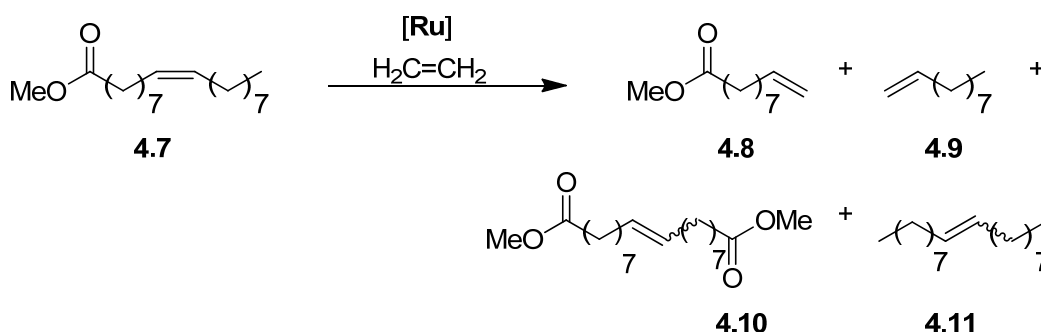
**Scheme 4.1.** Metathesis reactions during ethenolysis.***Ethenolysis Reaction******Self-Metathesis******Secondary Metathesis***

Side reactions that would reduce product selectivity include self-metathesis and secondary metathesis.<sup>6</sup> Self-metathesis occurs when the substrate-bound catalyst reacts with another



substrate molecule rather than ethylene, thereby yielding another internal olefin and ruthenium alkylidene species. Secondary metathesis involves further cross-metathesis of two desired terminal olefins to generate an internal olefin and release ethylene. Because the key steps involve propagation via a ruthenium methylidene, catalyst stability as a propagating methylidene is essential for viable ethenolysis reactions.

**Scheme 4.2.** Ethenolysis of methyl oleate.



A variety of ruthenium metathesis catalysts have been screened for kinetic selectivity for the ethenolysis of internal olefins (Figure 4.1).<sup>14</sup> Phosphine-based ruthenium catalysts (**4.1** and **4.2**, Figure 4.1) show high initial selectivity, where selectivity is defined as the percentage of the product mixture that is the desired olefin products **4.8** and **4.9**, for the ethenolysis of methyl oleate (Scheme 4.2). However, these complexes decompose due to the instability of the propagating methylidene species, resulting in a limited catalyst lifetime. Complex **4.1** catalyzes the ethenolysis of methyl oleate (**4.7**), with 93% selectivity for ethenolysis products **4.8** and **4.9** over self-metathesis products **4.10** and **4.11**. The yield (54%) is moderate, although the TON (5400) is good. The first generation chelate catalyst **4.2** improves selectivity slightly to 94%, but the yield (48%) and TON (4800) are lower.<sup>14</sup> Catalyst inhibition by ethenolysis products is reported for the first generation ruthenium

catalysts, and instability of the methylidene undermines the use of these catalysts.<sup>6,7</sup> Phoban ruthenium catalysts are reported to have some increased stability relative to first generation catalysts, while maintaining comparable selectivities and TONs.<sup>15</sup>

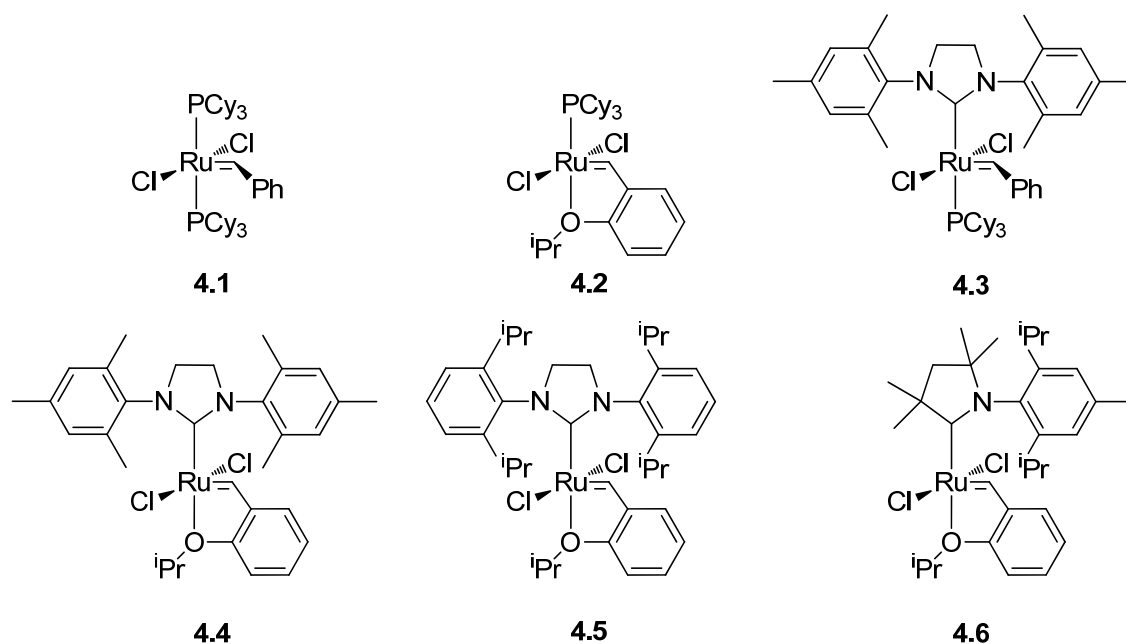


**Figure 4.1.** Example ruthenium catalysts previously studied for ethenolysis reactions.

NHC ruthenium catalysts are known to be very active for self-metathesis and cross-metathesis of methyl oleate with 2-butene (TON of up to 470,000).<sup>14,16</sup> These complexes propagate primarily as an alkylidene. Accordingly, the selectivity of these complexes (**4.3-4.5**, Figure 4.1) for the production of terminal olefins **4.8** and **4.9** is poor. It has been reported that complex **4.3** exhibits only 44% selectivity for ethenolysis products **8** and **9** with 28% yield at a TON of 2,800. Catalyst **4.4** was shown to display even lower selectivity at 33% and only 20% yield with a TON of 2,000. However, increasing the temperature from 40 °C to 60 °C improved the selectivity to 47% and the yield to 32%, with a TON of 3,200. More sterically hindered NHC ligands also improved selectivity.

Complex **4.5** afforded ethenolysis products **4.8** and **4.9** in 55% selectivity over **4.10** and **4.11**, with 38% yield and a TON of 3,800.<sup>16</sup> While *N*-aryl, *N*-aryl NHC-based ruthenium catalysts are generally more active and stable than first generation catalysts, they are significantly less selective for ethenolysis due to their propensity toward undergoing self-metathesis reactions.

Cyclic (alkyl)(amino)carbene (CAAC) ruthenium catalysts, such as **4.6**, have been found to be more selective for ethenolysis products over self-metathesis products, although improvements in selectivity, activity, and catalyst stability are still necessary for the reaction to be viable.<sup>6</sup> With complex **4.6**, selectivities as high as 92% have been achieved at 100 ppm loading, with 56% yield and a TON of 5600. Changing the isopropyl aryl substituents to ethyl substituents improved the TON to 35,000 at 10 ppm loading, although the selectivity was reduced to 83% and the yield to 35%. These complexes are unusual in that they exhibit a higher preference for propagation as a methyldiene relative to previously reported NHC-based complexes.<sup>17</sup>

Previous work studying degenerate metathesis reactions has demonstrated that greater catalyst preference for a methyldiene species appears to be related to selectivity for degenerate metathesis over productive metathesis.<sup>17</sup> Therefore, degenerate metathesis studies can be used as a means of identifying promising catalysts for ethenolysis reactions. For instance, CAAC catalysts, such as **4.6**, exhibit higher degenerate turnovers than **4.1**-**4.5**. Interestingly, unsymmetrical *N*-aryl, *N*-alkyl NHC catalysts show even higher non-productive turnovers to productive turnovers relative to CAAC-type NHC catalysts.<sup>17</sup> This led us to believe that these catalysts would show promising ethenolysis selectivity, with the

propensity to propagate as a methyldiene providing the desired kinetic selectivity for terminal olefin products over thermodynamically favored internal olefins.

The unusual stability of unsymmetrical *N*-aryl, *N*-alkyl NHC catalysts toward propagation as a methyldiene species and their application as catalysts for highly selective ethenolysis is described herein. These complexes exhibit good activity and are unusually stable to methyldiene propagation relative to previously reported NHC-based catalysts. Most of the catalysts also display good thermal stability, and all are stable to air and moisture. In comparison to standard NHC and phosphine derived ruthenium catalysts, these complexes exhibit longer lifetimes in cross-metathesis reactions, presumably as a result of their stability as the methyldiene.

## Results and Discussion

With the goal of improving both selectivity and TON during ethenolysis reactions, a variety of *N*-aryl, *N*-alkyl NHC complexes bearing different ligand substituents were designed and synthesized (Figure 4.2). Complex **4.12** was designed first to enhance the ethenolysis selectivity through increased steric bulk of the *N*-aryl, and primarily, the *N*-alkyl substituent. Initial screening of catalyst **4.12** for the ethenolysis of methyl oleate afforded promising results (Table 4.1, entry 4.1). At 150 psi of ethylene and 40 °C, 86% selectivity for ethenolysis products **4.8** and **4.9** over cross-metathesis products **4.10** and **4.11** was achieved, with 46% yield of **4.8** and **4.9** in 6 hours and a TON of 4,620 at a low catalyst loading of 100 ppm. The yield increased to 68% of ethenolysis products at a loading of 500 ppm, although the TON was reduced to 1,370. Lowering the loading of **4.12** to 10 ppm gave a significantly higher TON of 8,340, although the yield of **4.8** and **4.9** was



Complexes **4.12-4.21** were all compared for catalytic activity for the ethenolysis of methyl oleate at 100 ppm catalyst loading and 150 psi of ethylene (Table 4.1). Complex **4.13** exhibited lower kinetic selectivity compared to **4.12** (Table 4.1, entry 4.1), with 77% selectivity for **4.8** and **4.9** over **4.10** and **4.11** (Table 4.1, entry 4.2), presumably due to the decreased sterics of the *N*-aryl substituent (mesityl in complex **4.13** versus di-isopropyl in complex **4.12**). The TON was lower for **4.13** in comparison to **4.12** as well, likely a result of greater instability of **4.13** as a propagating methyldiene species. Catalyst **4.14** was very unstable and degraded early during the reaction, affording low conversion. Since the reaction equilibrium was not reached due to the catalyst's fast decomposition, the selectivity of **4.14** and is not reported. Crystal structures of complexes **4.12** and **4.15** confirmed that their bond lengths are consistent with previously reported NHC ruthenium complexes (Figures 4.3 and 4.4).

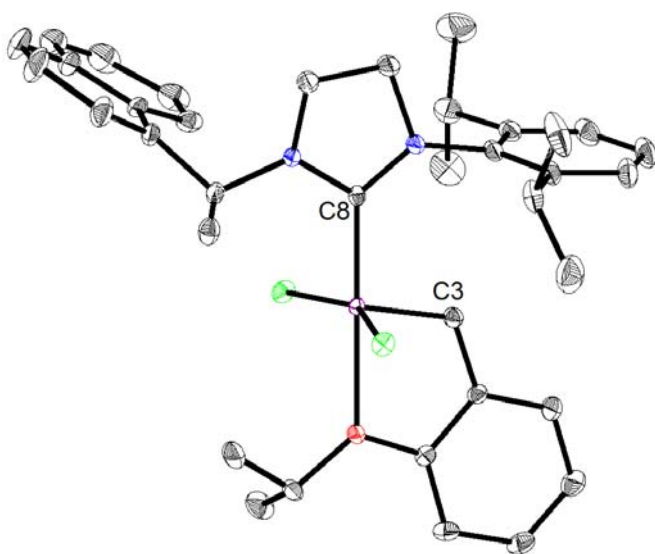


**Figure 4.3.** Crystal structure of complex **4.12** shown at the 50% ellipsoid probability level. Selected bond lengths: Ru-C3 = 1.83 Å, Ru-C8 = 1.98 Å, Ru-O = 2.26 Å.

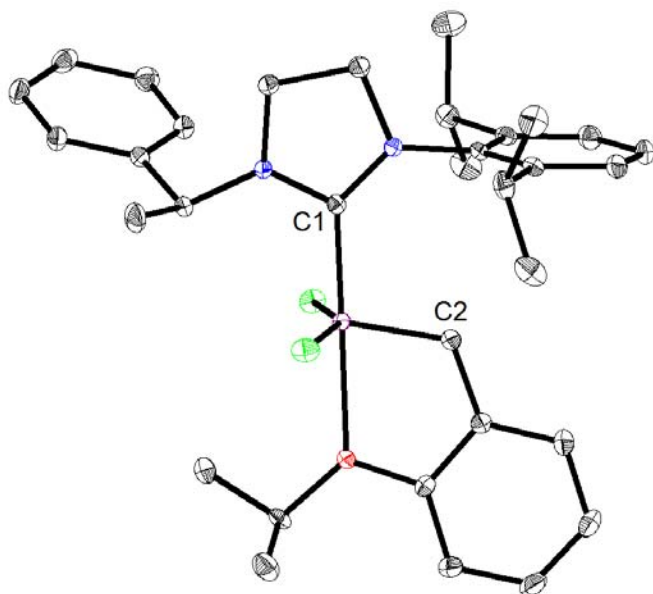


**Figure 4.4.** Crystal structure of complex **4.15** at the 50% ellipsoid probability level. Selected bond lengths: Ru-C2 = 1.83 Å, Ru-C1 = 1.97 Å, Ru-O = 2.28 Å.

The kinetic selectivities of **4.12**, **4.15**, and **4.16** were identical (86% for **4.8** and **4.9** over **4.10** and **4.11**), revealing that small changes in the sterics of the alkyl substituents do not have a significant impact on catalyst selectivity (Table 4.1, entries 4.1, 4.3, and 4.4). The more sterically demanding ligand substituents of **4.17** and **4.18** did slightly improve kinetic selectivity (Table 4.1, entries 4.5 and 4.6). High selectivities of 87% and 89% for **4.17** and **4.18**, respectively, were obtained, and both **4.17** and **4.18** displayed good TONs at 5,070 and 4,600, respectively. Catalyst **4.19** showed excellent kinetic selectivity at 95%, markedly higher than other reported ruthenium NHC catalysts and comparable to first generation ruthenium catalysts (Table 4.1, entry 4.7). Catalysts **4.20** and **4.21** both gave lower selectivity compared to the catalysts with a di-isopropyl *N*-aryl group on the NHC, as expected from the results with **4.13** and **4.14**. The selectivities of **4.20** and **4.21** were 69% and 79%, respectively (Table 4.1, entries 4.8 and 4.9). The yield (40%) and TON (3,080) of **4.21** were significantly better than that of **4.20** and **4.13**.

**Table 4.1.** Catalyst comparison for the ethenolysis of methyl oleate.

Entry <sup>a</sup>	Catalyst	% Conv. <sup>b</sup>	% Selectivity <sup>c</sup>	% Yield <sup>d</sup>	TON <sup>e</sup>
1	4.12	54	86	46	4620
2	4.13	11	77	9	845
3	4.15	52	86	45	4450
4	4.16	42	86	36	3600
5	4.17	59	87	51	5070
6	4.18	52	89	46	4604
7	4.19	15	95	15	1460
8	4.20	17	69	11	1120
9	4.21	40	79	31	3080

<sup>a</sup>The reactions were run neat for 6 hours at 40 °C and 150 psi of ethylene. The catalyst loading was 100 ppm.

<sup>b</sup>Conversion =  $100 - [(final \text{ moles of } \mathbf{4.7}) \times 100 / (initial \text{ moles of } \mathbf{4.7})]$ . <sup>c</sup>Selectivity = (moles of ethenolysis products **4.8** and **4.9**)  $\times 100 /$  (moles of total products **4.8** + **4.9** + **4.10** + **4.11**). <sup>d</sup>Yield = (moles of ethenolysis products **4.8** + **4.9**)  $\times 100 /$  (initial moles of **4.7**). <sup>e</sup>TON = yield  $\times [(moles \text{ of } \mathbf{4.7}) / (moles \text{ of catalyst})]$ .

Comparison of the various complexes screened shows a consistent trend that both *N*-aryl and *N*-alkyl groups with more sterically hindering substituents improve selectivity. Catalyst **4.19**, with the most sterically hindered *N*-alkyl ligand gave the best selectivity, and complexes with a di-isopropyl *N*-aryl group consistently gave significantly better selectivities than complexes with a mesityl *N*-aryl group. Additionally, di-isopropyl *N*-aryl groups enhance catalyst stability, leading to better product yields. This is believed to be due to slower decomposition of di-isopropyl *N*-aryl complexes. Since catalysts with more sterically hindered ligands also were less active, a balance in complex structure accounting for sterics leading to high selectivity but lower activity was targeted. Subsequent efforts were directed toward exploring catalyst loadings for the more promising catalysts for the ethenolysis of methyl oleate, with the objectives of improving yields, exploring low loadings, and establishing that selectivity is independent of catalyst loading (Table 4.2).



**Table 4.2.** Ethenolysis of methyl oleate using different catalyst loadings.

Entry <sup>a</sup>	Catalyst	Cat./MO (ppm)	Time (h)	Conv. (%) <sup>b</sup>	Selectivity (%) <sup>c</sup>	Yield (%) <sup>d</sup>	TON <sup>e</sup>
1	4.19	500	6	48	95	46	913
2	4.19	100	6	15	95	15	1460
3	4.19	50	6	5	96	5	1010
4	4.17	500	6	89	88	78	1570
5	4.17	100	6	59	87	51	5070
6	4.17	50	2	12	86	10	2050
7	4.16	500	2	83	86	72	1440
8	4.16	100	6	42	86	36	3600
9	4.16	50	6	12	87	10	2010
10	4.21	500	4	65	82	53	1060
11	4.21	100	6	40	79	31	3080
12	4.21	50	6	19	79	14	2880
13	4.21	20	2	4	80	3	1680
14	4.14	500	6	70	58	41	817
15	4.18	500	6	86	88	76	1520

<sup>a</sup>The reactions were run neat at 40 °C and 150 psi of ethylene. <sup>b</sup>Conversion =  $100 - [(final \text{ moles of } \mathbf{4.7}) \times 100 / (initial \text{ moles of } \mathbf{4.7})]$ . <sup>c</sup>Selectivity =  $(\text{moles of ethenolysis products } \mathbf{4.8} \text{ and } \mathbf{4.9}) \times 100 / (\text{moles of total products } \mathbf{4.8} + \mathbf{4.9} + \mathbf{4.10} + \mathbf{4.11})$ . <sup>d</sup>Yield =  $(\text{moles of ethenolysis products } \mathbf{4.8} + \mathbf{4.9}) \times 100 / (\text{initial moles of } \mathbf{4.7})$ . <sup>e</sup>TON =  $\text{yield} \times [(\text{moles of } \mathbf{4.7}) / (\text{moles of catalyst})]$ .

Raising the catalyst loading to 500 ppm showed significant improvement in yield, more than doubling it in many cases, for the same given amount of time. Specifically, going from a loading of 100 ppm to 500 ppm of **4.19** increased the ethenolysis product yield from 15% to 46% (Table 4.2, entries 4.1 and 4.2). Alternatively, lowering the catalyst loading to 50 ppm decreased the yield from 15% to 5% (Table 4.2, entry 4.3). Similar results were obtained for the other catalysts upon varying catalyst loading. Complex **4.17**, at 500 ppm loading, generated an ethenolysis product yield of 78% (Table 4.2, entry 4.4), compared to 51% at 100 ppm (Table 4.2, entries 4.5). Analogously, **4.16** gave ethenolysis yields of 72%

at 500 ppm (Table 4.2, entry 4.7), compared to 36% yield at 100 ppm (Table 4.2, entry 4.8). Conversion of methyl oleate increases with increasing catalyst loading, as demonstrated with **4.21** (Table 4.2, entries 4.10-4.13). Complexes **4.14** and **4.18** have markedly higher ethenolysis product yields at 500 ppm as well (Table 4.2, entries 4.14 and 4.15). While the selectivities remain constant at variable catalyst loading for most complexes, catalyst **4.14** shows increased selectivity at a 500 ppm loading compared to a 100 ppm loading (58% versus 19%). This is believed to be due to higher loading of catalyst **4.14** enabling it to come closer to its inherent selectivity for the reaction before it decomposes. Previous reported ruthenium metathesis catalyst studies have shown that having an ortho-H on the *N*-aryl ring increases the rate of catalyst decomposition.

Temperature-dependent studies were conducted using catalysts **4.17** and **4.16** to consider the effect of temperature on selectivity and TON (Table 4.3). Ethenolysis of methyl oleate was carried out at 40 °C, 50 °C, and 60 °C for each catalyst. The TON for both **4.17** and **4.16** increased at higher reaction temperatures, as did the product yield. A reaction temperature of 60 °C likely induces earlier catalyst decomposition, and may account for the lower TON and yield for **4.16** at 60 °C compared to 50 °C (Table 4.3, entry 4.6). For both catalysts, the more significant increase in TON and yield occurred in going from 40 °C to 50 °C, indicating that a further increase in temperature produces only minimal benefits, and may in fact initiate faster catalyst decomposition. The selectivity was noticeably reduced at higher temperatures, dropping from 87% to 81% for **4.17** and 86% to 81% for **4.16**, in going from 40 °C to 50 °C. The reduction in selectivity between 50 °C and 60 °C, however, was minimal. Ethenolysis reactions were not run below 40 °C as this would decrease both

the yield, undermining the catalysts' utility. Accordingly, 40 °C was determined to be the optimal temperature for the ethenolysis of methyl oleate catalyzed by these complexes.

**Table 4.3.** Temperature effects on the ethenolysis of methyl oleate.

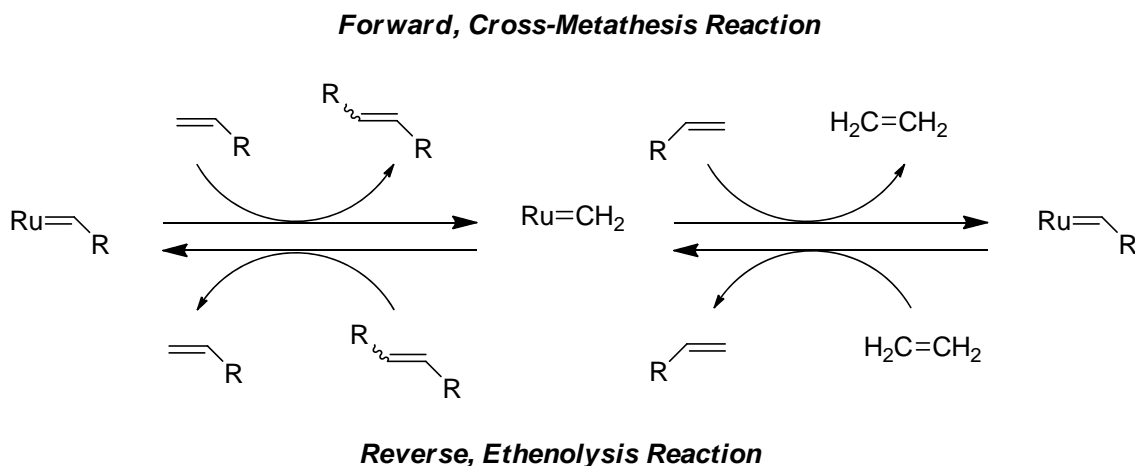
Entry <sup>a</sup>	Catalyst	Temp. (°C)	Time (h)	Conv. (%) <sup>b</sup>	Selectivity (%) <sup>c</sup>	Yield (%) <sup>d</sup>	TON <sup>e</sup>
<b>1</b>	<b>4.17</b>	40	6	59	87	51	5070
<b>2</b>	<b>4.17</b>	50	4	67	81	55	5460
<b>3</b>	<b>4.17</b>	60	4	68	81	55	5470
<b>4</b>	<b>4.16</b>	40	6	42	86	36	3600
<b>5</b>	<b>4.16</b>	50	6	51	81	41	4090
<b>6</b>	<b>4.16</b>	60	6	47	79	37	3680

<sup>a</sup>The reactions were run neat at 150 psi of ethylene. The catalyst loading was 100 ppm. <sup>b</sup>Conversion =  $100 - [(final\ moles\ of\ 4.7) \times 100 / (initial\ moles\ of\ 4.7)]$ . <sup>c</sup>Selectivity =  $(moles\ of\ ethenolysis\ products\ 4.8\ and\ 4.9) \times 100 / (moles\ of\ total\ products\ 4.8 + 4.9 + 4.10 + 4.11)$ . <sup>d</sup>Yield =  $(moles\ of\ ethenolysis\ products\ 4.8 + 4.9) \times 100 / (initial\ moles\ of\ 4.7)$ . <sup>e</sup>TON =  $yield \times [(moles\ of\ 4.7) / (moles\ of\ catalyst)]$ .

In order to evaluate catalyst propensity toward ethenolysis, a qualitative steady-state study was conducted to complement the ethenolysis results obtained. Observed selectivity in ethenolysis reactions is believed to arise from a catalyst's preference for the pathway favoring terminal olefins, manifested in its lack of cross-metathesis reactivity. This preference can be reflected in cross-metathesis reactions as well, where if ethylene generated by cross-metathesis of two terminal olefins is trapped in the reaction vessel, the forward cross-metathesis reaction will eventually reach a steady-state with ethenolysis of the internal olefin products with the generated ethylene, which affords the original terminal olefins (Scheme 4.3). Accordingly, relative preferences of different catalysts for terminal olefin versus internal olefin distributions can be determined by identifying the point at which the forward cross-metathesis reaction is equal to the reverse ethenolysis reaction. This will be observed when the conversion to internal olefin product no longer increases

(the steady-state has been reached) and requires that the catalyst is still active and undergoing metathesis turnovers. This method provides a qualitative means for comparing a given catalyst to others and determining its preference for forming terminal olefins (and similarly methylidene propagation) relative to the set of catalysts screened.

**Scheme 4.3.** Steady-state between cross-metathesis and ethenolysis.



For ease of measurement, homodimerization cross-metathesis was chosen as the model reaction, since the only possible product is the internal olefin dimer of the substrate. The reactions were carried out in a sealed NMR tube, preventing loss of generated ethylene, and the steady-state concentrations of cross-metathesis and ethenolysis products for each catalyst was measured. Although this setup does not yield absolute steady-state values, as the ethylene generated will be partitioned between the solution and the NMR tube head space, it does enable qualitative evaluation of relative steady-states for catalysts screened. The degree of conversion to CM product was evaluated for catalysts **4.17**, **4.19**, and second generation catalyst **4.4** in order to assess their relative propensities to undergo CM as compared to ethenolysis. Phosphine-based ruthenium catalyst **4.1** was also screened during

these experiments; however, **4.1** decomposed prior to reaching steady-state between CM and ethenolysis, and the data obtained was therefore not included. Catalysts **4.4**, **4.17**, and **4.19** did not undergo any decomposition during the course of the reaction, as confirmed by monitoring them by proton NMR spectroscopy.

Catalysts **4.4**, **4.17**, and **4.19**, were chosen to represent a range of selectivities for the ethenolysis of methyl oleate, with **4.4** showing a reported 33% selectivity, **4.17** showing 87% selectivity, and **4.19** showing 95% selectivity. In accordance with this data, catalyst **4.19** was predicted to reach steady-state between the forward and reverse reactions at the lowest conversion to CM product (higher preference for yielding ethenolysis products), and catalyst **4.4** was predicted to reach steady-state at the highest conversion to CM product. Catalyst **4.17** was expected to have a steady-state point between those of the other two complexes. Two substrates were employed for these experiments. First, the experiment was carried out using 1-hexene (Figure 4.5), and then a duplicate set of experiments were run with allyl chloride (Figure 4.6) to ascertain that the observed results were not substrate specific.

For the CM of 1-hexene and corresponding ethenolysis of 5-decene (Figure 4.5), the resulting relative steady-state values were as expected, with catalyst **4.19** showing the highest selectivity for 1-hexene (only 7 % conversion to 5-decene once steady-state was reached), relative to the other catalysts, and catalyst **4.4** showing the lowest selectivity for 1-hexene, indicated by it producing the greatest conversion to 5-decene (38% conversion) at its steady-state point. Catalyst **4.17** reached steady-state at 22% conversion of 1-hexene, in between that of **4.19** and **4.4**.

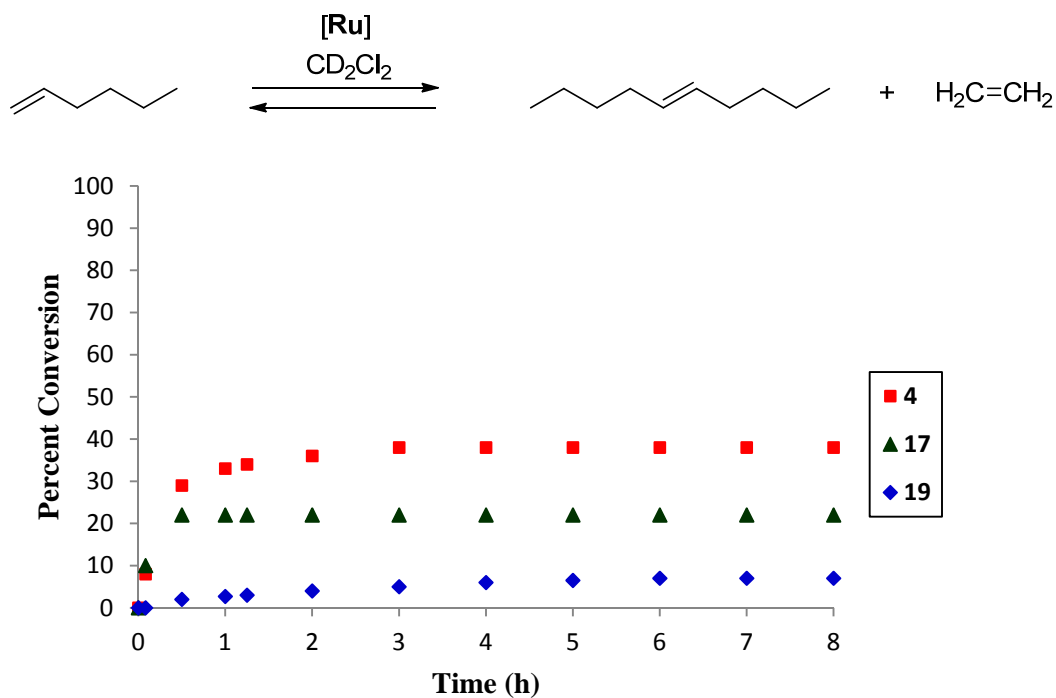


**Figure 4.5.** Steady-state between CM of 1-hexene and ethenolysis of 5-decene.

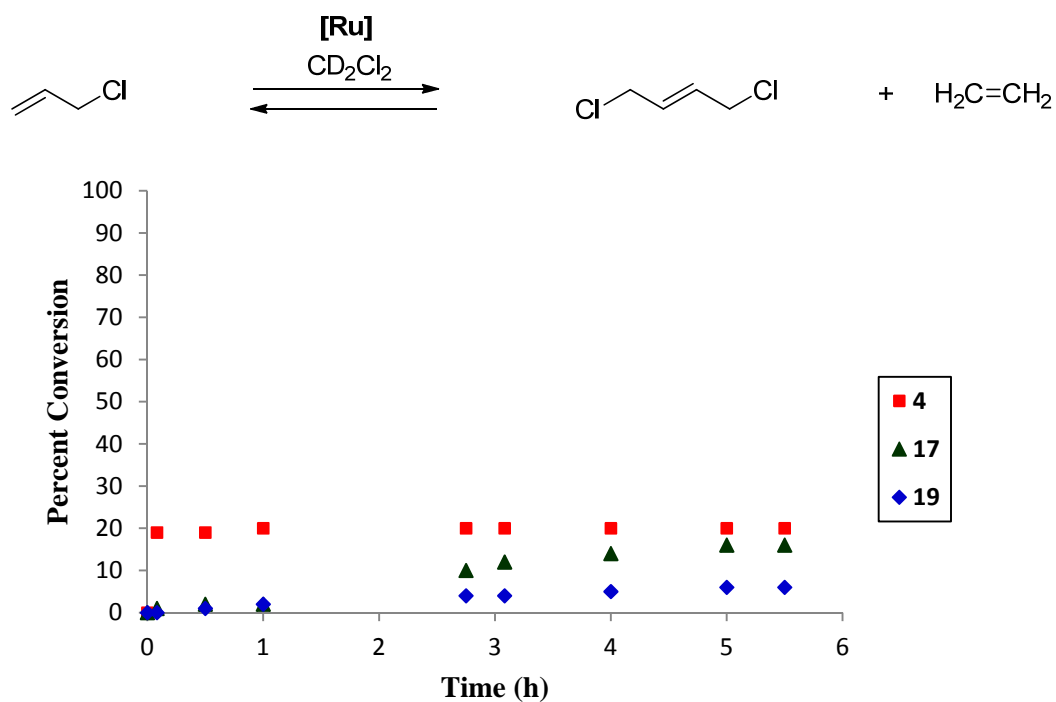


**Figure 4.6.** Steady-state between CM of allyl chloride and ethenolysis of 1,4-dichloro-2-butene.

When allyl chloride was used as the substrate (Figure 4.6), the same relative order of steady-state points was obtained for the catalysts studied. The data from both experiments corroborate the results found in the ethenolysis of methyl oleate, with **4.19** exhibiting the greatest preference for kinetic over thermodynamic products, and this class of *N*-aryl, *N*-alkyl catalysts showing greater preference for kinetic products than previous NHC-based ruthenium catalysts.

## Conclusion

We have developed highly selective *N*-aryl, *N*-alkyl NHC ruthenium catalysts for ethenolysis, with **4.19** exhibiting the highest selectivity for an NHC-based ruthenium metathesis catalyst to date. Catalyst loadings of 500 ppm afforded good yields of the ethenolysis products **4.8** and **4.9**. The TONs were modest for most of the catalysts screened, and future studies will be directed toward improving catalyst lifetime. These catalysts show unusual preference for generating kinetic products over thermodynamic products, believed to be controlled primarily through the NHC ligand sterics. Increasing the sterics of the NHC substituents enhances selectivity and, in general, improves stability as well, although a limit is reached where NHC ligands bearing extremely bulky substituents inhibit reactivity. The catalysts maintained good stability toward existing as a propagating methylenide species, making them attractive as catalysts for ethenolysis reactions. High selectivities, a challenging feature of ethenolysis reactions, were obtained for many of the complexes of this class of *N*-aryl, *N*-alkyl NHC catalysts.

## Experimental Section

### General considerations

All manipulations of air- or water-sensitive compounds were carried out under dry nitrogen using a glovebox or under dry argon utilizing standard Schlenk line techniques.  $^1\text{H}$  and  $^{13}\text{C}$  NMR spectra were recorded on a Varian Mercury ( $^1\text{H}$ , 300 MHz), a Varian Inova 400 ( $^1\text{H}$ , 400 MHz), a Varian Inova 500 ( $^1\text{H}$ , 500 MHz;  $^{13}\text{C}$ , 125 MHz), or an automated Varian Inova 500 ( $^1\text{H}$ , 500 MHz;  $^{13}\text{C}$ , 125 MHz) spectrometer and chemical shifts are reported in ppm downfield from  $\text{Me}_4\text{Si}$  by using the residual solvent peak as an internal standard. High resolution mass spectrometry (FAB) was done at the California Institute of Technology Mass Spectrometry Facility. X-ray crystallographic structures were obtained at the Beckman Institute X-ray Crystallography Laboratory at the California Institute of Technology.

### Materials

Deuterated methylene chloride was dried over calcium hydride and vacuum distilled, followed by three cycles of freeze-pump-thawing. Methyl oleate (>99%) was obtained from Nu-Chek-Prep (Elysian, MN) and stored over activated alumina. Prior to use, 1-hexene was dried over calcium hydride, vacuum distilled, and freeze-pump-thawed. Allyl chloride (99%) was purchased from Aldrich and used as received. Toluene and benzene were dried by passage through solvent purification systems.<sup>20</sup> Ruthenium precursors  $\text{RuCl}_2(\text{PCy}_3)(=\text{CH}-o\text{-O}^i\text{Pr}-\text{C}_6\text{H}_4)$  and  $\text{RuCl}_2(\text{PCy}_3)_2(=\text{CHPh})$  were received from Materia, Inc. All other reagents and solvents were used as purchased without further purification.



### **Procedure for the ethenolysis of methyl oleate**

Ethenolysis reactions were carried out using research-grade methyl oleate (>99%) that was purified by storage over activated alumina followed by filtration. The experiments were set up in a glove box under an atmosphere of argon. Methyl oleate was charged in a Fisher-Porter bottle equipped with a stir bar. A solution of ruthenium catalyst of an appropriate concentration was prepared in dry dichloromethane, and the desired volume of this solution was added to the methyl oleate. The head of the Fisher-Porter bottle was equipped with a pressure gauge and a dip-tube was adapted on the bottle. The system was sealed and taken out of the glove box to the ethylene line. The vessel was then purged with ethylene (polymer purity 99.9% from Matheson Tri Gas) for 5 minutes, pressurized to 150 psi, and placed in an oil bath at 40 °C. The reaction was monitored by collecting samples via the dip-tube at different reaction times. Prior to GC analysis, the reaction aliquots were quenched by adding a 1.0 M isopropanol solution of tris-(hydroxymethyl)phosphine (THMP) to each vial over the course of 2-3 hours. The samples were then heated for over an 1 hour at 60 °C, diluted with distilled water, extracted with hexanes and analyzed by gas chromatography (GC). The GC analyses were run using a flame ionization detector. Column: Rtx-5 from Restek (30 m × 0.25 mm (i.d.) × 0.25 µm film thickness. GC and column conditions: injection temperature, 250 °C; detector temperature, 280 °C; oven temperature, starting temperature, 100 °C; hold time, 1 min. The ramp rate was 10 °C/min to 250 °C, and the temperature was then held at 250 °C for 12 min. Carrier gas: Helium.

### **Cross-metathesis of 1-hexene/ ethenolysis of 5-decene steady-state experiments**

In a glovebox under a nitrogen atmosphere, 0.5 mL of dry  $\text{CD}_2\text{Cl}_2$  was added to an 8-inch NMR tube. 1-Hexene (18.9  $\mu\text{L}$ , 0.149 mmol) was added via a 25  $\mu\text{L}$  syringe, and the NMR tube was sealed with a septum cap. The appropriate amount of ruthenium catalyst (3 mol%) was added to a GC vial and dissolved in 0.25 mL of  $\text{CD}_2\text{Cl}_2$ . The GC vial was capped and brought out of the glovebox along with the NMR tube. An  $^1\text{H}$  NMR spectrum (Varian 500 MHz Spectrometer) was taken of the 1-hexene solution for time point  $t = 0$ , and the catalyst solution was subsequently injected into the NMR tube via syringe through the septum cap. The septum cap was wrapped with parafilm, and the reaction progress was monitored over time by  $^1\text{H}$  NMR spectroscopy. Catalyst stability was monitored by following the ruthenium benzylidene  $H$  peak over time, since catalyst decomposition causes the benzylidene  $H$  peak to shift or disappear altogether. Conversion of 1-hexene to 5-decene was determined by relative integration of the allylic  $\text{CH}_2$  protons of 5-decene to those of 1-hexene.  $^1\text{H}$  NMR of 1-hexene ( $\text{CD}_2\text{Cl}_2$ , 500 MHz):  $\delta$  5.83 (ddt,  $J = 17.0, 10.2, 6.7$  Hz, 1H), 5.02 – 4.96 (m, 1H), 4.92 (ddt,  $J = 10.2, 2.3, 1.2$  Hz, 1H), 2.08 – 2.02 (m, 2H) [ $\text{CH}_2$ ], 1.40 – 1.28 (m, 4H), 0.91 (t,  $J = 5.0$  Hz, 3H) ppm.  $^1\text{H}$  NMR of 5-decene ( $\text{CD}_2\text{Cl}_2$ , 500 MHz):  $\delta$  5.43 – 5.38 (m, 1H), 2.00 – 1.91 (m, 2H) [ $\text{CH}_2$ ], 1.34 – 1.28 (m, 4H), 0.90 (t,  $J = 5.0$  Hz, 3H) ppm.

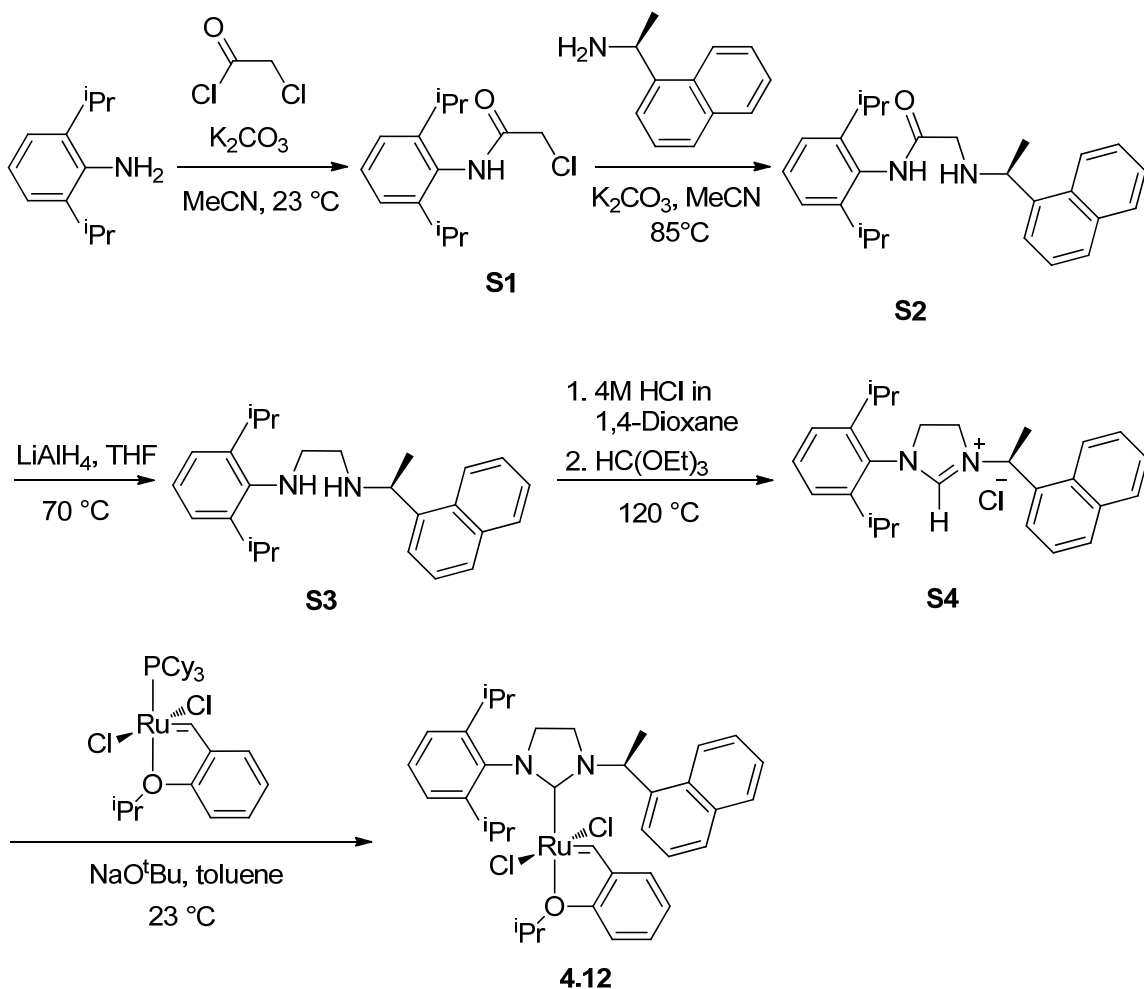
### **Cross-metathesis of allyl chloride/ ethenolysis of 1,4-dichloro-2-butene steady-state experiments**

In a glovebox under a nitrogen atmosphere, 0.5 mL of dry  $\text{CD}_2\text{Cl}_2$  was added to an 8-inch NMR tube, and the NMR tube was sealed with a septum cap. The appropriate amount of

ruthenium catalyst (3 mol%) was added to a GC vial and dissolved in 0.25 mL of  $\text{CD}_2\text{Cl}_2$ . The GC vial was capped and brought out of the glovebox along with the NMR tube. Allyl chloride (12.2  $\mu\text{L}$ , 0.150 mmol) was added via a 25  $\mu\text{L}$  syringe through the septum cap, which was then wrapped with parafilm.  $^1\text{H}$  NMR spectrum (Varian 500 MHz Spectrometer) was taken of the allyl chloride solution for time point  $t = 0$ , and the catalyst solution was subsequently injected into the NMR tube via syringe through the septum cap. The reaction progress was monitored over time by  $^1\text{H}$  NMR spectroscopy. Catalyst stability was monitored by following the ruthenium benzylidene  $H$  peak over time, since catalyst decomposition causes the benzylidene  $H$  to shift or disappear altogether. Conversion of allyl chloride to 1,4-dichloro-2-butene was determined by relative integration of the vinyl  $\text{H}_2\text{C}=\text{CHCH}_2\text{Cl}$  proton of allyl chloride to the vinyl  $\text{ClCH}_2\text{CH}=\text{CHCH}_2\text{Cl}$  protons of 1,4-dichloro-2-butene.  $^1\text{H}$  NMR of allyl chloride ( $\text{CD}_2\text{Cl}_2$ , 500 MHz):  $\delta$  5.98 (ddt,  $J = 10.0, 8.7, 6.6$  Hz, 1H), 5.35 (ddd,  $J = 16.9, 2.5, 1.3$  Hz, 1H), 5.21 (ddd,  $J = 10.1, 2.0, 0.9$  Hz, 1H), 4.09 – 4.05 (m, 2H) ppm.  $^1\text{H}$  NMR of 1,4-dichloro-2-butene ( $\text{CD}_2\text{Cl}_2$ , 500 MHz):  $\delta$  5.96 – 5.92 (m, 2H), 4.11 – 4.08 (m, 2H) ppm.

## Catalyst Syntheses

### Synthesis of **4.12**.



The procedure for synthesizing **S1**, **S2**, **S3**, and **S4** was very similar to that outlined in references 18, 19, and 21, with slight modifications.

**Synthesis of S1.** Anhydrous potassium carbonate (112.8 mmol, 15.6 grams) and acetonitrile (150 mL) were added to a 250 mL round bottom flask containing a stir bar. 2,6-Diisopropyl aniline (56.4 mmol, 10.0 mL) was added via syringe with stirring, and

chloroacetyl chloride (56.4 mmol, 4.5 mL) was then added dropwise. The reaction was stirred at room temperature for 43 hours, after which the resulting mixture was filtered through a thin pad of silica gel. The filtrate was concentrated under partial vacuum on a rotary evaporator, and hexanes were added to the obtained cream colored residue. The hexanes dissolved away the off-white color and the remaining white solids were filtered and washed with more hexanes to yield **S1** (11.33 g, 79% yield).  $^1\text{H}$  NMR ( $\text{CDCl}_3$ , 500 MHz):  $\delta$  7.79 (s, 1H), 7.32 (t,  $J$  = 8 Hz, 1H), 7.20 (d,  $J$  = 7 Hz, 2H), 4.27 (s, 2H), 3.02 (sept,  $J$  = 6.5 Hz, 2H), 1.21 (d,  $J$  = 7 Hz, 12H) ppm.  $^{13}\text{C}$  NMR ( $\text{CDCl}_3$ , 125 MHz):  $\delta$  165.45, 146.16, 130.12, 129.00, 123.83, 43.02, 29.08, 23.82 ppm.

Synthesis of **S2**. Anhydrous potassium carbonate (40.9 mmol, 5.65 grams) and **S1** (20.4 mmol, 5.19 g) were added to a 250 mL round bottom flask containing a stir bar. Acetonitrile (100 mL) was added, followed by (*S*)-(-)-1-(1-Naphthyl)ethylamine (20.4 mmol, 3.50 g). A reflux condenser was attached to the flask, and the reaction was heated at 85 °C for 37 hours with stirring. The crude reaction mixture was then filtered through a thin pad of silica gel, and the filtrate was concentrated *in vacuo*. The crude solids obtained were then dissolved in diethyl ether and loaded onto a silica gel column for purification (100% diethyl ether as the eluting solvent). Upon concentration of the fractions containing product, **S2** was obtained as a white solid (3.97 g, 50% yield).  $^1\text{H}$  NMR ( $\text{CDCl}_3$ , 500 MHz):  $\delta$  8.64 (s, 1H), 8.16 (d,  $J$  = 8.5 Hz, 1H), 7.92 – 7.88 (m, 1H), 7.80 (d,  $J$  = 8.2 Hz, 1H), 7.62 (d,  $J$  = 6.8 Hz, 1H), 7.56 – 7.43 (m, 3H), 7.28 – 7.26 (m, 1H), 7.16 (d,  $J$  = 7.7 Hz, 2H), 4.78 (q,  $J$  = 6.7 Hz, 1H), 3.59 – 3.42 (m, 2H), 3.02 – 2.85 (m, 2H), 2.20 (s, 1H), 1.63 (d,  $J$  = 6.6 Hz, 3H), 1.15 (d,  $J$  = 6.9 Hz, 6H), 1.13 (d,  $J$  = 6.9 Hz, 6H) ppm.  $^{13}\text{C}$  NMR ( $\text{CDCl}_3$ , 125 MHz):  $\delta$  171.23, 146.03, 139.92, 136.64, 134.01, 131.40, 129.39, 128.34,

128.10, 126.42, 125.86, 125.68, 123.63, 122.80, 50.95, 48.85, 29.09, 23.95, 23.68, 23.54 ppm.

Synthesis of **S3**. In a nitrogen atmosphere glovebox, **S2** (2.10 grams, 5.4 mmol) was added to a 100 mL round bottom flask containing a stir bar, followed by the addition of dry tetrahydrofuran (5 mL). In a separate flask, lithium aluminum hydride (0.820 grams, 21.6 mmol) was weighed out and dry THF (5 mL) was slowly added. This lithium aluminum hydride suspension was then very slowly added to the solution of **S2**, and the round bottom flask was sealed and brought out of the glovebox. The reaction was sealed heated at 70 °C for 5 days. The reaction mixture was then removed from the oil bath and allowed to cool. Water was slowly added to quench and the THF/water mixture was stirred for 3 hours. The mixture was then extracted with methylene chloride (4 x 20 mL). The combined organic layers were dried over MgSO<sub>4</sub> and filtered. Concentration of the filtrate afforded a clear oil. The oil (0.372 g) was a mixture of product **S3** and unreacted starting material **S2** (91% and 9%, respectively). This crude mixture was carried directly on to the next step in the synthesis. <sup>1</sup>H NMR (CDCl<sub>3</sub>, 500 MHz):  $\delta$  8.24 (d,  $J$  = 8.4 Hz, 1H), 7.91 – 7.87 (m, 1H), 7.78 (d,  $J$  = 8.1 Hz, 1H), 7.69 (d,  $J$  = 6.5 Hz, 1H), 7.55 – 7.46 (m, 3H), 7.11 – 7.07 (m, 2H), 7.05 (dd,  $J$  = 8.7, 6.4 Hz, 1H), 4.71 (q,  $J$  = 6.6 Hz, 1H), 3.32 (sept,  $J$  = 6.8 Hz, 2H), 3.03 – 2.94 (m, 2H), 2.91 – 2.81 (m, 2H), 1.56 (d,  $J$  = 6.6 Hz, 3H), 1.23 (d,  $J$  = 6.9 Hz, 6H), 1.21 (d,  $J$  = 6.9 Hz, 6H) ppm.

Synthesis of **S4**. **S3** (0.91 mmol, 0.372 g crude) was transferred to a 50 mL Schlenk tube containing a stir bar. Under an atmosphere of argon on the Schlenk line, 4M HCl in 1,4-dioxane (0.99 mL) was added via syringe through the septum cap. The mixture was stirred

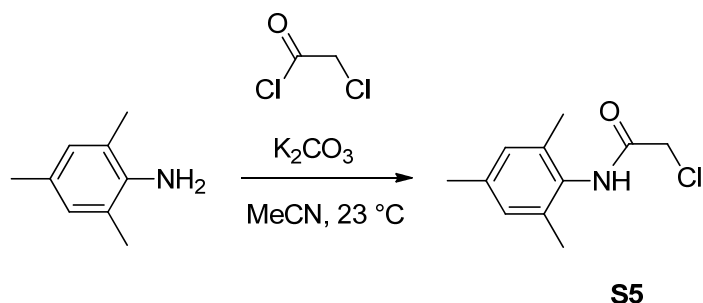
at room temperature for 2 hours. Vacuum was then applied to the Schlenk tube to remove excess HCl and 1,4-dioxane. The Schlenk tube was placed back under an argon atmosphere and anhydrous triethyl orthoformate (9.9 mmol, 1.65 mL) was added via syringe. The schlenk tube was sealed under the argon atmosphere and heated to 120 °C for 18 hours. After allowing the solution to cool, the crude mixture was added to a silica gel column to purify (solvent system 5% MeOH in CH<sub>2</sub>Cl<sub>2</sub>). A white powder (0.244 g, 64% yield) was obtained upon concentrating and drying the fractions containing product. <sup>1</sup>H NMR (CDCl<sub>3</sub>, 500 MHz):  $\delta$  10.00 (s, 1H), 8.55 (d,  $J$  = 8.5 Hz, 1H), 7.92-7.90 (m, 1H), 7.70 (t,  $J$  = 7 Hz, 1H), 7.62 (d,  $J$  = 7 Hz, 1H), 7.58 (d,  $J$  = 7 Hz, 1H), 7.56 (d,  $J$  = 7 Hz, 1H), 7.51 (t,  $J$  = 8 Hz, 1H), 7.38 (t,  $J$  = 8 Hz, 1H), 7.20-7.17 (m, 1H), 6.92 (q,  $J$  = 7 Hz, 1H), 4.25 (dt,  $J$  = 9.5 Hz,  $J$  = 11.5 Hz, 1H), 4.09 (dt,  $J$  = 8.5 Hz,  $J$  = 12 Hz, 1H), 3.94 (dt,  $J$  = 9.5 Hz,  $J$  = 12 Hz, 1H), 3.75 (dt,  $J$  = 8.5 Hz,  $J$  = 12 Hz, 1H), 2.85 (sept,  $J$  = 6.5 Hz, 1H), 2.70 (sept,  $J$  = 6.5 Hz, 1H), 2.05 (d,  $J$  = 6.5 Hz, 3H), 1.26 (d,  $J$  = 3 Hz, 3H), 1.25 (d,  $J$  = 3 Hz, 3H), 1.21-1.18 (m, 3H), 1.12 (d,  $J$  = 7 Hz, 3H) ppm. <sup>13</sup>C NMR (CDCl<sub>3</sub>, 125 MHz):  $\delta$  159.11, 146.63, 134.38, 131.27, 130.44, 129.33, 128.09, 126.83, 125.10, 123.55, 113.28, 100.83, 94.70, 86.57, 53.81, 53.21, 46.00, 29.18, 25.34, 25.13, 24.35, 24.24, 18.54 ppm.

Synthesis of **4.12**. In a nitrogen atmosphere glovebox, **S4** (1.35 mmol, 0.570 g), sodium *tert*-butoxide (2.46 mmol, 0.237 g), and RuCl<sub>2</sub>(PCy<sub>3</sub>)<sub>2</sub>(=CH-*o*-O<sup>*i*</sup>PrC<sub>6</sub>H<sub>4</sub>) (1.23 mmol, 0.740 g) were added to a 100 mL round bottom flask. Dry toluene (15 mL) was added to this mixture and the flask was sealed and brought out of the glovebox. The reaction was stirred at room temperature for 24 hours. The crude mixture was then loaded directly onto a silica gel column. The eluting solvent was 10% diethyl ether in pentane. The product was isolated from a green band that came off of the column. Concentration of fractions from

this green band afforded **4.12** as a dark green powder (0.382 grams, 40% yield).  $^1\text{H}$  NMR ( $\text{CDCl}_3$ , 500 MHz):  $\delta$  16.48 (s, 1H), 8.87 (d,  $J = 8\text{ Hz}$ , 1H), 7.90 (d,  $J = 7\text{ Hz}$ , 1H), 7.85 (d,  $J = 8\text{ Hz}$ , 1H), 7.70 (d,  $J = 7.5\text{ Hz}$ , 1H), 7.60 (t,  $J = 7.5\text{ Hz}$ , 1H), 7.57 – 7.47 (m, 3H), 7.41 – 7.32 (m, 3H), 6.91 (d,  $J = 8.5\text{ Hz}$ , 1H), 6.86 (d,  $J = 4.5\text{ Hz}$ , 2H), 5.11 (sept,  $J = 6\text{ Hz}$ , 1H), 3.86 – 3.78 (m, 4H), 3.52 – 3.46 (m, 1H), 3.33 (sept,  $J = 7\text{ Hz}$ , 1H), 3.20 (sept,  $J = 6.5\text{ Hz}$ , 1H), 2.48 (d,  $J = 7\text{ Hz}$ , 3H), 1.81 (d,  $J = 6\text{ Hz}$ , 3H), 1.64 (d,  $J = 6\text{ Hz}$ , 3H), 1.19 (m, 6H), 1.02 (d,  $J = 7\text{ Hz}$ , 3H), 0.88 – 0.85 (m, 3H) ppm.  $^{13}\text{C}$  NMR ( $\text{CDCl}_3$ , 125 MHz):  $\delta$  211.33, 152.83, 148.72, 148.67, 144.11, 138.37, 137.42, 134.20, 131.60, 129.80, 129.65, 128.89, 128.74, 126.07, 126.01, 125.41, 125.30, 125.17, 124.97, 124.33, 122.55, 122.51, 113.23, 75.26, 55.78, 54.87, 45.95, 28.18, 28.02, 25.98, 25.75, 24.15, 24.08, 22.59, 22.28, 20.39 ppm. High resolution mass spectrometry:  $[\text{C}_{37}\text{H}_{44}\text{Cl}_2\text{N}_2\text{ORu}][\text{M-H}]$  Calc. = 704.1875. Found = 704.1899.

The same synthetic procedure was used for the synthesis of complexes **4.13-4.20**, **4.22**, and **4.23**. Complexes **4.21** and **4.24** were made as discussed below.

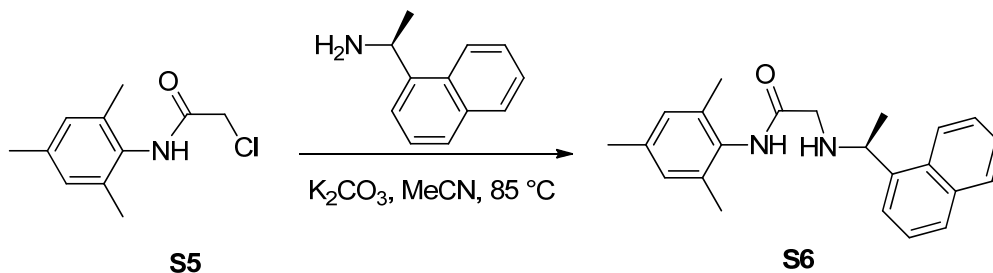
#### Synthesis of **4.13**.



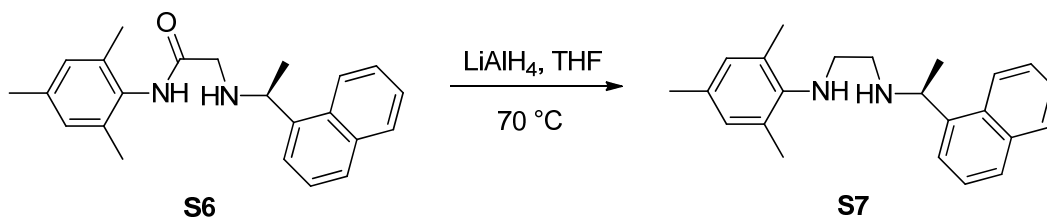
Compound **S5**. The product was isolated as white crystalline needles (25.413 g, 81% yield).  $^1\text{H}$  NMR ( $\text{CDCl}_3$ , 500 MHz):  $\delta$  7.77 (s, 1H), 6.92 (s, 2H), 4.25 (s, 2H), 2.28 (s, 3H),



2.20 (s, 6H) ppm.  $^{13}\text{C}$  NMR ( $\text{CDCl}_3$ , 125 MHz):  $\delta$  164.60, 137.79, 135.20, 130.17, 129.26, 43.02, 21.20, 18.43 ppm.

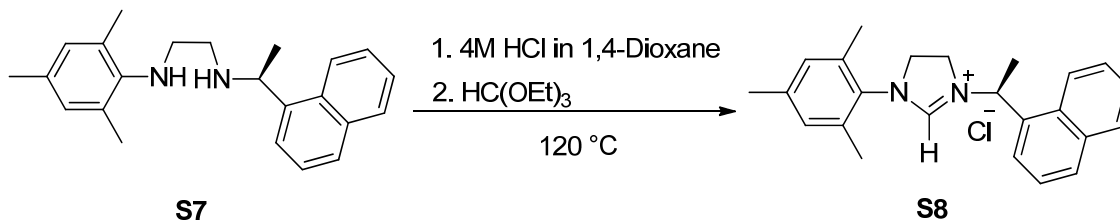


Compound **S6**. The product was isolated as white solids (2.750 g, 60% yield).  $^1\text{H}$  NMR ( $\text{CDCl}_3$ , 500 MHz):  $\delta$  8.60 (s, 1H), 8.17 (d,  $J$  = 8.4 Hz, 1H), 7.93 – 7.88 (m, 1H), 7.80 (d,  $J$  = 8.2 Hz, 1H), 7.62 (d,  $J$  = 6.7 Hz, 1H), 7.56 – 7.47 (m, 3H), 6.89 (s, 2H), 4.88 – 4.70 (m, 1H), 3.48 (q,  $J$  = 17.2 Hz, 2H), 2.27 (s, 3H), 2.13 (s, 6H), 1.63 (d,  $J$  = 6.6 Hz, 3H) ppm.  $^{13}\text{C}$  NMR ( $\text{CDCl}_3$ , 125 MHz):  $\delta$  170.43, 139.97, 136.71, 134.85, 134.10, 131.25, 131.16, 129.16, 128.91, 127.85, 126.21, 125.65, 125.58, 122.74, 54.03, 52.23, 50.69, 23.35, 21.04, 18.49 ppm.

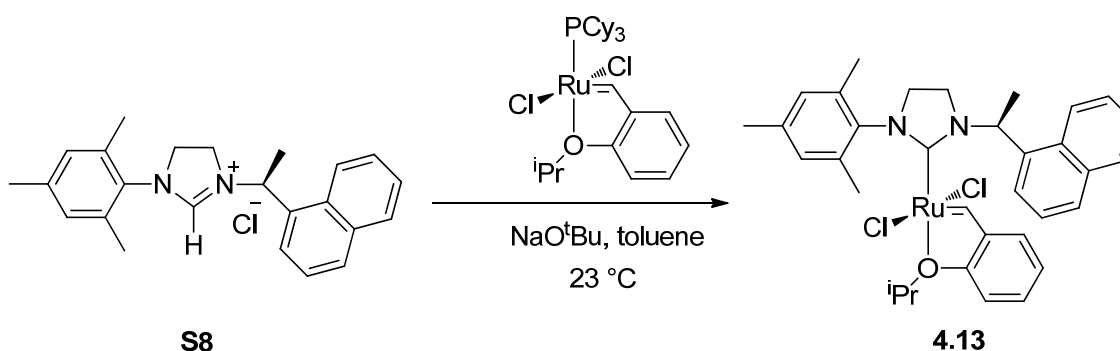


Compound **S7**. The reaction afforded 99% conversion to product (1.015 g of crude mixture isolated). This mixture was carried onto the next step crude without further purification.  $^1\text{H}$  NMR ( $\text{CDCl}_3$ , 500 MHz):  $\delta$  8.23 (d,  $J$  = 8.3 Hz, 1H), 7.89 (m,  $J$  = 7.7, 1.9 Hz, 1H), 7.77 (d,  $J$  = 8.1 Hz, 1H), 7.65 (dd,  $J$  = 7.1, 0.7 Hz, 1H), 7.55 – 7.45 (m, 3H), 6.85 – 6.82 (m,

2H), 4.67 (q,  $J = 6.6$  Hz, 1H), 3.08 – 3.01 (m, 2H), 2.85 – 2.77 (m, 2H), 2.27 (s, 6H), 2.25 – 2.22 (m, 3H), 1.54 (d,  $J = 6.6$  Hz, 3H) ppm.



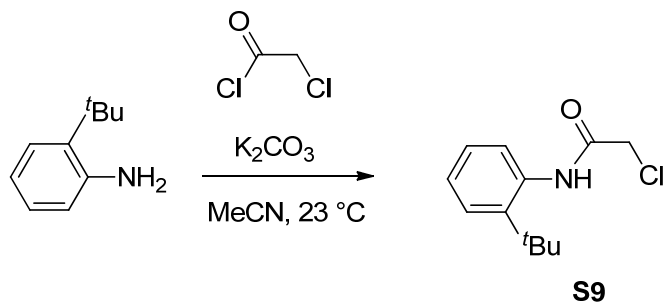
Compound **S8**. The product was purified by silica gel column chromatography (10% MeOH in  $\text{CH}_2\text{Cl}_2$ ) and isolated as a cream powder. Yield = 23% (0.582 g).  $^1\text{H}$  NMR ( $\text{CDCl}_3$ , 500 MHz):  $\delta$  10.10 (s, 1H), 8.51 (d,  $J = 8.4$  Hz, 1H), 7.69 – 7.66 (m, 2H), 7.62 (d,  $J = 6.5$  Hz, 1H), 7.58 – 7.55 (m, 2H), 7.52 (dd,  $J = 8.1, 7.2$  Hz, 1H), 6.91 (s, 2H), 6.76 – 6.73 (m, 1H), 4.17 – 4.02 (m, 2H), 4.00 – 3.87 (m, 1H), 3.73 – 3.62 (m, 1H), 2.30 (s, 3H), 2.27 (s, 3H), 2.23 (s, 3H), 2.05 (d,  $J = 6.8$  Hz, 3H) ppm.  $^{13}\text{C}$  NMR ( $\text{CDCl}_3$ , 125 MHz):  $\delta$  159.24, 140.41, 135.34, 134.26, 132.32, 131.11, 130.89, 130.26, 130.14, 129.29, 127.93, 126.71, 125.29, 124.77, 123.40, 53.84, 50.77, 45.99, 21.16, 18.73, 18.15 ppm.



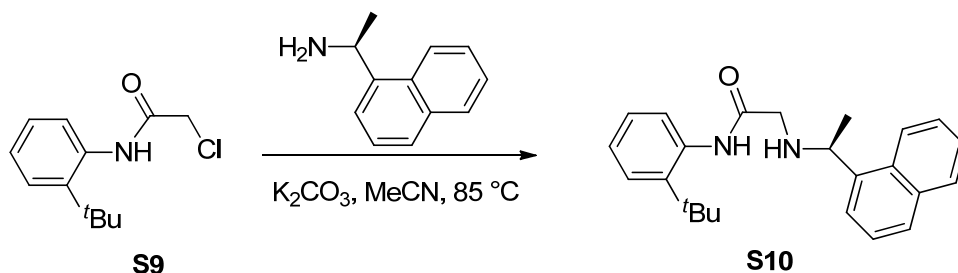
Complex **4.13**. The product was isolated as a green solid (14.2 mg) in 11% yield after purification by silica gel column chromatography (10% ether in pentane as the eluting solvent).  $^1\text{H}$  NMR ( $\text{CDCl}_3$ , 500 MHz):  $\delta$  16.51 (s, 1H), 8.69 (d,  $J = 8.1$  Hz, 1H), 7.93 –

7.88 (m, 1H), 7.83 (dd,  $J = 8.9, 4.1$  Hz, 1H), 7.69 (d,  $J = 7.2$  Hz, 1H), 7.57 – 7.45 (m, 4H), 7.17 (q,  $J = 6.7$  Hz, 1H), 7.09 (d,  $J = 3.7$  Hz, 2H), 6.95 – 6.87 (m, 3H), 5.10 (sept,  $J = 6.1$  Hz, 1H), 4.00 – 3.89 (m, 2H), 3.88 – 3.82 (m, 1H), 3.79 – 3.66 (m, 1H), 2.48 (s, 3H), 2.43 (s, 3H), 2.32 (s, 3H), 2.31 (s, 3H), 1.71 (d,  $J = 6.1$  Hz, 3H), 1.62 (d,  $J = 6.1$  Hz, 3H) ppm.  $^{13}\text{C}$  NMR ( $\text{CDCl}_3$ , 125 MHz):  $\delta$  210.97, 152.57, 144.77, 138.91, 138.58, 138.33, 138.30, 137.83, 134.25, 131.20, 129.99, 129.86, 129.79, 129.03, 128.59, 126.21, 125.93, 125.52, 124.95, 124.14, 123.04, 122.65, 113.20, 75.11, 56.34, 51.78, 46.77, 22.37, 22.33, 21.43, 21.09, 18.55, 18.51, 1.24 ppm. HRMS:  $[\text{C}_{34}\text{H}_{39}\text{Cl}_2\text{N}_2\text{ORu}]$   $[\text{M}^+]$  Calc. = 663.1484. Found = 663.1499.

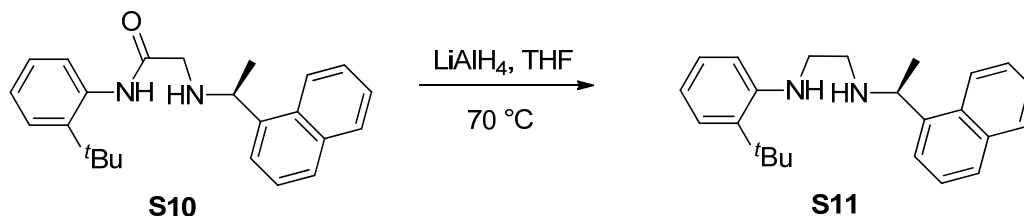
#### Synthesis of complex **4.14**.



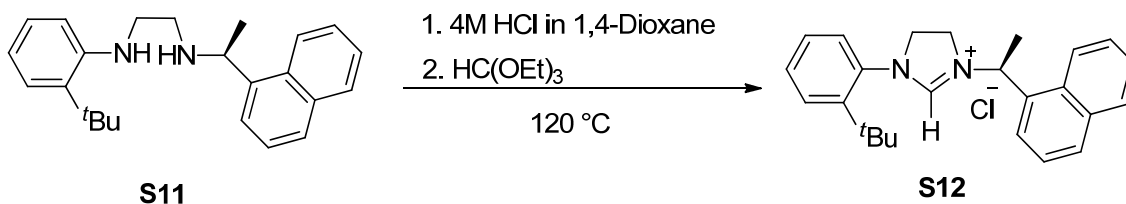
Compound **S9**. The product was isolated as white solids (21.441 g) in 71% yield.  $^1\text{H}$  NMR ( $\text{CDCl}_3$ , 500 MHz):  $\delta$  8.44 (s, 1H), 7.66 (dd,  $J = 10$  Hz, 3 Hz, 1H), 7.42 (dd,  $J = 10.5$  Hz, 3 Hz, 1H), 7.28 – 7.16 (m, 2 H), 4.26 (s, 2H), 1.43 (s, 9H) ppm.  $^{13}\text{C}$  NMR ( $\text{CDCl}_3$ , 125 MHz):  $\delta$  163.96, 142.52, 134.32, 127.11, 126.98, 126.89, 126.76, 43.38, 34.79, 30.83 ppm.



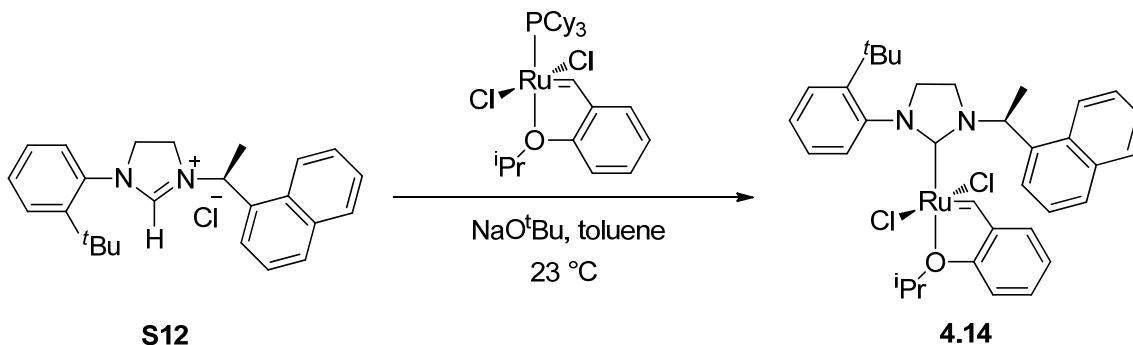
Compound **S10**. The product was purified by running a silica gel column using diethyl ether as the eluting solvent and isolated white solids (2.965 g) in 46% yield.  $^1\text{H}$  NMR ( $\text{CDCl}_3$ , 500 MHz):  $\delta$  9.51 (s, 1H), 8.11 (d,  $J = 8.3$  Hz, 1H), 7.90 (m, 1H), 7.85 – 7.82 (m, 1H), 7.80 (d,  $J = 8.1$  Hz, 1H), 7.59 (dd,  $J = 8.7, 4.0$  Hz, 1H), 7.55 – 7.47 (m, 3H), 7.40 (dd,  $J = 8.0, 1.5$  Hz, 1H), 7.26 – 7.22 (m, 1H), 7.17 – 7.15 (m, 1H), 4.80 – 4.77 (m, 1H), 1.63 – 1.61 (m, 3H), 1.46 (s, 9H) ppm.  $^{13}\text{C}$  NMR ( $\text{CDCl}_3$ , 125 MHz):  $\delta$  169.83, 140.96, 139.91, 135.33, 134.05, 131.16, 129.17, 127.86, 126.85, 126.47, 126.30, 125.74, 125.69, 125.55, 125.37, 122.57, 122.34, 53.87, 51.42, 34.62, 30.62, 23.41 ppm.



Compound **S11**. The reaction gave 95% conversion to product (1.703 g of crude mixture). The mixture was carried on to the next step crude without further purification.  $^1\text{H}$  NMR ( $\text{CDCl}_3$ , 500 MHz):  $\delta$  8.22 (d,  $J = 8.0$  Hz, 1H), 7.94 – 7.89 (m, 1H), 7.79 (d,  $J = 8.2$  Hz, 1H), 7.71 – 7.68 (m, 1H), 7.56 – 7.49 (m, 3H), 7.30 – 7.28 (m, 1H), 7.17 – 7.12 (m, 1H), 6.74 – 6.71 (m, 1H), 6.68 (dd,  $J = 8.1, 1.2$  Hz, 1H), 4.74 (q,  $J = 6.5$  Hz, 1H), 3.32 – 3.20 (m, 2H), 3.01 – 2.94 (m, 2H), 1.56 (d,  $J = 6.6$  Hz, 3H), 1.51 (s, 9H) ppm.



Compound **S12**. The product was isolated as a cream colored powder (0.476 g) in 60% yield.  $^1\text{H}$  NMR ( $\text{CDCl}_3$ , 500 MHz):  $\delta$  9.06 (s, 1H), 8.33 (d,  $J = 8.5$  Hz, 1H), 7.92 – 7.87 (m, 1H), 7.81 (d,  $J = 7.5$  Hz, 1H), 7.63 (t,  $J = 7.3$  Hz, 1H), 7.59 (d,  $J = 7.1$  Hz, 1H), 7.55 (t,  $J = 7.5$  Hz, 1H), 7.50 (t,  $J = 7.7$  Hz, 1H), 7.48 – 7.43 (m, 1H), 7.36 – 7.32 (m, 1H), 7.32 – 7.27 (m, 1H), 6.43 (m, 1H), 4.26 – 4.22 (m, 2H), 4.12 (dd,  $J = 21.5, 10.9$  Hz, 1H), 3.93 (m, 1H), 2.05 (d,  $J = 6.8$  Hz, 3H), 1.30 (s, 9H) ppm.  $^{13}\text{C}$  NMR ( $\text{CDCl}_3$ , 125 MHz):  $\delta$  158.73, 146.97, 134.46, 134.31, 132.79, 131.01, 130.83, 130.70, 130.19, 129.42, 128.62, 128.57, 127.88, 126.68, 125.45, 124.88, 123.06, 55.21, 54.86, 35.91, 32.29, 19.32 ppm.

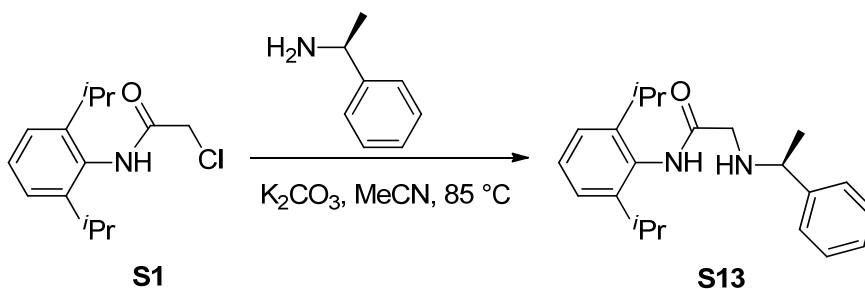


Complex **4.14**. The complex was purified by silica gel chromatography (10% ether in pentane) to obtain green solids (89.7 mg) in 13% yield. This complex was very unstable, and required storage under inert atmosphere. Complex **4.14** decomposed in solution, yielding a mixture of unidentifiable compounds in the  $^1\text{H}$  and  $^{13}\text{C}$  NMR spectra. High

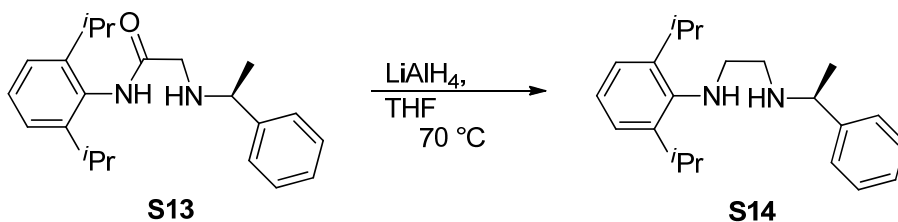
resolution mass spectrometry:  $[C_{35}H_{40}Cl_2N_2ORu][(M+H)-H_2]$  Calculated = 676.1562.

Found = 676. 1570.

Synthesis of complex **4.15**.

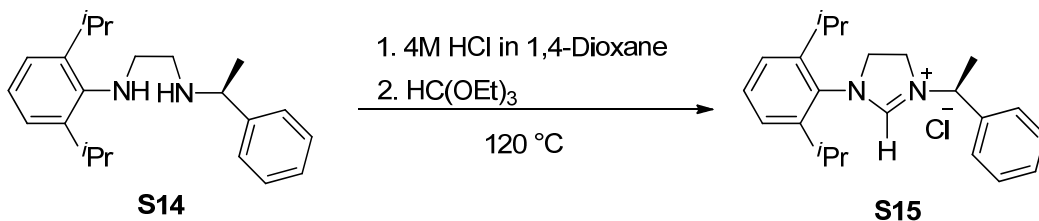


Compound **S13**. The product was isolated as white crystals (1.589 g) in 28% yield.  $^1\text{H}$  NMR ( $\text{CDCl}_3$ , 500 MHz):  $\delta$  8.68 (s, 1H), 7.39 – 7.32 (m, 4H), 7.32 – 7.26 (m, 2H), 7.18 (d,  $J = 7.7$  Hz, 2H), 3.90 (q,  $J = 6.6$  Hz, 1H), 3.51 – 3.27 (m, 2H), 3.04 – 2.94 (m, 2H), 1.47 (d,  $J = 6.6$  Hz, 3H), 1.21 (d,  $J = 6.9$  Hz, 6H), 1.19 (d,  $J = 6.9$  Hz, 6H) ppm.  $^{13}\text{C}$  NMR ( $\text{CDCl}_3$ , 125 MHz):  $\delta$  171.39, 146.03, 144.43, 131.41, 128.94, 128.33, 127.72, 126.73, 123.65, 58.73, 50.65, 29.08, 24.18, 23.88, 23.78 ppm.

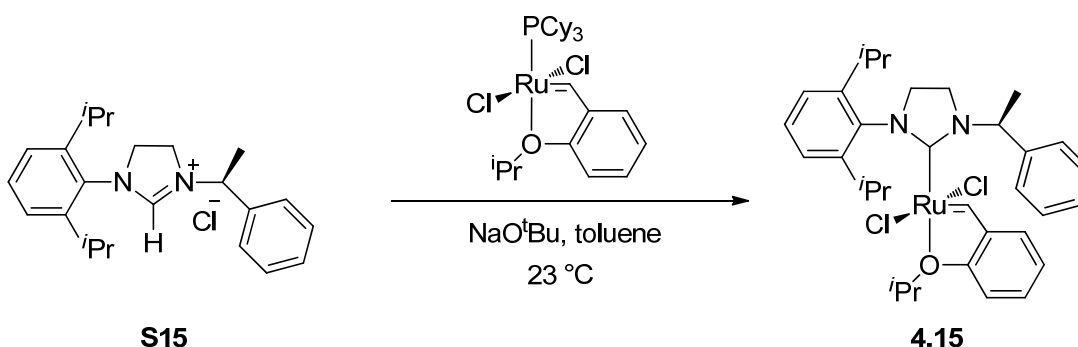


Compound **S14**. The reaction gave 89% conversion to product (0.904 g) as a pale yellow, viscous oil. The mixture was carried on crude to the next step.  $^1\text{H}$  NMR ( $\text{CDCl}_3$ , 500 MHz):  $\delta$  7.29 – 7.26 (m, 3H), 7.18 (m, 2H), 7.03 – 6.99 (m, 2H), 6.96 (dd,  $J = 8.4, 6.6$  Hz,

1H), 3.74 (q,  $J = 6.6$  Hz, 1H), 3.26 – 3.22 (m, 2H), 2.95 – 2.79 (m, 2H), 2.72 – 2.56 (m, 2H), 1.33 (d,  $J = 6.6$  Hz, 3H), 1.15 (d,  $J = 3.6$  Hz, 6H), 1.13 (d,  $J = 3.6$  Hz, 6H) ppm.



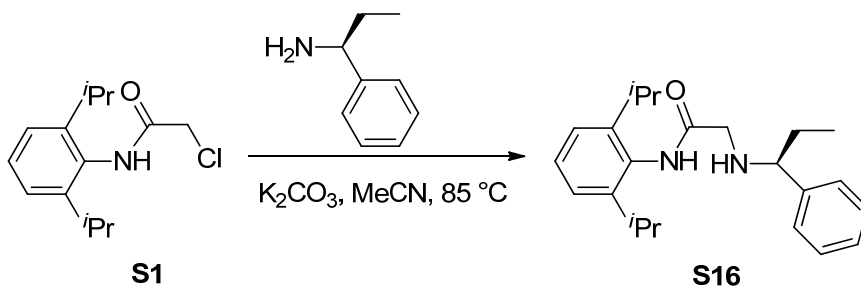
Compound **S15**. The product was isolated as a peach-colored powder (0.683 g) in 74% yield. <sup>1</sup>H NMR (CDCl<sub>3</sub>, 500 MHz):  $\delta$  9.98 (s, 1H), 7.60 – 7.55 (m, 2H), 7.46 – 7.36 (m, 4H), 7.24 – 7.21 (m, 2H), 6.17 (q,  $J = 7.0$  Hz, 1H), 4.24 – 4.09 (m, 2H), 4.07 – 3.95 (m, 2H), 2.91 (sept,  $J = 6.8$  Hz, 1H), 2.76 (sept,  $J = 6.8$  Hz, 1H), 1.82 (d,  $J = 7.0$  Hz, 3H), 1.32 (d,  $J = 6.8$  Hz, 3H), 1.28 (d,  $J = 7.0$  Hz, 3H), 1.27 (d,  $J = 7.0$  Hz, 3H), 1.21 (d,  $J = 5.6$  Hz, 3H) ppm. <sup>13</sup>C NMR (CDCl<sub>3</sub>, 125 MHz):  $\delta$  159.14, 146.73, 146.56, 137.57, 131.27, 130.37, 129.50, 129.29, 127.52, 125.10, 56.98, 53.28, 45.65, 29.10, 25.33, 25.21, 24.40, 24.15, 17.94 ppm.



Compound **4.15**. The complex was obtained by silica gel chromatography (10% ether in pentane as the eluting solvent) as a dark grayish-green powder (0.1107 g) in 14% yield. <sup>1</sup>H NMR (CDCl<sub>3</sub>, 500 MHz):  $\delta$  16.34 (s, 1H), 7.89 (d,  $J = 7.5$  Hz, 2H), 7.59 (t,  $J = 8$  Hz, 1H),

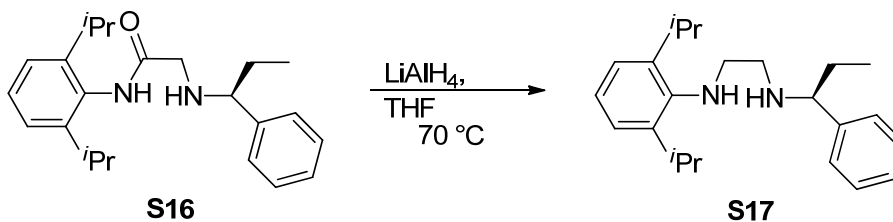
7.50 – 7.44 (m, 3H), 7.39 – 7.34 (m, 3H), 6.92 (d,  $J$  = 8 Hz, 1H), 6.88 – 6.85 (m, 2H), 6.64 (q,  $J$  = 6.5 Hz, 1H), 5.13 (sept,  $J$  = 6 Hz, 1H), 3.87 – 3.78 (m, 3H), 3.46 – 3.41 (m, 1H), 3.21 (sept,  $J$  = 7 Hz, 1H), 3.15 (sept,  $J$  = 6.5 Hz, 1H), 2.12 (d,  $J$  = 7 Hz, 3H), 1.77 (d,  $J$  = 6.5 Hz, 3H), 1.73 (d,  $J$  = 6 Hz, 3H), 1.20 (dd,  $J$  = 5.5 Hz,  $J$  = 1.5 Hz, 6H), 0.94 (d,  $J$  = 6.5 Hz, 3H), 0.88 (d,  $J$  = 7 Hz, 3H) ppm.  $^{13}\text{C}$  NMR ( $\text{CDCl}_3$ , 125 MHz):  $\delta$  208.77, 152.86, 148.78, 148.74, 143.97, 140.15, 138.09, 129.69, 129.60, 128.67, 128.44, 127.92, 125.08, 125.02, 122.55, 122.48, 113.20, 75.36, 57.59, 54.93, 43.17, 28.22, 28.12, 25.94, 25.73, 24.08, 22.42, 22.38, 17.65 ppm. HRMS:  $[\text{C}_{33}\text{H}_{42}\text{Cl}_2\text{N}_2\text{ORu}][\text{M-H}]$  Calc. = 654.1718. Found = 654.1725.

Synthesis of complex **4.16**.

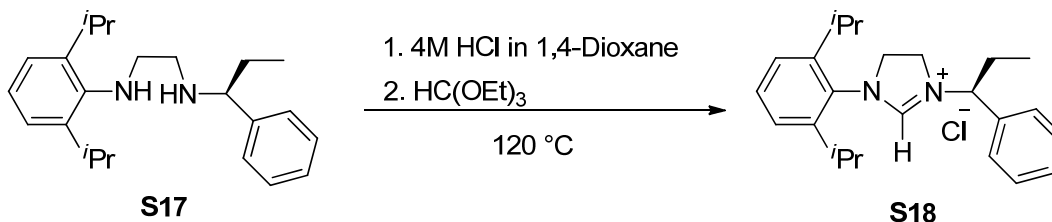


Compound **S16**. The product was isolated as white solids (4.351 g) in 42% yield.  $^1\text{H}$  NMR ( $\text{CDCl}_3$ , 500 MHz):  $\delta$  8.67 (s, 1H), 7.39 – 7.33 (m, 2H), 7.32 – 7.26 (m, 4H), 7.18 (d,  $J$  = 7.7 Hz, 2H), 3.60 (dd,  $J$  = 7.5, 6.4 Hz, 1H), 3.35 (s, 2H), 3.07 – 2.89 (m, 1H), 1.90 – 1.80 (m, 1H), 1.79 – 1.71 (m, 1H), 1.21 (d,  $J$  = 6.9 Hz, 6H), 1.19 (d,  $J$  = 6.9 Hz, 6H), 0.88 (t,  $J$  = 7.4 Hz, 3H) ppm.  $^{13}\text{C}$  NMR ( $\text{CDCl}_3$ , 125 MHz):  $\delta$  171.46, 146.03, 142.97, 131.44, 128.85, 128.79, 128.32, 127.74, 127.39, 126.49, 123.65, 65.50, 50.58, 31.00, 29.07, 23.87, 23.80, 11.15 ppm.

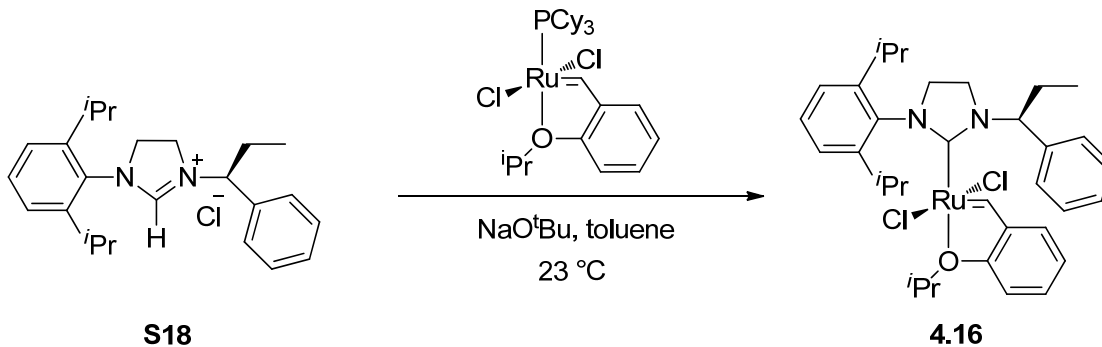




Compound **S17**. The reaction yielded 97% conversion to product (1.907 g). The mixture was carried on crude to the next step.  $^1\text{H}$  NMR ( $\text{CDCl}_3$ , 500 MHz):  $\delta$  7.35 – 7.30 (m, 2H), 7.29 – 7.26 (m, 2H), 7.24 – 7.21 (m, 1H), 7.08 (d,  $J$  = 1.5 Hz, 1H), 7.06 (s, 1H), 7.04 – 6.99 (m, 1H), 3.53 (dd,  $J$  = 7.5, 6.1 Hz, 1H), 3.29 (sept,  $J$  = 6.8 Hz, 2H), 2.94 (dt,  $J$  = 11.6, 5.7 Hz, 1H), 2.90 – 2.82 (m, 1H), 2.68 (t,  $J$  = 5.6 Hz, 2H), 1.84 – 1.72 (m, 1H), 1.72 – 1.60 (m, 1H), 1.22 (d,  $J$  = 3.6 Hz, 6H), 1.21 (d,  $J$  = 3.6 Hz, 6H), 0.86 (t,  $J$  = 10 Hz, 3H) ppm.

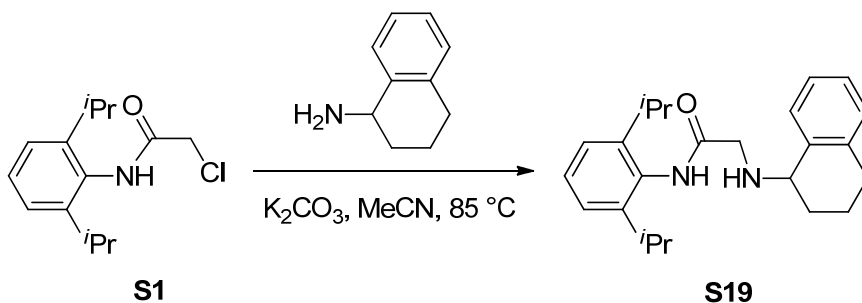


Compound **S18**. The product was isolated as fluffy white solids (0.530 g) in 25% yield.  $^1\text{H}$  NMR ( $\text{CDCl}_3$ , 500 MHz):  $\delta$  10.22 (s, 1H), 7.60 (d,  $J$  = 7.1 Hz, 2H), 7.49 – 7.35 (m, 4H), 7.24 – 7.21 (m, 2H), 5.96 (t,  $J$  = 7.8 Hz, 1H), 4.19 – 4.08 (m, 2H), 4.08 – 3.93 (m, 2H), 2.89 (dt,  $J$  = 13.6, 6.8 Hz, 1H), 2.77 (dt,  $J$  = 13.7, 6.9 Hz, 1H), 2.30 – 2.26 (m, 2H), 2.21 – 2.09 (m, 2H), 1.34 (d,  $J$  = 6.8 Hz, 3H), 1.30 (d,  $J$  = 4.2 Hz, 3H), 1.29 (d,  $J$  = 4.3 Hz, 3H), 1.22 (d,  $J$  = 6.8 Hz, 3H), 1.08 (t,  $J$  = 7.3 Hz, 3H) ppm.  $^{13}\text{C}$  NMR ( $\text{CDCl}_3$ , 125 MHz):  $\delta$  159.58, 146.67, 146.61, 136.33, 131.30, 130.35, 129.51, 129.31, 128.18, 125.13, 125.05, 62.77, 53.10, 45.49, 29.91, 29.23, 29.13, 25.33, 25.30, 24.20, 24.16, 10.85 ppm.



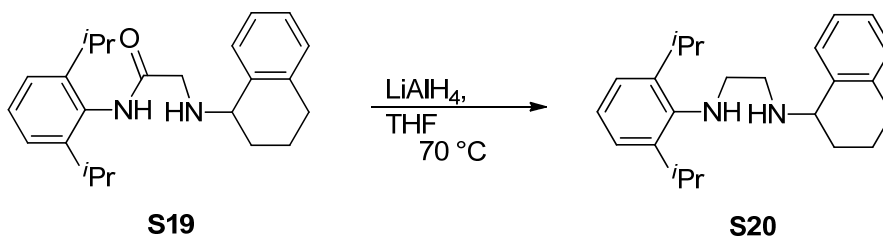
Compound **4.16**. The complex was obtained after silica gel column chromatography as a green powder (0.420 g) in 75% yield.  $^1\text{H}$  NMR ( $\text{CDCl}_3$ , 500 MHz):  $\delta$  16.37 (s, 1H), 7.94 (d,  $J = 7.4$  Hz, 2H), 7.58 (t,  $J = 7.8$  Hz, 1H), 7.53 – 7.49 (m, 1H), 7.47 (t,  $J = 6.8$  Hz, 2H), 7.40 – 7.34 (m, 3H), 6.94 (d,  $J = 8.3$  Hz, 1H), 6.87 (d,  $J = 4.4$  Hz, 2H), 6.24 (dd,  $J = 11.8$ , 2.9 Hz, 1H), 5.17 (sept,  $J = 6.1$  Hz, 1H), 3.94 – 3.81 (m, 3H), 3.82 – 3.72 (m, 1H), 3.56 – 3.45 (m, 1H), 3.20 (sept,  $J = 6.6$  Hz, 1H), 3.04 (sept,  $J = 6.8$  Hz, 1H), 2.88 – 2.85 (m, 1H), 2.53 – 2.39 (m, 1H), 1.85 (d,  $J = 6.1$  Hz, 3H), 1.82 (d,  $J = 6.1$  Hz, 3H), 1.21 (d,  $J = 6.9$  Hz, 3H), 1.14 (d,  $J = 6.9$  Hz, 3H), 1.07 (t,  $J = 7.3$  Hz, 3H), 0.90 (d,  $J = 6.7$  Hz, 3H), 0.88 (d,  $J = 6.6$  Hz, 3H) ppm.  $^{13}\text{C}$  NMR ( $\text{CDCl}_3$ , 125 MHz):  $\delta$  208.25, 152.81, 148.83, 148.71, 144.04, 138.09, 137.58, 129.68, 129.64, 129.61, 128.77, 128.10, 125.06, 125.00, 122.58, 122.49, 113.21, 75.23, 64.88, 54.96, 44.33, 28.14, 28.03, 25.87, 25.81, 25.32, 24.09, 24.03, 22.59, 22.45, 11.53 ppm. HRMS:  $[\text{C}_{34}\text{H}_{44}\text{Cl}_2\text{N}_2\text{ORu}][(\text{M}+\text{H})-\text{H}_2]$  Calc. = 668.1875. Found = 668.1871.

Synthesis of complex **4.17**.



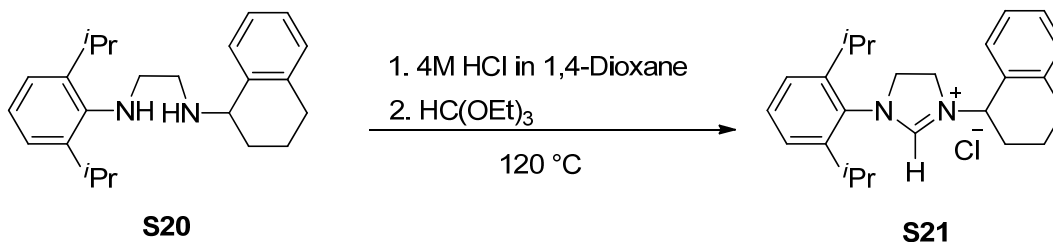
Compound **S19**. The product was isolated as cream colored solids (4.716 g) in 48% yield.

$^1\text{H}$  NMR ( $\text{CDCl}_3$ , 500 MHz):  $\delta$  8.85 (s, 1H), 7.43 (d,  $J = 6.6$  Hz, 1H), 7.28 (dd,  $J = 14.7$ , 7.1 Hz, 1H), 7.19 (d,  $J = 7.4$  Hz, 4H), 7.14 – 7.01 (m, 1H), 3.92 (broad s, 1H), 3.61 – 3.57 (m, 2H), 3.07 – 3.00 (m, 2H), 2.88 – 2.82 (m, 1H), 2.81 – 2.73 (m, 1H), 2.04 – 1.95 (m, 2H), 1.95 – 1.85 (m, 2H), 1.86 – 1.74 (m, 1H), 1.21 (d,  $J = 6.8$  Hz, 12H) ppm.  $^{13}\text{C}$  NMR ( $\text{CDCl}_3$ , 125 MHz):  $\delta$  171.68, 146.07, 138.16, 137.80, 129.54, 128.86, 128.35, 127.47, 126.26, 123.70, 56.56, 50.67, 29.55, 29.13, 29.00, 23.90, 19.25 ppm.



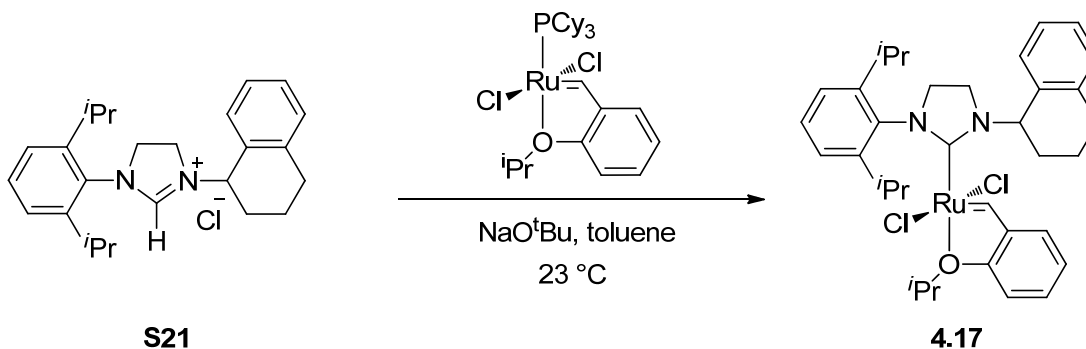
Compound **S20**. The reaction gave 53% conversion to product (2.355 g). The mixture was carried on crude to the next step.  $^1\text{H}$  NMR ( $\text{CDCl}_3$ , 500 MHz):  $\delta$  7.51 – 7.45 (m, 1H), 7.21 – 7.14 (m, 2H), 7.10 (d,  $J = 7.5$  Hz, 3H), 7.07 – 7.01 (m, 1H), 3.88 – 3.76 (m, 1H), 3.36 (sept,  $J = 6.8$  Hz, 2H), 3.08 – 2.99 (m, 2H), 3.00 – 2.88 (m, 2H), 2.88 – 2.80 (m, 1H), 2.80

– 2.70 (m, 1H), 2.05 – 1.93 (m, 2H), 1.90 – 1.81 (m, 1H), 1.80 – 1.69 (m, 1H), 1.24 (d,  $J = 6.8$  Hz, 12H) ppm.



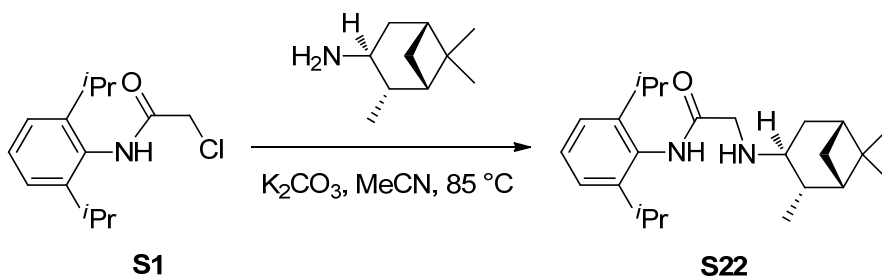
Compound **S21**. The product was isolated as cream colored solids (1.408 g) in 53% yield.

$^1\text{H}$  NMR ( $\text{CDCl}_3$ , 500 MHz):  $\delta$  9.01 (s, 1H), 7.52 – 7.46 (m, 1H), 7.42 (t,  $J = 7.8$  Hz, 1H), 7.25 – 7.21 (m, 3H), 7.19 – 7.15 (m, 2H), 5.99 (t,  $J = 5.5$  Hz, 1H), 4.69 – 4.55 (m, 1H), 4.41 – 4.28 (m, 1H), 4.23 – 4.07 (m, 2H), 3.02 (sept,  $J = 6.8$  Hz, 1H), 2.90 (sept,  $J = 6.9$  Hz, 1H), 2.82 (t,  $J = 12.3$  Hz, 2H), 2.29 – 2.31 (m, 1H), 2.20–2.22 (m, 1H), 2.07 – 1.95 (m, 1H), 1.87 – 1.76 (m, 1H), 1.32 (d,  $J = 5.1$  Hz, 3H), 1.31 (d,  $J = 6.6$  Hz, 6H), 1.24 (d,  $J = 6.8$  Hz, 3H) ppm.  $^{13}\text{C}$  NMR ( $\text{CDCl}_3$ , 125 MHz):  $\delta$  159.13, 147.11, 138.56, 131.36, 131.04, 130.09, 129.12, 129.04, 127.35, 125.34, 124.96, 56.61, 53.83, 47.18, 29.28, 29.00, 27.34, 25.35, 25.26, 24.39, 24.08, 19.45 ppm.



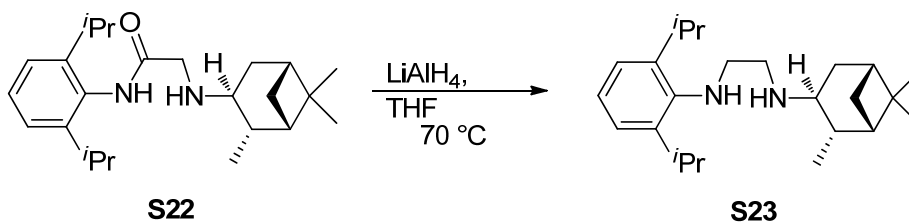
Compound **4.17**. The complex was purified by silica gel chromatography (eluting solvent starting at 10% ether in pentane and increased to 100% ether over 30 minutes) and isolated as a greenish-brown powder (0.910 g). Yield = 58%.  $^1\text{H}$  NMR ( $\text{CDCl}_3$ , 500 MHz):  $\delta$  16.32 (s, 1H), 7.92 (d,  $J = 7.8$  Hz, 1H), 7.61 (t,  $J = 7.8$  Hz, 1H), 7.53 – 7.43 (m, 1H), 7.40 (td,  $J = 8.1, 1.4$  Hz, 2H), 7.33 – 7.27 (m, 1H), 7.24 (d,  $J = 6.6$  Hz, 1H), 7.18 (d,  $J = 7.5$  Hz, 1H), 6.92 (d,  $J = 8.4$  Hz, 1H), 6.89 – 6.83 (m, 2H), 6.52 (dd,  $J = 10.4, 5.6$  Hz, 1H), 5.11 (sept,  $J = 6.1$  Hz, 1H), 4.11 – 3.85 (m, 2H), 3.78 (dd,  $J = 20.9, 10.1$  Hz, 1H), 3.63 – 3.60 (m, 1H), 3.25 – 3.22 (m, 2H), 3.16 – 3.01 (m, 1H), 3.00 – 2.80 (m, 2H), 2.24 – 2.10 (m, 1H), 2.09 – 1.92 (m, 2H), 1.79 (d,  $J = 6.1$  Hz, 3H), 1.69 (d,  $J = 6.1$  Hz, 3H), 1.28 (d,  $J = 6.9$  Hz, 3H), 1.22 (d,  $J = 10.0$  Hz, 3H), 0.98 (d,  $J = 6.7$  Hz, 3H), 0.90 (d,  $J = 6.7$  Hz, 3H) ppm.  $^{13}\text{C}$  NMR ( $\text{CDCl}_3$ , 125 MHz):  $\delta$  289.81, 209.36, 152.90, 148.80, 143.95, 138.76, 137.98, 134.74, 129.71, 129.53, 129.35, 129.32, 127.67, 126.37, 125.07, 125.02, 122.54, 122.48, 113.19, 75.27, 60.01, 55.09, 43.54, 30.05, 28.46, 28.34, 28.13, 25.98, 25.70, 24.10, 22.42, 22.40, 22.28 ppm. HRMS:  $[\text{C}_{35}\text{H}_{44}\text{Cl}_2\text{N}_2\text{ORu}][(\text{M}+\text{H})-\text{H}_2]$  Calc. = 680.1875. Found = 680.1877.

#### Synthesis of complex **4.18**.

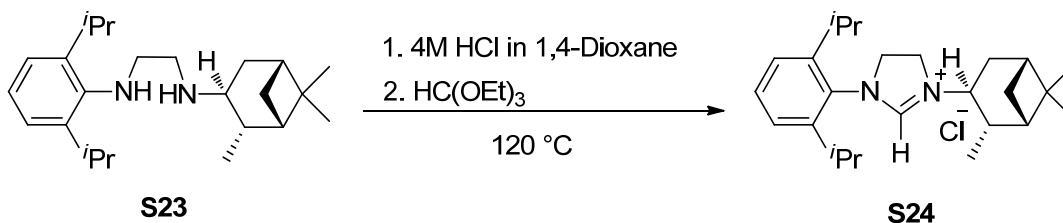


Compound **S22**. The product was isolated as white solids (3.118 g) in 65% yield.  $^1\text{H}$  NMR ( $\text{CDCl}_3$ , 500 MHz):  $\delta$  8.86 (s, 1H), 7.28 (dd,  $J = 13.6, 6.2$  Hz, 1H), 7.18 (d,  $J = 7.7$  Hz, 2H), 3.57 – 3.47 (m, 2H), 3.12 – 2.99 (m, 3H), 2.55 – 2.46 (m, 1H), 2.44 – 2.34 (m, 1H),

2.05 – 1.96 (m, 1H), 1.88 – 1.79 (m, 2H), 1.70 – 1.62 (m, 1H), 1.24 (s, 3H), 1.22 (d,  $J = 3.6$  Hz, 6H), 1.20 (d,  $J = 3.6$  Hz, 6H), 1.17 (d,  $J = 7.2$  Hz, 3H), 0.99 (s, 3H), 0.91 (d,  $J = 9.8$  Hz, 1H) ppm.  $^{13}\text{C}$  NMR ( $\text{CDCl}_3$ , 125 MHz):  $\delta$  171.72, 146.04, 131.52, 128.28, 123.67, 57.37, 50.31, 48.07, 45.79, 41.94, 38.77, 36.98, 34.55, 29.13, 28.02, 23.86, 23.82, 23.45, 21.77 ppm.

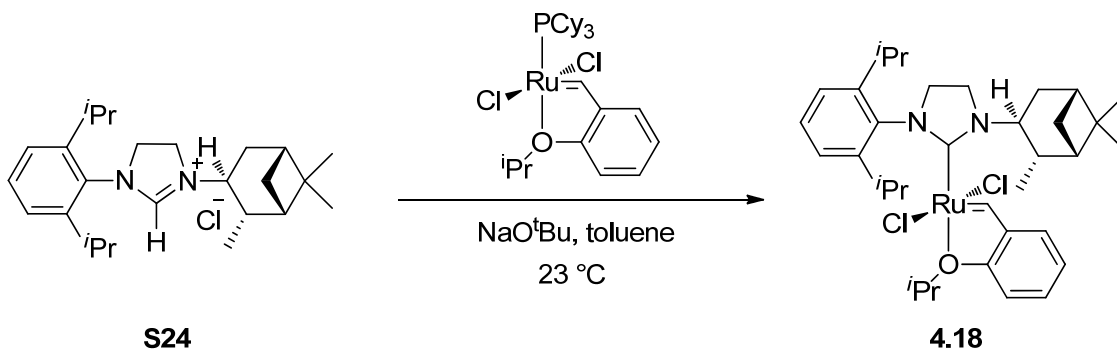


Compound **S23**. The product (1.44 g) was isolated as a clear oil. There was 87% conversion to product. The crude mixture was carried on directly to the next step.  $^1\text{H}$  NMR ( $\text{CDCl}_3$ , 500 MHz):  $\delta$  7.12 – 7.07 (m, 2H), 7.06 – 7.01 (m, 1H), 3.36 (sept,  $J = 5.0$  Hz, 2H), 3.06 – 2.99 (m, 1H), 2.98 – 2.89 (m, 3H), 2.88 – 2.78 (m, 1H), 2.43 – 2.32 (m, 2H), 2.01 – 1.89 (m, 1H), 1.84 – 1.74 (m, 2H), 1.65 – 1.60 (m, 1H), 1.25 (d,  $J = 6.8$  Hz, 12H), 1.23 (s, 3H), 1.15 (d,  $J = 7.2$  Hz, 3H), 0.99 (s, 3H), 0.96 (d,  $J = 9.6$  Hz, 1H) ppm.



Compound **S24**. Crude **S23** (0.724 g) was carried on directly to the reaction to synthesize **S24**. Product **S24** (0.238 g) was isolated as a cream colored powder in 30% yield.  $^1\text{H}$  NMR ( $\text{CDCl}_3$ , 500 MHz):  $\delta$  10.15 (s, 1H), 7.40 – 7.35 (m, 1H), 7.19 – 7.15 (m, 2H), 5.35 (dt,  $J =$

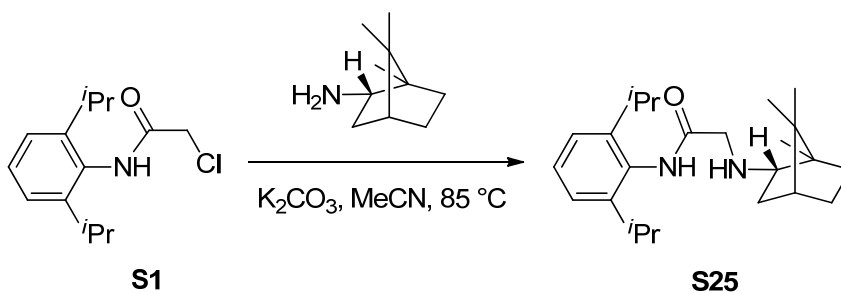
10.3, 7.3 Hz, 1H), 4.35 – 4.19 (m, 3H), 4.21 – 4.04 (m, 1H), 2.89 (sept,  $J = 5.0$  Hz, 1H), 2.74 (sept,  $J = 5.0$  Hz, 1H), 2.67 – 2.57 (m, 1H), 2.46 – 2.44 (m, 1H), 2.21 – 2.11 (m, 1H), 2.05 – 2.01 (m, 2H), 1.93 – 1.84 (m, 2H), 1.26 (d,  $J = 6.8$  Hz, 6H), 1.25 – 1.22 (m, 6H), 1.21 (s, 3H), 1.16 (d,  $J = 7.2$  Hz, 3H), 1.08 (s, 3H), 0.84 (d,  $J = 10.3$  Hz, 1H) ppm.  $^{13}\text{C}$  NMR ( $\text{CDCl}_3$ , 125 MHz):  $\delta$  160.18, 146.92, 146.39, 131.07, 130.40, 125.09, 124.84, 56.96, 53.29, 47.36, 44.00, 41.45, 40.43, 38.65, 35.28, 31.88, 29.17, 29.06, 28.20, 25.37, 25.17, 24.37, 24.10, 23.69, 20.02 ppm.



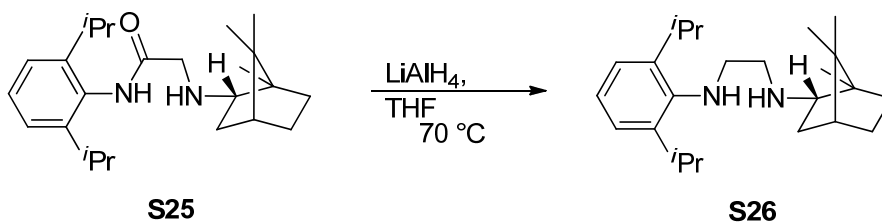
Compound **4.18**. The complex was purified by silica gel column chromatography (5% methanol in methylene chloride as the eluting solvent) to give 1.161g of grayish-green solids in 56% yield.  $^1\text{H}$  NMR ( $\text{CDCl}_3$ , 500 MHz):  $\delta$  16.37 (s, 1H), 7.59 (t,  $J = 7.8$  Hz, 1H), 7.53 – 7.45 (m, 1H), 7.41 – 7.33 (m, 2H), 6.92 (d,  $J = 8.3$  Hz, 1H), 6.86 (d,  $J = 4.3$  Hz, 2H), 5.59 (dt,  $J = 10.0, 6.3$  Hz, 1H), 5.13 – 5.11 (m, 1H), 4.07 – 4.05 (m, 2H), 4.00 – 3.94 (m, 1H), 3.95 – 3.79 (m, 1H), 3.25 – 3.03 (m, 3H), 2.52 (dtd,  $J = 13.9, 6.9, 1.3$  Hz, 1H), 2.49 – 2.38 (m, 1H), 2.19 – 2.06 (m, 1H), 2.00 – 1.98 (m, 2H), 1.78 (d,  $J = 6.1$  Hz, 3H), 1.76 (d,  $J = 6.1$  Hz, 3H), 1.57 (d,  $J = 7.0$  Hz, 3H), 1.31 (s, 3H), 1.25 (s, 3H), 1.22 (d,  $J = 4.1$  Hz, 3H), 1.21 (d,  $J = 4.1$  Hz, 3H), 1.05 (d,  $J = 9.9$  Hz, 1H), 0.90 (d,  $J = 3.2$  Hz, 3H), 0.88 (d,  $J = 3.2$  Hz, 3H) ppm.  $^{13}\text{C}$  NMR ( $\text{CDCl}_3$ , 125 MHz):  $\delta$  209.86, 152.66, 148.88, 148.65, 144.21,

138.40, 129.60, 129.56, 125.05, 125.00, 122.53, 122.51, 113.23, 75.06, 59.98, 54.90, 48.62, 43.34, 42.09, 41.10, 38.85, 34.54, 34.13, 28.19, 28.05, 26.01, 25.79, 24.08, 24.02, 23.78, 22.53, 22.49, 21.86 ppm. HRMS:  $[C_{35}H_{50}Cl_2N_2ORu][(M+H)-H_2]$  Calc. = 686.2344. Found = 686.2350.

Synthesis of complex **4.19**.

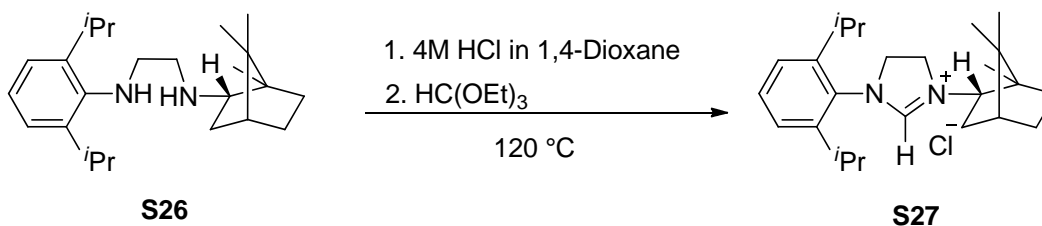


Compound **S25**. The product was isolated as white crystals (1.669 g) in 46% yield.  $^1\text{H}$  NMR ( $\text{CDCl}_3$ , 500 MHz):  $\delta$  8.78 (s, 1H), 7.30 – 7.25 (m, 1H), 7.18 (d,  $J = 7.7$  Hz, 2H), 3.64 – 3.32 (m, 2H), 3.04 (sept,  $J = 6.9$  Hz, 2H), 2.96 (d,  $J = 7.8$  Hz, 2H), 2.34 – 2.28 (m, 1H), 1.81 – 1.71 (m, 1H), 1.71 – 1.63 (m, 2H), 1.58 (s, 1H), 1.41 – 1.33 (m, 1H), 1.21 (d,  $J = 1.7$  Hz, 6H), 1.20 (d,  $J = 1.7$  Hz, 6H), 1.19 – 1.14 (m, 1H), 0.90 (s, 3H), 0.88 (s, 6H) ppm.  $^{13}\text{C}$  NMR ( $\text{CDCl}_3$ , 125 MHz):  $\delta$  171.83, 146.05, 131.52, 128.29, 123.68, 63.96, 51.66, 49.08, 48.47, 45.04, 38.21, 29.12, 28.65, 27.57, 23.91, 19.99, 18.72, 14.43 ppm.

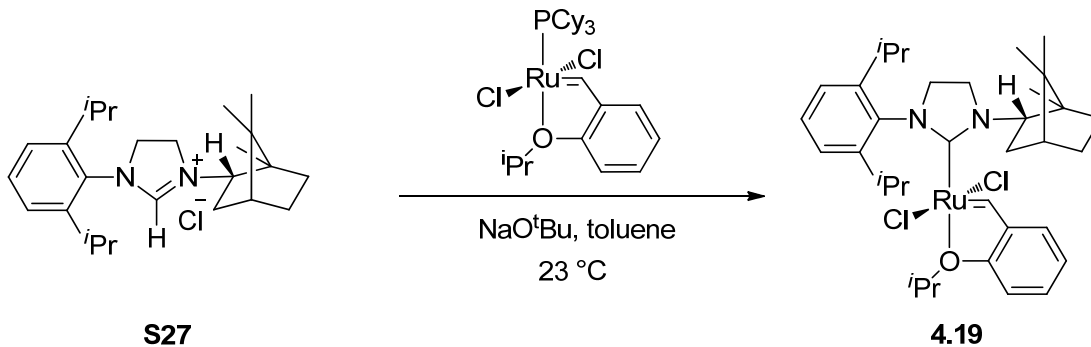




Compound **S26**. The reaction afforded 61% conversion to product (1.407 g). The mixture was carried on crude to the next step.  $^1\text{H}$  NMR ( $\text{CDCl}_3$ , 500 MHz):  $\delta$  7.09 – 7.06 (m, 2H), 7.04 – 6.99 (m, 1H), 3.35 (sept,  $J = 6.8$  Hz, 2H), 2.95 (m, 2H), 2.21 – 2.12 (m, 1H), 1.81 – 1.77 (m, 2H), 1.76 – 1.72 (m, 2H), 1.70 – 1.66 (m, 2H), 1.67 – 1.61 (m, 2H), 1.41 – 1.25 (m, 2H), 1.23 (d,  $J = 6.9$  Hz, 12H), 0.88 (s, 6H), 0.87 (s, 3H) ppm.

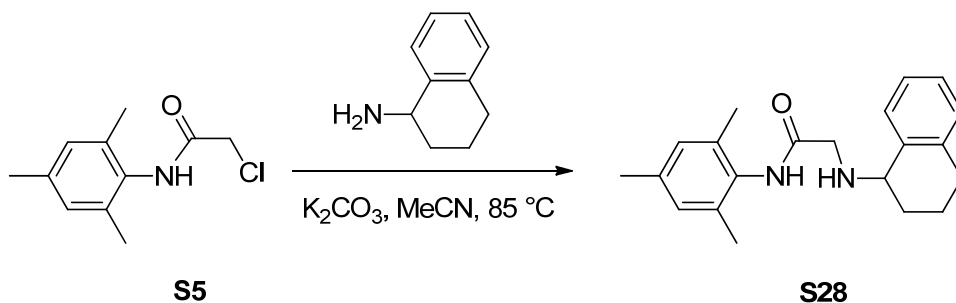


Compound **S27**. The product was isolated as cream-colored solids (0.349 g) in 36% yield.  $^1\text{H}$  NMR ( $\text{CDCl}_3$ , 500 MHz):  $\delta$  9.19 (s, 1H), 7.41 (t,  $J = 8$  Hz, 1H), 7.24 – 7.21 (m, 2H), 4.71 (broad d,  $J = 11$  Hz, 1H), 4.44 (t,  $J = 10.5$  Hz, 2H), 4.22 (t,  $J = 11$  Hz, 2H), 3.02 (sept,  $J = 6.5$  Hz, 1H), 2.89 (sept,  $J = 6.5$  Hz, 1H), 2.50 – 2.45 (m, 1H), 1.89 – 1.86 (m, 2H), 1.84 – 1.82 (m, 1H), 1.60 – 1.55 (m, 1H), 1.46 – 1.42 (m, 1H), 1.39 – 1.37 (m, 1H), 1.32 – 1.27 (m, 12H), 1.03 (s, 3H), 0.99 (s, 3H), 0.91 (s, 3H) ppm.  $^{13}\text{C}$  NMR ( $\text{CDCl}_3$ , 125 MHz):  $\delta$  159.62, 147.00, 146.62, 131.25, 130.28, 125.18, 125.04, 64.51, 53.40, 51.19, 50.83, 49.17, 44.71, 32.83, 29.10, 29.03, 28.72, 28.26, 25.35, 25.31, 24.47, 24.34, 19.77, 18.90, 14.32 ppm.

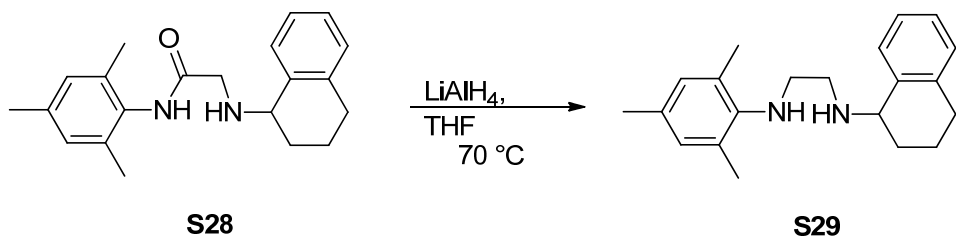


Compound **4.19**. The complex was purified by silica gel column chromatography (10% ether in pentane) to give a green powder (0.1544 g) in 34% yield.  $^1\text{H}$  NMR ( $\text{CDCl}_3$ , 500 MHz):  $\delta$  16.46 (s, 1H), 7.62 (t,  $J = 7.8$  Hz, 1H), 7.51 (ddd,  $J = 8.4, 7.1, 2.0$  Hz, 1H), 7.42 – 7.40 (m, 2H), 6.93 (d,  $J = 8.4$  Hz, 1H), 6.89 – 6.82 (m, 2H), 5.39 (ddd,  $J = 10.9, 5.4, 1.7$  Hz, 1H), 5.12 (sept,  $J = 6.2$  Hz, 1H), 4.23 (q,  $J = 9.3$  Hz, 1H), 4.07 – 4.11 (m, 1H), 3.94 – 3.98 (m, 2H), 3.22 (sept,  $J = 7.0$  Hz, 1H), 3.09 (sept,  $J = 6.6$  Hz, 1H), 2.91 – 2.75 (m, 1H), 2.17 – 2.03 (m, 1H), 2.00 – 1.92 (m, 1H), 1.90 (t,  $J = 4.5$  Hz, 1H), 1.78 (d,  $J = 6.1$  Hz, 3H), 1.75 (d,  $J = 6.1$  Hz, 3H), 1.71 – 1.64 (m, 2H), 1.46 – 1.41 (m, 1H), 1.33 (s, 3H), 1.25 (d,  $J = 5.1$  Hz, 3H), 1.23 (d,  $J = 7.4$  Hz, 6H), 1.01 (s, 3H), 0.94 (d,  $J = 6.6$  Hz, 3H), 0.89 (d,  $J = 6.7$  Hz, 3H) ppm.  $^{13}\text{C}$  NMR ( $\text{CDCl}_3$ , 125 MHz):  $\delta$  212.80, 152.60, 148.71, 148.35, 144.09, 138.54, 129.70, 129.61, 125.10, 125.07, 122.72, 122.48, 113.25, 74.93, 67.82, 55.93, 51.88, 49.09, 46.79, 44.39, 34.66, 30.49, 28.66, 28.11, 28.08, 25.95, 25.80, 24.06, 24.03, 22.82, 22.65, 20.01, 19.96, 16.18 ppm. HRMS:  $[\text{C}_{35}\text{H}_{50}\text{Cl}_2\text{N}_2\text{ORu}][(\text{M}+\text{H})-\text{H}_2]$  Calc. = 686.2344. Found = 686.2316.

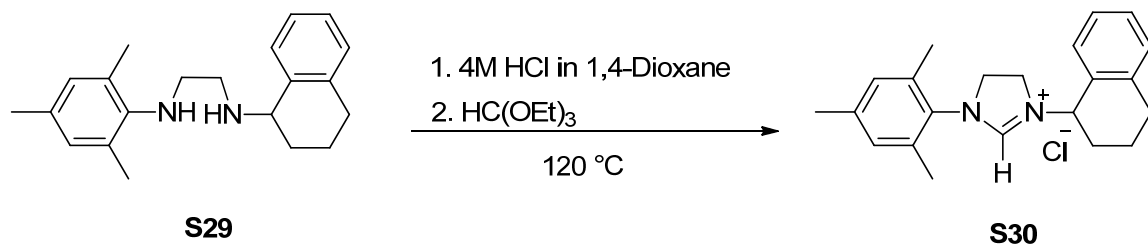
Synthesis of complex **4.20**.



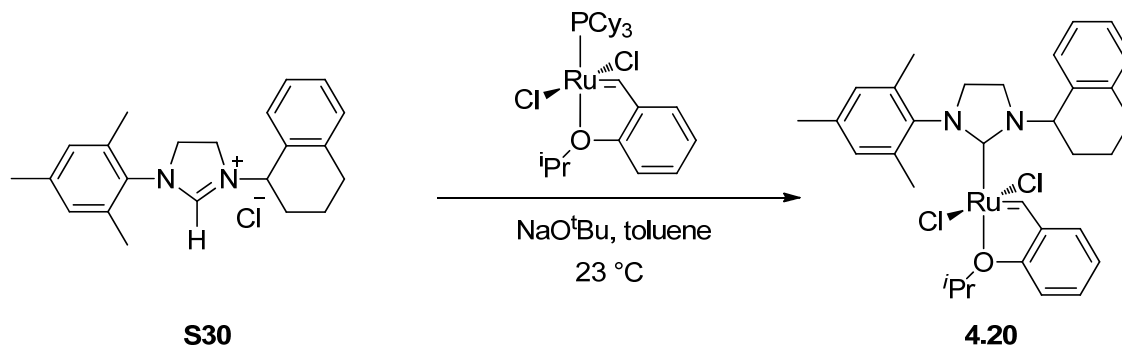
Compound **S28**. The product was isolated as white crystals (4.21 g) in 18% yield.  $^1\text{H}$  NMR ( $\text{CDCl}_3$ , 500 MHz):  $\delta$  8.82 (s, 1H), 7.44 – 7.41 (m, 1H), 7.22 – 7.16 (m, 2H), 7.14 – 7.10 (m, 1H), 6.91 (s, 2H), 3.90 (t,  $J = 4.6$  Hz, 1H), 3.58 (q,  $J = 17.3$  Hz, 2H), 2.89 – 2.72 (m, 2H), 2.27 (s, 3H), 2.19 (s, 6H), 2.01 – 1.93 (m, 2H), 1.93 – 1.85 (m, 1H), 1.85 – 1.73 (m, 1H) ppm.  $^{13}\text{C}$  NMR ( $\text{CDCl}_3$ , 125 MHz):  $\delta$  170.79, 138.20, 137.75, 137.00, 135.08, 131.38, 129.50, 129.14, 128.84, 127.41, 126.24, 56.41, 50.58, 29.52, 28.83, 21.11, 19.23, 18.64 ppm.



Compound **S29**. The reaction gave 99% conversion to product (0.720 g). The mixture was carried on crude to the next step.  $^1\text{H}$  NMR ( $\text{CDCl}_3$ , 500 MHz):  $\delta$  7.40 – 7.42 (m, 1H), 7.15 – 7.17 (m, 2H), 7.09 – 7.11 (m, 1H), 6.81 (s, 2H), 3.81 (s, 1H), 3.13 – 3.02 (m, 2H), 3.03 – 2.92 (m, 1H), 2.93 – 2.85 (m, 1H), 2.85 – 2.78 (m, 1H), 2.78 – 2.69 (m, 1H), 2.27 (s, 6H), 2.23 (s, 3H), 2.03 – 1.89 (m, 2H), 1.90 – 1.79 (m, 1H), 1.79 – 1.70 (m, 1H) ppm.



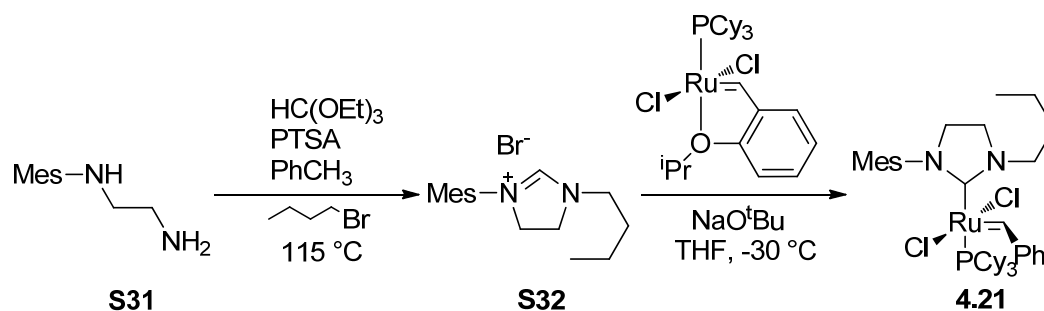
Compound **S30**. The product was isolated as white solids (0.202 g) in 25% yield.  $^1\text{H}$  NMR ( $\text{CDCl}_3$ , 500 MHz):  $\delta$  9.75 (s, 1H), 7.43 – 7.38 (m, 1H), 7.27 – 7.23 (m, 2H), 7.18 – 7.13 (m, 1H), 6.94 (s, 2H), 6.04 (t,  $J = 6.4$  Hz, 1H), 4.40 – 4.30 (m, 1H), 4.29 – 4.21 (m, 1H), 4.16 – 4.05 (m, 1H), 4.00 – 3.90 (m, 1H), 2.89 – 2.74 (m, 2H), 2.34 (s, 6H), 2.29 (s, 3H), 2.15 – 2.06 (m, 2H), 2.03 – 1.91 (m, 1H), 1.91 – 1.82 (m, 1H) ppm.  $^{13}\text{C}$  NMR ( $\text{CDCl}_3$ , 125 MHz):  $\delta$  160.01, 140.56, 138.64, 131.06, 130.88, 130.21, 130.06, 128.83, 128.43, 127.25, 56.64, 51.14, 46.07, 29.10, 27.92, 21.19, 20.13, 18.26 ppm.



Compound **4.20**. The complex was purified by silica gel column chromatography (10% ether in pentane) to afford a green powder (36.6 mg) in 11% yield.  $^1\text{H}$  NMR ( $\text{CDCl}_3$ , 500 MHz):  $\delta$  16.28 (s, 1H), 7.89 (d,  $J = 7.5$  Hz, 1H), 7.48 (dt,  $J = 7$  Hz,  $J = 2$  Hz, 1H), 7.26 (t,  $J = 7$  Hz, 1H), 7.21 (t,  $J = 6.5$  Hz, 1H), 7.15 (d,  $J = 7$  Hz, 1H), 7.07 (d,  $J = 3.5$  Hz, 2H), 6.93 – 6.88 (m, 3H), 6.48 – 6.45 (m, 1H), 5.11 (sept,  $J = 6.5$  Hz, 1H), 3.94 (quintet,  $J = 9.5$  Hz, 1H), 3.91 – 3.87 (m, 1H), 3.77 (quartet,  $J = 10.5$  Hz, 1H), 3.63 – 3.58 (m, 1H), 3.03 – 3.01

(m, 1H), 2.92 – 2.89 (m, 2H), 2.45 (s, 3H), 2.33 (s, 3H), 2.25 (s, 3H), 2.16 – 2.12 (m, 1H), 2.04 – 2.02 (m, 1H), 1.97 – 1.92 (m, 1H), 1.72 (d,  $J = 6$  Hz, 3H), 1.66 (d,  $J = 5.5$  Hz, 3H), 1.30 – 1.23 (m, 1H) ppm.  $^{13}\text{C}$  NMR ( $\text{CDCl}_3$ , 125 MHz):  $\delta$  293.00, 208.95, 152.59, 144.61, 144.59, 138.95, 138.70, 138.48, 138.44, 138.17, 134.64, 129.85, 129.70, 129.38, 129.30, 127.70, 126.40, 122.97, 122.67, 113.12, 75.15, 59.85, 51.80, 43.75, 30.01, 28.35, 22.40, 22.12, 22.09, 21.43, 18.46, 18.44 ppm. HRMS:  $[\text{C}_{32}\text{H}_{38}\text{Cl}_2\text{N}_2\text{ORu}][(\text{M}+\text{H})-\text{H}_2]$  Calc. = 638.1405. Found = 638.1436.

#### Synthesis of complex **4.21**.



Synthesis of **S31**. **S31** was made as outlined in reference 22.

Synthesis of **S32**. A Schlenk flask with a Teflon stopper was charged with **S31** (0.59 g, 3.31 mmol), 1-bromobutane (0.54 g, 3.97 mmol), *p*-toluene sulfonic acid monohydrate (0.031 g, 0.167 mmol),  $\text{CH(OEt)}_3$  (8 mL), and toluene (8 mL). The flask was sealed under air and heated to  $115\text{ }^\circ\text{C}$  for 10 h. After cooling to room temperature, an off-white precipitate formed and approximately 30 mL of ether was added to ensure full precipitation. The suspension was stirred for several hours after which the precipitate was collected by filtration and dried *in vacuo* to give **S32** (0.72 g, 67% yield) as an off-white solid.  $^1\text{H}$  NMR (400 MHz,  $\text{CDCl}_3$ )  $\delta$  8.97 (s, 1H), 6.39 (s, 2H), 3.76 (dd,  $J = 22.5, 8.2$  Hz,

4H), 3.42 (s, 2H), 1.77 (s, 9H), 1.20 (br s, 2H), 0.89 (br s, 2H), 0.46 (m, 3H).  $^{13}\text{C}$  NMR (101 MHz,  $\text{CDCl}_3$ )  $\delta$  158.74, 139.93, 135.15, 130.56, 129.78, 51.00, 48.86, 48.14, 29.08, 20.92, 19.44, 18.03, 13.59.

Synthesis of **4.21**. In a glovebox under a nitrogen atmosphere, a 100 mL RB flask was charged with **S32** (0.73 g, 2.25 mmol),  $\text{NaO}^t\text{Bu}$  (0.22 g, 2.25 mmol), and first generation Grubbs catalyst (1.23 g, 1.5 mmol). The flask was cooled to  $-30\text{ }^\circ\text{C}$  and prechilled THF (20 mL) was added. The reaction was stirred at  $-30\text{ }^\circ\text{C}$  for 15 min after which the flask was removed from the cold bath and allowed to stir at RT for 10 h. The flask was then exposed to air and concentrated *in vacuo* to give a brownish-red residue. The residue was dissolved in a minimal amount of benzene and loaded onto a silica gel column (150 mL) where it was flashed with 10% ether in pentane to collect residual first generation Grubbs catalyst as a purple band followed by 30% ether in pentane to collect **4.21** as a red/pink band. The appropriate fractions were concentrated to yield **4.21** (0.61 g, 63%) as a dark pink residue that could be lyophilized from benzene to give a pink powder.  $^1\text{H}$  NMR (500 MHz,  $\text{C}_6\text{D}_6$ )  $\delta$  19.51 (s, 1H), 7.17 (m, 4H), 6.99 (t,  $J = 7.4\text{ Hz}$ , 2H), 6.21 (br s, 1H), 4.29 (t,  $J = 7.1\text{ Hz}$ , 2H), 3.23 – 3.06 (m, 4H), 2.59 (q,  $J = 11.9\text{ Hz}$ , 3H), 2.35 (br s, 5H), 1.92 – 1.77 (m, 11H), 1.73 – 1.56 (m, 11H), 1.48 (q,  $J = 12.4\text{ Hz}$ , 6H), 1.33 – 1.08 (m, 10H), 1.06 – 0.96 (m, 3H) ppm.  $^{13}\text{C}$  NMR (126 MHz,  $\text{C}_6\text{D}_6$ )  $\delta$  220.22, 219.61, 151.74, 137.53, 137.48, 137.12, 129.14, 50.88, 50.66, 48.01, 47.99, 32.07, 31.95, 30.91, 29.95, 28.26, 28.19, 27.06, 21.04, 20.50, 18.82, 14.56 ppm.  $^{31}\text{P}$  NMR (121 MHz,  $\text{C}_6\text{D}_6$ )  $\delta$  32.58 ppm. HRMS: Calc. = 786.3150. Found = 786.3158.

**Acknowledgement.** Dr. Lawrence Henling and Dr. Michael Day for obtaining the X-ray crystallographic structures of complexes **4.12** and **4.15**.

The author thanks the *American Chemical Society* for the permission for the contents of this chapter. This research has been published in the *Journal of the American Chemical Society*. Article reference: Thomas, R. M.; Keitz, B. K.; Champagne, T. M.; Grubbs, R. H. *J. Am. Chem. Soc.* **2011**, *133*, 7490-7496.

## REFERENCES

1. (a) Grubbs, R. H. *Handbook of Metathesis*; Wiley-VCH: Weinheim, Germany, 2003. And references cited therein. (b) Cossy, J.; Arseniyadis, S.; Meyer, C. *Metathesis in Natural Product Synthesis*; Wiley-VCH: Weinheim, Germany, 2010.
2. Ritter, T.; Hejl, A.; Wenzel, A. G.; Funk, T. W.; Grubbs, R. H. *Organometallics* **2006**, *25*, 5740–5745.
3. (a) Fu, G. C.; Nguyen, S. T.; Grubbs, R. H. *J. Am. Chem. Soc.* **1993**, *115*, 9856–9857. (b) Chatterjee, A. K.; Morgan, J. P.; Scholl, M.; Grubbs, R. H. *J. Am. Chem. Soc.* **2000**, *122*, 3783–3784. (c) Trnka, T. M.; Grubbs, R. H. *Acc. Chem. Res.* **2001**, *34*, 18–29. (d) Love, J. A.; Morgan, J. P.; Trnka, T. M.; Grubbs, R. H. *Angew. Chem. Int. Ed.* **2002**, *41*, 4035–4037.
4. (a) Dias, E. L.; Nguyen, S. T.; Grubbs, R. H. *J. Am. Chem. Soc.* **1997**, *119*, 3887–3897. (b) Sanford, M. S.; Ulman, M.; Grubbs, R. H. *J. Am. Chem. Soc.* **2001**, *123*, 749–750. (c) Sanford, M. S.; Love, J. A.; Grubbs, R. H. *J. Am. Chem. Soc.* **2001**, *123*, 6543–6554.
5. (a) Chatterjee, A. K.; Choi, T. –L.; Sanders, D. P.; Grubbs, R. H. *J. Am. Chem. Soc.* **2003**, *125*, 11360–11370. (b) Ibrahim, I.; Yu, M.; Schrock, R. R.; Hoveyda, A. H. *J. Am. Chem. Soc.* **2009**, *131*, 3844–3845. (c) Malcolmson, S. J.; Meek, S. J.; Sattely, E. S.; Schrock, R. R.; Hoveyda, A. H. *Nature* **2008**, *456*, 933–937. (d) Jiang, A. J.; Zhao, Y.; Schrock, R. R.; Hoveyda, A. H. *J. Am. Chem. Soc.* **2009**, *131*, 16630–16631.
6. Anderson, D. R.; Ung, T.; Mkrtumyan, G.; Bertrand, G.; Grubbs, R. H.; Schrodi, Y. *Organometallics* **2008**, *27*, 563–566.
7. Burdett, K. A.; Harris, L. D.; Margl, P.; Maughon, B. R.; Mokhtar-Zadeh, T.; Saucier, P. C.; Wasserman, E. P. *Organometallics* **2004**, *23*, 2027–2047.
8. Mandelli, D.; Jannini, M. J. D. M.; Buffon, R.; Schuchardt, U. *Journal of the American Oil Chemists' Society* **1996**, *73*, 229–32.
9. Lysenko, Z.; Maughon, B. R.; Bicerano, J.; Burdett, K. A.; Christenson, C. P.; Cummins, C. H.; Dettloff, M. L.; Maher, J. M.; Schrock, A. K.; Thomas, P. J.; Varjian, R. D.; White, J. E. WO 2003/093215 A1 priority date of November 13 **2003**.
10. (a) Olson, E. S. US 2010/0191008 A1 priority date of July 29 **2010**. (b) DuBois, J. –L.; Sauvageot, O. WO 2010/103223 A1 priority date of September 16 **2010**. (c) Herbinet, O.; Pitz, W. J.; Westbrook, C. K. *Combustion and Flame* **2010**, *157*, 893–908.



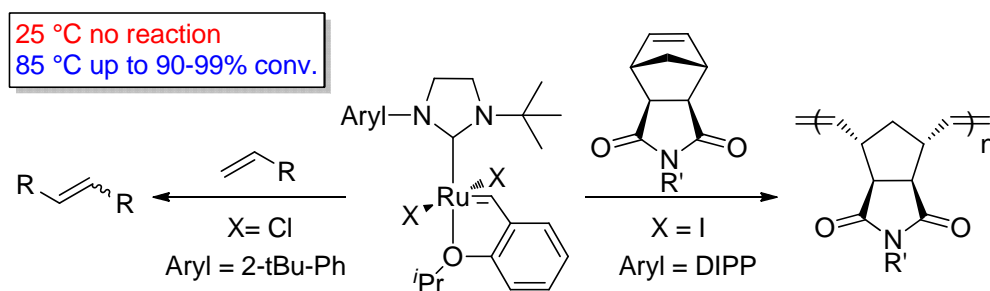
11. (a) Mol, J. C. *J. Mol. Cat. A: Chem.* **2004**, *213*, 39-45. (b) Kuhn, K. M.; Bourg, J. -B.; Chung, C. K.; Virgil, S. C.; Grubbs, R. H. *J. Am. Chem. Soc.* **2009**, *131*, 5313–5320.
12. Marinescu, S. C.; Schrock, R. R.; Müller, P.; Hoveyda, A. H. *J. Am. Chem. Soc.* **2009**, *131*, 10840–10841.
13. Hong, S. H.; Wenzel, A. G.; Salguero, T. T.; Day, M. W.; Grubbs, R. H. *J. Am. Chem. Soc.* **2007**, *129*, 7961–7968.
14. (a) Patel, J.; Mujcinovic, S.; Jackson, W. R.; Robinson, A. J.; Serelis, A. K.; Such, C. *Green Chemistry* **2006**, *8*, 450–454. (b) Bei, X.; Allen, D. P.; Pedersen, R. L. *Pharm. Technol.* **2008**, s18.
15. (a) Forman, G. S.; Bellabara, R. M.; Tooze, R. P.; Slawin, A. M. Z.; Karch, R.; Winde, R. *J. Organomet. Chem.* **2006**, *691*, 5513–5516. (b) Forman, G. S.; McConnell, A. E.; Hanton, M. J.; Slawin, A. M. Z.; Tooze, R. P.; van Rensburg, W. J.; Meyer, W. H.; Dwyer, C.; Kirk, M. M.; Serfontein, D. W. *Organometallics* **2004**, *23*, 4824–4827.
16. Schrodi, Y.; Ung, T.; Vargas, A.; Mkrtumyan, G.; Lee, C. W.; Champagne, T. M.; Pederson, R. L.; Hong, S. H. *Clean* **2008**, *36*, 669-673.
17. Stewart, I. C.; Keitz, B. K.; Kuhn, K. M.; Thomas, R. M.; Grubbs, R. H. *J. Am. Chem. Soc.* **2010**, *132*, 8534-8535.
18. Vehlow, K.; Maechling, S.; Blechert, S. *Organometallics* **2006**, *25*, 25–28.
19. Vehlow, K.; Wang, D.; Buchmeiser, M. R.; Blechert, S. *Angew. Chem. Int. Ed.* **2008**, *47*, 2615–2618.
20. Pangborn, A. B.; Giardello, M. A.; Grubbs, R. H.; Rosen, R. K.; Timmers, F. J. *Organometallics* **1996**, *15*, 1518–1520.
21. Paczal, A.; Bényei, A. C.; Kotschy, A. *J. Org. Chem.* **2006**, *71*, 5969–5979.
22. Carlin, R. B.; Moores, M. S. *J. Am. Chem. Soc.* **1962**, *84*, 4107–4112.

## Chapter 5

### THERMALLY STABLE, LATENT OLEFIN METATHESIS CATALYSTS

#### Abstract

Highly thermally stable *N*-aryl, *N*-alkyl *N*-heterocyclic carbene (NHC) ruthenium catalysts were designed and synthesized for latent olefin metathesis. These catalysts showed excellent latent behavior toward metathesis reactions, whereby the complexes were inactive at ambient temperature and initiated at elevated temperatures, a challenging property to achieve with second generation catalysts. A sterically hindered *N*-*tert*-butyl substituent on the NHC ligand of the ruthenium complex was found to induce latent behavior toward cross-metathesis reactions, and exchange of the chloride ligands for iodide ligands was necessary to attain latent behavior during ring-opening metathesis polymerization (ROMP). Iodide-based catalysts showed no reactivity toward ROMP of norbornene-derived monomers at 25 °C, and upon heating to 85 °C gave complete conversion of monomer to polymer in less than 2 hours. All of the complexes were very stable to air, moisture, and elevated temperatures up to at least 90 °C, and exhibited a long catalyst lifetime in solution at elevated temperatures.



## Introduction

Olefin metathesis is widely used as a method of constructing carbon–carbon double bonds.<sup>1</sup> Toward this end, highly efficient metathesis catalysts have been designed through improvement of activity,<sup>2</sup> stability,<sup>3</sup> and selectivity of the catalysts.<sup>4</sup> Recently, efforts have been directed toward the development of latent metathesis catalysts.<sup>5,6</sup> Latent catalysts are defined as complexes that show little or no activity at a particular (usually ambient) temperature and initiate only upon activation. This activation can be caused by a variety of different stimuli, including heat,<sup>7,8</sup> acid,<sup>9</sup> light,<sup>10–13</sup> and chemical activation.<sup>14</sup> Latent metathesis catalysts primarily have applications in polymer chemistry.<sup>14</sup> One such application is the advantage of preparing monomer solutions in a mold with a catalyst that is unreactive at ambient temperature, thus allowing for good mixing and even distribution of monomeric solution before initiating polymerization.<sup>7</sup>

Previous literature reports describe latent ruthenium catalysts whereby the initiators and organic ligand structure were altered to induce latency.<sup>15–17</sup> The structure of initiators, such as variations of the Hoveyda-type chelating ligand, has been particularly well-explored and documented.<sup>18–20</sup> Another approach toward tuning the latency of a catalyst involves manipulation of the *N*-heterocyclic carbene (NHC) ligand. This method of inducing latent behavior is attractive in that it enables a straightforward catalyst design and synthesis while maintaining the functional group tolerance and stability of second generation ruthenium catalysts. Reported herein is the investigation of four new ruthenium-based latent catalysts for cross-metathesis and ROMP that were prepared adopting this strategy.

## Results and Discussion

Since *N*-aryl, *N*-alkyl NHC ruthenium catalysts display good stability, complexes **5.1** and **5.2** bearing a sterically hindered *N*-*tert*-butyl substituent on the NHC were synthesized and screened for latent behavior during cross-metathesis (CM) and ring-opening metathesis polymerization (ROMP) reactions (Figure 5.1).<sup>21</sup> At ambient temperature, solutions of complexes **5.1** and **5.2** in CDCl<sub>3</sub> showed no decomposition by NMR spectroscopy over 14 days and were stable in air for over four months. Additionally, complexes **5.1** and **5.2** could be heated in chloroform at 60 °C for 5 days without any signs of decomposition, thus indicating good thermal stability. At 90 °C in toluene, catalysts **5.1** and **5.2** began showing slight decomposition after 30 hours. This observed catalyst stability was promising for applications in latent metathesis chemistry, where the catalyst must remain active at high temperature for the duration of the reaction. This thermal stability also renders these catalysts valuable for applications requiring elevated temperatures.

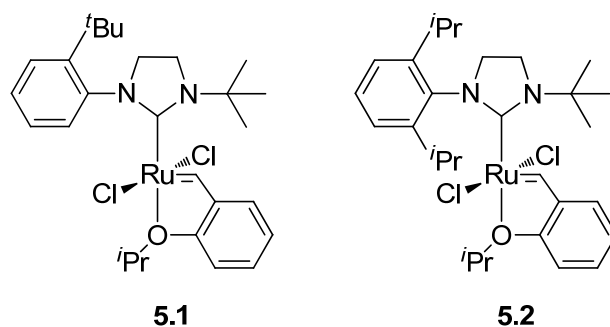


**Figure 5.1.** *N*-aryl, *N*-alkyl NHC ruthenium catalysts for latent olefin metathesis reactions.

Catalysts **5.1** and **5.2** were initially screened and compared for latency for the homodimerization of 1-hexene to 5-decene (Scheme 5.1). Both catalysts showed less than

5% conversion of 1-hexene after 24 hours at 25 °C while maintaining catalyst structural integrity as confirmed by  $^1\text{H}$  NMR spectroscopy (Table 5.1, entries 1 and 2). The reactions were subsequently heated at 85 °C for 24 hours, and the conversions were determined by  $^1\text{H}$  NMR spectroscopy (Table 5.1, entries 3 and 4). Both catalysts gave clean conversion of 1-hexene to 5-decene, without detectable side products by  $^1\text{H}$  NMR spectroscopy. Since catalyst **5.1** achieved 90% conversion of 1-hexene to 5-decene compared to 41% afforded by catalyst **5.2**, it was considered optimal for further latent cross-metathesis studies. Catalyst **5.2** was still active with no signs of decomposition after 24 hours at 85 °C. Presumably the better activity of catalyst **5.1** in relation to catalyst **5.2** is due to less steric hindrance of the former on the *N*-aryl ring (mono-*tert*-butyl versus di-isopropyl). Since both catalysts are latent for cross-metathesis of 1-hexene, the better activity of catalyst **5.1** is preferential for these reactions. The crystal structures of complexes **5.1** and **5.2** show expected geometry (Figure 5.2).<sup>21</sup>

**Scheme 5.1.** Latent olefin cross-metathesis of 1-hexene.

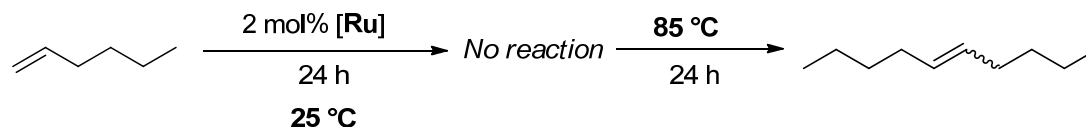


**Table 5.1.** Comparison of catalysts for latent homodimerization of 1-hexene.

Entry <sup>a</sup>	Catalyst	Temp. (°C)	Time (h)	% Conv. <sup>b</sup>
1	5.1	25	24	<5
2	5.2	25	24	<5
3	5.1	85	24	90
4	5.2	85	24	41

<sup>a</sup>The catalyst loading was 2 mol%. The concentration of 1-hexene in benzene was 0.5 M, and the reactions were carried out sealed under a nitrogen atmosphere. <sup>b</sup>The conversion was determined by  $^1\text{H}$  NMR spectroscopy. 1-Hexene was cleanly converted to 5-decene.

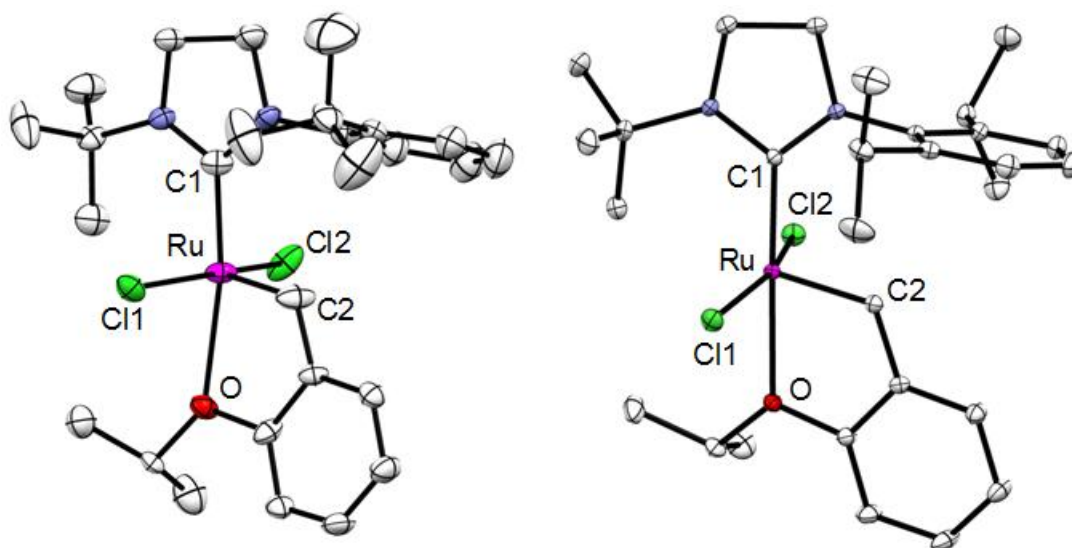
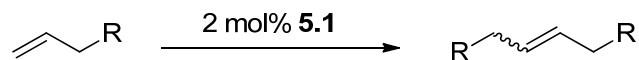


**Figure 5.2.** Crystal structures of complexes **5.1** (left) and **5.2** (right). Thermal ellipsoids set at 50% and hydrogen atoms omitted for clarity. Selected bond lengths (Å) and angles (deg.) for **5.1**: C1-Ru, 1.961; C2-Ru, 1.796; O-Ru 2.417; Cl1-Ru, 2.348; Cl2-Ru, 2.376; Cl-Ru-Cl, 7.43; C2-Ru-O, 77.95; and for **5.2**: C1-Ru, 1.982; C2-Ru, 1.837; O-Ru 2.312; Cl1-Ru, 2.369; Cl2-Ru, 2.348; Cl-Ru-Cl, 8.75; C2-Ru-O, 78.50.

Further studies were conducted with catalyst **5.1** to determine the optimal temperature for carrying out cross-metathesis reactions. In addition to 1-hexene, 1-octene, 5-hexenyl acetate, and 4-penten-1-ol were used as cross-metathesis substrates for homodimerization to assure that the observed results were general to simple alkyl olefins (Table 5.2). Catalyst **5.1** proved to be latent for these substrates even at 40 °C, showing no appreciable reactivity until 50 °C. Moderate conversion to product was obtained for all substrates at 60 °C; however, 85 °C was considered optimal for attaining good conversion of the starting material. The reactions gave the desired homocoupled product of these substrates as a mixture of *cis* and *trans* isomers. Following temperature optimization, substrate scope was subsequently explored to determine the general applicability of catalyst **5.1** (Table 5.2). For simple, longer chain olefins, catalyst **5.1** efficiently catalyzed conversion of terminal olefin to dimer product (Table 5.2, entries 5, 10, 13, and 16). Catalyst **5.1** showed lower reactivity

toward more sterically demanding olefins (Table 5.2, entries 18 and 20), as would be expected given the hindrance of the *N*-aryl, *N*-*tert*-butyl NHC ligand.

**Table 5.2.** Temperature optimization and substrate scope of catalyst **5.1**.

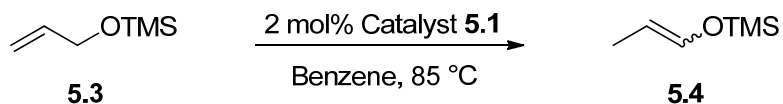


Entry <sup>a</sup>	Substrate	Temp. (°C)	Time (h)	% Conv. <sup>b</sup>
1		25	24	<5
2		40	24	5
3		50	24	11
4		60	30	35
5		85	24	90
6		25	22	0
7		40	22	2
8		50	22	13
9		60	30	26
10		85	15	89
11		25	22	0
12		40	22	0
13		85	22	62
14		25	22	0
15		40	22	<1
16		85	22	76
17		25	24	0
18		85	24	17
19		25	22	0
20		85	22	3

<sup>a</sup>The loading of catalyst **1** was 2 mol%. The concentration of substrate in benzene was 0.5 M, and the reactions were carried out sealed under a nitrogen atmosphere. <sup>b</sup>The conversion was determined by <sup>1</sup>H NMR spectroscopy. The reactions went cleanly to the target homodimerization products.

Functional groups were tolerated well when attached several carbon atoms away from the double bond. However, substrates with functional groups allylic to the olefin, particularly those containing oxygen, underwent significant olefin isomerization upon heating at 85 °C. While catalyst **5.1** was latent for allyl alcohol, allyl acetate, allyl ethyl ether, and allyl benzene at ambient temperature, subsequent heating of the reactions produced multiple isomerization products in addition to desired product, affording inseparable mixtures of olefinic cross-products. In contrast, catalyst **5.1** completely isomerized allyloxytrimethylsilane (**5.3**) to *cis*- and *trans*-propenyl trimethylsilyl ether (**5.4**) after 18 hours at 85 °C, and showed no subsequent cross-metathesis conversion of the internal olefin product (**5.4**) (Scheme 5.2).

**Scheme 5.2.** Isomerization of allyloxytrimethylsilane.

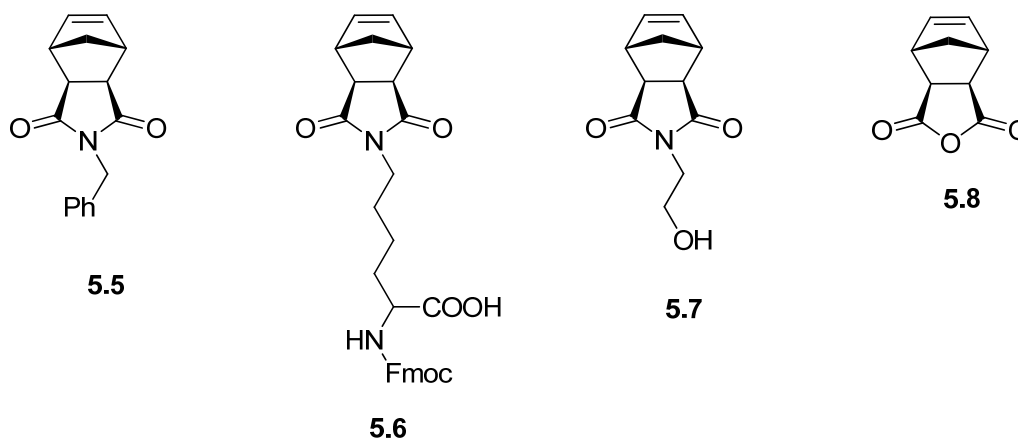


Since 1,4-benzoquinone has been reported to prevent olefin isomerization, this additive was tested in the homodimerization of allyl benzene and allyl ethyl ether to see if it would eliminate the observed isomerization and improve selectivity and yield of the desired product.<sup>22</sup> However, the addition of 0.1 equivalents of 1,4-benzoquinone resulted in catalyst decomposition. Interestingly, **5.1** showed no reactivity toward dienes, including 1,3-hexadiene, 1,3-pentadiene, and *trans*-1-phenyl-1,3-butadiene, even at an elevated temperature of 100 °C, possibly due to the low activity of the ruthenium vinylalkylidene intermediate.<sup>23</sup> Longer chain olefins were therefore considered ideal substrates since their conversions to desired homodimerization products were clean.



Toward the goal of developing a practical latent metathesis catalyst for ROMP applications, catalyst **5.1** was tested for polymerization of cyclooctadiene (COD) in benzene. In contrast to cross-metathesis reactions, 2 mol% of **5.1** initiated the ROMP of COD (0.7 M in benzene) at ambient temperature, giving 80% conversion to polymer after 35 minutes. Expectedly, higher conversion (90%) of COD to polymer was achieved by **5.1** at 85 °C in 35 minutes. Catalyst **5.2** was also active for the ROMP of COD (0.7M in benzene) at ambient temperature, affording 39% conversion to polymer in 19 hours.

**Figure 5.3.** ROMP monomers. Fmoc is fluorenylmethyloxycarbonyl.

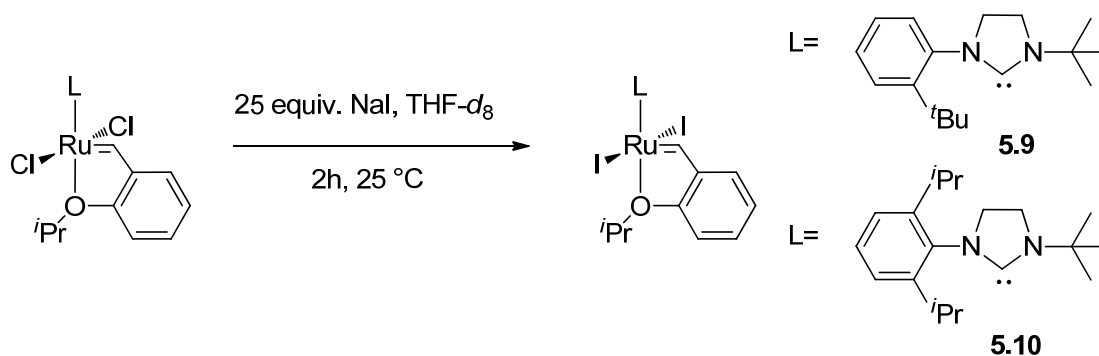


To gain more insight into the reactivity of these catalysts, we screened complex **5.2** for ROMP of norbornene-derived monomer **5.5**, since **5.2** would presumably show better latency than **5.1** due to its increased steric bulk. The increased sterics of **5.2** was expected to reduce its activity and necessitate higher temperature for initiation. Unfortunately, catalyst **5.2** polymerized **5.5** at 25 °C in tetrahydrofuran (THF), giving 56% conversion to polymer in 5 hours. These results showed that **5.1** and **5.2** were not effectively latent for ROMP as they were for cross-metathesis reactions. Therefore the complex structure was

modified to develop a catalyst that would display latent behavior toward ROMP of norbornene-derived monomers (Figure 5.3).

In effort to improve the latency of complexes **5.1** and **5.2** and thereby develop an effective latent catalyst for ROMP, complexes **5.1** and **5.2** were converted to complexes **5.9** and **5.10**, respectively, by *in situ* reaction with an excess of sodium iodide in THF according to literature procedure (Scheme 5.3).<sup>24</sup> While <sup>1</sup>H NMR chemical shifts of new complexes **5.9** and **5.10** are very similar to those of chlorine-based precursors, X-ray analysis unambiguously established the structure of **5.10** showing typical spacial arrangement for a second generation ruthenium catalyst (Figure 5.4).<sup>21</sup> Complex **5.10** was crystallized out of methanol as long, dark needles.

**Scheme 5.3.** Synthesis of complexes **5.9** and **5.10**.



It was anticipated that the effect of changing the chloride ligands to iodide ligands would induce latency for ROMP due to the iodide causing more steric hindrance for the association of the olefin substrate.<sup>25</sup> Ruthenium metathesis catalysts with iodide ligands are known to be slower initiators than those with chloride ligands.<sup>26</sup> Accordingly, this property was utilized to achieve latent ROMP catalysts.<sup>27</sup>

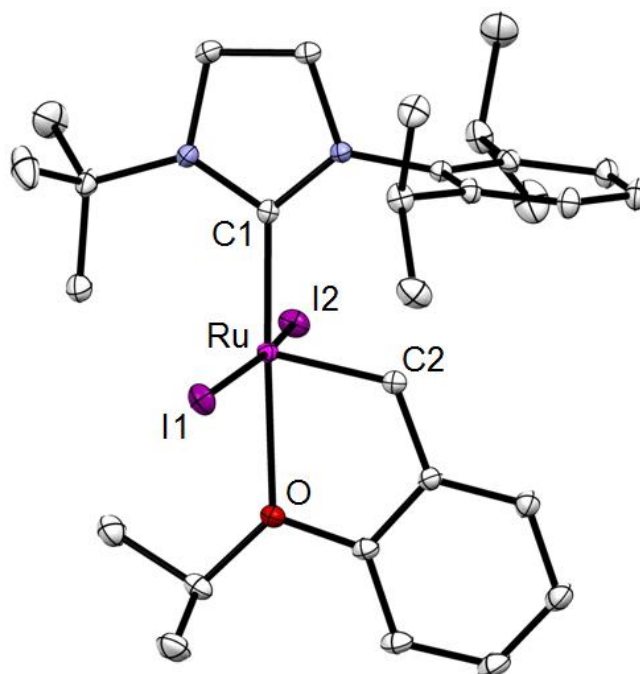


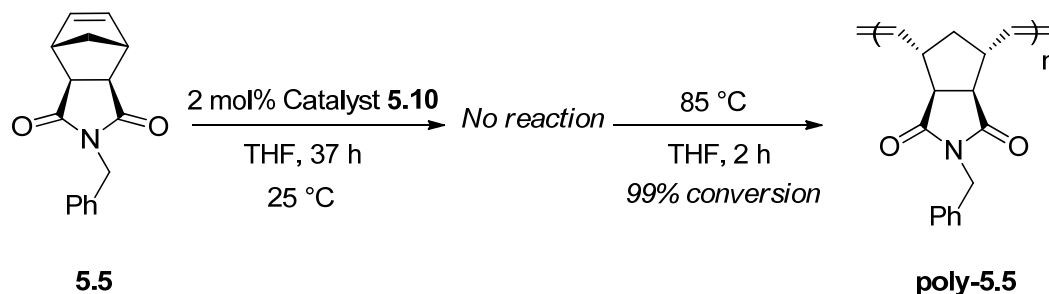
**Figure 5.4.** Crystal structure of **5.10**. Thermal ellipsoids set at 50% and hydrogen atoms omitted for clarity. Selected bond lengths (Å) and angles (deg.) for **5.10**: C1-Ru, 1.987; C2-Ru, 1.840; O-Ru 2.332; I1-Ru, 2.702; I2-Ru, 2.683; I-Ru-I, 6.66; C2-Ru-O, 78.09.

Since norbornene-derived polymers have numerous applications, research toward an efficient latent ROMP catalyst was focused on these monomers. Therefore norbornene-derived compounds **5.5-5.8**, representing a variety of functional groups and different degrees of steric hindrance, were explored as monomers for latent metathesis (Figure 5.3). Complexes **5.9** and **5.10** both proved to be latent for ROMP of **5.5**, affording no conversion of monomer **5.5** in THF after 4 hours at ambient temperature. Upon heating, >95% conversion to polymer was achieved with both catalysts **5.9** and **5.10** in 2 hours.

Due to better overall initiation, as well as superior latency after extended time periods, catalyst **5.10** was used for further latent ROMP studies. Catalyst **5.10** showed excellent latency at ambient temperature in THF, remaining stable but inactive for at least 24 hours, and subsequently initiating on heating to 85 °C in a sealed reaction vessel to give 99%

conversion to polymer **poly-5.5** (Scheme 5.4). This observed superior latent behavior of catalysts bearing iodide ligands compared to chloride ligands is consistent with previously reported reactivity trends for catalysts with different halogen ligands.<sup>28</sup>

**Scheme 5.4.** Latent ROMP of **5.5** with catalyst **5.10**.



The solvent also plays a role in the degree of latency of the catalysts, as THF proved to result in significantly improved latency at 25 °C for ROMP compared to benzene. Specifically, complex **5.10** showed excellent latency toward the ROMP of COD in THF at 25 °C, giving no polymerization product after 18 hours. However, repeating the same reaction with complex **5.10** using benzene as the solvent yields 28% conversion of COD to polymer after 30 minutes at 25 °C. THF may increase the latency of the catalysts by functioning as a coordinating solvent, thereby potentially slowing olefin association with ruthenium.

The results of latent ROMP of monomers **5.5-5.8** with catalyst **5.10** are presented in Table 5.3. Catalyst **5.10** was latent for the ROMP of all monomers screened, affording no reaction at 25 °C up to 37 hours. Excellent conversion was achieved in 2 hours at 85 °C for each of the monomers (Table 5.3, entries 2, 4, 6, and 8), and the corresponding polymers were isolated in good yield. The polydispersity index (PDI) was moderately low for the

polymerization of **5.5** and **5.6** (Table 5.3, entries 2 and 4), indicating good catalyst initiation and propagation. The PDI for the polymerization of **5.7** was significantly broader and for **5.8** was moderately broader (Table 5.3, entries 6 and 8, respectively), suggesting poorer catalyst initiation for these monomers.

**Table 5.3.** Latent ROMP of norbornene-derived monomers with catalyst **5.10**.

Entry <sup>a</sup>	Monomer	Temp. (°C)	Time (h)	% Conv. <sup>b</sup>	% Yield <sup>c</sup>	<i>M<sub>n</sub></i> (g/mol) <sup>d</sup>	PDI <sup>d</sup>
<b>1</b>	<b>5.5</b>	25	24	0	NA	NA	NA
<b>2</b>	<b>5.5</b>	85	2	99	81	24,300	1.16
<b>3</b>	<b>5.6</b>	25	37	0	NA	NA	NA
<b>4</b>	<b>5.6</b>	85	2	95	94	36,900	1.27
<b>5</b>	<b>5.7</b>	25	24	0	NA	NA	NA
<b>6</b>	<b>5.7</b>	85	2	99	48	2,000	3.25
<b>7</b>	<b>5.8</b>	25	37	0	NA	NA	NA
<b>8</b>	<b>5.8</b>	85	2	78	68	3,800	1.79

<sup>a</sup>The loading of catalyst **5.10** was 2 mol%. The substrate concentrations were 0.5M in THF, and the reactions were carried out sealed under a nitrogen atmosphere. <sup>b</sup>The conversion was determined by <sup>1</sup>H NMR spectroscopy. <sup>c</sup>Isolated polymer yield. <sup>d</sup>The molecular weight and PDI were determined by GPC.

## Conclusions

We have developed *N*-aryl, *N*-alkyl NHC ruthenium catalysts showing excellent latent behavior toward cross-metathesis and ROMP reactions, providing fine thermal control for initiation. These complexes demonstrate remarkable thermal stability over extended periods of time, enabling metathesis reactions to be successfully carried out at high temperatures. Exchanging out the chloride ligands for iodide ligands is important for producing complexes that are latent for ROMP. Catalyst studies showed that elevated temperatures are required for metathesis activity, and upon reacting at these temperatures, the catalysts afford good conversion of substrate to product. These *N*-aryl, *N*-*tert*-butyl

ruthenium complexes are attractive for applications in latent chemistry due to their properties and behavior, and their thermal stability lends them to be promising metathesis catalysts where elevated temperatures are required.

## Experimental Section

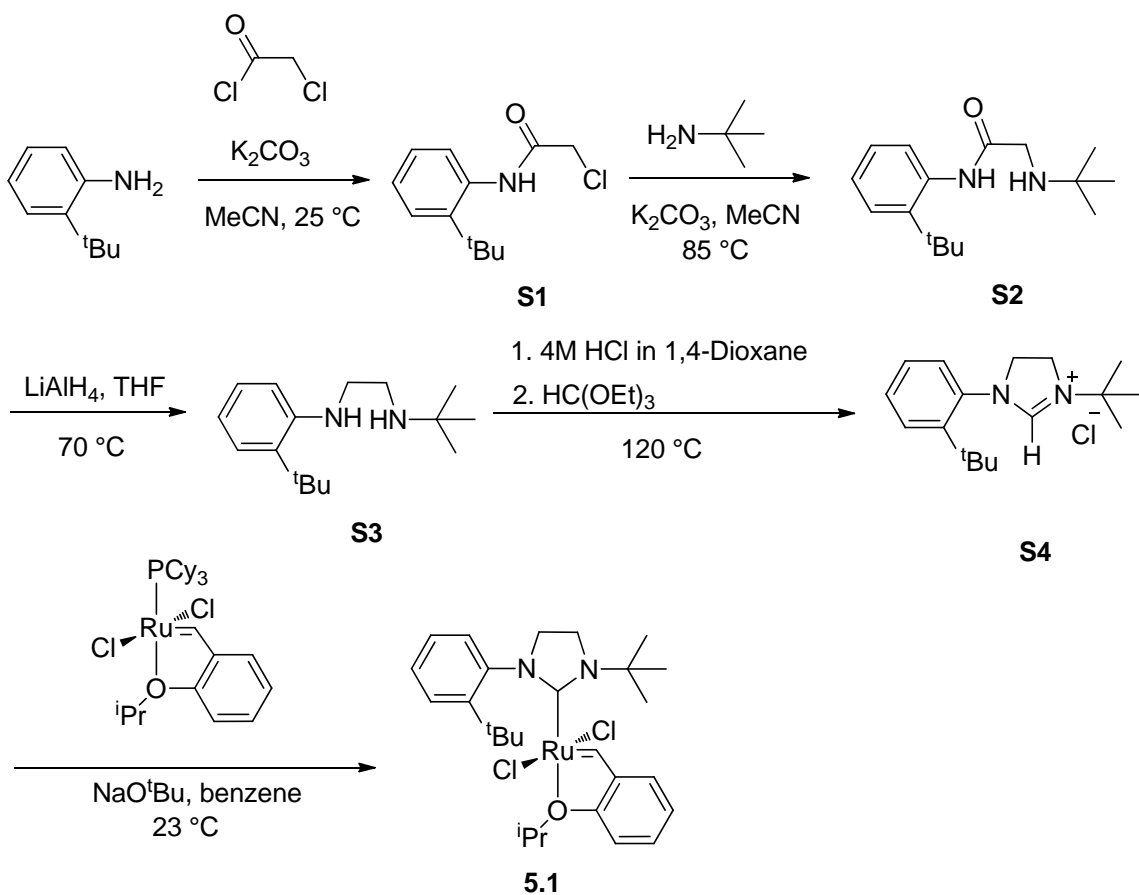
**General information.**  $^1\text{H}$  and  $^{13}\text{C}$  NMR spectra were recorded on a Varian Mercury ( $^1\text{H}$ , 300 MHz), a Varian Inova 400 ( $^1\text{H}$ , 400 MHz), a Varian Inova 500 ( $^1\text{H}$ , 500 MHz;  $^{13}\text{C}$ , 125 MHz), or an automated Varian Inova 500 ( $^1\text{H}$ , 500 MHz;  $^{13}\text{C}$ , 125 MHz) spectrometer and chemical shifts are reported in ppm downfield from  $\text{Me}_4\text{Si}$  by using the residual solvent peak as an internal standard. Gel permeation chromatography (GPC) analyses were carried out in HPLC grade tetrahydrofuran on two MZ-Gel 10  $\mu\text{m}$  columns (Analysetechnik) connected in series with a miniDAWN TREOS multiangle laser light scattering (MALLS) detector and an Optilab rex differential refractometer (both from Wyatt Technology). No calibration standards were used, and  $dn/dc$  values were obtained for each injection by assuming 100% mass elution from the columns. High resolution mass spectrometry (FAB) was done at the California Institute of Technology Mass Spectrometry Facility. X-ray crystallographic structures were obtained at the Beckman Institute X-ray Crystallography Laboratory at the California Institute of Technology. All air-sensitive reactions were conducted either in a nitrogen atmosphere glovebox or under an argon atmosphere using standard Schlenk-line techniques.

**Materials.** Toluene, benzene, benzene- $d_6$ , and tetrahydrofuran were dried by passage through solvent purification systems.<sup>29</sup> Ruthenium catalyst precursors  $\text{RuCl}_2(\text{PCy}_3)(=\text{CH}-o\text{-O}^i\text{Pr}-\text{C}_6\text{H}_4)$  and  $\text{RuCl}_2(\text{PCy}_3)_2(=\text{CHPh})$  were received from Materia, Inc. 1-Hexene was

dried over calcium hydride and distilled prior to use. 1-Octene, 5-hexenyl acetate, 4-penten-1-ol, 3-methyl-1-hexene, 3,5,5-trimethyl-1-hexene, allyl alcohol, allyl acetate, allyl ethyl ether, allyl benzene, and allyloxytrimethylsilane were degassed before use. All other reagents and solvents were used as purchased without further purification.

**Synthesis of Catalyst 5.1.** Catalyst **5.1** was synthesized following established procedures for making *N*-aryl, *N*-alkyl NHC ruthenium catalysts.<sup>21</sup>

**Scheme 5.5.** Synthesis of complex **5.1**.



Synthesis of **S1**. Anhydrous potassium carbonate (136.7 mmol, 18.9 grams) and acetonitrile (175 mL) were added to a 500 mL RB flask containing a stir bar. 2-*tert*-butyl aniline (134 mmol, 20.9 mL) was added via syringe with stirring, and chloroacetyl chloride (134 mmol, 10.7 mL) was then added dropwise. The reaction was stirred at room temperature for 48 hours, after which the resulting mixture was filtered through a thin pad of silica gel. The filtrate was concentrated under partial vacuum on a rotary evaporator, and hexanes were added to the obtained cream colored residue. The hexanes dissolved away the off-white color and the remaining white solids were filtered and washed with more hexanes to yield **S1** (20.40 g, 67% yield).  $^1\text{H}$  NMR ( $\text{CDCl}_3$ , 500 MHz):  $\delta$  8.44 (s, 1H), 7.66 (dd,  $J = 10$  Hz, 3 Hz, 1H), 7.42 (dd,  $J = 10.5$  Hz, 3 Hz, 1H), 7.28 – 7.16 (m, 2 H), 4.26 (s, 2H), 1.43 (s, 9H) ppm.  $^{13}\text{C}$  NMR ( $\text{CDCl}_3$ , 125 MHz):  $\delta$  163.96, 142.52, 134.32, 127.11, 126.98, 126.89, 126.76, 43.38, 34.79, 30.83 ppm.

Synthesis of **S2**. Anhydrous potassium carbonate (88.3 mmol, 12.2 grams) and **S1** (41.0 mmol, 9.2 g) were added to a 100 mL round bottom flask containing a stir bar. Acetonitrile (50 mL) was added, followed by *tert*-butyl amine (41.0 mmol, 4.3 mL). A reflux condenser was attached to the flask, and the reaction was heated at 85 °C for 40 hours with stirring. The crude reaction mixture was then filtered through a thin pad of silica gel, and the filtrate was concentrated *in vacuo*. The crude solids obtained were then dissolved in diethyl ether and loaded onto a silica gel column for purification (100% diethyl ether as the eluting solvent). The product was isolated as white solids (4.225 g) in 40% yield.  $^1\text{H}$  NMR ( $\text{CDCl}_3$ , 500 MHz):  $\delta$  9.74 (s, 1H), 7.97 (d,  $J = 8.0$  Hz, 1H), 7.38 (d,  $J = 7.9$  Hz, 1H), 7.23 (t,  $J = 7.6$  Hz, 1H), 7.10 (t,  $J = 7.6$  Hz, 1H), 3.40 (s, 2H), 1.45 (s,



9H), 1.16 (s, 9H) ppm.  $^{13}\text{C}$  NMR ( $\text{CDCl}_3$ , 125 MHz):  $\delta$  170.71, 140.42, 135.74, 127.02, 126.55, 125.11, 124.99, 51.49, 46.97, 34.68, 30.63, 29.24 ppm.

**Synthesis of S3.** In a nitrogen atmosphere glovebox, **S2** (4.2 grams, 16.0 mmol) was added to a 100 mL round bottom flask containing a stir bar, followed by the addition of dry tetrahydrofuran (THF) (50 mL). In a vial, lithium aluminum hydride (2.3 grams, 60.6 mmol) was weighed out and dry THF (15 mL) was slowly added. This lithium aluminum hydride suspension was then very slowly added to the solution of **S2**, and the round bottom flask was sealed and brought out of the glovebox. The reaction was heated at 70 °C for 6 days, and then removed from the oil bath and allowed to cool. Water was slowly added to quench, and the THF/water mixture was stirred for 3 hours. The mixture was then extracted with methylene chloride ( $6 \times 20$  mL). The combined organic layers were dried over  $\text{MgSO}_4$  and filtered. Concentration of the filtrate afforded a clear oil. The oil (4.10 g) was a mixture of product **S3** and unreacted starting material **S2** (95% and 5%, respectively). This crude mixture was carried directly on to the next step in the synthesis.  $^1\text{H}$  NMR ( $\text{CDCl}_3$ , 500 MHz):  $\delta$  7.27 – 7.23 (m, 1H), 7.13 (td,  $J = 8.0, 1.3$  Hz, 1H), 6.78 – 6.56 (m, 2H), 3.25 – 3.10 (m, 2H), 2.97 – 2.90 (m, 2H), 1.45 (s, 9H), 1.14 (s, 9H) ppm.

**Synthesis of S4.** **S3** (7.1 mmol, 1.76 g crude) was transferred to a 50 mL Schlenk tube containing a stir bar. Under an atmosphere of argon on the Schlenk line, 4M HCl in 1,4-dioxane (7.0 mL) was added via syringe through the septum cap. The mixture was stirred at room temperature for 2 hours. Vacuum was then applied to the Schlenk tube to remove excess HCl and 1,4-dioxane. The Schlenk tube was placed back under an argon atmosphere and anhydrous triethyl orthoformate (35.5 mmol, 5.9 mL) was added via syringe. The Schlenk tube was sealed under the argon atmosphere and heated to 120 °C

for 19 hours. After allowing the solution to cool, the crude mixture was added to a silica gel column for purification of the product (solvent system 5% MeOH in CH<sub>2</sub>Cl<sub>2</sub>). The product was isolated as a white powder (0.6549 g, 31% yield). <sup>1</sup>H NMR (CDCl<sub>3</sub>, 500 MHz):  $\delta$  8.21 (s, 1H), 8.09 (dd,  $J$  = 7.5, 1.9 Hz, 1H), 7.47 (dd,  $J$  = 7.7, 1.9 Hz, 1H), 7.35 (pd,  $J$  = 7.3, 1.8 Hz, 2H), 4.50 (t,  $J$  = 10.5 Hz, 2H), 4.32 (t,  $J$  = 10.4 Hz, 2H), 1.58 (s, 9H), 1.39 (s, 9H) ppm. <sup>13</sup>C NMR (CDCl<sub>3</sub>, 125 MHz):  $\delta$  156.27, 131.51, 131.29, 129.79, 129.51, 128.12, 127.66, 57.51, 55.10, 35.72, 32.24, 28.23, 25.79 ppm.

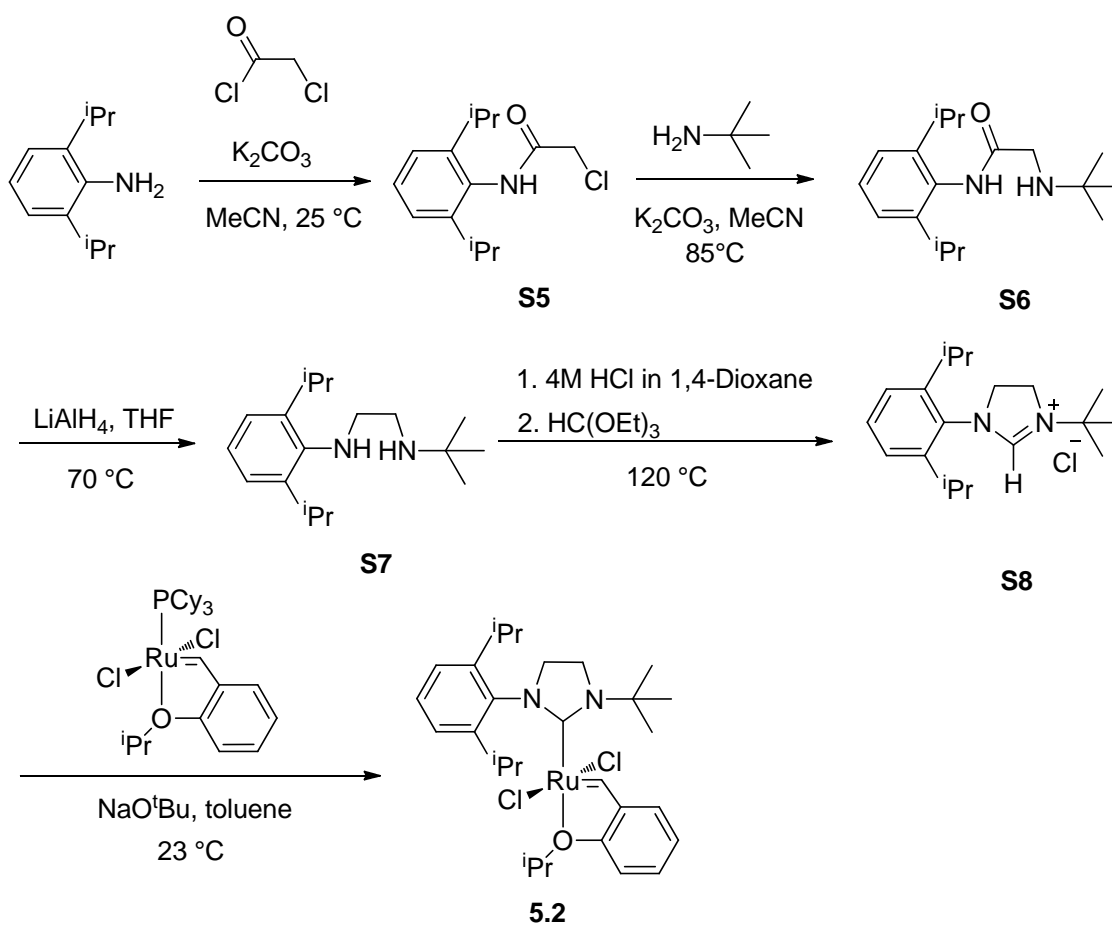
Synthesis of **5.1**. In a nitrogen atmosphere glovebox, **S4** (2.1 mmol, 0.620 g), sodium *tert*-butoxide (4.4 mmol, 0.420 g), and RuCl<sub>2</sub>(PCy<sub>3</sub>)(=CH-*o*-O<sup>*i*</sup>PrC<sub>6</sub>H<sub>4</sub>) (1.9 mmol, 1.16 g) were added to a 100 mL round bottom flask. Dry benzene (40 mL) was added to this mixture and the flask was sealed and brought out of the glovebox. The reaction was stirred at 30 °C for 12 hours. The crude mixture was then loaded directly onto a silica gel column. The eluting solvent was 10% diethyl ether in pentane, and the gradient was increased to 50% ether in pentane. The product was isolated from a green band that came off of the column. Concentration of fractions from this green band afforded **5.1** as a glittery, green powder (0.251 g) in 24% yield. <sup>1</sup>H NMR (CDCl<sub>3</sub>, 500 MHz):  $\delta$  16.99 (s, 1H), 7.75 (dd,  $J$  = 8.2, 1.4 Hz, 1H), 7.57 – 7.51 (m, 1H), 7.46 (ddd,  $J$  = 8.4, 7.1, 1.6 Hz, 1H), 7.24 (dd,  $J$  = 7.9, 1.6 Hz, 1H), 7.20 – 7.14 (m, 1H), 6.95 (d,  $J$  = 8.4 Hz, 1H), 6.88 (t,  $J$  = 7.4 Hz, 1H), 6.83 (dd,  $J$  = 7.5, 1.8 Hz, 1H), 5.15 – 5.00 (m, 1H), 4.17 – 4.08 (m, 1H), 3.97 – 3.81 (m, 2H), 3.75 – 3.71 (m, 1H), 2.26 (s, 6H), 1.66 (d,  $J$  = 6.2 Hz, 3H), 1.63 (d,  $J$  = 6.2 Hz, 3H), 1.52 (s, 6H) ppm. <sup>13</sup>C NMR (CDCl<sub>3</sub>, 125 MHz):  $\delta$  212.15, 153.33, 147.68, 144.93, 144.32, 132.48, 131.05, 129.33, 128.74, 128.39, 123.70, 122.78, 113.40, 77.48,

77.23, 76.98, 74.71, 57.93, 56.78, 46.01, 36.95, 32.58, 29.97, 22.71, 22.65 ppm. HRMS:  $[\text{C}_{27}\text{H}_{38}\text{Cl}_2\text{N}_2\text{ORu}] [(M+2)\text{-H}_2]$  Calc = 578.1405. Found = 578.1392.

### Synthesis of Catalyst **5.2**.

Complex **5.2** was synthesized in an analogous method to complex **5.1** (scheme 6).

**Scheme 5.6.** Synthesis of complex **5.2**.



Synthesis of **S5**. Anhydrous potassium carbonate (112.8 mmol, 15.6 grams) and acetonitrile (150 mL) were added to a 250 mL RB flask containing a stir bar. 2,6-Diisopropyl aniline (56.4 mmol, 10.0 mL) was added via syringe with stirring, and chloroacetyl chloride (56.4 mmol, 4.5 mL) was then added dropwise. The reaction was

stirred at room temperature for 43 hours, after which the resulting mixture was filtered through a thin pad of silica gel. The filtrate was concentrated under partial vacuum on a rotary evaporator, and hexanes were added to the obtained pale colored residue. The hexanes dissolved away the pale color and the remaining white solids were filtered and washed with more hexanes to yield **S5** (11.33 g, 79% yield).  $^1\text{H}$  NMR ( $\text{CDCl}_3$ , 500 MHz):  $\delta$  7.79 (s, 1H), 7.32 (t,  $J = 8$  Hz, 1H), 7.20 (d,  $J = 7$  Hz, 2H), 4.27 (s, 2H), 3.02 (sept,  $J = 6.5$  Hz, 2H), 1.21 (d,  $J = 7$  Hz, 12H) ppm.  $^{13}\text{C}$  NMR ( $\text{CDCl}_3$ , 125 MHz):  $\delta$  165.45, 146.16, 130.12, 129.00, 123.83, 43.02, 29.08, 23.82 ppm.

Synthesis of **S6**. Anhydrous potassium carbonate (42.3 mmol, 5.85 grams) and **S5** (20.6 mmol, 5.23 g) were added to a 100 mL round bottom flask containing a stir bar. Acetonitrile (40 mL) was added, followed by *tert*-butyl amine (20.6 mmol, 2.2 mL). A reflux condenser was attached to the flask, and the reaction was heated at 85 °C for 2 days with stirring. The crude reaction mixture was then filtered through a thin pad of silica gel, and the filtrate was concentrated *in vacuo*. The crude solids obtained were then dissolved in diethyl ether and loaded onto a silica gel column for purification (100% diethyl ether as the eluting solvent). The product was further purified by crystallization from layering methylene chloride (2 mL) with hexanes (10 mL). **S6** was obtained as white crystals (1.271 g, 33% yield).  $^1\text{H}$  NMR ( $\text{CDCl}_3$ , 500 MHz):  $\delta$  9.00 (s, 1H), 7.30 – 7.27 (m, 1H), 7.18 (d,  $J = 7.7$  Hz, 2H), 3.42 (s, 2H), 3.02 (sept,  $J = 6.9$  Hz, 2H), 1.21 (s, 6H), 1.20 (s, 6H), 1.18 (s, 9H) ppm.  $^{13}\text{C}$  NMR ( $\text{CDCl}_3$ , 125 MHz):  $\delta$  172.34, 145.91, 131.72, 128.17, 123.61, 51.40, 46.38, 29.32, 29.08, 23.80 ppm.

Synthesis of **S7**. In a nitrogen atmosphere glovebox, **S6** (0.702 grams, 2.42 mmol) was added to a 100 mL round bottom flask containing a stir bar, followed by the addition of

dry THF (5 mL). In a separate flask, lithium aluminum hydride (0.383 grams, 10.1 mmol) was weighed out and dry THF (5 mL) was slowly added. This lithium aluminum hydride suspension was then very slowly added to the solution of **S6**, and the round bottom flask was sealed and brought out of the glovebox. The reaction was heated while sealed at 70 °C for 5 days, after which it was removed from the oil bath and allowed to cool. Water was slowly added, and the mixture was then extracted with methylene chloride (4 x 20 mL). The combined organic layers were dried over MgSO<sub>4</sub> and filtered. Concentration of the filtrate afforded a clear oil. The oil (0.632 g) was a mixture of product **S7** and unreacted starting material **S6** (90% and 10%, respectively). This crude mixture was carried directly on to the next step in the synthesis. <sup>1</sup>H NMR (CDCl<sub>3</sub>, 500 MHz):  $\delta$  7.09 (d,  $J$  = 8.0 Hz, 2H), 7.05 – 7.00 (m, 1H), 3.32 – 3.35 (m, 2H), 2.95 (t,  $J$  = 5.6 Hz, 2H), 2.82 (t,  $J$  = 5.6 Hz, 2H), 1.24 (d,  $J$  = 6.8 Hz, 12H), 1.14 (s, 9H) ppm.

Synthesis of **S8**. **S7** (2.28 mmol, 0.631 g crude) was transferred to a 50 mL Schlenk tube containing a stir bar. Under an atmosphere of argon on the Schlenk line, 4M HCl in 1,4-dioxane (2.3 mL) was added via syringe through the septum cap. The mixture was stirred at room temperature for 2 hours. Vacuum was then applied to the Schlenk tube to remove excess HCl and 1,4-dioxane. The Schlenk tube was placed back under an argon atmosphere and anhydrous triethyl orthoformate (22.8 mmol, 3.8 mL) was added via syringe. The Schlenk tube was sealed under the argon atmosphere and heated to 120 °C for 18 hours. After allowing the solution to cool, the crude mixture was added to a silica gel column to purify (solvent system 5% MeOH in CH<sub>2</sub>Cl<sub>2</sub>). The product was isolated as a white powder (0.269 g) in 41% yield. <sup>1</sup>H NMR (CDCl<sub>3</sub>, 500 MHz):  $\delta$  8.69 (s, 1H), 7.41 (t,  $J$  = 7.5 Hz, 1H), 7.23 (d,  $J$  = 8 Hz, 2H), 4.53 (t,  $J$  = 10.5 Hz, 2H), 4.33 (t,  $J$  = 11.5 Hz,

2H), 2.94 (sept,  $J = 6.5$  Hz, 2H), 1.61 (s, 9H), 1.29 (d,  $J = 7$  Hz, 12H) ppm.  $^{13}\text{C}$  NMR ( $\text{CDCl}_3$ , 125 MHz):  $\delta$  156.64, 146.76, 131.28, 130.59, 125.12, 58.07, 54.00, 46.96, 29.07, 28.68, 25.16, 24.45 ppm.

Synthesis of **5.2**. In a nitrogen atmosphere glovebox, **S8** (0.464 mmol, 0.150 g), sodium *tert*-butoxide (1.0 mmol, 0.098 g), and  $\text{RuCl}_2(\text{PCy}_3)(=\text{CH}-o\text{-O}^i\text{PrC}_6\text{H}_4)$  (0.499 mmol, 0.300 g) were added to a 100 mL round bottom flask. Dry toluene (10 mL) was added to this mixture and the flask was sealed and brought out of the glovebox. The reaction was stirred at room temperature for 7 hours. The crude mixture was then loaded directly onto a silica gel column. The eluting solvent was 10% diethyl ether in pentane, and the gradient was increased to 50% ether in pentane. The product was isolated from a green band that came off of the column. Concentration of fractions from this green band afforded **5.2** as a dark green powder (0.097 grams, 35% yield).  $^1\text{H}$  NMR ( $\text{CDCl}_3$ , 500 MHz):  $\delta$  16.96 (s, 1H), 7.57 (t,  $J = 8$  Hz, 1H), 7.52 – 7.49 (m, 1H), 7.37 (d,  $J = 8$  Hz, 2H), 6.91 (d,  $J = 8.5$  Hz, 1H), 6.83 (t,  $J = 7.5$  Hz, 1H), 6.78 – 6.75 (m, 1H), 5.04 (sept,  $J = 6.5$  Hz, 1H), 3.98 – 3.95 (m, 2H), 3.90 – 3.86 (m, 2H), 3.14 (sept,  $J = 6.5$  Hz, 2H), 2.26 (s, 9H), 1.62 (d,  $J = 6\text{Hz}$ , 6H), 1.17 (d,  $J = 7$  Hz, 6H), 0.89 (d,  $J = 7$  Hz, 6H) ppm.  $^{13}\text{C}$  NMR ( $\text{CDCl}_3$ , 125 MHz):  $\delta$  208.29, 153.04, 148.51, 145.01, 139.37, 130.77, 129.50, 125.17, 123.79, 122.73, 113.40, 74.75, 56.53, 54.96, 45.96, 30.17, 28.07, 26.07, 24.23, 22.76 ppm. HRMS:  $[\text{C}_{35}\text{H}_{40}\text{Cl}_2\text{N}_2\text{ORu}] [(M+2)\text{-H}_2]$  Calculated = 676.1562. Found = 676.1570.

### Latent Cross-Metathesis Reactions

The latent cross-metathesis screens were carried out by two methods; both methods produced the same result. The first method of screening the catalysts for latency for

cross-metathesis of a substrate involved setting up two duplicate, identical experiments, with one reaction at 25 °C and the other reaction at 85 °C. The conversion of substrate to product for both reactions was measured by  $^1\text{H}$  NMR. The second method entailed taking one reaction and observing it over a given time period at 25 °C, and then taking an  $^1\text{H}$  NMR spectrum to determine the percent conversion, if any. This same exact reaction was subsequently heated at 85 °C. Both sets of experiments gave the same degree of latency at ambient temperature, and the same conversion to product upon heating for a given amount of time. Catalyst **5.1** gave a mixture of *cis* and *trans* product isomers, which had overlapping peaks in the NMR spectra.

### Representative Latent Cross-Metathesis of 1-hexene

In a nitrogen atmosphere glovebox, catalyst **5.1** (0.0047 mmol, 2.7 mg) was added to an NMR tube. Benzene- $d_6$  (0.50 mL) was added via syringe, followed by 1-hexene (0.24 mmol, 30  $\mu\text{L}$ ), which was added via a 50  $\mu\text{L}$  syringe. This gave a concentration of 1-hexene in benzene of 0.5M. The NMR tube was then sealed and the contents were mixed. The NMR tube was subsequently heated while sealed at 85 °C in an oil bath for 24 hours. An  $^1\text{H}$  NMR spectrum was taken to determine the percent conversion of 1-hexene to 5-decene, which was calculated to be 90%. The  $^1\text{H}$  NMR spectrum matched reported NMR spectra for this product.<sup>30,31</sup>  $^1\text{H}$  NMR of 5-decene (500 MHz,  $\text{C}_6\text{D}_6$ ):  $\delta$  5.41-5.47 (m, 2H), 1.93-2.07 (m, 4H), 1.22-1.37 (m, 8H), 0.88 (t,  $J = 7.1$  Hz, 6H) ppm.

### Latent Cross-Metathesis of 1-octene

Catalyst **5.1** (0.0053 mmol, 3.1 mg), benzene- $d_6$  (0.53 mL), and 1-octene (0.27 mmol, 42  $\mu\text{L}$ ) were added to an NMR tube. The NMR tube was then sealed and heated at 85 °C in

an oil bath for 22 hours. An  $^1\text{H}$  NMR spectrum was taken to determine the percent conversion of 1-octene to 7-tetradecene, which was calculated to be 76%. The  $^1\text{H}$  NMR spectrum matched reported NMR spectra for this product.<sup>31</sup>  $^1\text{H}$  NMR of 7-tetradecene (500 MHz,  $\text{C}_6\text{D}_6$ ):  $\delta$  5.42-5.49 (m, 2H), 1.97-2.09 (m, 4H), 1.20-1.40 (m, 12H), 0.89 (t,  $J$ = 7.1 Hz, 6H) ppm.

### **Latent Cross-Metathesis of 5-hexenyl acetate**

Catalyst **5.1** (0.005 mmol, 2.9 mg), benzene- $d_6$  (0.49 mL), and 5-hexenyl acetate (0.25 mmol, 40  $\mu\text{L}$ ) were added to an NMR tube. The NMR tube was then sealed and heated at 85  $^\circ\text{C}$  in an oil bath for 22 hours. An  $^1\text{H}$  NMR spectrum was taken to determine the percent conversion of 5-hexenyl acetate to 5-decenyl-1,10-diacetate, which was calculated to be 62%. The  $^1\text{H}$  NMR spectrum matched reported NMR spectra for this product.<sup>32</sup>  $^1\text{H}$  NMR of 5-decenyl-1,10-diacetate (500 MHz,  $\text{C}_6\text{D}_6$ ):  $\delta$  5.26-5.32 (m, 2H), 3.95-3.99 (m, 4H), 1.82-1.91 (m, 4H), 1.68 (s, 6H), 1.35-1.45 (m, 4H), 1.20-1.27 (m, 4H) ppm.

### **Latent Cross-Metathesis of 4-penten-1-ol**

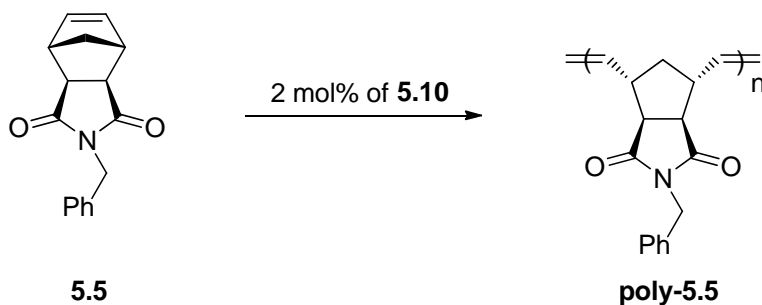
Catalyst **5.1** (0.0052 mmol, 3.0 mg), benzene- $d_6$  (0.51 mL), and 4-penten-1-ol (0.26 mmol, 26  $\mu\text{L}$ ) were added to an NMR tube. The NMR tube was then sealed and heated at 85  $^\circ\text{C}$  in an oil bath for 22 hours. An  $^1\text{H}$  NMR spectrum was taken to determine the percent conversion of 4-penten-1-ol to 4-octene-1,8-diol, which was calculated to be 89%. The  $^1\text{H}$  NMR spectrum matched reported NMR spectra for this product.<sup>33</sup>  $^1\text{H}$  NMR of 4-octene-1,8-diol (500 MHz,  $\text{C}_6\text{D}_6$ ):  $\delta$  5.28-5.52 (m, 2H), 3.42 (t,  $J$ = 6.5 Hz, 4H), 2.07-2.12 (m, 4H), 1.71 (s, 2H), 1.52-1.54 (m, 4H) ppm.



### Latent Cross-Metathesis of 3-methyl-1-hexene

Catalyst **5.1** (0.005 mmol, 2.9 mg), benzene-*d*<sub>6</sub> (0.51 mL), and 3-methyl-1-hexene (0.25 mmol, 36  $\mu$ L) were added to an NMR tube. The NMR tube was then sealed and heated at 85 °C in an oil bath for 22 hours. An <sup>1</sup>H NMR spectrum was taken to determine the percent conversion of 3-methyl-1-hexene to 4,7-dimethyl-5-decene, which was calculated to be 17%. <sup>1</sup>H NMR of 4,7-dimethyl-5-decene (500 MHz, C<sub>6</sub>D<sub>6</sub>):  $\delta$  5.24-5.27 (m, 2H), 1.93-1.98 (m, 2H), 1.15-1.27 (m, 8H), 0.99-1.01 (m, 6H), 0.86 (t, *J* = 7.3 Hz, 6H) ppm.

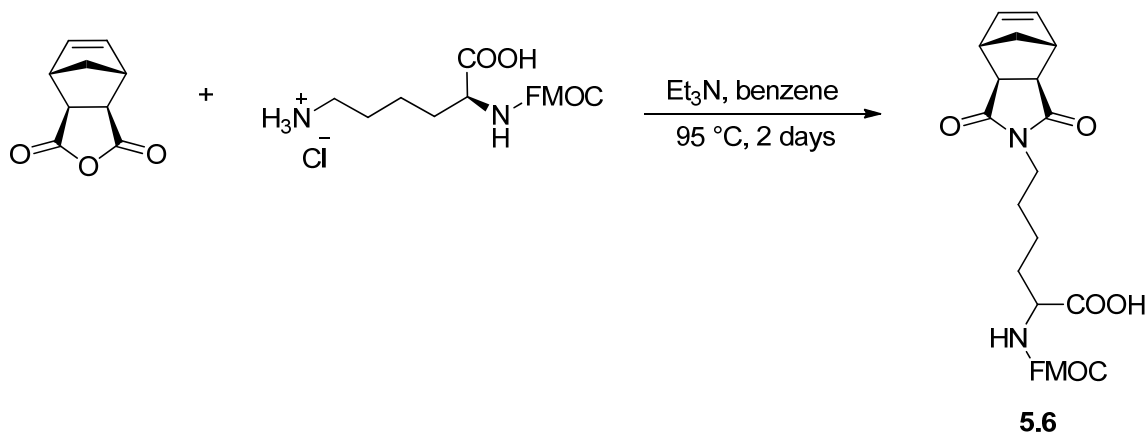
### Latent ROMP of Monomer 5.5



In a glovebox under a nitrogen atmosphere, complex **5.2** (0.0047 mmol, 2.9 mg) was added to an NMR tube. Subsequently, 25 equivalents of sodium iodide (0.12 mmol, 17.8 mg) were added (12.5 equivalents per chloride ligand), followed by the addition of THF-*d*<sub>8</sub> (0.89 mL) via syringe. The NMR tube was capped and the solution was mixed and left for 4 hours to allow the chloride ligands to exchange out for iodide ligands to give catalyst **5.10**. After 4 hours, monomer **5.5**<sup>34,35</sup> (0.25 mmol, 64 mg) was added to the NMR tube, and the reaction was carried out at 25 °C. After 24 hours at 25 °C, an <sup>1</sup>H NMR spectrum was taken of the reaction mixture. Based on <sup>1</sup>H NMR spectroscopy, there was

no conversion of monomer **5.5**. The NMR tube was then heated while sealed at 85 °C for 2 hours. After 2 hours at 85 °C, an  $^1\text{H}$  NMR spectrum was taken of the reaction mixture. There was complete conversion of monomer to polymer (99%). The polymer was precipitated in methanol, which was decanted off. The white polymer was filtered and washed with methanol and then dried under vacuum to afford 52 mg of polymer **poly-5.5** (81% isolated yield).  $^1\text{H}$  NMR of polymer **poly-5.5** (500 MHz,  $\text{CDCl}_3$ ):  $\delta$  7.30-7.45 (m, 5H), 5.77-5.86 (m, 2H), 4.68 (s, br, 2H), 3.03-3.12 (m, 2H), 2.68-2.79 (m, 2H), 2.15-2.25 (m, 1H), 1.69-1.77 (m, 1H) ppm.  $^{13}\text{C}$  NMR (125 MHz,  $\text{CDCl}_3$ ):  $\delta$  178.09, 136.15, 132.16, 131.95, 128.89, 128.83, 128.12, 51.20, 51.10, 46.05, 45.88, 42.39, 42.27 ppm. GPC data:  $M_n = 24,300$ , PDI = 1.16.

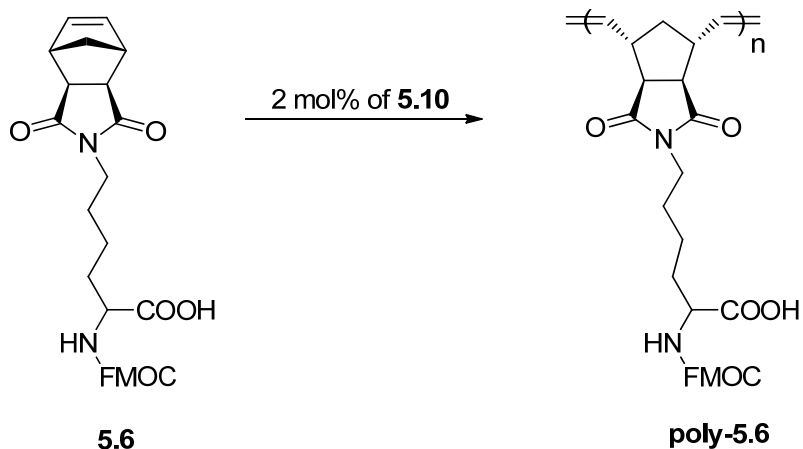
### Synthesis of monomer **5.6**



*cis*-5-Norbornene-*exo*-2,3-dicarboxylic anhydride (7.3 mmol, 1.2 g) and Fmoc-Lys-OH hydrochloride (7.6 mmol, 3.08 g) were dissolved in benzene (14 mL), and triethylamine (7.6 mmol, 1.06 mL) was added with stirring. The reaction was heated with a Dean-Stark trap at 95 °C for two days, after which the solution was cooled to room temperature. 1 M

HCl was added to the solution, and the mixture was extracted two times with methylene chloride. The combined organic layers were washed with brine, and subsequently dried over Na<sub>2</sub>SO<sub>4</sub>, filtered, and concentrated under vacuum. The product was purified by silica gel chromatography (3–10% methanol in ether). White solids (2.87 g) were isolated in 76% yield. <sup>1</sup>H NMR (500 MHz, CDCl<sub>3</sub>):  $\delta$  7.76 (d,  $J$  = 7.5 Hz, 2H), 7.64 – 7.59 (m, 2H), 7.39 (t,  $J$  = 7.4 Hz, 2H), 7.31 (t,  $J$  = 7.4 Hz, 2H), 6.25 (s, 2H), 4.32 – 4.45 (m, 3H), 4.22 (t,  $J$  = 6.9 Hz, 1H), 3.48 (t,  $J$  = 7.0 Hz, 1H), 3.45 – 3.35 (m, 1H), 3.26 (s, 2H), 2.67 (s, 2H), 1.89 – 1.98 (m, 1H), 1.72 – 1.83 (m, 1H), 1.66 – 1.53 (m, 2H), 1.50 (d,  $J$  = 9.8 Hz, 1H), 1.45 – 1.28 (m, 2H), 1.20 (d,  $J$  = 9.6 Hz, 1H) ppm. <sup>13</sup>C NMR (126 MHz, CDCl<sub>3</sub>):  $\delta$  178.53, 143.91, 141.51, 138.03, 138.00, 127.95, 127.30, 125.35, 120.20, 110.20, 68.86, 67.36, 48.06, 47.36, 45.37, 42.96, 38.17, 31.56, 27.41, 22.60 ppm.

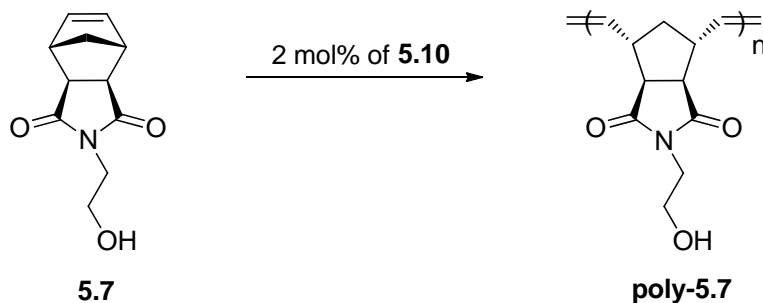
### Latent ROMP of Monomer **5.6**



In a glovebox under a nitrogen atmosphere, complex **5.2** (0.0028 mmol, 1.7 mg) was added to an NMR tube. Subsequently, 25 equivalents of sodium iodide (0.07 mmol, 11.1

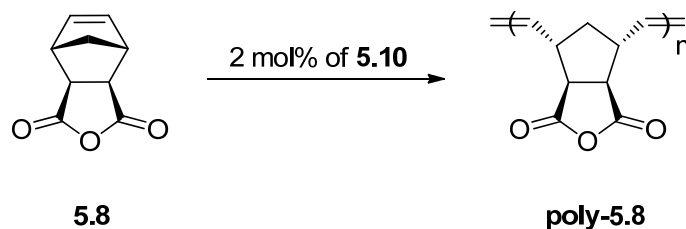
mg) were added, followed by the addition of THF- $d_8$  (0.54 mL) via syringe. The NMR tube was capped and the solution was mixed and left for 4 hours to allow the chloride ligands to exchange out for iodide ligands to give catalyst **5.10**. After 4 hours, monomer **5.6** (0.15 mmol, 76 mg) was added to the NMR tube, and the reaction was carried out at 25 °C. After 37 hours at 25 °C, a  $^1\text{H}$  NMR spectrum was taken of the reaction mixture. Based on  $^1\text{H}$  NMR spectroscopy, there was no conversion of monomer **5.6**. The NMR tube was then heated while sealed at 85 °C for 2 hours. After 2 hours at 85 °C, a  $^1\text{H}$  NMR spectrum was taken of the reaction mixture. There was 95% conversion of monomer to polymer **poly-5.6**. The polymer was precipitated in methanol, with the addition of pentane, which was decanted off. The white polymer was filtered and washed with methanol and then pentane, and dried under vacuum to afford 71.5 mg of **poly-5.6** (94% isolated yield).  $^1\text{H}$  NMR of polymer **poly-5.6** (500 MHz, THF- $d_8$ ):  $\delta$  7.73-7.78 (m, 2H), 7.62-7.69 (m, 2H), 7.30-7.36 (m, 2H), 7.23-7.29 (m, 2H), 5.62-5.74 (m, 2H), 4.27-4.35 (m, 2H), 4.17-4.25 (m, 2H), 3.35-3.43 (m, 2H), 2.80-2.95 (m, 2H), 2.25-2.70 (m, 6H), 1.46-1.62 (m, 2H+1H), 1.32-1.41 (m, 1H) ppm. GPC data:  $M_n$  = 36,900, PDI = 1.27.

### Latent ROMP of Monomer 5.7



In a glovebox under a nitrogen atmosphere, complex **5.2** (0.0048 mmol, 2.9 mg) was added to an NMR tube. Subsequently, 25 equivalents of sodium iodide (0.12 mmol, 18 mg) were added, followed by the addition of THF-*d*<sub>8</sub> (0.91 mL) via syringe. The NMR tube was capped and the solution was mixed and left for 4 hours to allow the chloride ligands to exchange out for iodide ligands to give catalyst **5.10**. After 4 hours, monomer **5.7**<sup>36</sup> (0.24 mmol, 50 mg) was added to the NMR tube, and the reaction was carried out at 25 °C. After 24 hours at 25 °C, a <sup>1</sup>H NMR spectrum was taken of the reaction mixture. Based on <sup>1</sup>H NMR spectroscopy, there was no conversion of monomer **5.7**. The NMR tube was then heated while sealed at 85 °C for 2 hours. After 2 hours at 85 °C, a <sup>1</sup>H NMR spectrum was taken of the reaction mixture. There was complete conversion of monomer to polymer. The polymer was precipitated in pentane, which was decanted off. The white polymer was filtered and washed with pentane and then dried under vacuum to afford 24.1 mg of polymer **poly-5.7** (48% isolated yield). <sup>1</sup>H NMR of polymer **poly-5.7** (500 MHz, THF-*d*<sub>8</sub>): δ 6.24-6.31 (m, 2H), 3.57-3.63 (m, 2H), 3.51-3.56 (m, 2H), 3.10-3.17 (m, 2H), 2.64-2.68 (m, 2H), 1.37-1.42 (m, 2H) ppm. <sup>13</sup>C NMR (125 MHz, THF-*d*<sub>8</sub>): δ 178.34, 138.77, 59.36, 48.72, 46.26, 43.55, 41.80 ppm. GPC data: *M*<sub>n</sub> = 2,000, PDI = 3.25.

### Latent ROMP of Monomer **5.8**



In a glovebox under a nitrogen atmosphere, complex **5.2** (0.0054 mmol, 3.3 mg) was added to an NMR tube. Subsequently, 25 equivalents of sodium iodide (0.14 mmol, 21

mg) were added, followed by the addition of THF- $d_8$  (1.0 mL) via syringe. The NMR tube was capped and the solution was mixed and left for 4 hours to allow the chloride ligands to exchange out for iodide ligands to give catalyst **5.10**. After 4 hours, monomer **5.8** (0.28 mmol, 46 mg) was added to the NMR tube, and the reaction was carried out at 25 °C. After 37 hours at 25 °C, a  $^1\text{H}$  NMR spectrum was taken of the reaction mixture. Based on  $^1\text{H}$  NMR spectroscopy, there was no conversion of monomer **5.8**. The NMR tube was then heated while sealed at 85 °C for 2 hours. After 2 hours at 85 °C, a  $^1\text{H}$  NMR spectrum was taken of the reaction mixture. There was 78% conversion of monomer to polymer. The polymer was precipitated in pentane, which was decanted off. The white polymer was filtered and washed with pentane and then dried under vacuum to afford 31.1 mg of polymer **poly-5.8** (68% isolated yield).  $^1\text{H}$  NMR of polymer **poly-5.8** (500 MHz, THF- $d_8$ ):  $\delta$  5.40-5.53 (m, 2H), 2.87-2.98 (m, 2H), 2.76-2.84 (m, 2H), 1.95-2.06 (m, 1H), 1.25-1.37 (m, 1H) ppm.  $^{13}\text{C}$  NMR (125 MHz, THF- $d_8$ ):  $\delta$  174.35, 173.57, 133.12, 53.56, 51.59, 46.31, 46.19, 46.08, 39.96, 30.75 ppm. GPC data:  $M_n$  = 3,800, PDI = 1.79.

**Acknowledgement.** Dr. Rosemary Conrad for the synthesis of monomer **5.6**.

The author thanks the *American Chemical Society* for permission for the contents of this chapter. This research has been published in *Organometallics*. Article reference: Thomas, R. M.; Fedorov, A.; Keitz, B. K.; Grubbs, R. H. *Organometallics* **2011**, 30, 6713-6717.

## REFERENCES

1. (a) Trnka, T. M.; Grubbs, R. H. *Acc. Chem. Res.* **2001**, *34*, 18–29. (b) Hoveyda, A. H.; Zhugralin, A. R. *Nature* **2007**, *450*, 243–251. (c) Chatterjee, A. K.; Morgan, J. P.; Scholl, M.; Grubbs, R. H. *J. Am. Chem. Soc.* **2000**, *122*, 3783–3784. (d) Fu, G. C.; Nguyen, S. T.; Grubbs, R. H. *J. Am. Chem. Soc.* **1993**, *115*, 9856–9857.
2. Ritter, T.; Hejl, A.; Wenzel, A. G.; Funk, T. W.; Grubbs, R. H. *Organometallics* **2006**, *25*, 5740–5745.
3. Kuhn, K. M.; Bourg, J. B.; Chung, C. K.; Virgil, S. C.; Grubbs, R. H. *J. Am. Chem. Soc.* **2009**, *131*, 5313–5320.
4. (a) Endo, K.; Grubbs, R. H. *J. Am. Chem. Soc.* **2011**, *133*, 8525–8527.
5. (b) Chatterjee, A. K.; Choi, T. L.; Sanders, D. P.; Grubbs, R. H. *J. Am. Chem. Soc.* **2003**, *125*, 11360–11370.
6. Monsaert, S.; Lozano Vila, A.; Drozdak, R.; Van Der Voort, P.; Verpoort, F. *Chem. Soc. Rev.* **2009**, *38*, 3360–3372.
7. Szadkowska, A.; Grela, K. *Current Organic Chemistry* **2008**, *12*, 1631–1647.
8. Hejl, A.; Day, M. W.; Grubbs, R. H. *Organometallics* **2006**, *25*, 6149–6154.
9. Ung, T.; Hejl, A.; Grubbs, R. H. *Organometallics* **2004**, *23*, 5399–5401.
10. Samec, J. S.; Keitz, B. K.; Grubbs, R. H. *J. Organomet. Chem.* **2010**, *695*, 1831–1837.
11. Wang, D.; Wurst, K.; Knolle, W.; Decker, U.; Prager, L.; Naumov, S.; Buchmeiser, M. R. *Angew. Chem. Int. Ed.* **2008**, *47*, 3267–3270.
12. Ginzburg, Y.; Anaby, A.; Vidavsky, Y.; Diesendruck, C. E.; Ben-Asuly, A.; Goldberg, I.; Lemcoff, N. G. *Organometallics* **2011**, *30*, 3430–3437.
13. Wang, D.; Wurst, K.; Buchmeiser, M. R. *Chem. Eur. J.* **2010**, *16*, 12928–12934.
14. Kost, T.; Sigalov, M.; Goldberg, I.; Ben-Asuly, A.; Lemcoff, N. G. *J. Organomet. Chem.* **2008**, *693*, 2200–2203.
15. (a) Monsaert, S.; Ledoux, N.; Drozdak, R.; Verpoort, F. *J. Polym. Sci. Part A: Polym. Chem.* **2010**, *48*, 302–310. (b) Zirngast, M.; Pump, E.; Leitgeb, A.; Albering, J. H.; Slugovc, C. *Chem. Comm.* **2011**, *47*, 2261–2263.
16. Lexer, C.; Burtscher, D.; Perner, B.; Tzur, E.; Lemcoff, G. N.; Slugovc, C. *J. Organomet. Chem.* **2011**, *696*, 2466–2470.

17. Hudson, D. M.; Valerte, E. J.; Schachner, J.; Limbach, M.; Müller, K.; Schanz, H. *J. ChemCatChem* **2011**, *3*, 297–301.
18. Diesendruck, C. E.; Vidavsky, Y.; Ben-Asuly, A.; Lemcoff, N. G. *Journal of Polymer Science: Part A: Polymer Chemistry* **2009**, *47*, 4209–4213.
19. Ben-Asuly, A.; Tzur, E.; Diesendruck, C. E.; Sigalov, M.; Goldberg, I.; Lemcoff, N. G. *Organometallics* **2008**, *27*, 811–813.
20. Kabro, A.; Roisnel, T.; Fischmeister, C.; Bruneau, C. *Chem. Eur. J.* **2010**, *16*, 12255–12261.
21. Szadkowska, A.; Gstrein, X.; Burtscher, D.; Jarzemska, K.; Wozniak, K.; Slugovc, C.; Grela, K. *Organometallics* **2010**, *29*, 117–124.
22. Thomas, R. M.; Keitz, B. K.; Champagne, T. M.; Grubbs, R. H. *J. Am. Chem. Soc.* **2011**, *133*, 7490–7496.
23. Hong, S. H.; Sanders, D. P.; Lee, C. W.; Grubbs, R. H. *J. Am. Chem. Soc.* **2005**, *127*, 17160–17161.
24. (a) Nguyen, S. T.; Johnson, L. K.; Grubbs, R. H. *J. Am. Chem. Soc.* **1992**, *114*, 3974–3975. (b) Schwab, P.; France, M. B.; Ziller, J. W.; Grubbs, R. H. *Angew. Chem. Int. Ed.* **1995**, *34*, 2039–2041.
25. Funk, T. W.; Berlin, J. M.; Grubbs, R. H. *J. Am. Chem. Soc.* **2006**, *128*, 1840–1846.
26. Hejl, A. Ph.D. Dissertation, California Institute of Technology, **2007**.
27. Sanford, M. S.; Love, J. A.; Grubbs, R. H. *J. Am. Chem. Soc.* **2001**, *123*, 6543–6554.
28. Catalyst **10** was investigated for latent RCM of diethyl diallylmalonate; however, the complex never initiated even at 85 °C for this substrate. Catalyst **2**, with chloride ligands in place of iodide ligands, showed low activity for RCM of diethyl diallylmalonate at 25 °C. These complexes were therefore concluded to not be optimal for latent RCM.
29. Wappel, J.; Urbina-Blanco, C. A.; Abbas, M.; Albering, J. H.; Saf, R.; Nolan, S. P.; Slugovc, C. *Beilstein J. Org. Chem.* **2010**, *6*, 1091–1098.
30. Pangborn, A. B.; Giardello, M. A.; Grubbs, R. H.; Rosen, R. K.; Timmers, F. J. *Organometallics* **1996**, *15*, 1518–1520.
31. Kim, I. S.; Dong, G. R.; Jung, Y. H. *J. Org. Chem.* **2007**, *72*, 5424–5426.
32. Jiang, A. J.; Zhao, Y.; Schrock, R. R.; Hoveyda, A. H. *J. Am. Chem. Soc.* **2009**, *131*, 16630–16631.

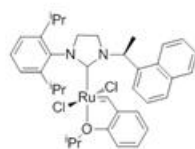


33. Pederson, R. L.; Fellows, I. M.; Ung, T. A.; Ishihara, H.; Hajela, S. P. *Adv. Synth. Catal.* **2002**, *344*, 728–735.
34. Keitz, B. K.; Endo, K.; Herbert, M. B.; Grubbs, R. H. *J. Am. Chem. Soc.* **2011**, *133*, 9686–9688.
35. Wang, D.; Wurst, K.; Knolle, W.; Decker, U.; Prager, L.; Naumov, S.; Buchmeiser, M. R. *Angew. Chem. Int. Ed.* **2008**, *47*, 3267–3270.
36. Haigh, D. M.; Kenwright, A. M.; Khosravi, E. *Macromolecules* **2005**, *38*, 7571–7579.
37. Matson, J. B.; Grubbs, R. H. *J. Am. Chem. Soc.* **2008**, *130*, 6731–6733.

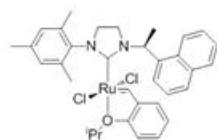
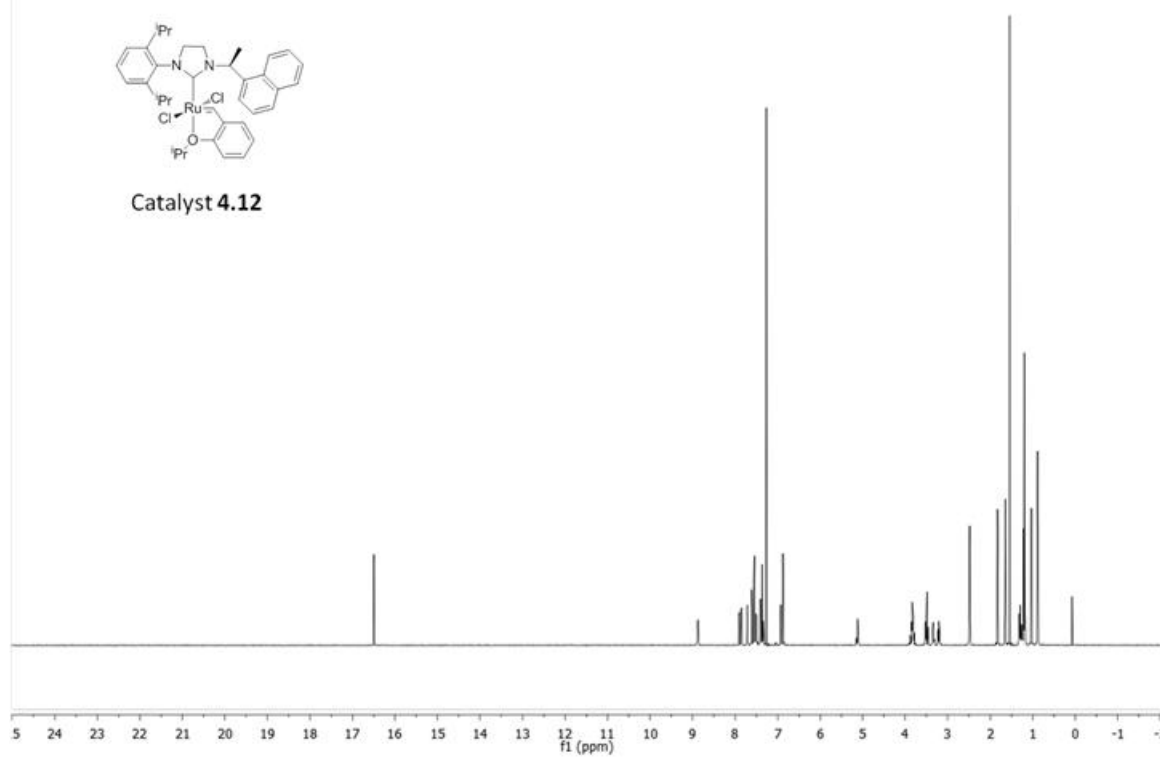
***APPENDIX A***

<sup>1</sup>H NMR Spectra of Chapter 4 Catalysts in CDCl<sub>3</sub>

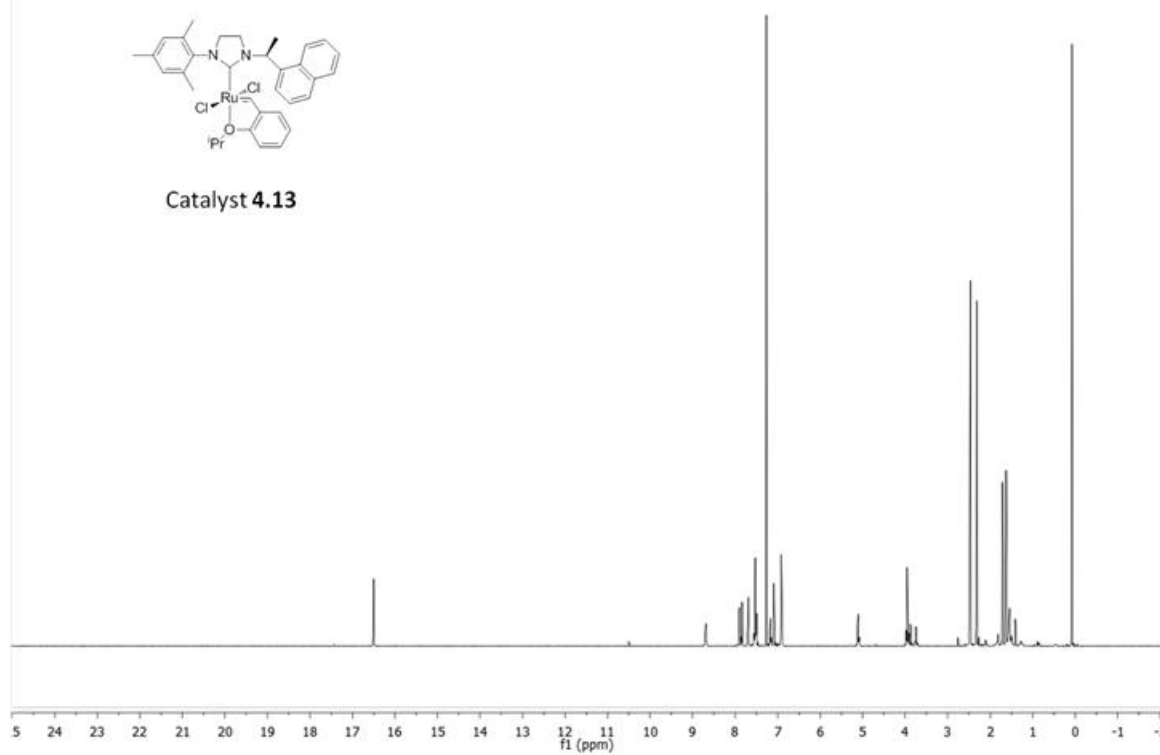
X-Ray Crystallographic Data of Catalysts **12** and **15**

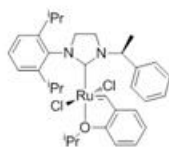


Catalyst 4.12

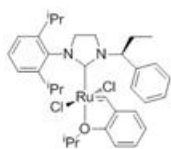
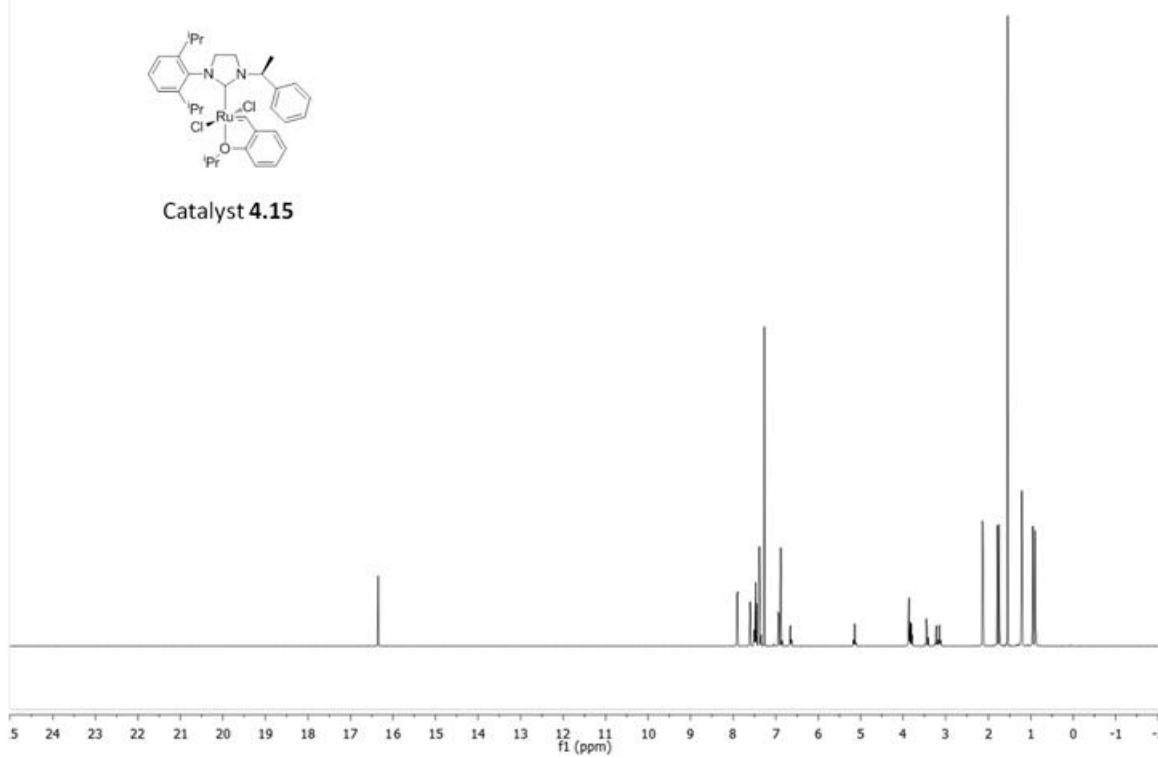


Catalyst 4.13

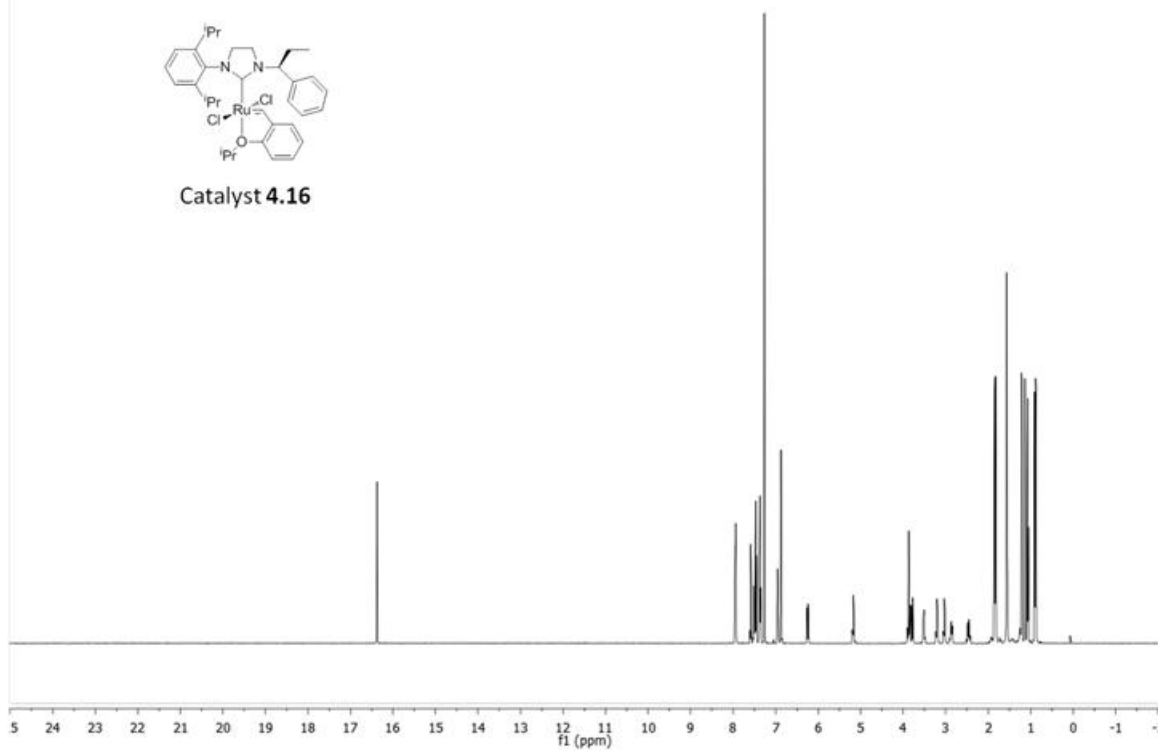


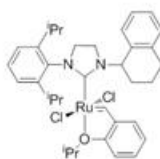


Catalyst 4.15

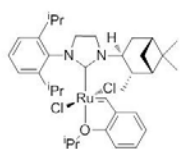
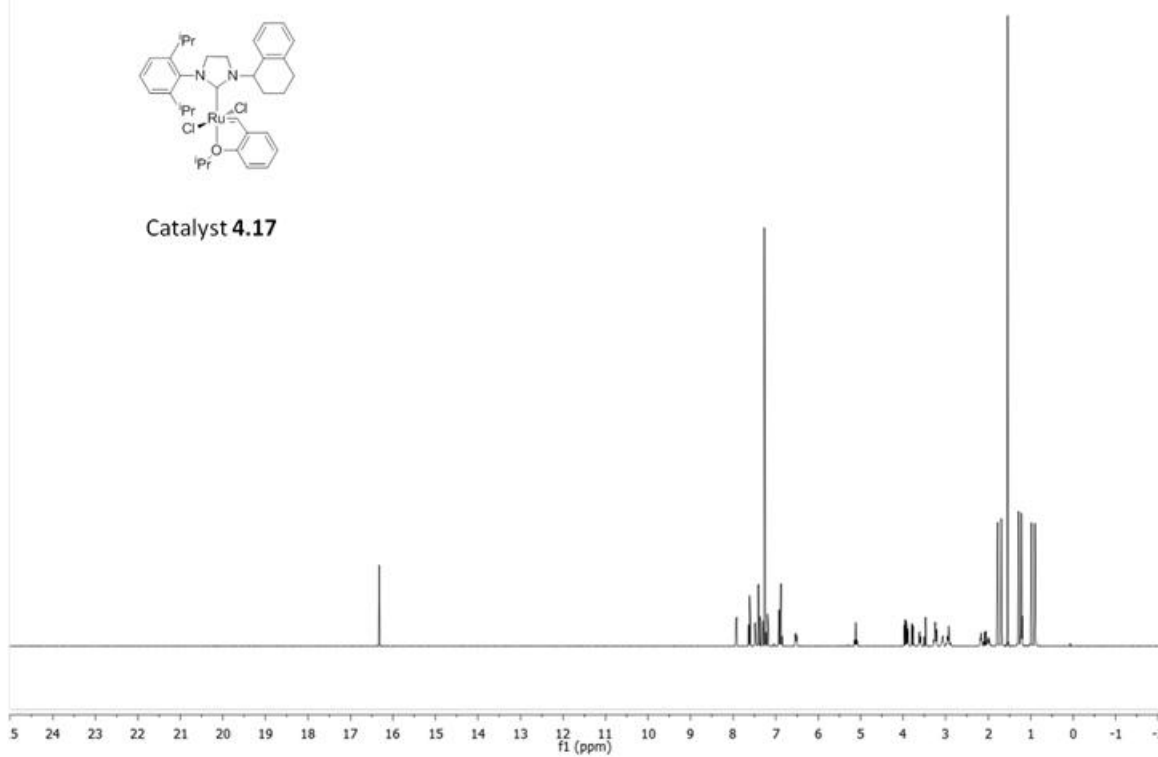


Catalyst 4.16

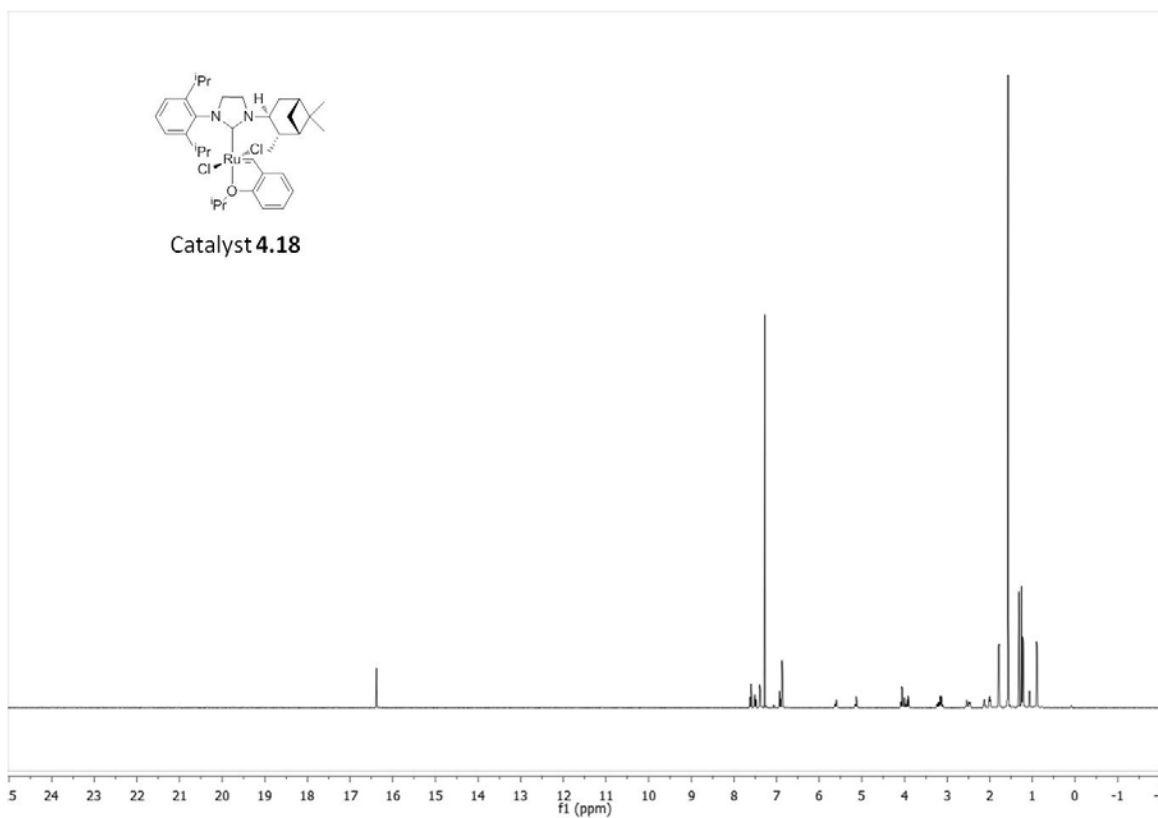


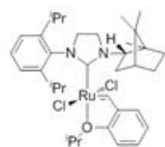


Catalyst 4.17

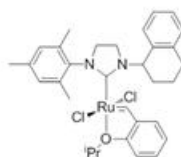
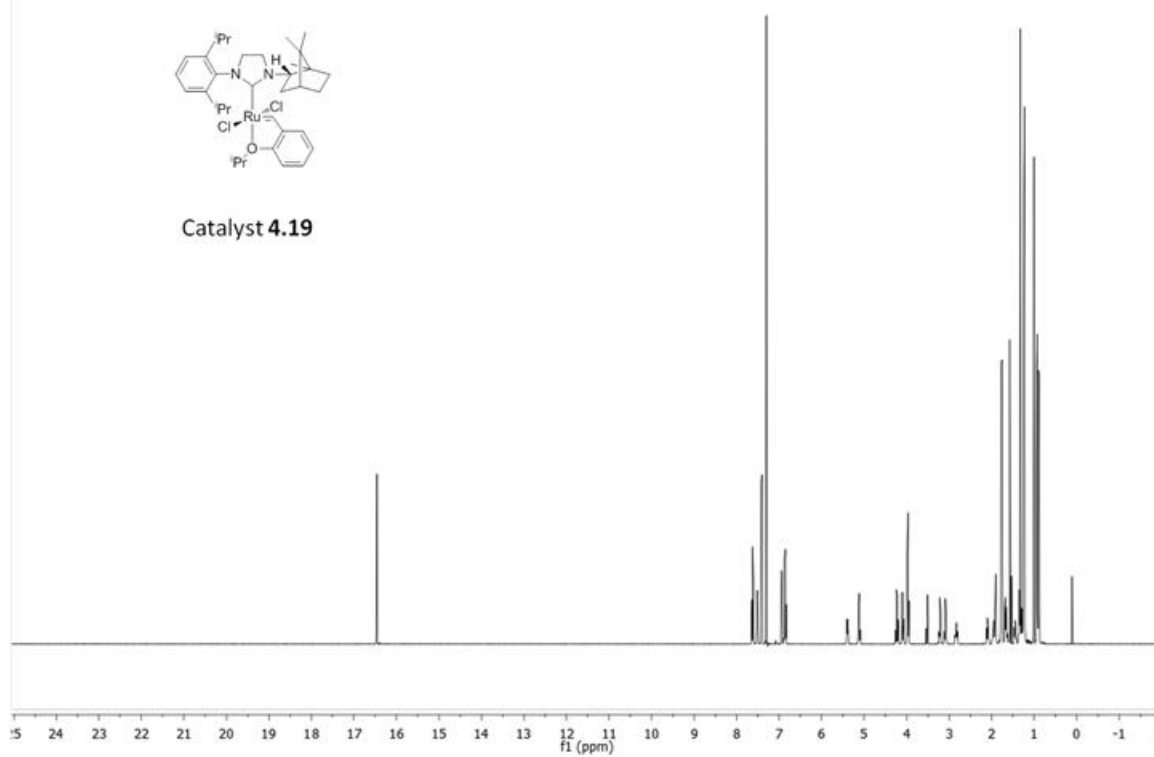


Catalyst 4.18

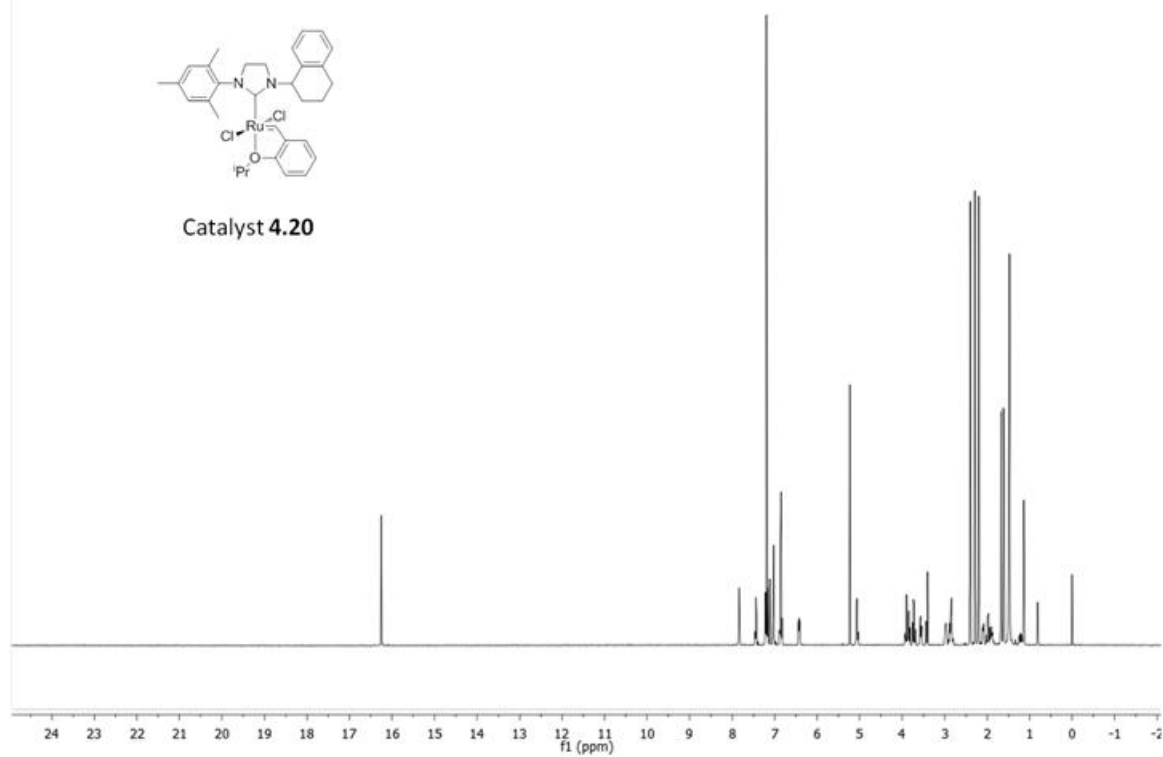




Catalyst 4.19



Catalyst 4.20



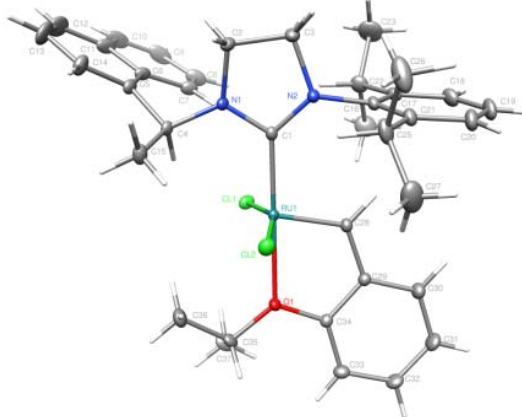
X-ray Crystallographic Data of Catalysts **12** and **15**.**Crystallographic Data for Complex 12**Contents

Table A.1. Crystal data


Figures Minimum overlap

Table A.2. Atomic Coordinates

Table A.3. Selected bond distances and angles



**Table A.1. Crystal data and structure refinement for Complex 12 (CCDC 804197).**

Empirical formula	$C_{37}H_{44}N_2OCl_2Ru$	
Formula weight	704.71	
Crystallization solvent	Ether/pentane	
Crystal habit	Block	
Crystal size	0.21 x 0.15 x 0.14 mm <sup>3</sup>	
Crystal color	Olive green	
<b>Data Collection</b>		
Type of diffractometer	Bruker KAPPA APEX II	
Wavelength	0.71073 Å MoK $\alpha$	
Data Collection Temperature	100(2) K	
$\theta$ range for 9729 reflections used in lattice determination	2.61° to 41.69°	
Unit cell dimensions	$a = 10.4912(4)$ Å $b = 12.2508(5)$ Å $c = 13.7547(5)$ Å	$\alpha = 90^\circ$ $\beta = 105.157(2)^\circ$ $\gamma = 90^\circ$
Volume	1706.33(11) Å <sup>3</sup>	
Z	2	
Crystal system	Monoclinic	
Space group	P 2 <sub>1</sub>	
Density (calculated)	1.372 Mg/m <sup>3</sup>	
F(000)	732	
Data collection program	Bruker APEX2 v2009.7-0	
$\theta$ range for data collection	2.01° to 47.06°	
Completeness to $\theta = 47.06^\circ$	99.6%	
Index ranges	$-21 \leq h \leq 21$ , $-20 \leq k \leq 25$ , $-28 \leq l \leq 28$	
Data collection scan type	$\omega$ scans; 16 settings	
Data reduction program	Bruker SAINT-Plus v7.66A	
Reflections collected	106745	
Independent reflections	28701 [ $R_{int} = 0.0449$ ]	
Absorption coefficient	0.647 mm <sup>-1</sup>	
Absorption correction	None	
Max. and min. transmission	0.9149 and 0.8761	



**Table A.1 (cont.)****Structure solution and Refinement**

Structure solution program	SHELXS-97 (Sheldrick, 2008)
Primary solution method	Direct methods
Secondary solution method	Difference Fourier map
Hydrogen placement	Difference Fourier map
Structure refinement program	SHELXL-97 (Sheldrick, 2008)
Refinement method	Full matrix least-squares on $F^2$
Data/ restraints/parameters	2870 / 1/564
Treatment of hydrogen atoms	Unrestrained
Goodness-of-fit on $F^2$	1.115
Final R indices [ $I > 2\sigma(I)$ , 24952 reflections]	$R1 = 0.0270$ , $wR2 = 0.0390$
R indices (all data)	$R1 = 0.0351$ , $wR2 = 0.0399$
Type of weighting scheme used	Sigma
Weighting scheme used	$w = 1 / \sigma^2(F_o^2)$
Max shift/error	0.006
Average shift/error	0.000
Absolute structure determination	Anomalous differences
Absolute structure parameter	-0.024(6)
Largest diff. peak and hole	0.970 and -1.147 e.Å <sup>-3</sup>

**Special Refinement Details**

Crystals were mounted on a glass fiber using Paratone oil then placed on the diffractometer under a nitrogen stream at 100K.

Refinement of  $F^2$  against ALL reflections. The weighted R-factor ( $wR$ ) and goodness of fit ( $S$ ) are based on  $F^2$ , conventional R-factors ( $R$ ) are based on  $F$ , with  $F$  set to zero for negative  $F^2$ . The threshold expression of  $F^2 > 2\sigma(F^2)$  is used only for calculating R-factors(gt) etc. and is not relevant to the choice of reflections for refinement. R-factors based on  $F^2$  are statistically about twice as large as those based on  $F$ , and R-factors based on ALL data will be even larger.

All esds (except the esd in the dihedral angle between two l.s. planes) are estimated using the full covariance matrix. The cell esds are taken into account individually in the estimation of esds in distances, angles and torsion angles; correlations between esds in cell parameters are only used when they are defined by crystal symmetry. An approximate (isotropic) treatment of cell esds is used for estimating esds involving l.s. planes.

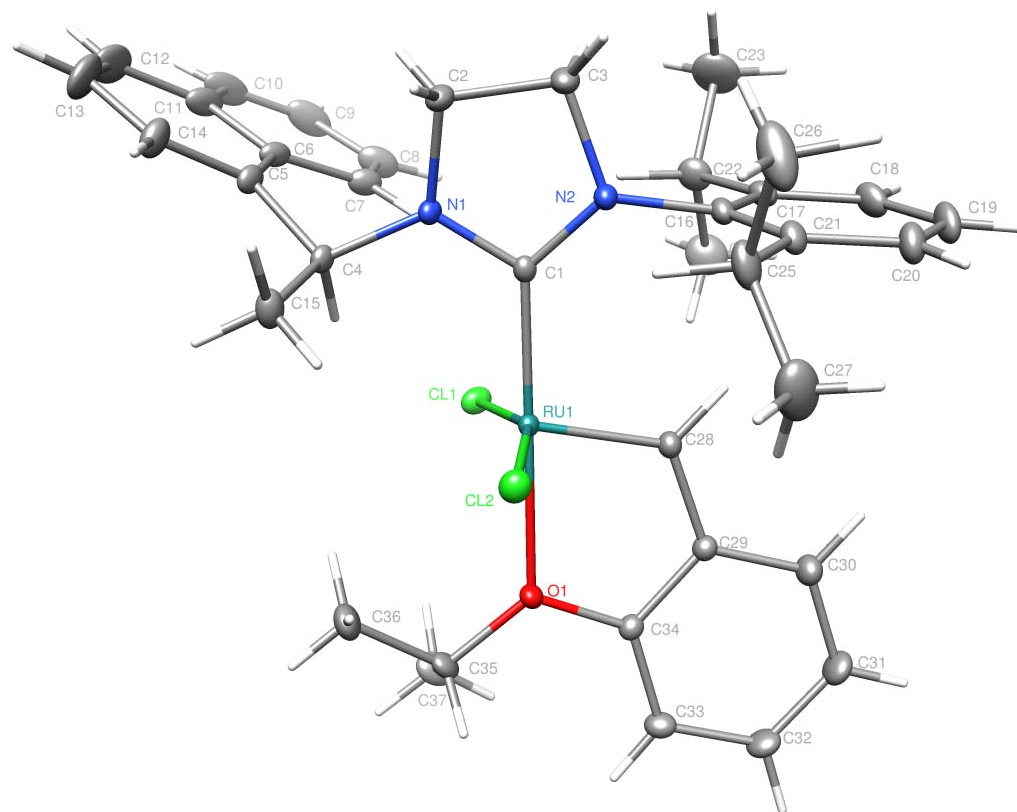


**Table A.2. Atomic coordinates ( $\times 10^4$ ) and equivalent isotropic displacement parameters ( $\text{\AA}^2 \times 10^3$ ) for Complex 12 (CCDC 804197).  $U(\text{eq})$  is defined as the trace of the orthogonalized  $U^{\text{ij}}$  tensor.**

	x	y	z	$U_{\text{eq}}$
Ru(1)	81(1)	1809(1)	8021(1)	9(1)
Cl(1)	-1652(1)	1481(1)	6604(1)	15(1)
Cl(2)	1091(1)	2118(1)	9733(1)	15(1)
O(1)	-270(1)	89(1)	8485(1)	13(1)
N(1)	-514(1)	4135(1)	7603(1)	12(1)
N(2)	1464(1)	3804(1)	7448(1)	13(1)
C(1)	388(1)	3328(1)	7638(1)	11(1)
C(2)	44(1)	5229(1)	7559(1)	17(1)
C(3)	1243(1)	4970(1)	7180(1)	19(1)
C(4)	-1764(1)	4020(1)	7887(1)	12(1)
C(5)	-2802(1)	4822(1)	7304(1)	15(1)
C(6)	-3361(1)	4682(1)	6245(1)	16(1)
C(7)	-2852(1)	3933(1)	5658(1)	18(1)
C(8)	-3438(1)	3786(1)	4652(1)	25(1)
C(9)	-4590(1)	4365(1)	4183(1)	32(1)
C(10)	-5098(1)	5113(1)	4718(1)	32(1)
C(11)	-4485(1)	5311(1)	5749(1)	24(1)
C(12)	-4956(1)	6122(1)	6299(1)	35(1)
C(13)	-4348(1)	6300(1)	7286(1)	35(1)
C(14)	-3275(1)	5640(1)	7800(1)	24(1)
C(15)	-1536(1)	4090(1)	9024(1)	18(1)
C(16)	2588(1)	3297(1)	7225(1)	14(1)
C(17)	2504(1)	2974(1)	6231(1)	16(1)
C(18)	3646(1)	2555(1)	6026(1)	22(1)
C(19)	4814(1)	2463(1)	6776(1)	24(1)
C(20)	4863(1)	2774(1)	7751(1)	22(1)
C(21)	3753(1)	3200(1)	8001(1)	16(1)
C(22)	1233(1)	3028(1)	5398(1)	21(1)
C(23)	1358(2)	3805(1)	4562(1)	40(1)
C(24)	796(1)	1891(1)	4972(1)	31(1)
C(25)	3832(1)	3516(1)	9081(1)	22(1)
C(26)	4626(1)	4565(1)	9379(1)	35(1)
C(27)	4417(1)	2590(1)	9812(1)	36(1)
C(28)	1427(1)	1091(1)	7676(1)	13(1)
C(29)	1588(1)	-67(1)	7888(1)	12(1)
C(30)	2628(1)	-669(1)	7694(1)	18(1)
C(31)	2764(1)	-1771(1)	7934(1)	21(1)
C(32)	1860(1)	-2270(1)	8367(1)	19(1)
C(33)	802(1)	-1703(1)	8557(1)	15(1)
C(34)	683(1)	-596(1)	8318(1)	12(1)
C(35)	-1372(1)	-349(1)	8836(1)	16(1)
C(36)	-2004(1)	620(1)	9210(1)	25(1)
C(37)	-2324(1)	-962(1)	7997(1)	25(1)

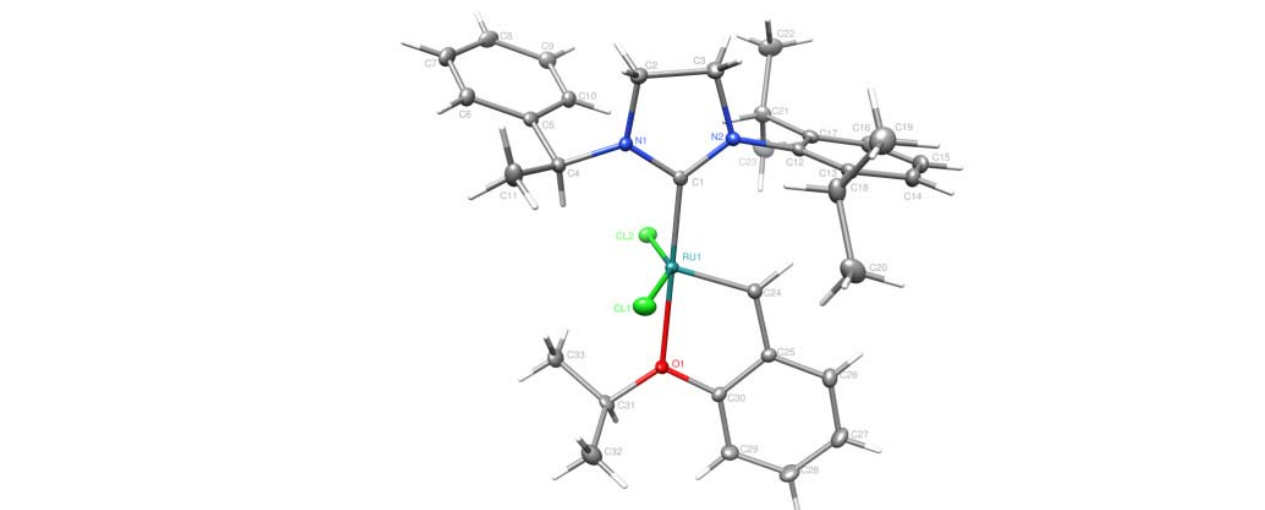
**Table A.3. Selected bond lengths [ $\text{\AA}$ ] and angles [ $^\circ$ ] for Complex 12 (CCDC 804197).**

Ru(1)-C(28)	1.8285(8)	C(28)-Ru(1)-C(1)	101.08(3)
Ru(1)-C(1)	1.9831(7)	C(28)-Ru(1)-O(1)	79.54(3)
Ru(1)-O(1)	2.2601(5)	C(1)-Ru(1)-O(1)	179.01(3)
Ru(1)-Cl(1)	2.3273(2)	C(28)-Ru(1)-Cl(1)	100.77(3)
Ru(1)-Cl(2)	2.3459(2)	C(1)-Ru(1)-Cl(1)	94.87(2)
		O(1)-Ru(1)-Cl(1)	85.760(16)
		C(28)-Ru(1)-Cl(2)	99.27(3)
		C(1)-Ru(1)-Cl(2)	93.05(2)
		O(1)-Ru(1)-Cl(2)	86.079(16)
		Cl(1)-Ru(1)-Cl(2)	156.580(8)

### Crystallographic Data for Complex 15

## Contents

Table A.4. Crystal data  
 Figures Minimum overlap  
 Table A.5. Atomic Coordinates  
 Table A.6. Selected bond distances and angles



**Complex 15**

**Note:** Crystallographic data have been deposited at the CCDC, 12 Union Road, Cambridge CB2 1EZ, UK and copies can be obtained on request, free of charge, by quoting the publication citation and the deposition number 804198.

**Table A.4. Crystal data and structure refinement for Complex 15 (CCDC 804198).**

Empirical formula	$C_{33}H_{42}N_2OCl_2Ru$
Formula weight	654.66
Crystallization Solvent	Ether/pentane
Crystal Habit	Block
Crystal size	0.22 x 0.18 x 0.16 mm <sup>3</sup>
Crystal color	Green



### Data Collection

Type of diffractometer	Bruker KAPPA APEX II
Wavelength	0.71073 Å MoK $\alpha$
Data Collection Temperature	100(2) K
$\theta$ range for 9859 reflections used in lattice determination	2.56° to 36.04°
Unit cell dimensions	$a = 10.5474(3)$ Å $b = 15.6796(5)$ Å $c = 19.1646(6)$ Å
	$\alpha = 90^\circ$ $\beta = 90^\circ$ $\gamma = 90^\circ$
Volume	3169.42(17) Å <sup>3</sup>
Z	4
Crystal system	Orthorhombic
Space group	P 2 <sub>1</sub> 2 <sub>1</sub> 2 <sub>1</sub>
Density (calculated)	1.372 Mg/m <sup>3</sup>
F(000)	1360
Data collection program	Bruker APEX2 v2009.7-0
$\theta$ range for data collection	2.33° to 36.56°
Completeness to $\theta = 36.56^\circ$	99.9%
Index ranges	$-17 \leq h \leq 17$ , $-25 \leq k \leq 26$ , $-31 \leq l \leq 32$
Data collection scan type	$\omega$ scans; 8 settings
Data reduction program	Bruker SAINT-Plus v7.66A
Reflections collected	79037
Independent reflections	15623 [ $R_{int} = 0.0482$ ]
Absorption coefficient	0.691 mm <sup>-1</sup>
Absorption correction	None
Max. and min. transmission	0.8975 and 0.8629

**Table A.4(cont.)****Structure solution and Refinement**

Structure solution program	SHELXS-97 (Sheldrick, 2008)
Primary solution method	Direct methods
Secondary solution method	Difference Fourier map
Hydrogen placement	Difference Fourier map
Structure refinement program	SHELXL-97 (Sheldrick, 2008)
Refinement method	Full matrix least-squares on F <sup>2</sup>
Data/restraints/ parameters	15623/0 /520
Treatment of hydrogen atoms	Unrestrained
Goodness-of-fit on F <sup>2</sup>	1.069
Final R indices [I>2σ(I), 14090 reflections]	R1 = 0.0250, wR2 = 0.0341
R indices (all data)	R1 = 0.0306, wR2 = 0.0349
Type of weighting scheme used	Sigma
Weighting scheme used	$w=1/\sigma^2(F_o^2)$
Max shift/error	0.004
Average shift/error	0.000
Absolute structure determination	Anomalous differences
Absolute structure parameter	-0.036(9)
Largest diff. peak and hole	0.685 and -0.647 e.Å <sup>-3</sup>

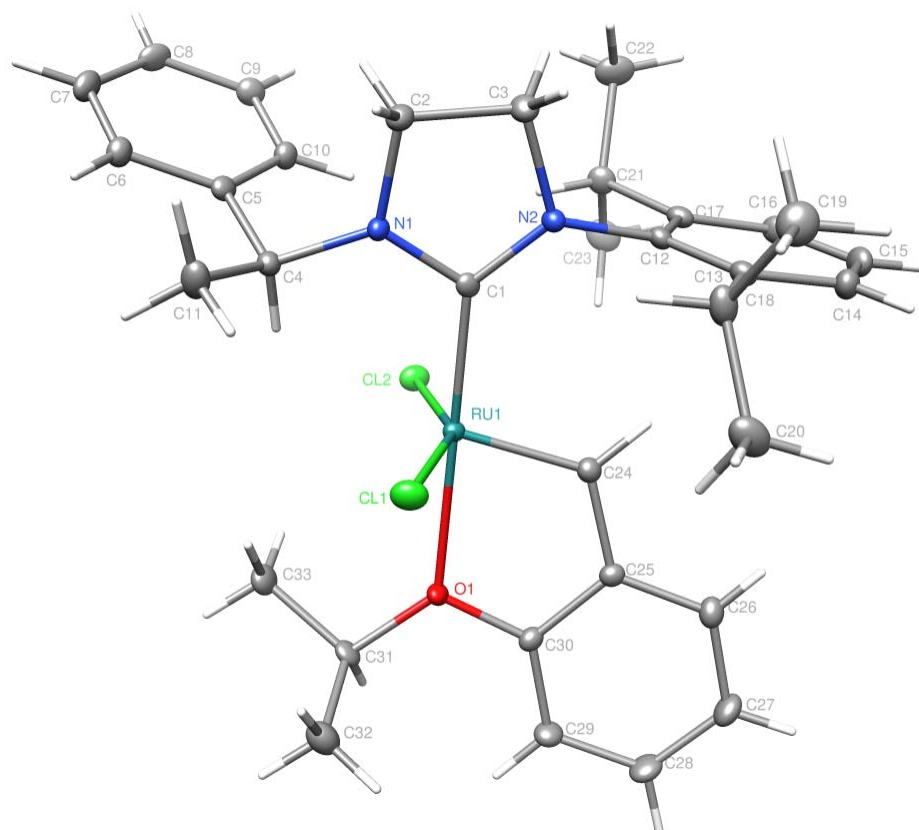




**Table A.5. Atomic coordinates ( $\times 10^4$ ) and equivalent isotropic displacement parameters ( $\text{\AA}^2 \times 10^3$ ) for Complex 15 (CCDC 804198).  $U(\text{eq})$  is defined as the trace of the orthogonalized  $U^{\text{ij}}$  tensor.**

	x	y	z	$U_{\text{eq}}$
Ru(1)	8746(1)	8200(1)	6998(1)	9(1)
Cl(1)	7182(1)	9179(1)	6690(1)	17(1)
Cl(2)	10509(1)	7349(1)	6764(1)	15(1)
O(1)	7462(1)	7156(1)	6562(1)	13(1)
N(1)	10320(1)	9698(1)	6918(1)	11(1)
N(2)	10035(1)	9425(1)	8017(1)	11(1)
C(1)	9782(1)	9144(1)	7367(1)	10(1)
C(2)	10905(1)	10434(1)	7261(1)	14(1)
C(3)	10816(1)	10202(1)	8028(1)	16(1)
C(4)	10404(1)	9590(1)	6162(1)	13(1)
C(5)	11792(1)	9530(1)	5950(1)	13(1)
C(6)	12276(1)	9946(1)	5364(1)	15(1)
C(7)	13554(1)	9897(1)	5198(1)	18(1)
C(8)	14376(1)	9439(1)	5617(1)	18(1)
C(9)	13911(1)	9015(1)	6199(1)	17(1)
C(10)	12637(1)	9053(1)	6357(1)	15(1)
C(11)	9656(1)	10290(1)	5787(1)	20(1)
C(12)	9834(1)	8985(1)	8667(1)	10(1)
C(13)	8785(1)	9215(1)	9074(1)	13(1)
C(14)	8641(1)	8814(1)	9717(1)	16(1)
C(15)	9495(1)	8204(1)	9943(1)	18(1)
C(16)	10521(1)	7987(1)	9529(1)	16(1)
C(17)	10724(1)	8371(1)	8885(1)	12(1)
C(18)	7801(1)	9859(1)	8829(1)	17(1)
C(19)	7751(2)	10640(1)	9305(1)	23(1)
C(20)	6501(1)	9439(1)	8758(1)	23(1)
C(21)	11889(1)	8147(1)	8458(1)	15(1)
C(22)	13084(1)	8560(1)	8767(1)	23(1)
C(23)	12085(2)	7179(1)	8395(1)	22(1)
C(24)	8080(1)	7757(1)	7801(1)	12(1)
C(25)	7095(1)	7116(1)	7757(1)	11(1)
C(26)	6461(1)	6800(1)	8340(1)	15(1)
C(27)	5545(1)	6167(1)	8270(1)	18(1)
C(28)	5273(1)	5846(1)	7614(1)	20(1)
C(29)	5886(1)	6148(1)	7023(1)	16(1)
C(30)	6776(1)	6795(1)	7096(1)	11(1)
C(31)	7182(1)	6921(1)	5836(1)	13(1)
C(32)	5913(1)	7266(1)	5607(1)	22(1)
C(33)	8244(1)	7275(1)	5401(1)	19(1)

**Table A.6. Selected bond lengths [ $\text{\AA}$ ] and angles [ $^\circ$ ] for Complex 15 (CCDC 804198).**

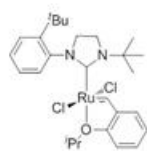
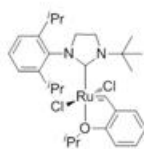
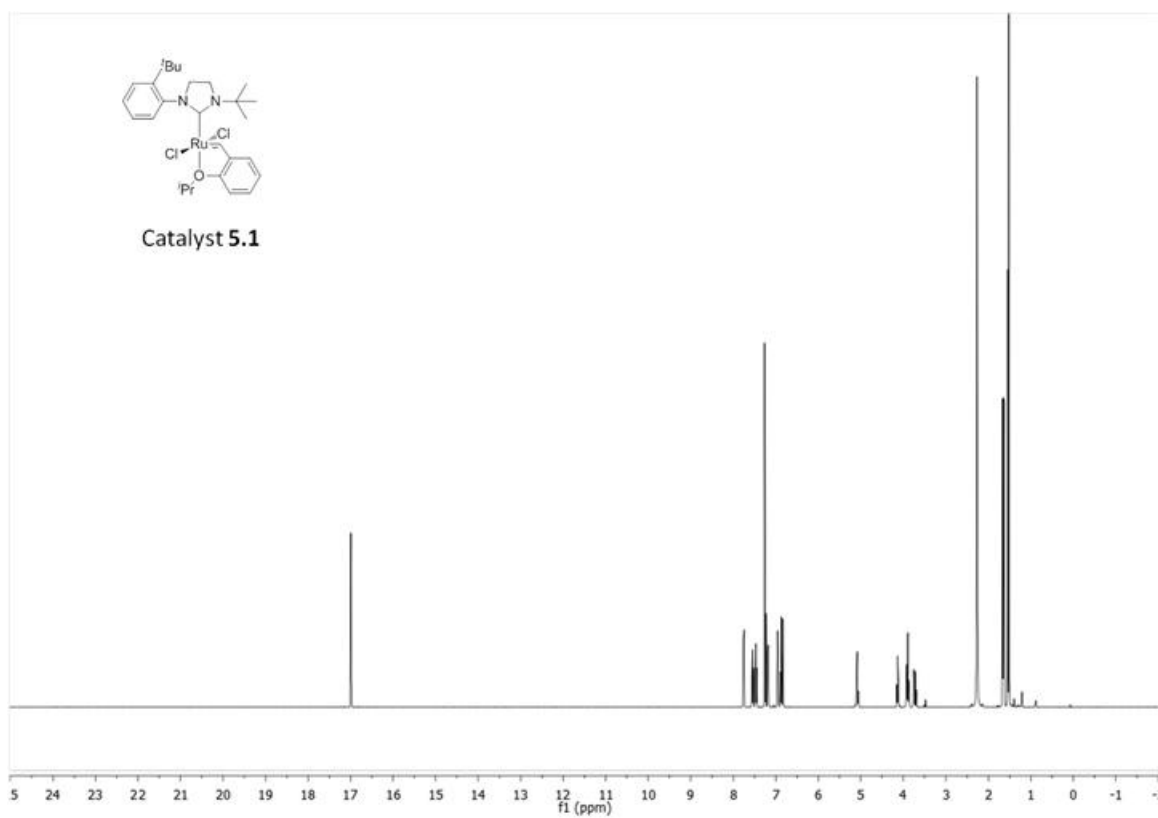
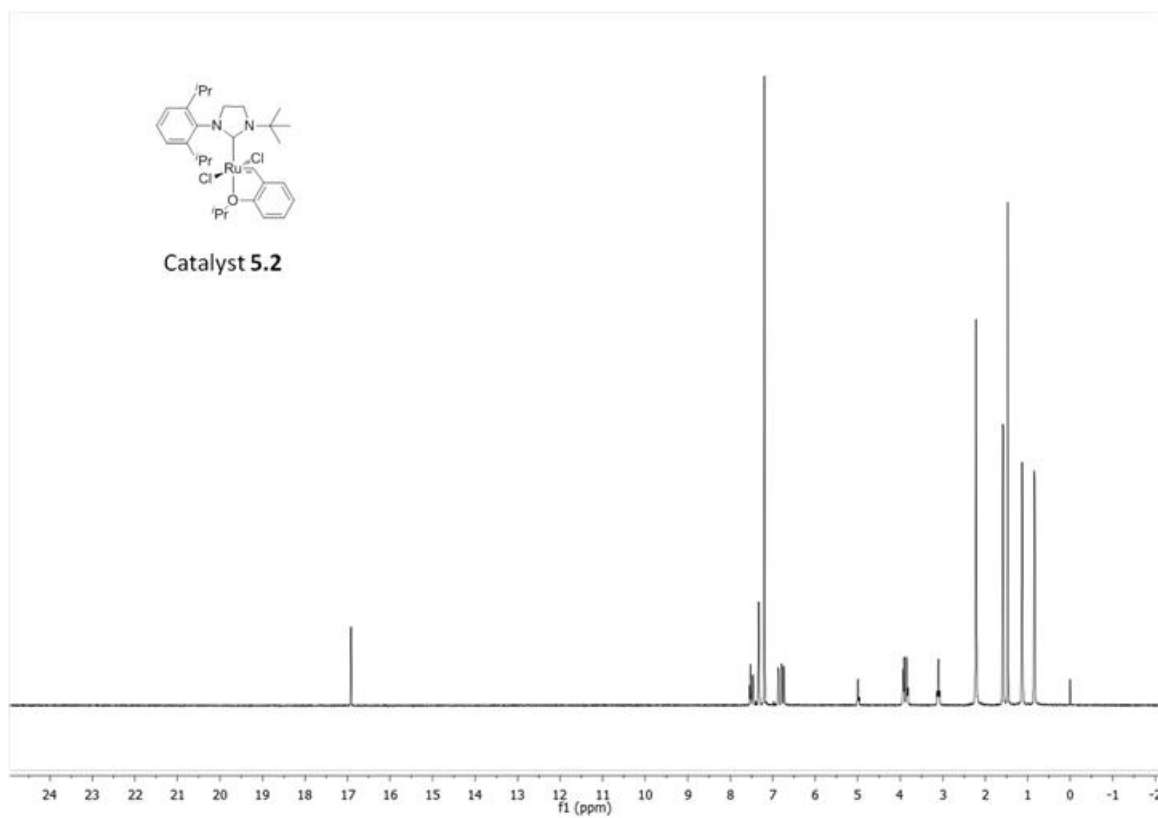
Ru(1)-C(24)	1.8287(12)	C(24)-Ru(1)-C(1)	101.32(5)
Ru(1)-C(1)	1.9707(11)	C(24)-Ru(1)-O(1)	78.95(4)
Ru(1)-O(1)	2.2834(8)	C(1)-Ru(1)-O(1)	177.03(4)
Ru(1)-Cl(1)	2.3289(3)	C(24)-Ru(1)-Cl(1)	101.10(4)
Ru(1)-Cl(2)	2.3336(3)	C(1)-Ru(1)-Cl(1)	89.36(3)
		O(1)-Ru(1)-Cl(1)	87.70(2)
		C(24)-Ru(1)-Cl(2)	104.50(4)
		C(1)-Ru(1)-Cl(2)	93.25(3)
		O(1)-Ru(1)-Cl(2)	89.53(2)
		Cl(1)-Ru(1)-Cl(2)	153.208(12)

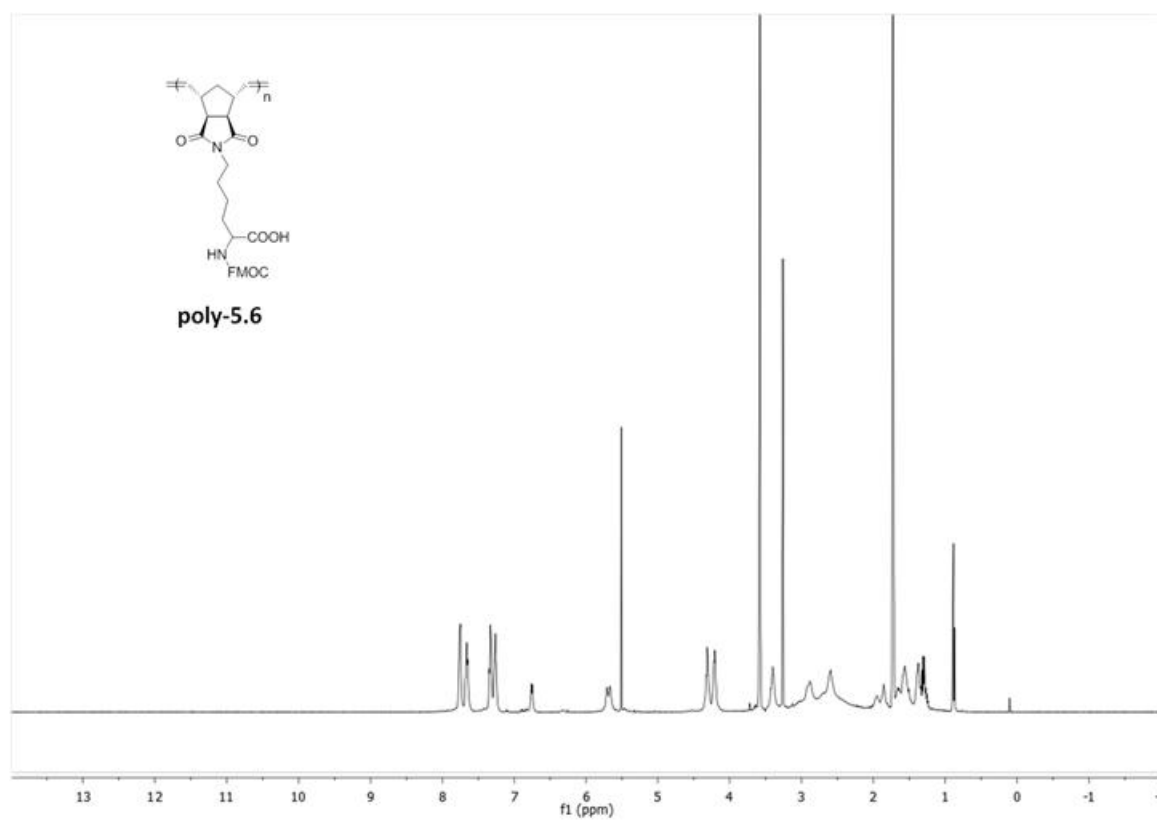
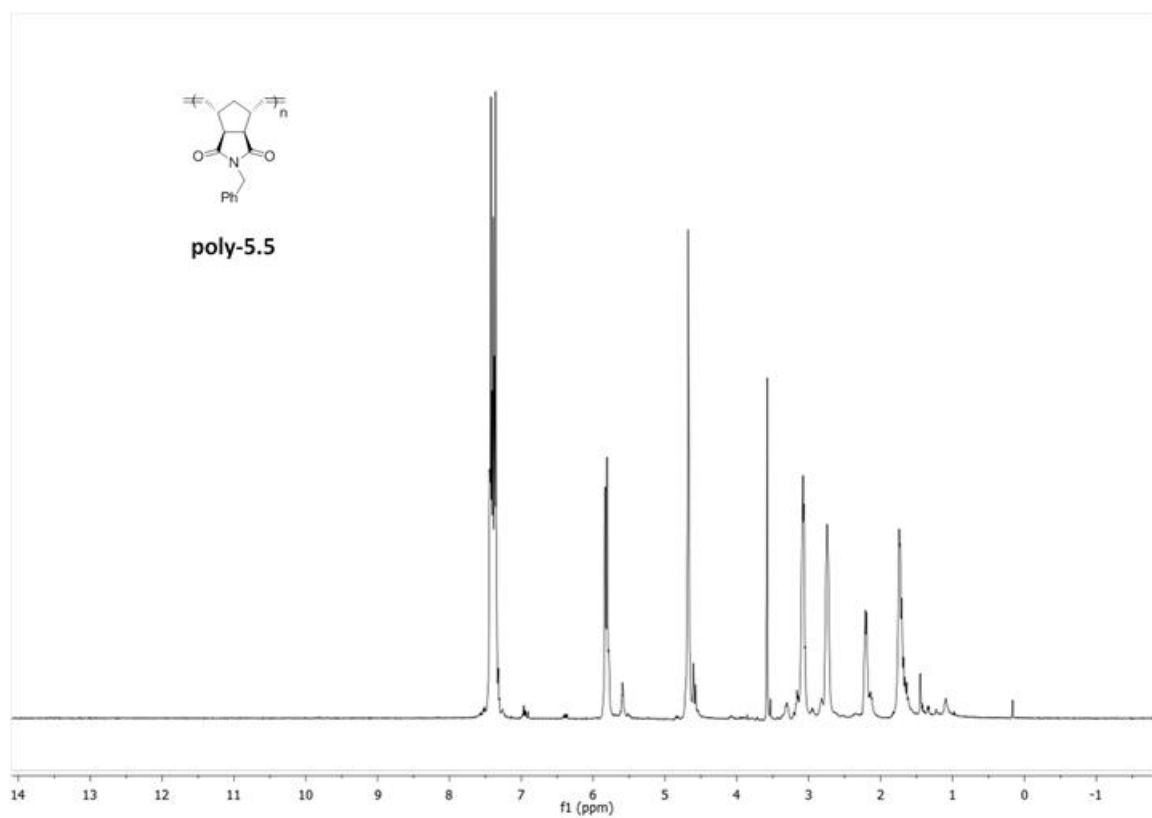
The Bruker KAPPA APEXII X-ray diffractometer was purchased via an NSF CRIF:MU award to the California Institute of Technology, CHE-0639094.

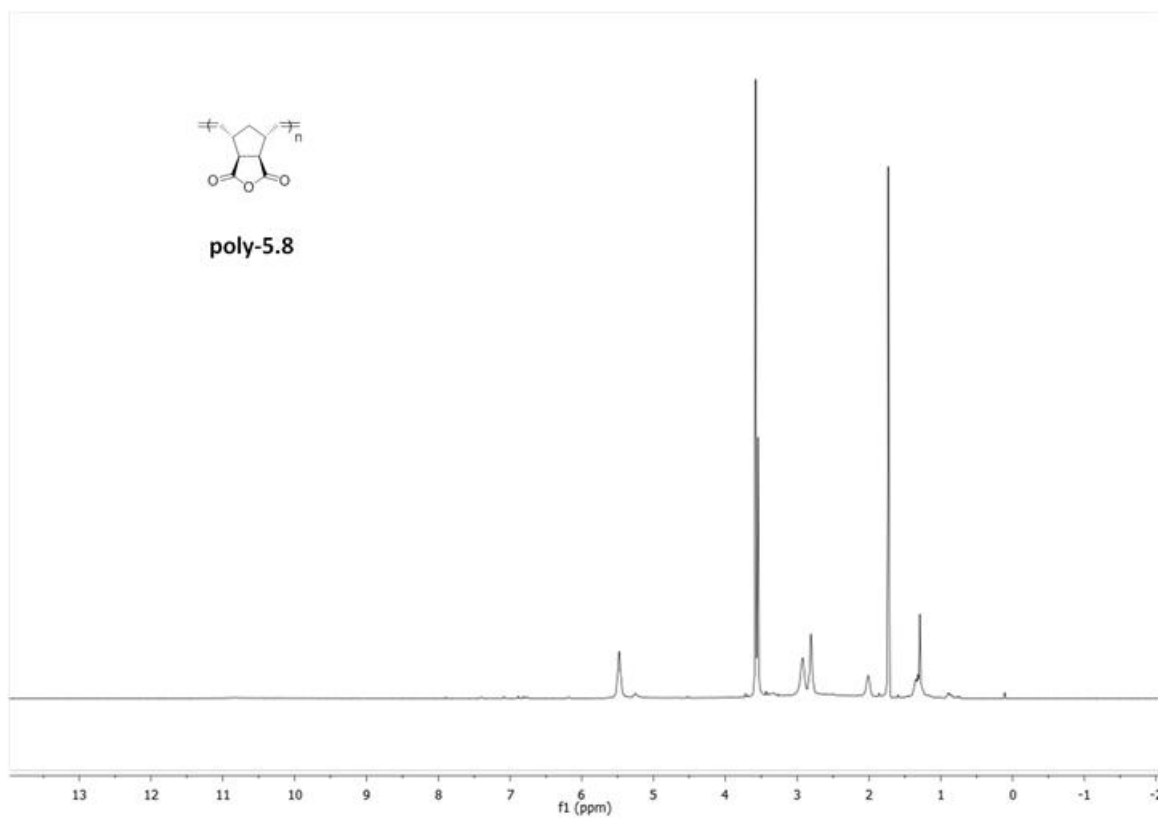
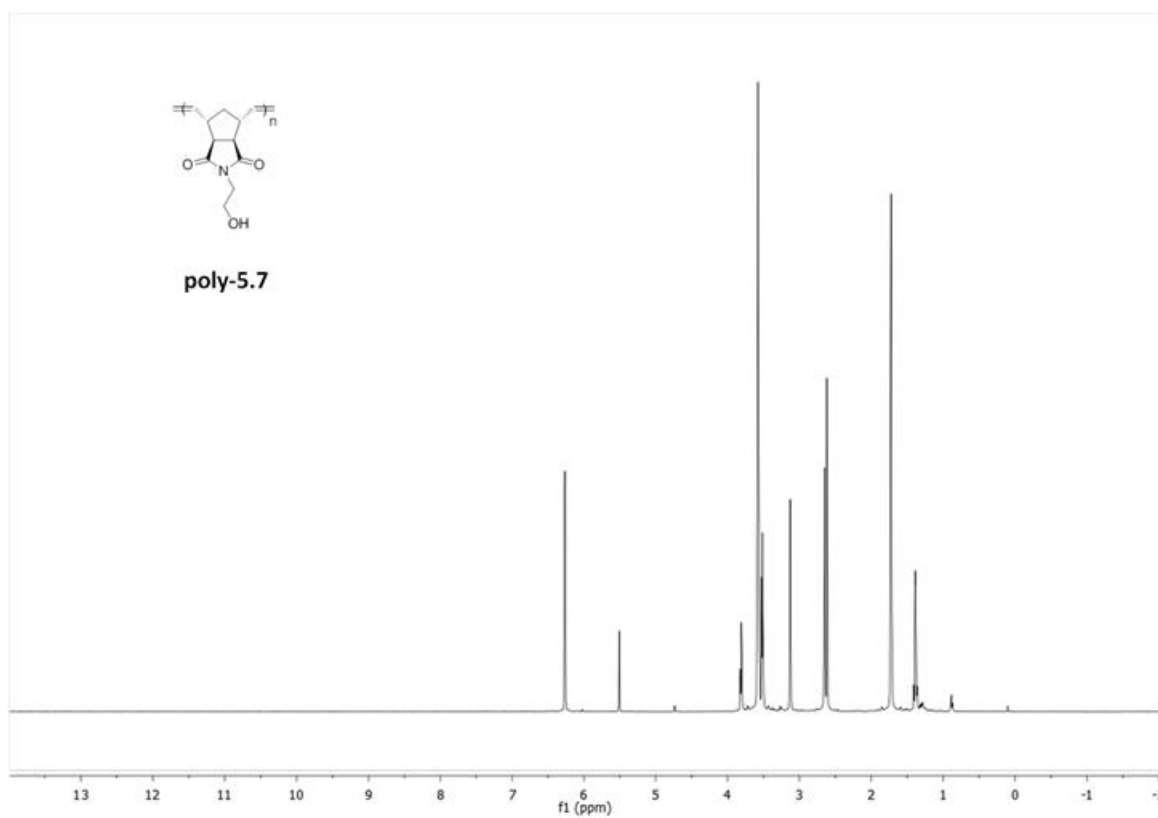
***APPENDIX B***

<sup>1</sup>H NMR Spectra of Chapter 5 Catalysts in CDCl<sub>3</sub> and Polymers in THF-*d*<sub>8</sub>

X-Ray Crystallographic Data of Catalysts **2** and **10**

**Catalyst 5.1****Catalyst 5.2**





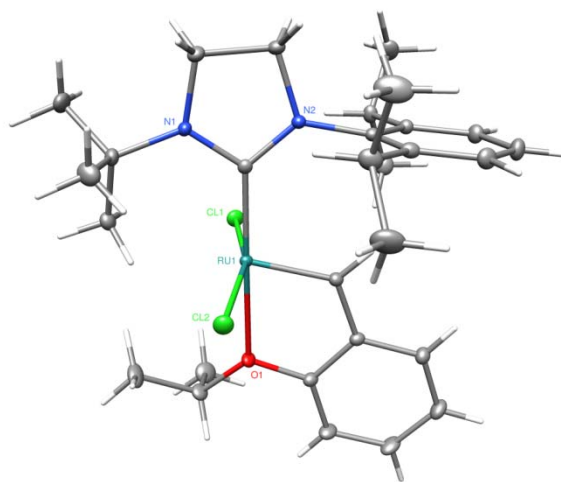
X-Ray Crystallographic Data for Catalysts **2** and **10**.**Crystallographic Data for Complex 2**Contents

Table B.1. Crystal data

Figures Minimum overlap

Table B.2. Atomic Coordinates

Table B.3. Selected bond distances and angles

**Complex 2**

**Note:** The crystallographic data have been deposited in the Cambridge Database (CCDC) and has been placed on hold pending further instructions from me. The deposition number is 835698. Ideally the CCDC would like the publication to contain a footnote of the type: "Crystallographic data have been deposited at the CCDC, 12 Union Road, Cambridge CB2 1EZ, UK and copies can be obtained on request, free of charge, by quoting the publication citation and the deposition number 835698."



**Table B.1. Crystal data and structure refinement for Complex 2 (CCDC 835698).**

Empirical formula	C <sub>54</sub> H <sub>42</sub> N <sub>2</sub> OCl <sub>2</sub> Ru	
Formula weight	606.62	
Crystallization Solvent	Diethyl ether/pentane	
Crystal Habit	Block	
Crystal size	0.36 x 0.31 x 0.30 mm <sup>3</sup>	
Crystal color	Dark green	
<b>Data Collection</b>		
Type of diffractometer	Bruker KAPPA APEX II	
Wavelength	0.71073 Å MoKα	
Data Collection Temperature	100(2) K	
θ range for 9613 reflections used in lattice determination	2.44° to 55.04°	
Unit cell dimensions	a = 10.4674(4) Å b = 15.4184(7) Å c = 18.7885(9) Å	α= 90° β= 103.545(2)° γ= 90°
Volume	2947.9(2) Å <sup>3</sup>	
Z	4	
Crystal system	Monoclinic	
Space group	P 2 <sub>1</sub> /n	
Density (calculated)	1.367 Mg/m <sup>3</sup>	
F(000)	1264	
Data collection program	Bruker APEX2 v2009.7-0	
θ range for data collection	2.05° to 55.60°	
Completeness to θ = 55.60°	98.5%	
Index ranges	-23 ≤ h ≤ 24, -35 ≤ k ≤ 35, -43 ≤ l ≤ 34	
Data collection scan type	ω scans; 17 settings	
Data reduction program	Bruker SAINT-Plus v7.66A	
Reflections collected	233734	
Independent reflections	38104 [R <sub>int</sub> = 0.0414]	
Absorption coefficient	0.736 mm <sup>-1</sup>	
Absorption correction	None	
Max. and min. transmission	0.8093 and 0.7774	

**Table B.1 (cont.)****Structure solution and Refinement**

Structure solution program	SHELXS-97 (Sheldrick, 2008)
Primary solution method	Direct methods
Secondary solution method	Difference Fourier map
Hydrogen placement	Difference Fourier map
Structure refinement program	SHELXL-97 (Sheldrick, 2008)
Refinement method	Full matrix least-squares on $F^2$
Data/restraints/parameters	38104/0/484
Treatment of hydrogen atoms	Unrestrained
Goodness-of-fit on $F^2$	1.907
Final R indices [ $I > 2\sigma(I)$ , 26773 reflections]	$R1 = 0.0284$ , $wR2 = 0.0494$
R indices (all data)	$R1 = 0.0539$ , $wR2 = 0.0505$
Type of weighting scheme used	Sigma
Weighting scheme used	$w = 1/\sigma^2(F_o^2)$
Max shift/error	0.009
Average shift/error	0.000
Largest diff. peak and hole	2.382 and -2.006 e.Å <sup>-3</sup>

**Special Refinement Details**

Crystals were mounted on a glass fiber using Paratone oil then placed on the diffractometer under a nitrogen stream at 100K.

Refinement of  $F^2$  against ALL reflections. The weighted R-factor ( $wR$ ) and goodness of fit ( $S$ ) are based on  $F^2$ , conventional R-factors ( $R$ ) are based on  $F$ , with  $F$  set to zero for negative  $F^2$ . The threshold expression of  $F^2 > 2\sigma(F^2)$  is used only for calculating R-factors(gt) etc. and is not relevant to the choice of reflections for refinement. R-factors based on  $F^2$  are statistically about twice as large as those based on  $F$ , and R-factors based on ALL data will be even larger.

All esds (except the esd in the dihedral angle between two l.s. planes) are estimated using the full covariance matrix. The cell esds are taken into account individually in the estimation of esds in distances, angles and torsion angles; correlations between esds in cell parameters are only used when they are defined by crystal symmetry. An approximate (isotropic) treatment of cell esds is used for estimating esds involving l.s. planes.

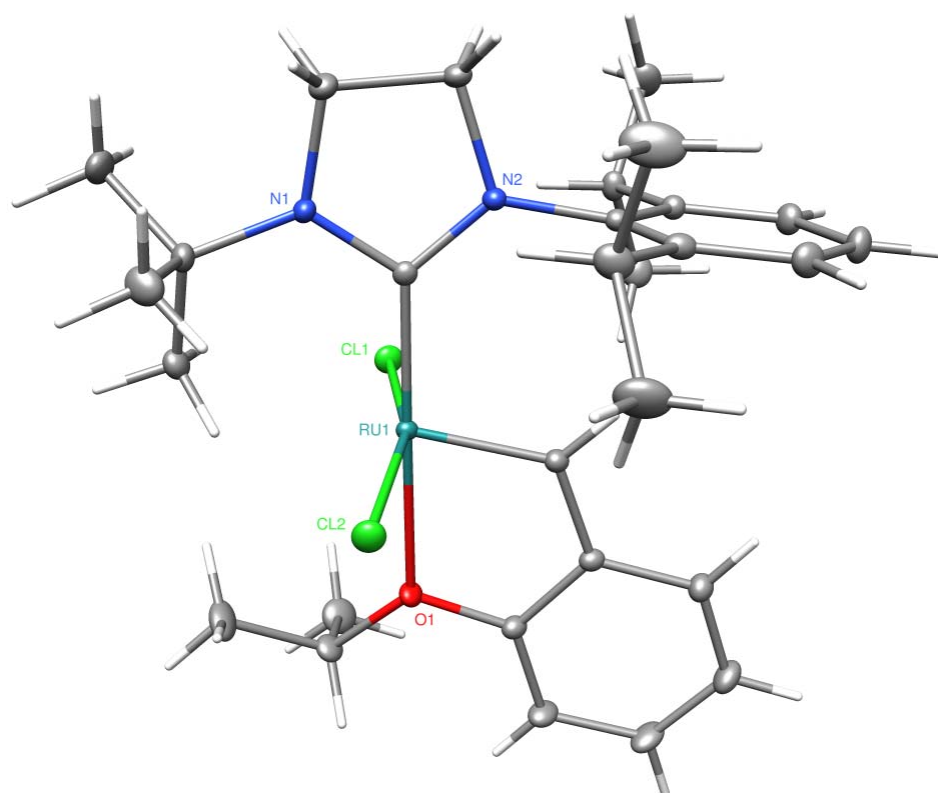


**Table B.2. Atomic coordinates ( $\times 10^4$ ) and equivalent isotropic displacement parameters ( $\text{\AA}^2 \times 10^3$ ) for Complex 2 (CCDC 835698).  $U(\text{eq})$  is defined as the trace of the orthogonalized  $U^{ij}$  tensor.**

	x	y	z	$U_{\text{eq}}$
Ru(1)	9987(1)	2339(1)	7515(1)	8(1)
Cl(1)	12114(1)	2923(1)	7722(1)	14(1)
Cl(2)	7939(1)	1712(1)	6941(1)	15(1)
O(1)	10934(1)	1025(1)	7342(1)	12(1)
N(1)	9053(1)	4133(1)	7171(1)	12(1)
N(2)	9094(1)	3848(1)	8315(1)	10(1)
C(1)	9289(1)	3494(1)	7690(1)	9(1)
C(2)	8539(1)	4932(1)	7432(1)	16(1)
C(3)	8723(1)	4769(1)	8244(1)	13(1)
C(4)	8828(1)	4021(1)	6364(1)	14(1)
C(5)	9222(1)	4862(1)	6035(1)	24(1)
C(6)	7381(1)	3818(1)	6042(1)	22(1)
C(7)	9686(1)	3296(1)	6188(1)	15(1)
C(8)	9111(1)	3457(1)	9010(1)	9(1)
C(9)	10265(1)	3477(1)	9567(1)	10(1)
C(10)	10214(1)	3152(1)	10252(1)	14(1)
C(11)	9063(1)	2812(1)	10378(1)	17(1)
C(12)	7933(1)	2798(1)	9818(1)	16(1)
C(13)	7926(1)	3126(1)	9127(1)	12(1)
C(14)	11558(1)	3816(1)	9449(1)	13(1)
C(15)	12006(1)	4622(1)	9915(1)	21(1)
C(16)	12618(1)	3113(1)	9625(1)	19(1)
C(17)	6664(1)	3118(1)	8531(1)	16(1)
C(18)	5657(1)	3744(1)	8717(1)	27(1)
C(19)	6091(1)	2208(1)	8398(1)	27(1)
C(20)	10070(1)	1802(1)	8397(1)	10(1)
C(21)	10614(1)	939(1)	8523(1)	10(1)
C(22)	10704(1)	491(1)	9181(1)	13(1)
C(23)	11258(1)	-329(1)	9285(1)	17(1)
C(24)	11726(1)	-709(1)	8725(1)	19(1)
C(25)	11653(1)	-283(1)	8064(1)	16(1)
C(26)	11097(1)	533(1)	7967(1)	11(1)
C(27)	11546(1)	721(1)	6756(1)	15(1)
C(28)	13010(1)	857(1)	6972(1)	22(1)
C(29)	10885(1)	1216(1)	6076(1)	24(1)

**Table B.3. Selected bond lengths [ $\text{\AA}$ ] and angles [ $^\circ$ ] for Complex 2 (CCDC 835698).**

Ru(1)-C(20)	1.8371(6)	C(20)-Ru(1)-C(1)	101.32(2)
Ru(1)-C(1)	1.9819(6)	C(20)-Ru(1)-O(1)	78.50(2)
Ru(1)-O(1)	2.3119(4)	C(1)-Ru(1)-O(1)	176.351(19)
Ru(1)-Cl(1)	2.34782(17)	C(20)-Ru(1)-Cl(1)	100.386(18)
Ru(1)-Cl(2)	2.36860(17)	C(1)-Ru(1)-Cl(1)	89.969(16)
		O(1)-Ru(1)-Cl(1)	86.487(12)
		C(20)-Ru(1)-Cl(2)	94.195(19)
		C(1)-Ru(1)-Cl(2)	96.502(16)
		O(1)-Ru(1)-Cl(2)	87.144(12)
		Cl(1)-Ru(1)-Cl(2)	162.582(6)

## Crystallographic Data for Complex 10

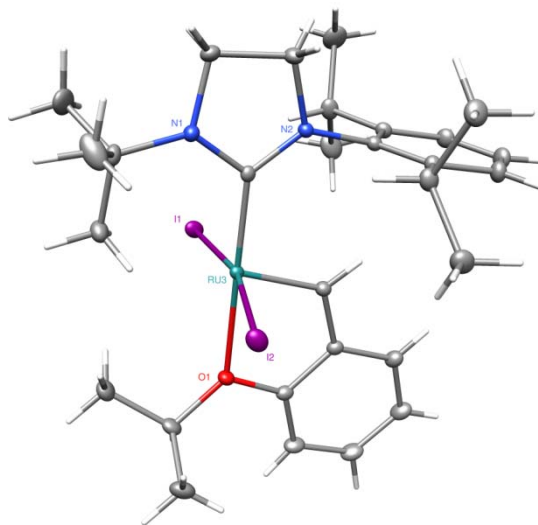
### Contents

Table B.4. Crystal data

Figures Minimum overlap

Table B.5. Atomic Coordinates


Table B.6. Selected bond distances and angles



Complex 10

**Note:** The crystallographic data have been deposited in the Cambridge Database (CCDC) and has been placed on hold pending further instructions from me. The deposition number is 834513. Ideally the CCDC would like the publication to contain a footnote of the type: "Crystallographic data have been deposited at the CCDC, 12 Union Road, Cambridge CB2 1EZ, UK and copies can be obtained on request, free of charge, by quoting the publication citation and the deposition number 834513."

**Table B.4. Crystal data and structure refinement for Complex 10 (CCDC 834513).**

Empirical formula	C <sub>29</sub> H <sub>42</sub> N <sub>2</sub> OI <sub>2</sub> Ru	
Formula weight	789.52	
Crystallization Solvent	Methanol	
Crystal Habit	Block	
Crystal size	0.26 x 0.21 x 0.20 mm <sup>3</sup>	
Crystal color	Brown/green	
<b>Data Collection</b>		
Type of diffractometer	Bruker KAPPA APEX II	
Wavelength	0.71073 Å MoKα	
Data Collection Temperature	100(2) K	
θ range for 9641 reflections used in lattice determination	2.43° to 50.93°	
Unit cell dimensions	a = 9.3566(5) Å b = 16.7642(9) Å c = 19.5715(11) Å	α = 90° β = 91.693(3)° γ = 90°
Volume	3068.6(3) Å <sup>3</sup>	
Z	4	
Crystal system	Monoclinic	
Space group	P 2 <sub>1</sub> /n	
Density (calculated)	1.709 Mg/m <sup>3</sup>	
F(000)	1552	
Data collection program	Bruker APEX2 v2009.7-0	
θ range for data collection	2.39° to 51.13°	
Completeness to θ = 51.13°	99.6%	
Index ranges	-20 ≤ h ≤ 16, -36 ≤ k ≤ 36, -42 ≤ l ≤ 42	
Data collection scan type	ω scans; 23 settings	
Data reduction program	Bruker SAINT-Plus v7.66A	
Reflections collected	308907	
Independent reflections	33668 [R <sub>int</sub> = 0.0423]	
Absorption coefficient	2.546 mm <sup>-1</sup>	
Absorption correction	Semi-empirical from equivalents	
Max. and min. transmission	0.7501 and 0.6618	

**Table 4 (cont.)****Structure solution and Refinement**

Structure solution program	SHELXS-97 (Sheldrick, 2008)
Primary solution method	Direct methods
Secondary solution method	Difference Fourier map
Hydrogen placement	Difference Fourier map
Structure refinement program	SHELXL-97 (Sheldrick, 2008)
Refinement method	Full matrix least-squares on $F^2$
Data/restraints/parameters	33668/0/484
Treatment of hydrogen atoms	Unrestrained
Goodness-of-fit on $F^2$	1.709
Final R indices [ $I > 2\sigma(I)$ , 27456 reflections]	$R1 = 0.0258$ , $wR2 = 0.0396$
R indices (all data)	$R1 = 0.0399$ , $wR2 = 0.0408$
Type of weighting scheme used	Sigma
Weighting scheme used	$w = 1/\sigma^2(F_o^2)$
Max shift/error	0.002
Average shift/error	0.000
Largest diff. peak and hole	2.411 and -1.012 e.Å <sup>-3</sup>

**Special Refinement Details**

Crystals were mounted on a glass fiber using Paratone oil then placed on the diffractometer under a nitrogen stream at 100K.

Refinement of  $F^2$  against ALL reflections. The weighted R-factor ( $wR$ ) and goodness of fit ( $S$ ) are based on  $F^2$ , conventional R-factors ( $R$ ) are based on  $F$ , with  $F$  set to zero for negative  $F^2$ . The threshold expression of  $F^2 > 2\sigma(F^2)$  is used only for calculating R-factors(gt) etc. and is not relevant to the choice of reflections for refinement. R-factors based on  $F^2$  are statistically about twice as large as those based on  $F$ , and R-factors based on ALL data will be even larger.

All esds (except the esd in the dihedral angle between two l.s. planes) are estimated using the full covariance matrix. The cell esds are taken into account individually in the estimation of esds in distances, angles and torsion angles; correlations between esds in cell parameters are only used when they are defined by crystal symmetry. An approximate (isotropic) treatment of cell esds is used for estimating esds involving l.s. planes.



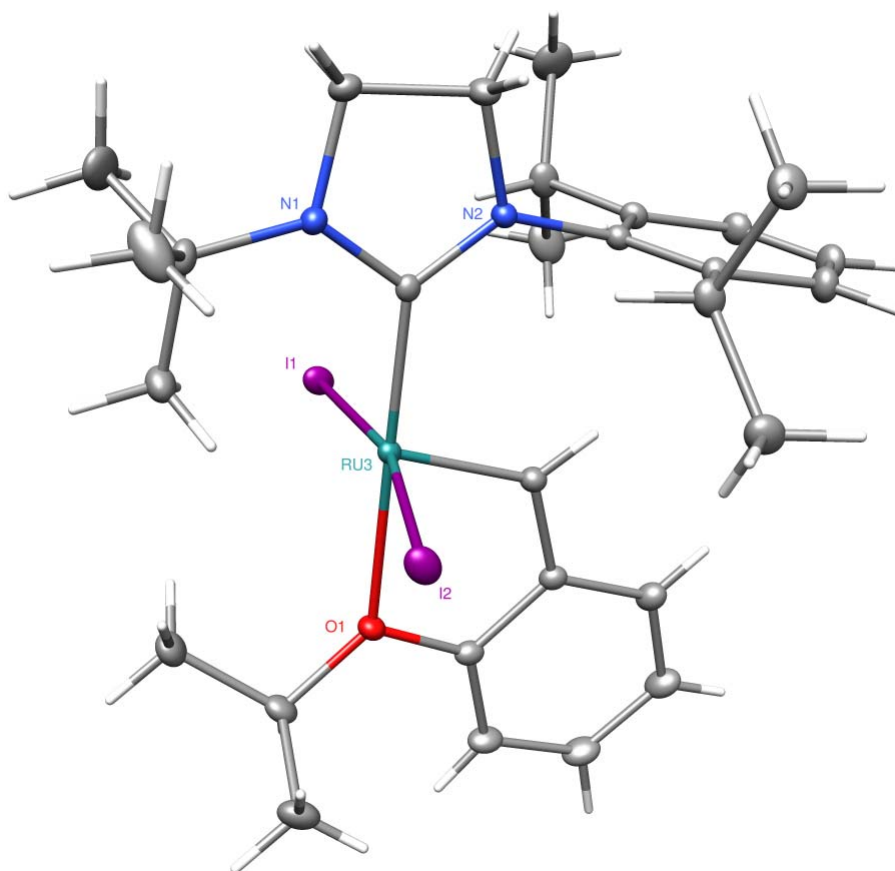


**Table B.5. Atomic coordinates ( $\times 10^4$ ) and equivalent isotropic displacement parameters ( $\text{\AA}^2 \times 10^3$ ) for Complex 10 (CCDC 834513).  $U(\text{eq})$  is defined as the trace of the orthogonalized  $U^{\text{ij}}$  tensor.**

	x	y	z	$U_{\text{eq}}$
Ru(3)	887(1)	1859(1)	2567(1)	9(1)
I(1)	2863(1)	728(1)	2374(1)	14(1)
I(2)	-1280(1)	2922(1)	2459(1)	15(1)
O(1)	-775(1)	833(1)	2414(1)	13(1)
N(1)	2984(1)	3088(1)	2197(1)	12(1)
N(2)	2998(1)	2968(1)	3309(1)	10(1)
C(1)	2370(1)	2694(1)	2721(1)	9(1)
C(2)	4193(1)	3590(1)	2432(1)	15(1)
C(3)	3974(1)	3642(1)	3193(1)	15(1)
C(4)	2663(1)	3056(1)	1453(1)	14(1)
C(5)	4053(1)	2920(1)	1078(1)	30(1)
C(6)	1980(1)	3852(1)	1233(1)	28(1)
C(7)	1640(1)	2383(1)	1266(1)	20(1)
C(8)	2780(1)	2762(1)	4009(1)	10(1)
C(9)	3648(1)	2172(1)	4318(1)	12(1)
C(10)	3493(1)	2016(1)	5012(1)	15(1)
C(11)	2513(1)	2435(1)	5394(1)	17(1)
C(12)	1682(1)	3022(1)	5082(1)	15(1)
C(13)	1799(1)	3203(1)	4390(1)	12(1)
C(14)	4744(1)	1705(1)	3926(1)	16(1)
C(15)	6256(1)	2020(1)	4085(1)	26(1)
C(16)	4658(1)	811(1)	4080(1)	26(1)
C(17)	886(1)	3870(1)	4087(1)	14(1)
C(18)	1407(1)	4674(1)	4376(1)	18(1)
C(19)	-702(1)	3744(1)	4232(1)	20(1)
C(20)	533(1)	1576(1)	3455(1)	12(1)
C(21)	-415(1)	916(1)	3592(1)	11(1)
C(22)	-677(1)	659(1)	4259(1)	15(1)
C(23)	-1583(1)	18(1)	4370(1)	18(1)
C(24)	-2226(1)	-368(1)	3813(1)	19(1)
C(25)	-2004(1)	-119(1)	3146(1)	16(1)
C(26)	-1097(1)	524(1)	3039(1)	12(1)
C(27)	-1552(1)	519(1)	1811(1)	16(1)
C(28)	-713(1)	749(1)	1189(1)	21(1)
C(29)	-3064(1)	850(1)	1786(1)	22(1)

**Table B.6. Selected bond lengths [ $\text{\AA}$ ] and angles [ $^\circ$ ] for Complex 10 (CCDC 834513).**

Ru(3)-C(20)	1.8398(7)	C(20)-Ru(3)-C(1)	100.54(3)
Ru(3)-C(1)	1.9870(7)	C(20)-Ru(3)-O(1)	78.09(3)
Ru(3)-O(1)	2.3318(5)	C(1)-Ru(3)-O(1)	177.09(2)
Ru(3)-I(1)	2.68323(12)	C(20)-Ru(3)-I(1)	95.47(2)
Ru(3)-I(2)	2.70214(12)	C(1)-Ru(3)-I(1)	92.160(18)
		O(1)-Ru(3)-I(1)	85.431(14)
		C(20)-Ru(3)-I(2)	95.07(2)
		C(1)-Ru(3)-I(2)	93.815(19)
		O(1)-Ru(3)-I(2)	88.879(14)
		I(1)-Ru(3)-I(2)	166.731(3)

The Bruker KAPPA APEXII X-ray diffractometer was purchased via an NSF CRIF:MU award to the California Institute of Technology, CHE-0639094.